University of Alberta

Channel and frequency offset estimation for OFDM-based systems

By

Wei Zhang

A thesis submitted in partial fulfillment of the

requirements for the degree of

Doctor of Philosophy

In Communications

Electrical and Computer Engineering Department

Spring,2011

Edmonton, Alberta

Examining Committee

Dr. Chintha Tellambura, Electrical and Computer Engineering Department
(Supervisor)

Dr. Witold Pedrycz, Electrical and Computer Engineering Department

Dr. Hai Jiang, Electrical and Computer Engineering Department

Dr. Mike MacGregor, Computing Science

Dr. Xianbin Wang, University of Western Ontario
(External examiner)

dedication

To my husband Garry, my son Lucas.

To my parents and sisters.

Abstract

Orthogonal frequency-division multiplexing (OFDM) has been employed in several current and future 4-th generation (4G) wireless standards. Frequency offsets in OFDM introduce intercarrier interference (ICI). Channel estimations are also required.

This thesis focuses on the channel and frequency offset estimation for OFDM-based systems. For cooperative-relay OFDM with frequency offsets, where inter-relay interference (IRI) exists, channel estimation is developed. Optimal pilot designs are proposed by minimizing the IRI in the mean square error (MSE) of the least square (LS) channel estimation. The impact of frequency offset on the channel estimation accuracy is derived. The pairwise error probability (PEP) with both the frequency offset and channel estimation errors is evaluated. The power allocation is discussed.

For multiple-input multiple-output (MIMO) OFDM systems, channel and frequency offset estimation errors are investigated. The signal-to-interference-and-noise ratio (SINR) is first analyzed given channel and frequency offset estimation errors. The bit error rate (BER) is then approximated for multiple-antenna reception with maximal ratio combing (MRC) and equal gain combining (EGC).

For orthogonal frequency-division multiplexing access (OFDMA) systems, the variance of the frequency offset estimation is derived as a function of SINR and signal-to-noise ratio (SNR). This variance information is exploited to improve the accuracy of frequency offset estimators. A successive interference cancelation (SIC)-based frequency offset estimator is also developed.

The accuracy of frequency offset estimation of the OFDMA uplink can also be improved by using the cooperative relaying. Both conventional amplify-and-forward (AF) relays and new decode-and-compensate-and-forward (DcF) relays are studied. The frequency offset estimate is derived from combining different link estimates. In addition, when CSI is available, a scheme is proposed to adaptively switch between the

cooperative and conventional (no relaying) transmissions to optimize the frequency offset estimation.

Acknowledgements

My first and most earnest gratitude goes to my supervisor, Prof. Chintha Tellambura for his continuous encouragement, invaluable advice, and unbelievable generosity. He teaches not only the knowledge itself, but also how to look into the problems. In every sense, this thesis could never have come into existence without his help. These years to be under his supervision will be remembered as one of most memorable part of the life.

I would like to sincerely thank my committee members who have given their time to read this manuscript and offered valuable comments to improve the contents of this dissertation.

Much respect to my labmates and friends. Special thanks go to Mr. Zhongshan Zhang, Ms. Yu Fu, Ms. Hua Shao, Mr. Luqing Wang for their inspiring discussions and help. I am grateful to all my colleagues and also friends for making the lab a 'warm' place filled with both academic discussions and fun of cross-cultural entertainments. Staying with them has always been so enjoyable.

Finally, I give my thanks to my husband Garry Li, Lucas and our families. Their endless love and unmeasurable support have always been one of the impetuses for my endeavor.

I cannot acknowledge enough all the peoples who have given me help of this kind or that. This list of acknowledgements will be ended with not only a 'thank you' but also a warm memory.

List of Tables

2.1 Performance Comparison Between AF and DF Modes 47

3.2 Parameters for BER Simulation in MIMO OFDM Systems 70

4.3 Subcarrier Allocation in OFDMA Uplink Transmission (Bandwidth = 10 MHz, DFT Length = 256, CP = 16) 98

4.4 Subcarrier Allocation in OFDMA Uplink Transmission with New Accessed Users (Bandwidth = 10 MHz, DFT Length = 256, CP = 16) . . 100

5.5 Performance Improvement in the Proposed Cooperative Scheme With and Without Feedback from the Base Station over the Conventional Non-cooperative Algorithm 119

5.6 Performance Improvement in the Proposed Cooperative Scheme with Feedback as a Function of M 120

List of Figures

1.1 Block diagram of an OFDM system. 4
1.2 OFDM symbol spectrum with sampling points: only four subcarriers are shown: (a) no frequency offset, and (b) frequency offset present. . . 6
1.3 SINR degradation in the presence of frequency offset. 8
1.4 Illustration of MRC and EGC. 11
1.5 Block diagram of a MIMO OFDM link. 11
1.6 A simplified single relay cooperation model. 13
1.7 Example of subcarrier allocation schemes: (a) subband CAS, (b) interleaved CAS, and (c) generalized CAS. 16
1.8 Example of pilots in a block of 9 OFDM symbols with 16 subcarriers. . 18

2.9 Transceiver system model of the proposed cooperative transmission. . . 33
2.10 Normalized MSE of channel estimation in either conventional transmission ($\alpha = 1$) or the proposed cooperative transmission ($0 < \alpha < 1$). 48
2.11 PEP of the proposed cooperative transmission with $L = 2$ and $\sigma_e^2 = 10^{-3}$. 49
2.12 PEP of the proposed cooperative transmission with $L = 4$ and $\sigma_e^2 = 10^{-3}$. 51
2.13 PEP of the proposed cooperative transmission with $L = 16$ and $\sigma_e^2 = 10^{-3}$. 52
2.14 PEP of the proposed cooperative transmission as a function of σ_e^2 with $L = 4, 8$. 53
2.15 PEP of the proposed cooperative transmission as a function of SNR with $L = 4$, $M = 16$ and $\sigma_e^2 = 10^{-2}, 10^{-3}$. 54

3.16 SINR reduction due to the residual frequency offset in MIMO OFDM systems. 71
3.17 BER degradation due to the residual frequency offset in MIMO OFDM systems. 72

3.18 BER with QPSK when $(N_t = 1, N_r = 1)$. 73
3.19 BER with 16-QAM when $(N_t = 1, N_r = 1)$. 74
3.20 BER with QPSK when $(N_t = 2, N_r = 2)$. 75
3.21 BER with 16-QAM when $(N_t = 2, N_r = 2)$. 76
3.22 BER with QPSK when $(N_t = 2, N_r = 4)$. 77
3.23 BER with 16-QAM when $(N_t = 2, N_r = 4)$. 78

4.24 Structure of OFDMA uplink transmission. 82
4.25 SINR reduction introduced by non-zero frequency offset in OFDMA systems. 88
4.26 Minimum variance of the frequency offset in a noisy OFDMA system. . 90
4.27 Receiver structure for OFDMA uplink frequency offset estimation. . . . 93
4.28 SINR estimation in OFDMA uplink. 95
4.29 SIC-based frequency offset estimation. 97
4.30 Performance comparison between conventional estimator and the proposed estimator. 99
4.31 Performance comparison between conventional estimator and the proposed estimator when there is one new user accessing the base station. 101
4.32 Performance comparison between conventional estimator and the proposed estimator when there are multiple new users simultaneously accessing the base station. 102
4.33 Performance comparison between conventional estimator and the proposed estimator by using a uniform RV to approximate the Gaussian distributed frequency offsets. 103

5.34 Channel outage probability as a function of N_u in OFDMA. 110
5.35 PDF of $\nu_{\max}$ in cooperation OFDMA uplink transmission. 111
5.36 Adaptive cooperation in OFDMA uplink frequency offset estimation. . 117

5.37 Cooperative frequency offset estimation as a function of α without feedback from the base station. 118
5.38 BER by using the proposed cooperative frequency offset estimation with feedback from the base station. 121

Acronyms

Acronyms	Definition
4G	Fourth generation
A/D	Analog-to-digital converter
ADSL	Asymmetric digital subscriber line
AF	Amplify-and-forward
AWGN	Additive white Gaussian noise
B3G	Beyond third generation
BER	Bit error rate
BS	Base station
CP	Cyclic prefix
CSI	Channel state information
CRLB	Cramer-Rao lower bound
D/A	Digital-to-analog converter
DAB	Digital audio broadcasting
DcF	Decode-and-compensate-and-forward
DF	Decode-and-forward
DFT	Discrete Fourier transform
DVB	Digital video broadcasting
EGC	Equal gain combining
FIM	Fisher information matrix
FEQ	Frequency-domain equalizer
FFT	Fast Fourier transform
HDSL	High-bit-rate digital subscriber line
i.i.d.	Identical independent distribution
IAI	Inter-antenna interference

Acronyms	Definition
ICI	Inter-carrier interference
IFFT	Inverse fast Fourier transform
IRI	Inter-relay interference
ISI	Inter-symbol interference
LS	Least squares
LTE	Long Term Evolution
MAI	Multiple access interference
MCM	Multi-carrier modulation
MIMO	Multiple-input multiple-output
MISO	Multiple-input single-output
ML	Maximum likelihood
MMSE	Minimum mean squared error
MRC	Maximal ratio combining
MS	Mobile station
MSE	Mean squared error
MUI	Multiuser interference
OFDM	Orthogonal frequency-division multiplexing
OFDMA	Orthogonal frequency-division multiple access
PDF	Probability density function
PEP	Pairwise error probability
P/S	Parallel-to-serial conversion
PSK	Phase shift keying
QAM	Quadrature amplitude modulation
QPSK	Quadrature phase shift keying
RV	Random variable
SNR	Signal-to-noise ratio
SIC	Successive interference cancellation
SIR	Signal-to-interference ratio

Acronyms	**Definition**
SINR	Signal-to-interference-and-noise ratio
STC	Space-time coding
VC	Virtual carrier
WLAN	Wireless local area network
ZF	Zero forcing

Notation

$\jmath$	$\sqrt{-1}$
$(\cdot)^*$	Complex conjugation
$(\cdot)^T$	Transpose
$(\cdot)^H$	Conjugate transpose
$(\cdot)^\dagger$	Moore-Penrose pseudo-inverse
$\delta(\cdot)$	Dirac delta function
$\arg(\cdot)$	Argument
$\otimes$	Convolution
$\mathbf{A}$	The matrix $\mathbf{A}$
$[\mathbf{A}]_{nk}$	The (n,k)th entry of the matrix $\mathbf{A}$
$\mathbf{A}^{-1}$	The inverse matrix of $\mathbf{A}$
$\mathbf{a}$	The vector $\mathbf{a}$
$a[n]$	The nth entry of the vector $\mathbf{a}$
$\mathfrak{R}(\cdot)$	Real part of the argument
$\mathfrak{I}(\cdot)$	Imaginary part of the argument
$\mathbb{E}(\cdot)$	Expectation of the argument
$\|\|(\cdot)\|\|^2$	2-norm of the argument
$\text{trace}(\mathbf{M})$	The trace of the matrix $\mathbf{M}$
$\mathcal{CN}(\mu,\sigma^2)$	A complex Gaussian random variable (RV) with mean μ and variance σ^2
$\mathbf{I}_N$	The $N \times N$ identity matrix
$\mathbf{0}_{M\times N}$	$M \times N$ all-zero matrix
$\text{diag}(\mathbf{a})$	The diagonal matrix formed by vector $\mathbf{a}$
$\lfloor a \rfloor$	The maximum integer part of a

Contents

1 Introduction **1**

1.1 OFDM Systems . . . 2

1.1.1 Wireless Channel . . . 2

1.1.2 OFDM . . . 3

1.1.3 MIMO OFDM . . . 7

1.1.4 Cooperative OFDM . . . 12

1.1.5 OFDMA . . . 15

1.2 Channel Estimation Techniques . . . 16

1.3 Frequency Offset Estimation Techniques . . . 20

1.4 Motivation . . . 22

1.5 Structure and Contributions . . . 24

2 Cooperative OFDM Channel Estimation **27**

2.1 Introduction . . . 27

2.2 Cooperative OFDM Signal Model . . . 28

2.2.1 Channel Model . . . 28

2.2.2 OFDM Signal Model . . . 29

2.2.3 First Time Slot (Preamble Period) . . . 29

2.2.4 Second Time Slot . . . 30

2.3 Channel Estimation . . . 32

2.3.1 Channel Estimation in the First Time Slot . . . 32

2.3.2 Pilot Design to Eliminate IRI in the Second Time Slot . . . 33

2.3.3 Effect of Imperfect Frequency Offset Estimation on Channel Estimation . . . 38

2.4 Effect of Frequency Offset and Channel Estimation Errors on PEP . . . 41

2.4.1 SINR Analysis 42
2.4.2 PEP for the AF Mode 44
2.4.3 PEP for the DF Mode 45
2.5 Numerical Results 47
2.6 Conclusions 52

3 BER of MIMO OFDM Systems with Frequency Offset and Channel Estimation Errors 55
3.1 Introduction 55
3.2 MIMO OFDM Signal Model 56
3.3 SINR Analysis in MIMO OFDM Systems 58
3.3.1 SINR Analysis without Receiver Combining 58
3.3.2 SINR Analysis with EGC 63
3.3.3 SINR Analysis with MRC 64
3.4 BER Performance 65
3.4.1 BER without Receiver Combining 68
3.4.2 BER with EGC 68
3.4.3 BER with MRC 69
3.4.4 Complexity of the Infinite-Series Representation of BER 69
3.5 Numerical Results 69
3.6 Conclusions 74

4 Robust OFDMA Uplink Frequency Offset Estimation 79
4.1 Introduction 79
4.2 OFDMA Uplink Signal Model 81
4.3 Interference Analysis in OFDMA Systems 85
4.3.1 Interference Reduction by Using Pre-Projector Method 85
4.3.2 SINR Analysis 87
4.3.3 Frequency Offset Analysis 87

4.4 Iterative Frequency Offset Estimation 89
4.4.1 ML Estimation 89
4.4.2 SIC-based Algorithm by Using Known Pilots/Training Sequences 91
4.5 Improving Estimators by Exploiting the Frequency Offset Variance in OFDMA Uplink 92
4.5.1 The SIC-based Algorithm with the Variance of the Frequency Offsets 94
4.5.2 Conventional Differential Algorithms with the Variance Knowledge 96
4.6 Numerical Results 98
4.7 Conclusions 104

5 OFDMA Uplink Frequency Offset Estimation via Cooperative Relaying 105

5.1 Introduction 105
5.2 Cooperative OFDMA Uplink Signal Model 106
5.2.1 Channel Model 107
5.2.2 The First Time Slot 108
5.2.3 The Second Time Slot 109
5.3 Frequency Offset Estimation in the Cooperative Scheme 113
5.3.1 Without CSI Feedback from the Base Station 115
5.3.2 With CSI Feedback from the Base Station 115
5.3.3 Adaptive Switching Between Cooperative and Conventional Non-Cooperative Transmissions 116
5.4 Numerical Results 116
5.5 Conclusions 120

6 Conclusions and Future Work 123

6.1 Conclusions 123
6.2 Future Work 125

Appendix **127**

A $D_{i;m}^{k}$ in Chapter 3 **127**

A.1 $D_{i;m}^{k}$ for Without Combining 127

A.2 $D_{i;m}^{\mathrm{EGC}}$ for EGC 128

A.3 $D_{i;m}^{\mathrm{MRC}}$ for MRC 130

B Appendix for Chapter 5 **133**

B.1 Analysis of FIM 133

B.2 SINR Analysis 134

Bibliography **136**

Chapter 1

Introduction

Wireless communication industry continues to evolve from the 3rd generation (3G) systems. For example, Long Term Evolution (LTE) [1] has been standardized for the emerging pre-4th generation (4G) wireless communications. The peak data rate provided by LTE systems is expected to be more than 100 Mb/s in the downlink, allowing these systems to provide diversified multimedia services effortlessly. However, since the radio spectrum is limited, improved physical-layer modulation methods are required to achieve such high-data rates.

Orthogonal frequency-division multiplexing (OFDM) [2], a special case of multi-carrier modulation, is a candidate for 4G wireless due to its inherent robustness to frequency-selective fading and the low-complexity of its receiver. OFDM can be combined with other advanced techniques to boost the performance of the LTE systems. For example, the LTE downlink employs orthogonal frequency-division multiple access (OFDMA) for multi-user access ability. Moreover, multiple-input multiple-output (MIMO) and OFDM improve the data throughput [3, 4]. Due to these advantages, OFDM has also been implemented for several other wireless standards, including IEEE 802.11 wireless local area network (WLAN) standard, IEEE 802.16 metropolitan area network (MAN) standard, and IEEE 802.20 mobile broadband wireless networks (MBWA) [5, 6]. OFDM has also been used in a number of other systems, from voice-band modems such as asymmetric digital subscriber line (ADSL), high-bit-rate digital subscriber line (HDSL) to broadcast standards including digital video broadcasting (DVB) [7], digital audio broadcasting (DAB) [8], and high-definition television (HDTV) [9]. For all OFDM systems, channel and frequency offset estimation are two

critical issues of the system design.

1.1 OFDM Systems

OFDM divides a wideband frequency-selective channel to an equivalent set of narrowband frequency-flat subchannels. This division is achieved by splitting the input high-rate data stream into a number of substreams that are transmitted in parallel over orthogonal subcarriers. The orthogonality between the subcarriers prevents interference between the closely spaced subcarriers as well as allows the subcarriers spectra to overlap, making OFDM highly spectrally efficient. Moreover, a cyclic prefix (CP) added at the transmitter reduces the receiver complexity by allowing discrete Fourier transform (DFT) demodulation and one-tap frequency-domain equalization (FEQ) [10].

1.1.1 Wireless Channel

To comprehend the benefits of OFDM, the basic characteristics of the wireless channel must be understood. The wireless channel is characterized by multipath propagation; i.e., the transmitted signal arrives at the receiving antenna via different paths. These paths experience different attenuations and time delays, giving rise to delay spread. Doppler spread happens when there is a relative motion between the transmitter and receiver. Key parameters of the channel are the coherence bandwidth and coherence time, which are inversely proportional to the delay spread and Doppler spread, respectively [11].

Depending on the bandwidth and symbol period of the transmitted signal, the wireless channel may manifest four different types of fading on the transmitted signal. When the signal bandwidth is smaller than the coherence bandwidth of the channel, the channel is frequency-flat or flat fading. Otherwise, the channel is frequency-selective.

When the symbol period is smaller than the coherence time of the channel, the channel is time-invariant. Otherwise, the channel is time-varying [11]. In high-data rate transmissions, because of the wide bandwidth of the transmitted signal, the channel becomes frequency-selective [11].

Such a multipath-fading channel can be modeled by the complex impulse response as [2, 12]

$$h(\tau, t) = \sum_{l=0}^{L-1} h_l(t)\delta(t - \tau_l(t)), \tag{1.1}$$

where $h(\tau, t)$ is the baseband equivalent channel response at time t due to an impulse applied at time $t-\tau$, $\delta(\cdot)$ is the dirac delta function, and $h_l(t)$ and $\tau_l(t)$ are the complex gain and the propagation delay of the l-th path. The discrete-time equivalent channel can be expressed as the samples $h[l] = h(lT_s)$, where T_s is the sampling period. Thus, when the sequence of symbols $x[n]$ is directly transmitted over the multipath channel $h[l]$, the received signal is given by the convolution of the symbol sequence with the channel impulse response [2],

$$y[n] = \sum_{l=0}^{L-1} h[l]x[n-l] + w[n] = h[0]x[n] + \underbrace{\sum_{l=1}^{L-1} h[l]x[n-l]}_{ISI} + w[n], \tag{1.2}$$

where $w[n]$ is an additive noise term and the second term of the right is the inter-symbol interference (ISI), which needs to be removed to correctly recover the transmitted sequence. ISI can be eliminated by OFDM, which is described next.

1.1.2 OFDM

The block diagram of an OFDM system is shown in Figure 1.1. The source bit stream may include source coding, channel coding, and bit interleaving. The transmitter maps the source bit stream to modulation symbols from a complex constellation such as phase-shift keying (PSK) or quadrature amplitude modulation (QAM). The different constellations maybe be used for different subcarriers, if bit loading algorithms are

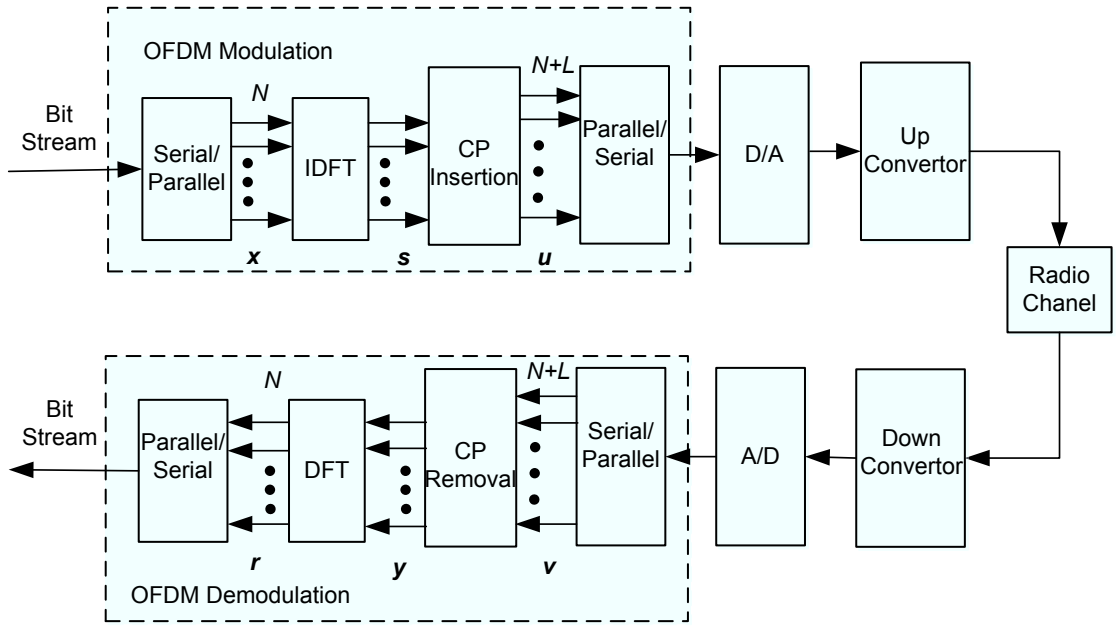

Figure 1.1: Block diagram of an OFDM system.

used [10]. An OFDM symbol is generated by taking the inverse discrete Fourier transform (IDFT) of N modulation symbols, where N is the size of the IDFT. In practice, the IDFT can be implemented with a computationally efficient inverse fast Fourier transform (IFFT).

Let $\{X(0), X(1), \ldots, X(N-1)\}$ be a block of N data symbols after the serial-to-parallel conversion. The IDFT of the data block is

$$s_n = \sum_{k=0}^{N-1} X(k) e^{\frac{\jmath 2\pi nk}{N}}, \quad n = 0, 1, \ldots, N-1, \tag{1.3}$$

where the imaginary unit $\jmath = \sqrt{-1}$. These time-domain samples are the time-domain OFDM symbol $\{s_n, n = 0, \ldots, N-1\}$. To mitigate the effects of ISI caused by the channel delay spread, each time-domain OFDM symbol $\{s_n, n = 0, \ldots, N-1\}$ is preceded by a CP, which is simply a repetition of the last N_g time samples. The length of the CP N_g is at least equal to the channel order L to completely mitigate ISI.

Because of the CP, the linear convolution of transmitted symbols with channel (see

Eq. (1.2)) is transformed to a circular convolution. Then the output of DFT demodulation is the multiplication of the frequency-domain OFDM symbol $\mathbf{X} = (X(0), X(1), \ldots, , X(N-1))^T$ and the channel response in the frequency domain [10], i.e.,

$$\mathbf{r} = \mathbf{HX} + \mathbf{w}, \tag{1.4}$$

where $\mathbf{H} = \text{diag}\{H[0], \ldots, H[N-1]\}$, $H[n] = \sum_{l=0}^{L-1} h(l) e^{-\frac{\jmath 2\pi nl}{N}}$ is the complex channel frequency response at subcarrier n, and $\mathbf{w}$ is an additive white Gaussian noise (AWGN) vector. The n-th element of $\mathbf{r}$ is then expressed as

$$r[n] = H[n]X(n) + w[n], \quad 0 \le n \le N-1. \tag{1.5}$$

Eq. (1.5) shows that OFDM transmission over a frequency-selective channel, given by (1.2), is equivalent to data transmission over N parallel subchannels.

If the gain of the n-th subcarrier $H[n]$ can be estimated as $\hat{H}[n]$, $X(n)$ is then detected by one tap FEQ as

$$\hat{X}(n) = \frac{r[n]}{\hat{H}[n]} = \frac{X(n)H[n]}{\hat{H}[n]} + \frac{\mathbf{w}[n]}{\hat{H}[n]}. \tag{1.6}$$

Sensitivity to Frequency Offset

The received signal of the n-th subcarrier in Eq. (1.5) is only valid for OFDM systems without a carrier frequency offset. When there is a frequency offset between the transmitter carrier frequency and the receiver carrier frequency, the received signals are expressed as [13]

$$r[n] = H[n]X(n)\frac{\sin(\pi\varepsilon)}{N\sin(\frac{\pi\varepsilon}{N})} e^{\frac{\jmath\pi\varepsilon(N-1)}{N}} + \underbrace{\sum_{m=0, m\neq n}^{N-1} H[m]X(m)\frac{\sin[\pi(m-n+\varepsilon)]}{N\sin\left[\frac{\pi(m-n+\varepsilon)}{N}\right]} e^{\frac{\jmath\pi(m-n+\varepsilon)(N-1)}{N}}}_{\text{ICI}} + w[n], \tag{1.7}$$

where ε is the normalized frequency offset, defined as $\varepsilon = f_o/\Delta f$, f_o is the frequency offset, and Δf is the frequency separation between subcarriers. The first term of the

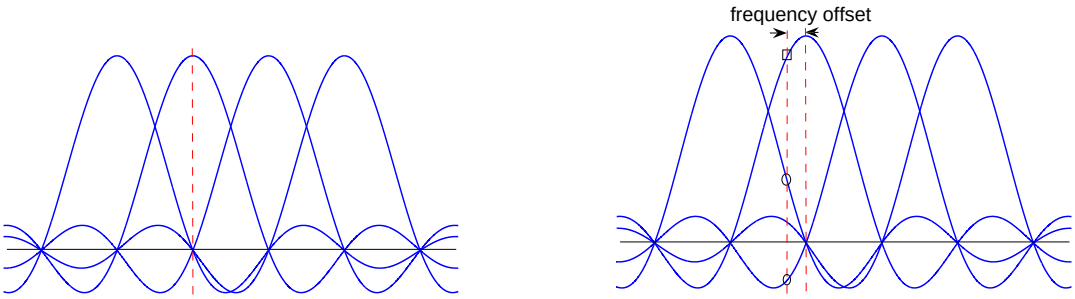

(a) (b)

Figure 1.2: OFDM symbol spectrum with sampling points: only four subcarriers are shown: (a) no frequency offset, and (b) frequency offset present.

right side of (1.7) is the useful signal part at the desired subcarrier and the second term represents the inter-carrier interference (ICI) introduced by other subcarriers.

The frequency offset may arise due to two reasons: first, a carrier frequency mismatch can exist between the transmitter and receiver oscillators; second, a Doppler shift can arise due to relative motion between the transmitter and the receiver.

In practical systems, the mismatch of the transmitter and the receiver oscillators embodies the different frequency shifts of the transmit and receive oscillators from the designated carrier frequency. The causes of the frequency shift are the oscillator instability, which can be due to aging, humidity, temperature, electromagnetic interference (EMI), and pressure. The oscillator stability is measured by unit of parts-per-million (ppm) with 1 ppm = 10^{-6}. For example, the stability of a typical mobile handset crystal may vary from 2 ppm to 12 ppm [14, 15], which translates to a frequency offset in the range of 2 to 12 kHz at a carrier frequency of 2 GHz.

The relative motion between the transmitter and receiver causes a shift in the received signal frequency, called the Doppler shift. The Doppler shift depends on the velocity and direction of the motion of the mobile with respect to the direction of the arrival of the received multipath wave. The Doppler shift introduced by the mobile movement is given by $f_d = f_m \cos\theta$, where f_m is the maximum Doppler shift and θ is the

angle of arrival. The maximum Doppler shift $f_m = \frac{v}{c} f_c$, where v is the mobile speed, c is the speed of light and f_c is the carrier frequency. For a vehicle moving at 100 km/h, the Doppler shift is about 185 Hz at a carrier frequency of 2 GHz. The Doppler shift in terrestrial mobile communications may vary from 1 Hz to several hundred of Hz.

With the frequency offset, the receiver cannot sample correctly at the center frequencies of the subcarriers (Figure 1.2 (b)). The signal amplitude of the desired subcarrier is then reduced. The nonzero sidelobes of other subcarriers cause ICI. The effect of frequency offset can be seen in (1.7), with two main effects clearly visible. First, the desired subcarrier is attenuated because it is no longer sampled at the peak of the subcarrier, which results in the amplitude $\frac{\sin(\pi\epsilon)}{N\sin(\frac{\pi\epsilon}{N})}$ and the phase shift $\theta = e^{j\pi\varepsilon(N-1)/N}$ factors. Second, adjacent subcarriers cause interference, as they are not sampled at their zero-crossings. The resulting ICI degrades the system performance. The signal-to-noise ratio (SNR) degradation caused by the frequency offset is roughly proportional to the square of the normalized frequency offset [16]. Since the frequency offset introduces interference, signal-to-interference-and-noise ratio (SINR), the ratio of the signal power to the sum of the interference power and noise power, is a suitable measure of the sensitivity of OFDM systems to frequency offset (Figure 1.3). In Figure 1.3, SNR = 12 dB. Clearly, when the frequency offset ε increases, the SINR decreases dramatically. For example, when $\varepsilon = 0.5$, the SINR is only -12 dB. The performance effect varies strongly with the choice of the signal constellation. Naturally, constellations with fewer points can tolerate larger frequency errors than larger constellations.

1.1.3 MIMO OFDM

Thus far, the discussion has been limited to single-input single-output (SISO) OFDM, where one transmit and one receive antenna are employed. MIMO systems employ multiple antennas at the receiver and/or transmitter [4, 17–19] to improve the performance of OFDM systems. By exploiting the spatial dimension, the MIMO approach significantly increases the spectral efficiency and link reliability without additional

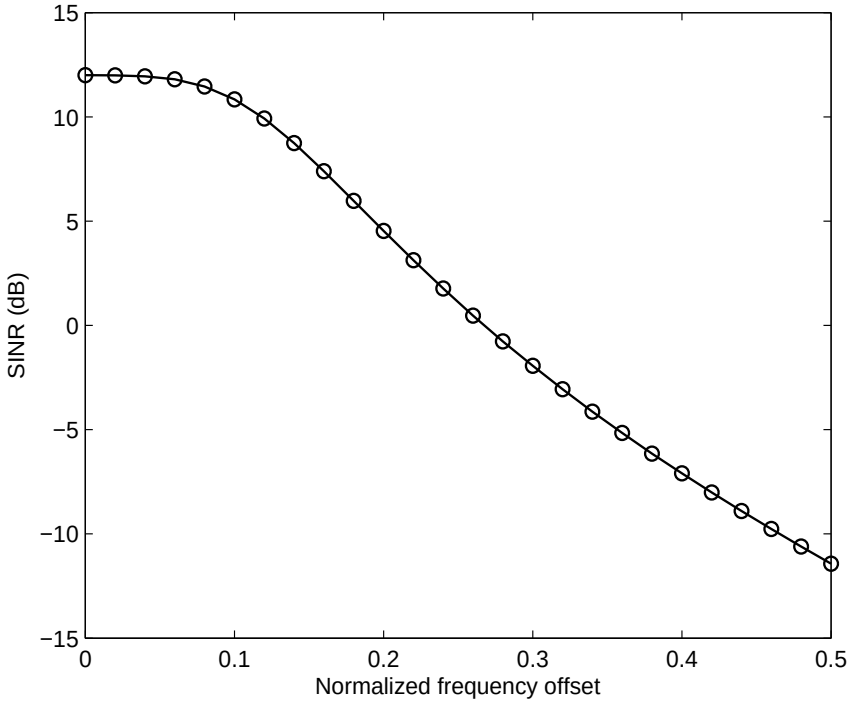

Figure 1.3: SINR degradation in the presence of frequency offset.

bandwidth or transmit power. By transforming the frequency-selective MIMO channel to a set of flat-fading MIMO channels, MIMO and OFDM can operate together at a high-throughput mode, the diversity mode or the combination of both [20]. Such systems achieve high spectral efficiencies and/or a large coverage area that are critical for future-generation wireless networks. MIMO OFDM is already included in wireless communication standards such as IEEE 802.11n, LTE and IEEE 802.16a MAN [1].

MIMO techniques that are developed for single-carrier systems can be readily extended to MIMO OFDM systems and can enhance the transmission reliability with spatial diversity by using space-time coding (STC) techniques [21, 22] and boost the system capacity with spatial multiplexing (SM) by simultaneously transmitting multiple data streams [23, 24].

Spatial diversity

Spatial diversity techniques mainly aim to improve the reliability of data transmission. Diversity is achieved by multiple independent spatial channels, which allow the receiver to combat signal fading and gain spatial diversity [4]. For any diversity technique, the performance improvement may be measured by the rate at which the error probability decreases at high SNR. This rate is much bigger than that for systems with no diversity. At high SNR, the decreasing rate is given by the slope of the plot of the symbol error rate (SER) against the SNR on a log-log scale. The absolute value of the slope is called the diversity order, which is strictly defined as [25]

$$m = -\lim_{\gamma \to \infty} \frac{\log P_{\mathrm{SER}}(\gamma)}{\log \gamma}, \tag{1.8}$$

where γ is the SNR and $P_{\mathrm{SER}}(\gamma)$ is the SER at γ. A large diversity order is desirable because the SER is then reduced at a faster rate. In a MIMO system, it is possible to provide a maximum or full diversity order equal to the product of the number of transmit antennas and the number of receive antennas, i.e., $N_T \times N_R$, where N_T and N_R are the number of the transmit and receive antennas respectively [17].

Diversity order is maximized by space-time block codes (STBCs) [26–28], which rely on coding across transmit antennas. Orthogonal STBC (OSTBC) obtains full $N_T \times N_R$ order diversity with low decoding complexity. These codewords consist only linear combinations of several symbols and their conjugates, and encoding therefore only requires linear processing. A well-known OSTBC is the Alamouti code for two transmit antennas, which can achieve full $2N_R$ order diversity and has been adopted in several 3G cellular standards [29, 30]. The Alamouti code takes two time slot to transmit two symbols x_1 and x_2. In the first time slot, x_1 and x_2 are transmitted from antenna 1 and 2, respectively, following by $-x_2^*$ and x_1^* transmitted from antenna 1 and 2 respectively during the second time slot. Hence, the Alamouti codeword can be

represented as

$$\mathbf{X} = \begin{pmatrix} x_1 & -x_2^* \\ x_2 & x_1^* \end{pmatrix},$$

which satisfies the OSTBC design criterion [17]

$$\mathbf{X}^H\mathbf{X} = (\sum_{u=1}^{U} |x_u|^2)\mathbf{I}_{N_T}.$$

Another approach to improve the diversity order is to use receive antenna diversity techniques, which combine the independent received signals on each receive antenna. Two popular examples are maximal-ratio combining (MRC) and equal-gain combining (EGC). MRC and EGC for n receive antennas are shown in Figure 1.4. The channel between the transmit antenna to the i-th receive antenna is denoted as h_i. The received signal on the i-th receive antenna r_i, will be multiplied with c_i, and the resulting signals will be summed up to generate the output. $c_i = h_i^*$ for MRC case, and $c_i = h_i^*/|h_i|$ for EGC case. The output of MRC and EGC can be expressed as

$$\begin{aligned} r_{\text{MRC}} &= \sum_{i=0}^{n-1} |h_i|^2 + \sum_{i=0}^{n-1} h_i^* w_i, \\ r_{\text{EGC}} &= \sum_{i=0}^{n-1} |h_i| + \sum_{i=0}^{n-1} w_i h_i^*/|h_i|. \end{aligned} \tag{1.9}$$

The SNR of the MRC output is the sum of SNRs on each branch and MRC achieves full diversity order. EGC performs slightly worse than MRC, and this is the price paid for the reduced complexity of using equal weight gains.

Spatial Multiplexing

Some MIMO systems are primarily designed to increase the data rate but not the diversity order. SM is one such MIMO technique, which uses a layered approach to increase the data rate. The achievable increase is proportional to $\min(N_T, N_R)$, where N_T and N_R are the number of the transmit and receive antennas respectively. One popular example of such system is the vertical-Bell Laboratories layered space-time (V-BLAST) suggested by Foschini *et al.* [18, 31]. These systems do not achieve full spatial diversity.

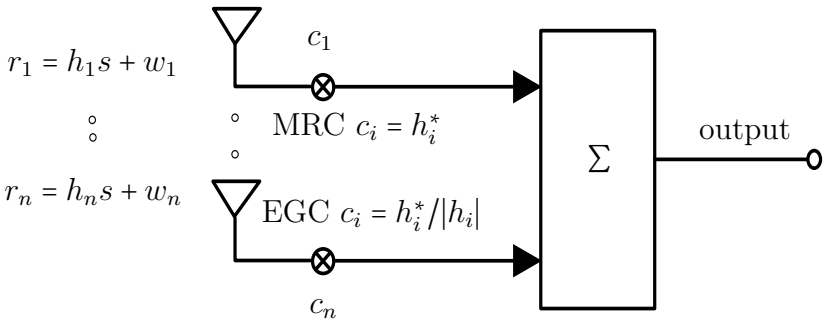

Figure 1.4: Illustration of MRC and EGC.

MIMO OFDM

A MIMO OFDM link (Figure 1.5) has N_t transmit antennas and N_r receive antennas. The MIMO encoder processes and outputs N_t parallel output symbol steams. Just as in SISO OFDM, the symbol streams over each transmit antenna are first IDFT modulated and appended with CPs. At each of the receive antennas, the CP is stripped off and DFT demodulation is performed.

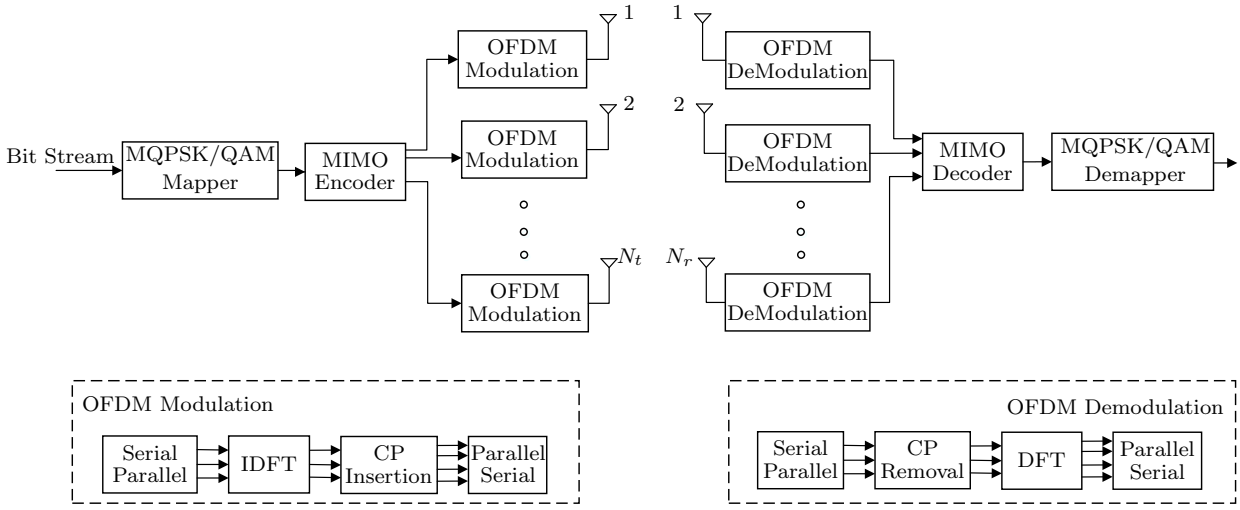

Figure 1.5: Block diagram of a MIMO OFDM link.

As mentioned before, OFDM transforms the frequency-selective channel to a set of parallel flat-fading channels. Thus in MIMO OFDM, every OFDM subcarrier is effectively tranmitted over a MIMO flat-fading channel. Single-carrier MIMO techniques can easily be extended to MIMO OFDM systems. For example, space-time coding can be thus extended to MIMO OFDM systems, resulting in space-frequency coding. Receive antenna diversity can also be extended to MIMO OFDM by combing the received signals on the subcarriers. SM and MIMO OFDM can maximize the data rate by transmitting independent data streams over transmit antennas. Again, for each subcarrier, the input-output relationship of MIMO OFDM reduces to that for single-carrier MIMO, and the receiver architecture of MIMO OFDM system for SM is identical to that for MIMO systems with single-carrier modulation.

MIMO OFDM is also sensitive to frequency offset. Over the $\{u, v\}$-th channel between the u-th receive antenna and the v-th transmit antenna, frequency offset $\varepsilon_{u,v}$ may exist. In multiuser OFDM, different users will have distinct values of frequency offsets. In the most general case, the frequency offset between each transmit-receive antenna pair may be different, i.e., the maximum possible number of frequency offset values is $N_t \times N_r$ [32, 33].

1.1.4 Cooperative OFDM

As already mentioned, multiple antennas achieve enhanced spectral efficiency and/or the improved link reliability. However, the cost increases because each transmit/receive antenna pair requires a dedicated radio frequency chain. In cellular applications, for example, packaging multiple antennas to the cellular mobile handset devices may not be practical due to size and power constraints. Moreover, the propagation environment might not support MIMO because, for example, there is not enough scattering [34].

The above limitations of MIMO are overcome by cooperative relaying [35–37]. A virtual multiple-antenna array is created with distributed multiple nodes. The use of relays may lead to expanded coverage, system wide power saving, and better immunity

against signal fading [34]. The cost of the system could be significantly reduced, and the complexity of the packaging multiple antennas in physical size limited terminals is eliminated. Relay protocols are included in beyond third generation (B3G) and 4G systems [38]. A concise single relay node cooperative communications model is shown in Figure 1.6. Independent channels between the source and the destination are generated via the introduction of a relay node. A typical cooperation strategy can be modeled with two phases.

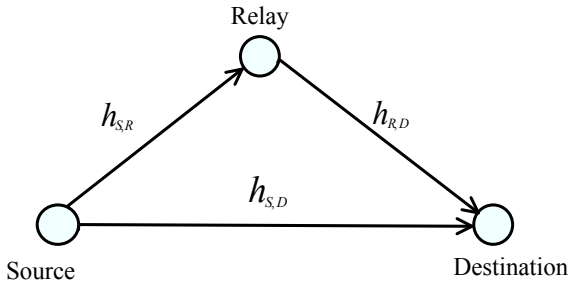

Figure 1.6: A simplified single relay cooperation model.

In phase 1, the source broadcasts information to the destination and the relay. The received signals $y_{S,D}$ and $y_{S,R}$ at the destination and the relay, respectively, can be written as

$$y_{S,D} = \sqrt{P_1} h_{S,D} x + \eta_{S,D}, \tag{1.10}$$

$$y_{S,R} = \sqrt{P_1} h_{S,R} x + \eta_{S,R}, \tag{1.11}$$

where P_1 is the transmitted power at the source, x is the transmitted information symbol, $\eta_{S,D}$ and $\eta_{S,R}$ are additive noise with variance N_0 at the destination and relay, respectively. In Equations (1.10) and (1.11), $h_{S,D}$ and $h_{S,R}$ are the channel coefficients from the source to the destination and the relay, respectively.

In phase 2, the relay can help the source by forwarding or retransmitting to the destination. The relay operation can be amplify-and-forward (AF) or decode-and-forward (DF). For an AF relay, the relay amplifies the received signal and forwards it

to the destination with transmitted power P_2. In this case, the received signal at the destination in phase 2 is specified as

$$y_{R,D} = \frac{\sqrt{P_2}}{\sqrt{P_1|h_{S,R}|^2 + N_0}} h_{R,D} y_{S,R} + \eta_{R,D} = \frac{\sqrt{P_1 P_2}}{\sqrt{P_1|h_{S,R}|^2 + N_0}} h_{R,D} h_{S,R} x + \eta'_{R,D}, \quad (1.12)$$

where $h_{R,D}$ is the channel coefficient from the relay to the destination, $\eta_{R,D}$ is an additive noise term, and

$$\eta'_{R,D} = \frac{\sqrt{P_2}}{\sqrt{P_1|h_{S,R}|^2 + N_0}} h_{R,D} \eta_{S,R} + \eta_{R,D} \quad (1.13)$$

with variance $\left(\frac{P_2|h_{R,D}|^2}{P_1|h_{S,R}|^2 + N_0} + 1\right) N_0$.

In phase 2, for DF relaying, on the other hand, if the relay is able to decode the transmitted symbol correctly, then it forwards the decoded symbol with power P_2 to the destination; otherwise, it does not forward. The received signal at the destination in phase 2 in this case can be modeled as

$$y_{R,D} = \sqrt{\tilde{P}_2} h_{R,D} x + \eta_{R,D}, \quad (1.14)$$

where $\tilde{P}_2 = P_2$ if the relay decodes the transmitted symbol correctly, otherwise $\tilde{P}_2 = 0$. AF relays lead to low complexity relay transceivers and lower power consumption because it does not decode. Another advantage of AF relays is that they are transparent to adaptive modulation techniques, which may be employed by the source. However, as Equation (1.13) shows, AF relaying forwards noise to the destination.

In multiple relay scenarios, since a virtual antenna array is created, the conventional space-time codes can be used in a distributed fashion. More specifically, the relay's antenna is considered as one antenna element in the antenna array. For distributed STBC operating in an AF mode, Nabar *et al.* [39,40] derived pairwise error probability (PEP) expressions. They show that the original design criteria for conventional STBC still apply for the design of distributed STBC schemes. Many relay studies have focused on flat-fading channels, where single-carrier systems are of interest.

However, the use of relays in frequency-selective broadband channels is important as well. Of course, frequency-selective fading is mitigated by OFDM. Coding for such

channels is space-frequency coding, which can also be employed in a distributed fashion [41]. The spatial separation of the relays presents multiple frequency offsets, which proposes design challenges for cooperative OFDM systems. The impact of frequency offsets on channel estimation for cooperative OFDM networks is investigated in Chapter 2.

1.1.5 OFDMA

OFDMA is a variant of OFDM that is deployed to serve multiple users simultaneously. Hence, the available subcarriers are divided into several mutually exclusive clusters that are assigned to distinct users for simultaneous transmission. The orthogonality among subcarriers guarantees protection against multiple access interference (MAI) while the adoption of a dynamic subcarrier assignment strategy provides the system with high flexibility in resource management [42]. Since subcarriers can be shared by all users, this structure is also called multi-user OFDM.

Three possible methods to distribute 16 subcarriers among 4 users are illustrated in Figure 1.7. In the subband carrier assignment scheme (CAS), adjacent subcarriers are allocated to each user. The main drawback of CAS is that a deep fade might hit a substantial number of subcarriers of a given user. This problem is avoided by adopting the interleaved CAS (Figure 1.7(b)), where the subcarriers of each user are uniformly spaced over the signal bandwidth. The generalized CAS, shown in Figure 1.7(c), allows dynamic resource allocation and provides more flexibility than subband or interleaved CAS [42].

For an OFDMA system, in the downlink transmission, the base station transmits signals to multiple users. In the uplink transmission, multiple users transmit data to the same base station. All these transmissions can be affected by frequency offsets. OFDMA is thus highly sensitive to frequency offsets, and inaccurate compensation of the frequeny offset destroys the orthogonality among subcarriers and produces ICI as well as MAI.

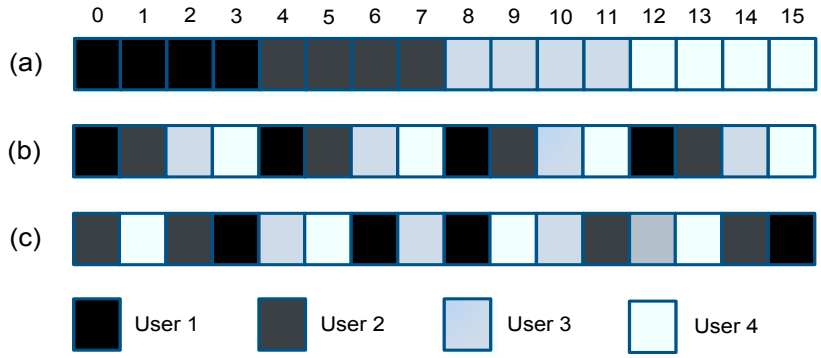

Figure 1.7: Example of subcarrier allocation schemes: (a) subband CAS, (b) interleaved CAS, and (c) generalized CAS.

In the downlink transmission, the frequency offset must be estimated for each user [42]. This can be accomplished by using the same methods available for single-user OFDM systems. In the uplink transmission, the received signal at the base station is the sum of signals transmitted by different users, each of which is affected by frequency offset errors. Accordingly, frequency offset estimation in the OFDMA uplink is a multiparameter estimation problem. It is investigated in Chapter 4.

1.2 Channel Estimation Techniques

For both SISO OFDM and MIMO OFDM systems, accurate channel state information (CSI) is needed at the receiver to realize the benefits of OFDM, such as simplified frequency domain equalization. CSI can be needed in the following circumstances:

- CSI is directly needed for equalization (Eq. (1.6)).
- If CSI is available at the transmitter, OFDM can adaptively allocate transmit power and load bits to match the channel so that the optimal bit error rate (BER) and/or ideal water filling capacity of a frequency-selective channel can be approached [43].

- CSI is essential in MIMO OFDM systems for diversity combining and interference suppression [44].

Hence, the quality of CSI greatly influences the overall system performance.

Channel estimation techniques can be categorized as data-aided or non-data-aided (blind) techniques [45–50]. Data-aided techniques are based on the transmission of pilot (reference) symbols. Non-data-aided or blind estimation relies only on the received symbols, such as the presence of CP, virtual carriers (VCs) and the finite alphabet property of the input data, and thus improves spectrum efficiency. Nevertheless, blind estimation generally requires long estimation latency, due to the requirement of many signal samples, and entails high complexity. For these reasons, this thesis focuses on data-aided channel estimation only.

In data-aided channel estimation, pilot tones may occupy all subcarriers of one OFDM symbol. This is called a block-type pilot symbol or preamble and has been developed for slow fading channels. The estimator then uses the least square (LS) or minimum mean-square error (MMSE) algorithms [51]. In [52], a low-rank approximation is applied to linear MMSE by using the frequency correlation of the channel to decrease the complexity of MMSE. In such systems, CSI is estimated prior to data transmission. When CSI changes significantly, a retaining pilot sequence is transmitted. In a fast time-varying environment, such systems must continually retrain to re-estimate CSI. Wiener filtering based on a known channel correlation function can be used to improve the channel estimation [53].

In contrast to block-type pilots, comb-type pilot symbols or scattered pilots are allocated to several subcarriers of one OFDM symbol. Channel estimation algorithms then require two steps: first, the channel gains of the pilot subcarriers are estimated and second, the channel gains of remaining subcarriers are obtained by interpolation. The number of such pilots is a trade-off between data rate and channel estimation performance [54, 55].

In a fast time-varying environment, channel variations cannot be neglected. Pilot symbols repetition must then be sufficient to track the time-varying channel. This concept is demonstrated in Figure 1.8, which shows a block of 9 OFDM symbols with 16 subcarriers. The channel is first estimated at the time-frequency locations of the pilot symbols, and a two-dimensional interpolation estimates the channel at the other time and frequency locations [10].

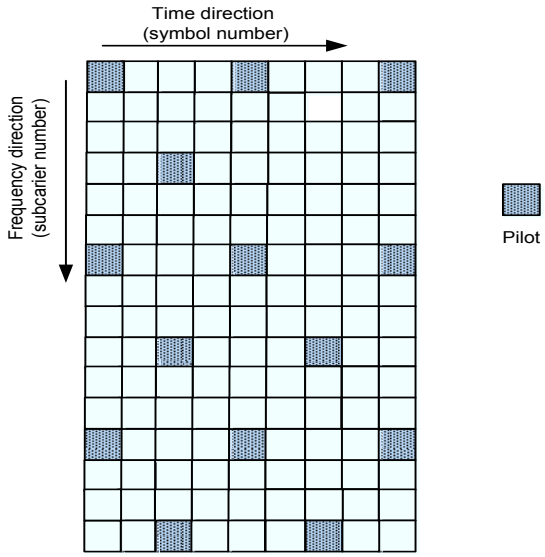

Figure 1.8: Example of pilots in a block of 9 OFDM symbols with 16 subcarriers.

As mentioned before, channel estimation algorithms includes LS and MMSE. The essential difference between these two is that the channel coefficients are treated as deterministic but unknown constants in the former, and as random variables of a stochastic process in the latter. MMSE channel estimation is treated in [52, 53, 56–59] and has been shown to give better accuracy than LS estimation [52]. This better performance of MMSE is due to the exploiting of the channel correlation statistics, which can be frequency-domain correlation for slow fading channels or both time and frequency domain for fasting fading channels. If channel correlation is unavailable, a robust channel estimator that is insensitive to the channel statistics is proposed in [59]

by analyzing the mismatch of the estimator-to-channel statistics. However, without using any channel statistics, the least mean square (LMS) algorithm can adaptively estimate the channel [60], which exploits the time and/or frequency domain correlation.

The number of pilots, their values and locations should be carefully selected, so as to achieve a good estimation performance and to reduce the pilot overhead. For fast fading channels, more pilots must be multiplexed with data symbols in order to track channel variations. Pilot design for OFDM systems has therefore received much attention [61–67]. The literature treats optimizing and analyzing the pilot locations, the total number of pilots, and the power allocated to the pilots relative to the data symbols [64].

The design of pilot tones was first proposed in [61], where the placement of the pilots that minimize the MSE of the LS channel estimate is shown to be equally powered and equally spaced. Optimal placement of training symbols is considered in [62] for block-fading channels, with regard to maximizing a lower bound on the training-based capacity on MMSE channel estimation. For OFDM systems, the optimal placement of pilot tones is equal spacing in frequency domain. Optimal pilots for OFDM with regard to the capacity based on MMSE channel estimation is also presented in [63]. Whereas in [64], the optimal pilot design and placement for block-fading channels are explored for single-carrier systems by minimizing the Cramer-Rao lower bound (CRLB). The same problem was addressed in [65]. For fast fading channels, the number and placement of pilots for OFDM systems are presented in [66] based on BER. The pilot pattern is proposed to cluster two neighboring pilots together so as to increase the channel estimation accuracy. A new pilot placement is also presented in [67] to save the number of pilots needed.

1.3 Frequency Offset Estimation Techniques

Eq.(1.7) shows that the frequency offset introduces the ICI. Even a frequency offset that is a small fraction of the subcarrier spacing can lead to serious performance degradation [10, 16]. This high sensitivity to the frequency offset requires the receiver to estimate and correct the frequency offset of the received signal to eliminate the ICI. The frequency offset estimation thus becomes a major task to ensure reliable receiver operation.

Similar to channel estimation, frequency offset estimation can also be generally categorized into data-aided methods and non-data-aided (blind) methods. The blind estimators may exploit the redundancy of CP [68,69], or the orthogonality between VCs and the information-bearing subcarriers [70–74]. The data-aided methods yield much better performance than that of blind methods at the cost of bandwidth efficiency. As for data-aided estimators, the pilots are named preamble when the pilot tones are allocated to all subcarriers of one OFDM symbol, as to distinguish from the pilots that are multiplexed with the data in one OFDM symbol.

One typical data-aided frequency offset estimation approach is to employ preambles composed by some repetitive parts which remain identical after passing through the transmission channel except for a phase shift produced by the frequency offset [13, 75, 76]. The frequency offset is thus estimated by measuring the induced phase shift. This method was originally employed by Moose in [13], where the phase shift between two successive identical blocks is measured. More precisely, denote $r_1[n]$ and $r_2[n]$ as the DFT output corresponding to the two training OFDM symbols, which are same. Then, if channel remains constant for two consecutive OFDM symbols, $r_1[n]$ and $r_2[n]$ can be written as

$$r_1[n] = H[n]x[n] + \eta_1[n] \tag{1.15}$$

$$r_2[n] = H[n]x[n]e^{j2\pi\varepsilon P/N} + \eta_2[n], \tag{1.16}$$

where $H[n]$ is the channel frequency response at n-th subcarrier, $x[n]$ is n-th element

of the training signal, which is same over the two OFDM symbols, $\eta_1[n]$ and $\eta_2[n]$ are noise terms and $P = N + N_g$ is the length of one OFDM symbol. From (1.15) and (1.16), an estimate of ε can be computed as

$$\hat{\varepsilon} = \frac{1}{2\pi(P/N)} \arg\left\{ \sum_{n=0}^{N-1} r_2[n] r_1^*[n] \right\}. \tag{1.17}$$

Several improved methods have been proposed to use multiple identical signal parts in one time domain OFDM symbol [13, 75–77]. For example, two identical halves are employed in [75] and the estimation range is proportional to the number of identical signal parts. Optimal periodic training sequences for frequency offset estimation have been proposed in [78]. These preambles are suitable for initial (coarse) frequency offset estimation, since the frequency offset estimation can be acquired during a short time after the start of transmission. Although the estimation range can be increased by shortening the preamble duration, this is achieved at the cost of decreased estimation accuracy.

Pilots enable the tracking of the variable frequency offset, which may be generated by a time-varying channel. The frequency offset can also be tracked by measuring the phase shift of pilot symbols in two consecutive OFDM symbols by using the similar way of the estimation with preambles [79, 80]. Since the pilots are multiplexed with the data steam, data generates the interference on pilots when frequency offset exists. The two neighbor pilots on each OFDM symbol are grouped and designed in [81] to decrease the data-interference. One data-pilot-multiplexed scheme is also derived in [82] to decrease this data-interference, where the two data tones adjacent to pilots are specially designed. Under the assumption that the channel remains constant during two consecutive OFDM blocks, this data-interference is eliminated in the method proposed in [83] by doing exhaustive search of all possible frequency offsets. A consistent estimate of the frequency offset is obtained in [84] by using distinctive spaced pilot tones and pilot-design criteria is discussed in [85] to provide both consistency and robustness.

Typically, channel and frequency offset estimators are developed separately. However, frequency offset and CSI can be estimated jointly. For example, the joint frequency offset and CSI estimator proposed in [86] utilizes the repetitive signal structure of preambles. A maximum-likelihood estimator (MLE) is studied in [87] and an adaptive MLE algorithm which iterates between estimating the frequency offset and the channel parameters is also proposed to decrease the complexity of MLE. The pilot symbols in each OFDM symbol are also exploited in [88] with recursive least-squares (RLS) estimation and in an iterative manner [89]. Both pilots and VCs are exploited in [90] by using an approximate MLE procedure.

1.4 Motivation

In the literature, channel and frequency offset estimation have been extensively investigated for SISO OFDM and MIMO OFDM systems. However, in the environment of the new cooperative networks, little work has been done for these estimation issues and extending these approaches from MIMO systems to cooperative networks is not straightforward. One major reason is that multiple frequency offsets are possible in distributed cooperative networks due to the different oscillators and Doppler shifts of spatially separated nodes. Moreover, the channel gain of cascaded source-to-relay and relay-to-destination links is not complex Gaussian. The channel and frequency offset estimation in cooperative OFDM systems is thus highly challenging and of interest.

To the best of our knowledge, only a few papers have studied the channel and frequency offset estimation issues for cooperative OFDM systems. Channel estimation algorithms have been proposed for single-carrier single-AF-relay networks in [91–93] and for AF OFDM in [94]. However, none of these considered the multiple frequency offsets in the cooperative networks. In the presence of multiple frequency offsets, simultaneous transmission of signals from different relays give rise to inter-relay interference (IRI) at the destination, which may degrade the performance of the channel estimation.

So in cooperative OFDM systems, which kind of pilots for channel estimation could eliminate this IRI and thus increase the channel estimation? In the thesis, the pilots design will be proposed for both AF and DF relay OFDM networks.

Multiple frequency offsets also present in the received signals at the base station in OFDMA uplink transmission. Thus frequency offset estimation becomes a multi-parameter estimation problem, and have been widely researched for OFDMA uplink with subband CAS [95, 96], interleaved CAS [97], and generalized CAS [97, 98, 98], respectively. The dynamic allocation strategy of generalized CAS provides the system with the flexibility and makes the frequency offset estimation task more challenging than with other two CAS.

These estimators are designed on a case-by-case basis. Is there a general method that could provide a framework to improve the accuracy of almost all existing estimators? This question is novelly answered with two proposed methods. One method is to exploit the variance of the frequency offset, the other method is to utilize the cooperation protocols.

Although high accuracy channel and frequency offset estimators have been proposed for OFDM-based systems, in practical systems, their estimation are not perfect. The impact of the frequency offset and channel estimation errors need to be analyzed to finally judge the performance the frequency offset and the channel estimators on the system performance. This analysis can also be helpful to choose suitable estimation methods for the target system performance since there is often a balance between the complexity and the accuracy. Previously, BER performance has been investigated only in the presence of frequency offset for SISO OFDM systems. [99,100]. Further research work should be carried out for other OFDM systems. We did anlysis for MIMO OFDM systems in the presence of frequency offset estimation errors, as well as the channel estimation errors. The analysis procedure could be used for the analysis for other OFDM systems, such as OFDMA and cooperative OFDM systems.

1.5 Structure and Contributions

This thesis proposes several channel and frequency offset estimation algorithms for cooperative OFDM and OFDMA systems. The BER is also derived for MIMO OFDM systems by considering the channel and frequency estimation errors. The main contributions are as follows:

Chapter 2: Channel Estimation for Cooperative OFDM Systems

In cooperative systems, CSI is needed for data detection. Most existing works assume perfect channel information is available. This assumption is based upon the common belief that the channel estimation for a relay network could be built upon by estimating the individual channels sequentially [35, 36]. For example, the relay first estimates the source-to-relay channel $h_{R,S}$ and then the destination estimates the relay-to-destination channel $h_{D,R}$. However, this works only for the DF relays where phase 1 and phase 2 are conducted independently. For AF relays, as can be seen from (1.12), $h_{R,S}$ is essential for the destination to estimate $h_{D,R}$. Thus, the relay need to inform the destination the estimate of $h_{R,S}$, which results in the bandwidth and power efficiency reduction, as well as the delayed processing. As well, the transmission of channel estimation will introduce further distortions. To overcome these drawbacks, a channel estimation scheme was proposed in [91] for single-carrier systems, where the overall channel from the source to the destination $h_{D,R}h_{R,S}$ is estimated at the destination only.

In this chapter, this idea is generalized to channel estimation for OFDM modulated AF relay networks with multiple relays. The DF case is also investigated. A two-time slot cooperative channel estimation protocol is proposed. Firstly, pilot designs are derived for both AF and DF relays by minimizing the inter-relay-interference (IRI), which occurs due to the simultaneous relay retransmissions. Secondly, given the channel order, the constrained maximum number of AF and DF relays are found for the proposed channel estimation scheme. Moreover, the pairwise error probability

(PEP) of cooperative OFDM with orthogonal space-frequency block coding in cooperative OFDM due to both the frequency offset and channel estimation errors is also evaluated. The optimal power allocation ratio between the source and the relays to minimize the PEP is also derived. The performance comparisons between AF and DF in terms of the PEP is also provided.

Chapter 3: BER analysis of MIMO OFDM

Although frequency offset and channel estimators are of high accuracy, in practical systems, they are not perfect. The residual frequency offset and channel estimation errors therefore impact the BER performance.

Due to this fact, it is important to analyze the BER for MIMO OFDM with frequency offset and channel estimation errors. Our analysis exploits the fact that for unbiased estimators, both channel estimation errors and frequency offset estimation errors are zero-mean random variables (RVs) [101]. The statistics of these RVs are used to derive the degradation in the received SINR, based on the analysis of the ICI and inter-antenna-interference (IAI). The BER of MIMO OFDM is derived as an infinite series. The BERs of MIMO OFDM under two receive antenna diversity techniques, MRC and EGC, are also derived. This analysis provides insights on the impact of frequency offset and channel estimation errors on the system performance.

Chapter 4: OFDMA Uplink Frequency Offset Estimation by Exploiting the Variance of Frequency Offsets

In this chapter, a frequency offset estimation scheme is proposed to improve the performance of existing frequency offset algorithms by exploiting the variance of frequency offsets. First, by the analysis of the MAI, which is introduced in OFDMA systems by frequency offsets, the CRLB for the variance of frequency offset estimation of each user is derived and further expressed as the function of the SNR. An estimation of the variance of the frequency offset is then derived as a function of SINR and SNR. Under the assumption of uniformly distributed frequency offsets, an estimation of the range of frequency offsets is derived.

For conventional differential frequency offset estimation algorithms, the accuracy improvement is validated with simulation. More specifically, the scenario of new users accessing the base station is studied and the proposed scheme shows a considerable performance improvement over estimators without the variance knowledge. For the successive interference cancellation (SIC)-based iterative frequency offset estimator, the proposed scheme saves several iterations.

Chapter 5: OFDMA Uplink Frequency Offset Estimation via Cooperative Relaying

In this chapter, a frequency offset estimation scheme is proposed for OFDMA uplink to improve the performance. This scheme exploits cooperation with multiple relays. Only the relay with the best source to relay channel is selected. The uplink frequency offset estimation is shown to be improved via cooperative relaying. Conventional AF relays are investigated, and a new type of relay called decode-and-compensate-and-forward (DcF) relay is proposed and investigated. The destination node first generates the frequency offset estimates of the transmission from the source node in the first time slot and the transmission from the relay node in the second time slot. The two frequency offset estimates are then combined to minimize the MSE.

When CSI is available at each mobile node, power allocation between the source and the relays can be adaptively adjusted to optimize the cooperative scheme in terms of frequency offset estimation error variance. To further improve the frequency offset estimation, a scheme, where with the knowledge of CSI, the relays adaptively switch between the cooperative and conventional (no relaying) transmissions, is proposed. The simulation reveals that the frequency offset estimation accuracy in the DcF mode is somewhat worse than the AF mode, but, both modes outperform the conventional transmission.

Chapter 2

Cooperative OFDM Channel Estimation

In this chapter, channel estimation has been investigated for OFDM modulated multi-relay networks. A two-time slot channel estimation protocol is proposed [102]. Pilots designs for AF and DF relays are derived by minimizing the inter-relay-interference (IRI) in the mean squared error (MSE) of the channel estimation, which occurs due to the simultaneous relay retransmissions. The constrained maximum number of AF and DF relays are found for the proposed channel estimation scheme. Moreover, pairwise error probability (PEP) with orthogonal space-frequency block coding is evaluated with frequency offset and channel estimation errors. The optimal power allocation ratio between the source and the relays to minimize the PEP is also derived for AF and DF relay networks.

2.1 Introduction

Conventional communication systems require accurate CSI. The same holds for cooperative systems. However, a commonly-used assumption is that channel estimation is available for relay networks by separating estimations of source-to-relay and relay-to-destination links, which are carried out at the relays and destination, respectively. Separating the channel estimation in AF has the drawback of reducing the bandwidth and power efficiency since the relays need to inform the destination the CSI. When both the transmission of source-to-relay and from relay-to-destination are considered,

the cascaded AF channel, which is not Gaussian, is analyzed in [103]. Channel estimation algorithms have been proposed for single-carrier AF relay networks [91–93], and impact of imperfect channel estimation is analyzed in [104]. Channel estimation for AF OFDM with single relay is investigated in [94], which method achieves the optimal CRLB. Channel estimation for AF OFDM is also studied in [105]. Using Alamouti-coded pilot symbols, channel estimation is provided for a cooperative OFDM system in [106].

Since frequency offset degrades the quality of channel estimation, its impact cannot be ignored. Several channel estimators have been proposed for MIMO OFDM systems in the presence or absence of frequency offset [107–109]. For cooperative OFDM channel estimation, these estimators can not be adapted directly and the effect of frequency offset has not thoroughly been investigated. Moreover, for AF OFDM, the convolution of the $S \to R$ and $R \to D$ channels yields the non-Gaussian $S \to R \to D$ channel. Optimal pilot design for cooperative OFDM networks with frequency offsets for AF, as well as DF relays, is provided here.

2.2 Cooperative OFDM Signal Model

Consider a network with S, k-th relay $R_k, k \in \{1, \ldots, M\}$ and D. In the first time slot, the $S \to D$ and $S \to R_k$ transmissions take place. In the second time slot, $R_k \to D$ transmissions take place.

2.2.1 Channel Model

The time-invariant channel impulse response between node a and node b is modelled as

$$h_{a,b}(\tau) = \sum_{l=0}^{L-1} h_{a,b}[l]\delta\left(\tau - lT_s\right), \tag{2.1}$$

where $h_{a,b}[l]$ is the l-th the channel gain, and $T_s = 1/B$ with B representing the total bandwidth. The delays are $\{0, T_s, 2T_s, \ldots, (L-1)T_s\}$. L is the channel order, and

is same for any pair of nodes. For brevity, define $\tilde{\mathbf{h}}_{a,b} = [h_{a,b}(0), h_{a,b}(1), \cdots, h_{a,b}(L-1)]^T$. The frequency-domain channel coefficient matrix is $\mathbf{H}_{a,b} = \text{diag}\{H_{a,b}[0], \cdots, H_{a,b}[N-1]\}$, where $H_{a,b}[n] = \sum_{d=0}^{L-1} h_{a,b}(d) e^{-\frac{j2\pi nd}{N}}$ is the channel frequency response on the n-th subcarrier.

The channel gains $h_{a,b}(l)$ are modeled as complex Gaussian zero-mean random variables (RVs). Both the $S \to D$ and $R_k \to D$ channels suffer large-scale fading and small-scale fading. The distance between S and R_k is much smaller than that between S and D or that between R_k and D. An identical large-scale fading coefficient $\mathcal{L}_u$ is used for each $S \to D$ or $R_k \to D$ channel. The large-scale fading coefficient $\mathcal{L}_u$ can be approximated as $\mathcal{L}_u = d_{D,S}^{-q}/2$ (or $\mathcal{L}_u = d_{D,R_k}^{-q}/2$), where $d_{a,b}$ represents the distance between nodes a and b and $2 \le q \le 6$ [110].

2.2.2 OFDM Signal Model

The node S transmits the symbol vector $\tilde{\mathbf{X}}_S = [X_S[0], X_S[1], \cdots, X_S[N-1]]$, where N is the number of subcarriers. This signal $\tilde{\mathbf{X}}_S$ can be decomposed as $\tilde{\mathbf{X}}_S = \tilde{\mathbf{X}}_S^d + \tilde{\mathbf{X}}_S^p$, where $\tilde{\mathbf{X}}_S^d$ and $\tilde{\mathbf{X}}_S^p$ are $N \times 1$ data and pilot vectors. Data entries of $\tilde{\mathbf{X}}_S$, PSK or QAM symbols, are modeled as zero mean and unit-variance RVs. In general, a total of $\mathcal{N}_p$ pilots are allocated per symbol. Therefore, $\tilde{\mathbf{X}}_S^p$ is non-zero only at locations $(\theta_1, \cdots, \theta_{\mathcal{N}_p})$, where $0 \le \theta_1 < \cdots < \theta_{\mathcal{N}_p} \le N-1$.

2.2.3 First Time Slot (Preamble Period)

The received signal samples at the destination D and the k-th relay R_k are given by

$$y_{D,1}(n) = \frac{\sqrt{\alpha \bar{P}}}{N} \sum_{i=0}^{N-1} X_S[i] H_{D,S}[i] e^{\frac{j2\pi n\left(i+\varepsilon_{D,S}\right)}{N}} + w_{D,1}(n), \tag{2.2a}$$

$$y_{R_k,1}(n) = \frac{\sqrt{\alpha \bar{P}}}{N} \sum_{i=0}^{N-1} X_S[i] H_{R_k,S}[i] e^{\frac{j2\pi n\left(i+\varepsilon_{R_k,S}\right)}{N}} + w_{R_k}(n), \tag{2.2b}$$

where $n = 0, 1, \cdots, N-1$, α is the power allocation ratio between S and the set of relays R_k $(0 \le \alpha \le 1)$, $\bar{P}$ is the average power of each subcarrier. $\varepsilon_{b,S}$ is the normalized

frequency offset between nodes S and b ($b \in \{R_k, D\}$), $w_{D,1}(n)$ and $w_{R_k}(n)$ are AWGN samples with $\{w_{D,1}(n), w_{R_k}(n)\} \sim \mathcal{CN}(0, \sigma_w^2)$.

The received samples at D and R_k are $\mathbf{y}_{D,1} = [y_{D,1}(0), y_{D,1}(1), \cdots, y_{D,1}(N-1)]^T$ and $\mathbf{y}_{R_k,1} = [y_{R_k,1}(0), y_{R_k,1}(1), \cdots, y_{R_k,1}(N-1)]^T$. The post-DFT demodulator outputs are then

$$\mathbf{r}_{D,1} = \mathbf{F}^H \mathbf{y}_{D,1} = \underbrace{\sqrt{\alpha N \bar{P}} \mathbf{E}_{D,S}^{\text{cir}} \mathbf{X}_S^p \mathbf{F}_{(L)}^H}_{\mathbf{P}_{D,S}\ (N \times L)} \tilde{\mathbf{h}}_{D,S} + \underbrace{\sqrt{\alpha N \bar{P}} \mathbf{E}_{D,S}^{\text{cir}} \mathbf{X}_S^d \mathbf{F}_{(L)}^H}_{\text{Interference}} \tilde{\mathbf{h}}_{D,S} + \underbrace{\mathbf{F}^H \mathbf{w}_{D,1}}_{\boldsymbol{\eta}_{D,1}\ (N \times 1)}, \tag{2.3a}$$

$$\mathbf{r}_{R_k,1} = \mathbf{F}^H \mathbf{y}_{R_k,1} = \underbrace{\sqrt{\alpha N \bar{P}} \mathbf{E}_{R_k,S}^{\text{cir}} \mathbf{X}_S^p \mathbf{F}_{(L)}^H}_{\mathbf{P}_{R_k,S}\ (N \times L)} \tilde{\mathbf{h}}_{R_k,S} + \underbrace{\sqrt{\alpha N \bar{P}} \mathbf{E}_{R_k,S}^{\text{cir}} \mathbf{X}_S^d \mathbf{F}_{(L)}^H}_{\text{Interference}} \tilde{\mathbf{h}}_{R_k,S} + \underbrace{\mathbf{F}^H \mathbf{w}_{R_k}}_{\boldsymbol{\eta}_{R_k,1}\ (N \times 1)}, \tag{2.3b}$$

where $\mathbf{w}_{D,1} = [w_{D,1}(0), w_{D,1}(1), \cdots, w_{D,1}(N-1)]^T$, $\mathbf{w}_{R_k} = [w_{R_k}(0), w_{R_k}(1), \cdots, w_{R_k}(N-1)]^T$, and the IDFT matrix $\mathbf{F}$ is defined as $[\mathbf{F}]_{nk} = (1/\sqrt{N}) e^{\jmath 2\pi nk/N}$ for $0 \le (n,k) \le N-1$. The frequency-offset dependent matrix $\mathbf{E}_{a,b}$ is defined by $\mathbf{E}_{a,b} = \text{diag}\left\{1, e^{\frac{\jmath 2\pi \varepsilon_{a,b}}{N}}, \cdots, e^{\frac{\jmath 2\pi \varepsilon_{a,b}(N-1)}{N}}\right\}$. $\mathbf{E}_{a,b}^{\text{cir}} = \mathbf{F}^H \mathbf{E}_{a,b} \mathbf{F}$ is a circulant matrix that specified by the frequency offset $\varepsilon_{a,b}$, $\mathbf{F}_{(L)}$ is the first L rows of $\mathbf{F}$, and $\mathbf{X}_S = \mathbf{X}_S^d + \mathbf{X}_S^p$ is an $N \times N$ diagonal matrix with $\mathbf{X}_S^d = \text{diag}\{\tilde{\mathbf{X}}_S^d\}$ and $\mathbf{X}_S^p = \text{diag}\{\tilde{\mathbf{X}}_S^p\}$.

2.2.4 Second Time Slot

The relays retransmit the received signal to D. The total power equally allocated to all the relays is $(1-\alpha)N\bar{P}$.

AF Mode

In this case, each relay simply retransmits the received signal to the destination. The received symbol at the destination D is $\mathbf{y}_{D,2}^{\text{AF}} = \rho_R \sqrt{\frac{(1-\alpha)\bar{P}}{M}} \sum_{k=1}^{M} \mathbf{E}_{D,R_k} \mathbf{F} \mathbf{H}_{D,R_k} \mathbf{r}_{R_k,1} + \mathbf{w}_{D,2}$, where $\rho_R = \dfrac{1}{\sqrt{\alpha \bar{P} + \sigma_w^2}}$ represents the amplifying coefficients at each relay. The received signal at the destination D can be demodulated as

$$
\begin{aligned}
\mathbf{r}_{D,2}^{\mathrm{AF}} &= \mathbf{F}^H \mathbf{y}_{D,2}^{\mathrm{AF}} \\
&= \mathbf{F}^H \rho_R \sqrt{\frac{(1-\alpha)\bar{P}}{M}} \sum_{k=1}^{M} \mathbf{E}_{D,R_k} \mathbf{F} \mathbf{H}_{D,R_k} \mathbf{r}_{R_k,1} + \mathbf{F}^H \mathbf{w}_{D,2} \\
&= \frac{Q_2(\alpha)}{\sqrt{N}} \sum_{k=1}^{M} \mathbf{F}^H \mathbf{E}_{D,R_k} \mathbf{F} \mathbf{H}_{D,R_k} \mathbf{r}_{R_k,1} + \mathbf{F}^H \mathbf{w}_{D,2} \\
&= Q_1(\alpha) \sum_{k=1}^{M} \overbrace{\mathbf{F}^H \underbrace{\mathbf{E}_{D,R_k} \mathbf{E}_{R_k,S}}_{=\mathbf{E}_{D,R_k,S}}}^{=\mathbf{E}^{\mathrm{cir}}_{D,R_k,S}} \mathbf{H}_{R_k,S} \mathbf{H}_{D,R_k} \tilde{\mathbf{X}}_S^p + Q_1(\alpha) \sum_{k=1}^{M} \mathbf{E}^{\mathrm{cir}}_{D,R_k,S} \mathbf{H}_{R_k,S} \mathbf{H}_{D,R_k} \tilde{\mathbf{X}}_S^d \\
&\quad + \frac{Q_2(\alpha)}{\sqrt{N}} \sum_{k=1}^{M} \mathbf{E}^{\mathrm{cir}}_{D,R_k} \mathbf{H}_{D,R_k} \mathbf{F}^H \mathbf{w}_{R_k} + \mathbf{F}^H \mathbf{w}_{D,2} \\
&= Q_1(\alpha) \sum_{k=1}^{M} \mathbf{E}^{\mathrm{cir}}_{D,R_k,S} (\mathbf{X}_S^d + \mathbf{X}_S^p) \mathbf{F}^H_{(2L-1)} \left(\tilde{\mathbf{h}}^T_{R_k,S} \otimes \tilde{\mathbf{h}}^T_{D,R_k} \right)^T \\
&\quad + \frac{Q_2(\alpha)}{\sqrt{N}} \sum_{k=1}^{M} \mathbf{E}^{\mathrm{cir}}_{D,R_k} \mathbf{H}_{D,R_k} \mathbf{F}^H \mathbf{w}_{R_k} + \mathbf{F}^H \mathbf{w}_{D,2},
\end{aligned}
\tag{2.4}
$$

where $Q_1(\alpha) = \sqrt{\dfrac{\alpha(1-\alpha)N\bar{P}^2}{M(\alpha\bar{P}+\sigma_w^2)}}$, $Q_2(\alpha) = \sqrt{\dfrac{(1-\alpha)N\bar{P}}{M(\alpha\bar{P}+\sigma_w^2)}}$, $\mathbf{E}^{\mathrm{cir}}_{D,R_k,S} = \mathbf{F}^H \mathbf{E}_{D,R_k} \mathbf{E}_{R_k,S} \mathbf{F} = \mathbf{E}^{\mathrm{cir}}_{D,S}$, $\tilde{\mathbf{h}}_{D,R_k,S} = \left(\tilde{\mathbf{h}}^T_{R_k,S} \otimes \tilde{\mathbf{h}}^T_{D,R_k} \right)^T$, and $\otimes$ denotes convolution. Equation (2.4) can further be simplified as

$$
\begin{aligned}
\mathbf{r}_{D,2}^{\mathrm{AF}} &= \sum_{k=1}^{M} \underbrace{Q_1(\alpha) \mathbf{E}^{\mathrm{cir}}_{D,R_k,S} \mathbf{X}_S^d \mathbf{F}^H_{(2L-1)} \tilde{\mathbf{h}}_{D,R_k,S}}_{\mathbf{D}^{\mathrm{AF}}_{D,R_k,S} \ (N \times (2L-1))} \\
&\quad + \sum_{k=1}^{M} \underbrace{Q_1(\alpha) \mathbf{E}^{\mathrm{cir}}_{D,R_k,S} \mathbf{X}_S^p \mathbf{F}^H_{(2L-1)}}_{\mathbf{P}^{\mathrm{AF}}_{D,R_k,S} \ (N \times (2L-1))} \tilde{\mathbf{h}}_{D,R_k,S} + \underbrace{\sum_{k=1}^{M} Q_2(\alpha) \mathbf{E}^{\mathrm{cir}}_{D,R_k} \mathbf{W}_\eta \mathbf{F}^H_{(L)} \tilde{\mathbf{h}}_{D,R_k} + \mathbf{F}^H \mathbf{w}_{D,2}}_{\boldsymbol{\eta}^{\mathrm{AF}}_{D,2}},
\end{aligned}
\tag{2.5}
$$

DF Mode

Each DF relay decodes and re-encodes the received signal. Unlike the AF mode, the DF mode can eliminate the additive noise and interference that accumulated in the relays.

It is assumed that m out of M relays can correctly decode, and the received symbol at node D is $\mathbf{y}_{D,2}^{\mathrm{DF}} = \sqrt{\frac{(1-\alpha)\bar{P}}{m}} \sum_{k=1}^{m} \mathbf{E}_{D,R_k}\mathbf{F}\mathbf{H}_{D,R_k}\tilde{\mathbf{X}}_{R_k} + \mathbf{w}_{D,2}$. The post-DFT output of $\mathbf{y}_{D,2}^{\mathrm{DF}}$ is

$$\begin{aligned}\mathbf{r}_{D,2}^{\mathrm{DF}} &= \mathbf{F}^H\mathbf{y}_{D,2}^{\mathrm{DF}} \\ &= \sum_{k=1}^{m} \underbrace{\sqrt{\frac{(1-\alpha)N\bar{P}}{m}}\mathbf{E}_{D,R_k}^{\mathrm{cir}}\mathbf{X}_{R_k}^{d}\mathbf{F}_{(L)}^{H}\tilde{\mathbf{h}}_{D,R_k}}_{\mathbf{D}_{D,R_k}^{\mathrm{DF}}\ (N\times L)} \\ &\quad + \sum_{k=1}^{m} \underbrace{\sqrt{\frac{(1-\alpha)N\bar{P}}{m}}\mathbf{E}_{D,R_k}^{\mathrm{cir}}\mathbf{X}_{R_k}^{p}\mathbf{F}_{(L)}^{H}}_{\mathbf{P}_{D,R_k}^{\mathrm{DF}}\ (N\times L)}\tilde{\mathbf{h}}_{D,R_k} + \underbrace{\mathbf{F}^H\mathbf{w}_{D,2}}_{\boldsymbol{\eta}_{D,2}^{\mathrm{DF}}}.\end{aligned} \tag{2.6}$$

A transceiver system model diagram for the proposed cooperative transmission is illustrated in Figure 2.9, where the cooperation is performed in two time slots, and transceivers for both AF and DF relaying modes are given out.

2.3 Channel Estimation

Since D receives from S only in the first time slot, conventional LS estimation is possible. However, in the second time slot, D receives multiple simultaneous relay transmissions, resulting in inter-relay interference (IRI).

2.3.1 Channel Estimation in the First Time Slot

From Equation (2.3), the LS estimation of the $S \to D$ channel response $\tilde{\mathbf{h}}_{D,S}$ is given by $\hat{\tilde{\mathbf{h}}}_{D,S} = \mathbf{P}_{D,S}^{\dagger}\mathbf{r}_{D,1}$, where $\mathbf{P}_{D,S}^{\dagger} = \left(\mathbf{P}_{D,S}^{H}\mathbf{P}_{D,S}\right)^{-1}\mathbf{P}_{D,S}^{H}$. The MSE of $\hat{\tilde{\mathbf{h}}}_{D,S}$ is obtained as $\mathrm{MSE}\left(\hat{\tilde{\mathbf{h}}}_{D,S}\right) = (1/L)\mathbb{E}\left\{\left\|\hat{\tilde{\mathbf{h}}}_{D,S} - \tilde{\mathbf{h}}_{D,S}\right\|_2^2\right\}$. Similarly, that for the $S \to R_k$ channel response is $\mathrm{MSE}\left(\hat{\tilde{\mathbf{h}}}_{R_k,S}\right) = (1/L)\mathbb{E}\left\{\left\|\hat{\tilde{\mathbf{h}}}_{R_k,S} - \tilde{\mathbf{h}}_{R_k,S}\right\|_2^2\right\}$

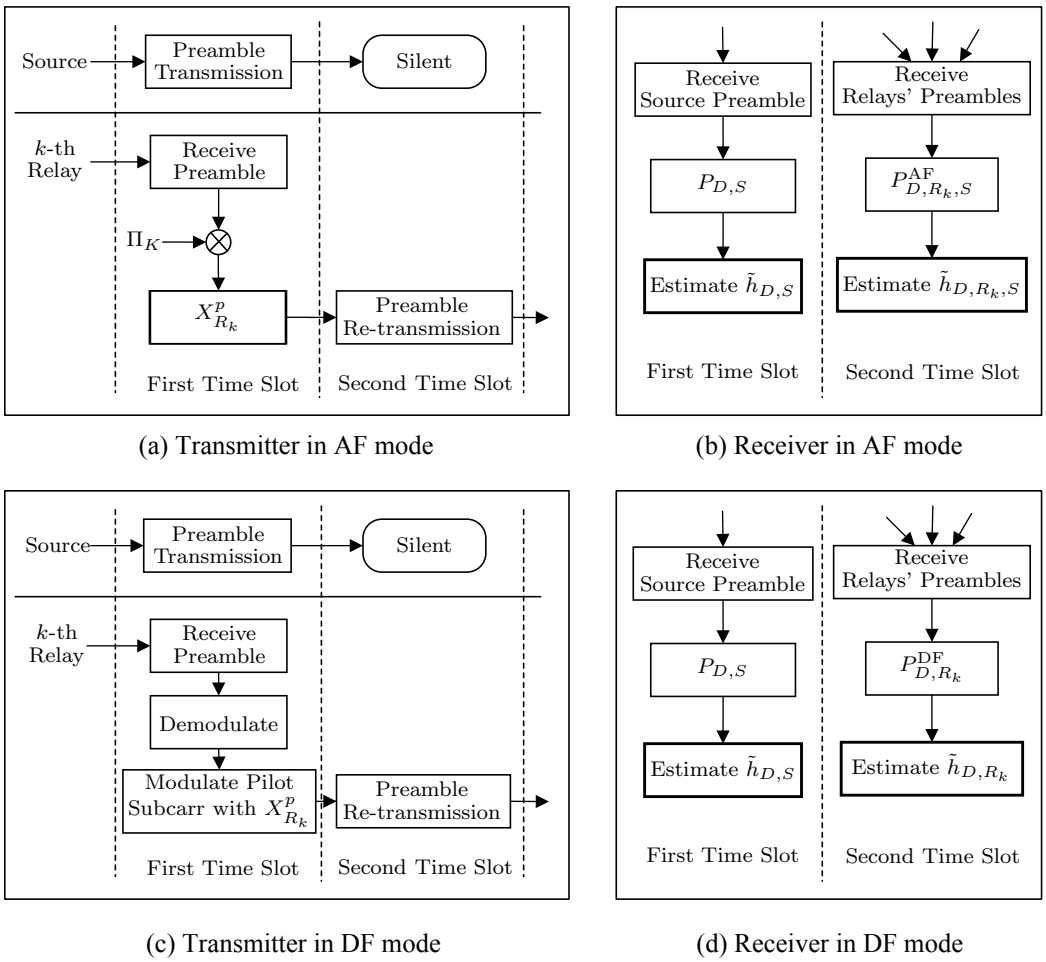

Figure 2.9: Transceiver system model of the proposed cooperative transmission.

2.3.2 Pilot Design to Eliminate IRI in the Second Time Slot

Since the identical pilot, i.e., $\mathbf{X}_S^p$, is received at each relay in the first time slot, the received pilot at the destination D in the second time slot is also $\mathbf{X}_S^p$, if the relays simply retransmit the received signal without modifying it. In this case, the destination D does not know where the received pilot comes from, and, therefore, it can not identify $\tilde{\mathbf{h}}_{D,R_k,S}$ in the AF mode (or $\tilde{\mathbf{h}}_{D,R_k}$ in the DF mode).

With multiple relay transmissions, the IRI must be eliminated to minimize the MSE. Define $\mathbf{P}_2^{\mathrm{AF}} = [\mathbf{P}^{\mathrm{AF}}_{D,R_1,S}, \ldots, \mathbf{P}^{\mathrm{AF}}_{D,R_M,S}]$, $\mathbf{D}_2^{\mathrm{AF}} = [\mathbf{D}^{\mathrm{AF}}_{D,R_1,S}, \ldots, \mathbf{D}^{\mathrm{AF}}_{D,R_M,S}]$, $\mathbf{h}_{DRS} =$

$[\tilde{\mathbf{h}}_{D,R_1,S},\ldots,\tilde{\mathbf{h}}_{D,R_M,S}]^T$, and Equation (2.5) can be rewritten as

$$\mathbf{r}_{D,2}^{\mathrm{AF}} = \mathbf{P}_2^{\mathrm{AF}}\mathbf{h}_{DRS} + \mathbf{D}_2^{\mathrm{AF}}\mathbf{h}_{DRS} + \boldsymbol{\eta}_{D,2}^{\mathrm{AF}}, \tag{2.7}$$

where $\mathbf{P}_2^{\mathrm{AF}}$ and $\mathbf{D}_2^{\mathrm{AF}}$ are the pilot and data matrices with the frequency offset component. By defining the pseudo-inverse of $\mathbf{P}_2^{\mathrm{AF}}$ as $(\mathbf{P}_2^{\mathrm{AF}})^{\dagger} = \left((\mathbf{P}_2^{\mathrm{AF}})^H\mathbf{P}_2^{\mathrm{AF}}\right)^{-1}(\mathbf{P}_2^{\mathrm{AF}})^H$, the LS estimation of $\mathbf{h}_{DRS}$ is given by

$$\hat{\mathbf{h}}_{DRS} = (\mathbf{P}_2^{\mathrm{AF}})^{\dagger}\mathbf{r}_{D,2}^{\mathrm{AF}} = \mathbf{h}_{DRS} + (\mathbf{P}_2^{\mathrm{AF}})^{\dagger}\mathbf{D}_2^{\mathrm{AF}}\mathbf{h}_{DRS} + (\mathbf{P}_2^{\mathrm{AF}})^{\dagger}\boldsymbol{\eta}_k. \tag{2.8}$$

The MSE of the LS estimator $\hat{\mathbf{h}}_{DRS}$ can be expressed as

$$\mathrm{MSE}\left(\hat{\mathbf{h}}_{DRS}\right) = \frac{\mathrm{trace}\left\{\mathbf{V}^H\left((\mathbf{P}_2^{\mathrm{AF}})^H\mathbf{P}_2^{\mathrm{AF}}\right)^{-2}\mathbf{V}\boldsymbol{\Phi}_2^{\mathrm{AF}}\right\}}{(2L-1)M} + \frac{\sigma^2_{\eta_{D,2}^{\mathrm{AF}}}\mathrm{trace}\left\{\left(\mathbf{P}_k^H\mathbf{P}_k\right)^{-1}\right\}}{(2L-1)M}, \tag{2.9}$$

where $\boldsymbol{\Phi}_2^{\mathrm{AF}} = \mathbb{E}\{\mathbf{h}_{DRS}\mathbf{h}_{DRS}^H\}$ and $\mathbf{V} = (\mathbf{P}_2^{\mathrm{AF}})^H\mathbf{D}_2^{\mathrm{AF}}$ ($\mathbf{V}$ represents the power spread of $\mathbf{D}_2^{\mathrm{AF}}$ to the signal space of $\mathbf{P}_2^{\mathrm{AF}}$). The interference of the pilots, contributed by the data subcarriers is noise-like, and it is hard to minimize the first part of $\mathrm{MSE}\left(\hat{\mathbf{h}}_{DRS}\right)$. Therefore, the optimal pilots should be designed to minimize $\mathrm{trace}\left((\mathbf{P}_2^{\mathrm{AF}})^H\mathbf{P}_2^{\mathrm{AF}}\right)^{-1}$.

The matrix $(\mathbf{P}_2^{\mathrm{AF}})^H\mathbf{P}_2^{\mathrm{AF}}$ can be represented as

$$(\mathbf{P}_2^{\mathrm{AF}})^H\mathbf{P}_2^{\mathrm{AF}} = \begin{bmatrix} \mathbf{G}_{1,1} & \cdots & \mathbf{G}_{1,M} \\ \vdots & \ddots & \vdots \\ \mathbf{G}_{M,1} & \cdots & \mathbf{G}_{M,M} \end{bmatrix},$$

where $\mathbf{G}_{m,n} = (\mathbf{P}_{D,R_m,S}^{\mathrm{AF}})^H\mathbf{P}_{D,R_n,S}^{\mathrm{AF}}$. $\mathbf{G}_{m,n} = \mathbf{G}_{n,m}^H$ represents the IRI. The IRI analysis of DF mode is in a similar way. The IRI between different relays can be eliminated if

$$\left(\mathbf{P}_{D,R_k,S}^{\mathrm{AF}}\right)^H\mathbf{P}_{D,R_i,S}^{\mathrm{AF}} = \mathbf{O}_{(2L-1)\times(2L-1)} \quad \text{(AF Mode)} \tag{2.10a}$$

$$\left(\mathbf{P}_{D,R_k}^{\mathrm{DF}}\right)^H\mathbf{P}_{D,R_i}^{\mathrm{DF}} = \mathbf{O}_{L\times L} \quad \text{(DF Mode)} \tag{2.10b}$$

is satisfied for each $i \neq k$. In DF mode, (2.10) can be easily satisfied by modulating different pilots in different relays before their retransmission. However, in AF mode, (2.10) cannot be satisfied unless each relay modifies to its received pilot.

AF Mode

A modified AF relaying mode is applied in each relay to satisfy (2.10). The k-th relay R_k multiplies its received signal $\mathbf{y}_{R_k,1}$ by a premodulation matrix $\mathbf{\Pi}_k$ and retransmits. The received signal at D can then be demodulated as

$$\tilde{\mathbf{r}}_{D,2}^{\mathrm{AF}} = \mathbf{F}^H \sum_{k=1}^{M} \mathbf{E}_{D,R_k} \mathbf{F} \mathbf{\Pi}_k \mathbf{y}_{R_k,1} \tag{2.11}$$

and it can further be resolved as

$$\begin{aligned}\tilde{\mathbf{r}}_{D,2}^{\mathrm{AF}} = & \sum_{k=1}^{M} Q_1(\alpha) \mathbf{E}_{D,R_k}^{\mathrm{cir}} \mathbf{\Pi}_k \mathbf{E}_{R_k,S}^{\mathrm{cir}} \mathbf{X}_S^d \mathbf{F}_{(2L-1)}^H \tilde{\mathbf{h}}_{D,R_k,S} \\ & + \underbrace{\sum_{k=1}^{M} Q_1(\alpha) \underbrace{\mathbf{E}_{D,R_k}^{\mathrm{cir}} \mathbf{\Pi}_k \mathbf{E}_{R_k,S}^{\mathrm{cir}} \mathbf{X}_S^p}_{=\mathbf{E}_{D,S}^{\mathrm{cir}} \mathbf{X}_{R_k}^p} \mathbf{F}_{(2L-1)}^H \tilde{\mathbf{h}}_{D,R_k,S}}_{\tilde{\mathbf{P}}_{D,R_k,S}^{\mathrm{AF}}} + \underbrace{\sum_{k=1}^{M} Q_2(\alpha) \mathbf{E}_{D,R_k}^{\mathrm{cir}} \mathbf{\Pi}_k \mathbf{W}_\eta \mathbf{F}_{(L)}^H \tilde{\mathbf{h}}_{D,R_k} + \mathbf{F}^H \mathbf{w}_{D,2}}_{\tilde{\boldsymbol{\eta}}_{D,2}^{\mathrm{AF}}},\end{aligned} \tag{2.12}$$

where $\mathbf{X}_{R_k}^p$ is the retransmitted pilot for the relay R_k. $\mathbf{X}_{R_k}^p$ is a unique pilot of R_k and different from $\mathbf{X}_S^p$. (2.12) can be understood as each relay uses a unique premodulation matrix $\mathbf{\Pi}_k$ to do some modification to its pilot subcarriers (how to obtain $\mathbf{\Pi}_k$ will be discussed later). The LS channel estimation is $\hat{\mathbf{h}}_{DRS} = (\mathbf{P}_2^{\mathrm{AF}})^\dagger \tilde{\mathbf{r}}_{D,2}^{\mathrm{AF}}$, where $\mathbf{P}_2^{\mathrm{AF}} = \begin{bmatrix} \tilde{\mathbf{P}}_{D,R_1,S}^{\mathrm{AF}} & \cdots & \tilde{\mathbf{P}}_{D,R_M,S}^{\mathrm{AF}} \end{bmatrix}$, and $h_{DRS} = [\tilde{h}_{D,R_1,S}^T, \cdots, \tilde{h}_{D,R_M,S}^T]^T$. In this relaying network, all the pilots are modulated in one symbol, and the pilot subcarriers are shared by all nodes. The pilots that satisfy (2.10) for the k-th node in the AF mode is resolved as

$$\begin{aligned} \left[\mathbf{X}_{R_k}^p\right]_{\theta_i\theta_i} &= e^{\frac{j2\pi\theta_i(k-1)(2L-1)}{N}}, \quad k = 1, \cdots, M, i = 1, \cdots, \mathcal{N}_p \\ s.t. \quad & (2L-1)M \le \mathcal{N}_p \le N, \quad \frac{N}{\mathcal{N}_p} = \text{integer}; \\ & \frac{\theta_i(k-l)(2L-1)}{N} \neq \text{integer}, \quad k \neq l; \\ & \theta_2 - \theta_1 = \theta_3 - \theta_2 = \cdots = \theta_{\mathcal{N}_p} - \theta_{\mathcal{N}_p-1} = \frac{N}{\mathcal{N}_p}. \end{aligned} \tag{2.13}$$

By using the pilot defined in (2.13), the MSE of $\hat{\mathbf{h}}_{DRS}$ is given by

$$\begin{aligned}\mathrm{MSE}\left(\hat{\mathbf{h}}_{DRS}\right) &= \frac{1}{(2L-1)M}\mathbb{E}\left\{\left\|\hat{\mathbf{h}}_{DRS}-\mathbf{h}_{DRS}\right\|_2^2\right\} \\ &= \frac{(N-\mathcal{N}_p)\cdot\mathrm{trace}\left\{\mathbf{\Phi}_2^{\mathrm{AF}}\right\}}{\mathcal{N}_p(2L-1)M} + \frac{\sigma_w^2\sum_{k=1}^{M}\mathrm{trace}\left\{\mathbf{\Phi}_{D,R_k}^{\mathrm{AF}}\right\}}{\alpha\mathcal{N}_p(2L-1)M\bar{P}} + \frac{M(\alpha\bar{P}+\sigma_w^2)\sigma_w^2}{\alpha(1-\alpha)\mathcal{N}_p\bar{P}^2},\end{aligned} \tag{2.14}$$

where $\mathbf{\Phi}_2^{\mathrm{AF}} = \mathbb{E}\left\{\mathbf{h}_{DRS}\mathbf{h}_{DRS}^H\right\}$, and $\mathbf{\Phi}_{D,R_k}^{\mathrm{AF}} = \mathbb{E}\left\{\tilde{\mathbf{h}}_{D,R_k}\tilde{\mathbf{h}}_{D,R_k}^H\right\}$.

Now derive $\mathbf{\Pi}_k$ to satisfy $\mathbf{E}_{D,R_k}^{\mathrm{cir}}\mathbf{\Pi}_k\mathbf{E}_{R_k,S}^{\mathrm{cir}}\mathbf{X}_S^p = \mathbf{E}_{D,S}^{\mathrm{cir}}\mathbf{X}_{R_k}^p$. Without loss of generality, we assume that the pilot with $m=1$ is allocated to S, and that $\mathbf{X}_{R_k}^p$ can be represented as $\mathbf{X}_{R_k}^p = \mathbf{\Lambda}_k\mathbf{X}_S^p$, where $\mathbf{\Lambda}_k$ is a diagonal matrix with $[\mathbf{\Lambda}_k]_{\theta_i\theta_i} = e^{\frac{\jmath 2\pi\theta_i(k-1)(2L-1)}{N}}$, and $[\mathbf{\Lambda}_k]_{ll} = 0$ for each $l \neq \theta_i$. Note that $\mathbf{E}_{D,S}^{\mathrm{cir}} = \mathbf{E}_{D,R_k}^{\mathrm{cir}}\mathbf{E}_{R_k,S}^{\mathrm{cir}}$ is satisfied for each k, so the problem is reduced to finding $\mathbf{\Pi}_k$ to make $\mathbf{\Pi}_k\mathbf{E}_{R_k,S}^{\mathrm{cir}} = \mathbf{E}_{R_k,S}^{\mathrm{cir}}\mathbf{\Lambda}_k$, which is resolved as

$$\mathbf{\Pi}_k = \mathbf{E}_{R_k,S}^{\mathrm{cir}}\mathbf{\Lambda}_k(\mathbf{E}_{R_k,S}^{\mathrm{cir}})^{-1} = \mathbf{F}^H\mathbf{E}_{R_k,S}\mathbf{F}\mathbf{\Lambda}_k\mathbf{F}^H\mathbf{E}_{R_k,S}^{-1}\mathbf{F}. \tag{2.15}$$

Since $\mathbf{\Pi}_k$ modifies only the pilot subcarriers by performing a phase rotation to the received pilots at R_k, the data subcarriers remain unaffected.

Note that the pilot given in (2.13) eliminates the IRI only when the number of relays does not exceed a specified value. The following Lemma provides the maximum number of relays in the AF mode.

Lemma 1—Maximum Number of Relays in the AF Mode: In AF mode, to minimize the variance error of the LS estimator for each $S \to R \to D$ channel, the maximum number of active relays that simultaneously retransmit is $M \leq \left\lfloor \frac{N}{2L-1} \right\rfloor$.

Proof: In AF mode, the channel order for all the $S \to R \to D$ channels is $2L-1$. From (2.13), the condition of $(2L-1)M \leq \mathcal{N}_p \leq N$ must be satisfied for the pilot design, and consequently, $M \leq \left\lfloor \frac{N}{2L-1} \right\rfloor$.

□

Lemma 1 indicates that the maximum number of active relays is inversely proportional to $2L-1$. Since the achievable cooperative is proportional to the number of

relays, this condition describe a tradeoff between the channel estimation ability and the achievable diversity gain.

DF Mode

Each active relay retransmits in the second time slot by modulating the pilot subcarriers with its own pilot but without changing the data subcarriers. The LS channel estimation is then given by $\hat{\mathbf{h}}_{DR} = (\mathbf{P}_2^{\mathrm{DF}})^{\dagger}\mathbf{r}_{D,2}^{\mathrm{DF}}$, where $\mathbf{P}_2^{\mathrm{DF}} = \begin{bmatrix} \mathbf{P}_{D,R_1}^{\mathrm{DF}} & \cdots & \mathbf{P}_{D,R_m}^{\mathrm{DF}} \end{bmatrix}$ and $\mathbf{h}_{DR} = \left[\tilde{\mathbf{h}}_{D,R_1}^T, \cdots, \tilde{\mathbf{h}}_{D,R_m}^T\right]^T$.

The optimal pilot for R_k in the DF mode is given by

$$\begin{aligned} \left[\mathbf{X}_{R_k}^p\right]_{\theta_i\theta_i} &= e^{\frac{\jmath 2\pi\theta_i(k-1)L}{N}}, \quad k = 1, \cdots, M, i = 1, \cdots, \mathcal{N}_p \\ s.t. \quad & LM \le \mathcal{N}_p \le N, \quad \frac{N}{\mathcal{N}_p} = \text{integer}; \\ & \frac{\theta_i(k-l)L}{N} \ne \text{integer}, \quad k \ne l; \\ & \theta_2 - \theta_1 = \theta_3 - \theta_2 = \cdots = \theta_{\mathcal{N}_p} - \theta_{\mathcal{N}_p - 1} = \frac{N}{\mathcal{N}_p}. \end{aligned} \tag{2.16}$$

By using (2.16), the MSE of $\hat{\mathbf{h}}_{DR}$ is

$$\mathrm{MSE}\left(\hat{\mathbf{h}}_{DR}\right) = \frac{1}{Lm}\mathbb{E}\left\{\left\|\hat{\mathbf{h}}_{DR} - \mathbf{h}_{DR}\right\|_2^2\right\} = \frac{N - \mathcal{N}_p}{\mathcal{N}_p} \cdot \frac{\mathrm{trace}\left\{\mathbf{\Phi}_2^{\mathrm{DF}}\right\}}{Lm} + \frac{m\sigma_w^2}{(1-\alpha)\mathcal{N}_p\bar{P}}, \tag{2.17}$$

where $\mathbf{\Phi}_2^{\mathrm{DF}} = \mathbb{E}\left\{\mathbf{h}_{DR}\mathbf{h}_{DR}^H\right\}$.

As with the AF mode, the maximum number of relays is constrained. The following Lemma provides this maximum number.

Lemma 2—Maximum Number of Relays in the DF Mode: In DF mode, to achieve the optimal channel estimation for each $S \to R \to D$ channel, the maximum number of active relays that simultaneously retransmit is $M \le \lfloor N/L \rfloor$.

Proof: In DF mode, the channel order for each $R \to D$ channel is L. From (2.16), the condition of $LM \le \mathcal{N}_p \le N$ must be satisfied for the optimal pilot design, and we can easily conclude that $M \le \lfloor N/L \rfloor$.

□

2.3.3 Effect of Imperfect Frequency Offset Estimation on Channel Estimation

Up to now, a perfect frequency offset knowledge is assumed. However, frequency offset estimation errors do exist in physical applications. Denote $e_{a,b}$ as the estimation error of $\varepsilon_{a,b}$. At node D, $\mathbf{E}_{D,z}$, $z = \{S, R_k\}$, can be estimated as

$$\begin{aligned}\hat{\mathbf{E}}_{D,z} &= \text{diag}\left\{1, e^{\frac{\jmath 2\pi\hat{\varepsilon}_{D,z}}{N}}, \cdots, e^{\frac{\jmath 2\pi\hat{\varepsilon}_{D,z}\times(N-1)}{N}}\right\} \\ &\cong \mathbf{E}_{D,z} + \overbrace{\jmath e_{D,z} \cdot \underbrace{\text{diag}\left\{0, \frac{2\pi}{N}, \cdots, \frac{2\pi\times(N-1)}{N}\right\}}_{\mathbf{\Omega}} \cdot \mathbf{E}_{D,z}}^{\Delta\mathbf{E}_{D,z}}.\end{aligned} \tag{2.18}$$

Using $\hat{\mathbf{P}}_{D,S}$, $\hat{\mathbf{P}}_2^{\text{AF}}$ and $\hat{\mathbf{P}}_2^{\text{DF}}$ to represent the estimated $\mathbf{P}_{D,S}$, $\mathbf{P}_2^{\text{AF}}$ and $\mathbf{P}_2^{\text{DF}}$, respectively, we have

$$\hat{\mathbf{P}}_{D,S} = \sqrt{\alpha N\bar{P}}\hat{\mathbf{E}}_{D,S}^{\text{cir}}\mathbf{X}_S^p\mathbf{F}_{(L)}^H = \underbrace{\sqrt{\alpha N\bar{P}}\mathbf{E}_{D,S}^{\text{cir}}\mathbf{X}_S^p\mathbf{F}_{(L)}^H}_{\mathbf{P}_{D,S}} + \underbrace{\sqrt{\alpha N\bar{P}}\Delta\mathbf{E}_{D,S}^{\text{cir}}\mathbf{X}_S^p\mathbf{F}_{(L)}^H}_{\Delta\mathbf{P}_{D,S}}. \tag{2.19}$$

$$\hat{\mathbf{P}}_2^{\text{AF}} = \mathbf{P}_2^{\text{AF}} + \underbrace{Q_1(\alpha)\ \mathbf{F}^H\Delta\mathbf{E}_{D,S}\mathbf{F}\mathbf{X}_{R_1}^p\mathbf{F}_{(2L-1)}^H \quad \cdots \quad \mathbf{F}^H\Delta\mathbf{E}_{D,S}\mathbf{F}\mathbf{X}_{R_M}^p\mathbf{F}_{(2L-1)}^H}_{\Delta\mathbf{P}_2^{\text{AF}}} \tag{2.20}$$

$$\hat{\mathbf{P}}_2^{\text{DF}} = \mathbf{P}_2^{\text{DF}} + \underbrace{\sqrt{\frac{(1-\alpha)N\bar{P}}{m}}\mathbf{F}^H\Delta_2^{\text{DF}}\mathbf{F}_{(L)}^H}_{\Delta\mathbf{P}_2^{\text{DF}}}, \tag{2.21}$$

where $\Delta_2^{\mathrm{DF}} = \left[\Delta\mathbf{E}_{D,R_1}\mathbf{F}\mathbf{X}_{R_1}^{p} \ldots \Delta\mathbf{E}_{D,R_m}\mathbf{F}\mathbf{X}_{R_m}^{p}\right]$. $\hat{\mathbf{P}}_{D,S}^{\dagger}$ can be expressed as

$$\begin{aligned}
\hat{\mathbf{P}}_{D,S}^{\dagger} &= \left(\hat{\mathbf{P}}_{D,S}^{H}\hat{\mathbf{P}}_{D,S}\right)^{-1}\hat{\mathbf{P}}_{D,S}^{H} \\
&= \left(\underbrace{\mathbf{P}_{D,S}^{H}\mathbf{P}_{D,S}}_{=\alpha\bar{P}\mathbf{I}_{\mathcal{N}_p}} + \underbrace{\Delta\mathbf{P}_{D,S}^{H}\mathbf{P}_{D,S} + \mathbf{P}_{D,S}^{H}\Delta\mathbf{P}_{D,S} + \Delta\mathbf{P}_{D,S}^{H}\Delta\mathbf{P}_{D,S}}_{\mathbf{BSB}^{H}}\right)^{-1}\left(\mathbf{P}_{D,S} + \Delta\mathbf{P}_{D,S}\right)^{H} \\
&= \frac{1}{\alpha\bar{P}}\left(\mathbf{I}_{\mathcal{N}_p} - \mathbf{B}\left(\mathbf{B}^{H}\mathbf{B} + \alpha\bar{P}\mathbf{S}^{-1}\right)^{-1}\mathbf{B}^{H}\right)\left(\mathbf{P}_{D,S} + \Delta\mathbf{P}_{D,S}\right)^{H} \\
&= \mathbf{P}_{D,S}^{\dagger} + \underbrace{\left(\mathbf{P}_{D,S}^{H}\mathbf{P}_{D,S}\right)^{-1}\Delta\mathbf{P}_{D,S}^{H} - \frac{1}{\alpha\bar{P}}\mathbf{B}\left(\mathbf{B}^{H}\mathbf{B} + \alpha\bar{P}\mathbf{S}^{-1}\right)^{-1}\mathbf{B}^{H}\left(\mathbf{P}_{D,S} + \Delta\mathbf{P}_{D,S}\right)^{H}}_{\Delta\mathbf{P}_{D,S}^{\dagger}},
\end{aligned} \tag{2.22}$$

where $\mathbf{S} = \mathrm{diag}\{\lambda_0, \lambda_1, \cdots, \lambda_{N-1}\}$, $\lambda_i = \frac{4\pi i e_{D,S}}{N}\sin\left(\frac{2\pi i e_{D,S}}{N}\right) + \frac{4\pi^2 i^2 e_{D,S}^2}{N^2}$, and $\mathbf{B} = \mathbf{F}_{(L)}\mathbf{X}_{S}^{pH}\mathbf{F}^{H}$. We also have

$$\mathbf{B}^{H}\mathbf{B} = \alpha\bar{P}\begin{bmatrix} \mathbf{I}_{\mathcal{N}_p} & \mathbf{O}_{\mathcal{N}_p\times(N-\mathcal{N}_p)} \\ \mathbf{O}_{(N-\mathcal{N}_p)\times\mathcal{N}_p} & \mathbf{O}_{(N-\mathcal{N}_p)\times(N-\mathcal{N}_p)} \end{bmatrix}. \tag{2.23}$$

From (2.22)-(2.23), the matrix $\left(\mathbf{B}^{H}\mathbf{B} + \alpha\bar{P}\mathbf{S}^{-1}\right)^{-1}$ must be a diagonal matrix. Using $\tilde{\lambda}_i$ to represent the i-th eigenvalue of $\left(\mathbf{B}^{H}\mathbf{B} + \alpha\bar{P}\mathbf{S}^{-1}\right)^{-1}$, we have

$$\tilde{\lambda}_i = \begin{cases} \frac{\lambda_i}{\alpha\bar{P}(\lambda_i+1)}, & 0 \le i \le \mathcal{N}_p - 1, \\ \frac{\lambda_i}{\alpha\bar{P}}, & \mathcal{N}_p \le i \le N-1. \end{cases} \tag{2.24}$$

For small frequency offset errors, λ_i can be approximated as $\lambda_i \cong \frac{12\pi^2 i^2 e_{D,S}^2}{N^2}$. When $\lambda_i \ll 1$, $\tilde{\lambda}_i \cong \lambda_i$ for each $0 \le i \le N-1$.

From (2.22), the first item in $\Delta\mathbf{P}_{D,S}^{\dagger}$ is a function of $e_{D,S}$, but the second item in $\Delta\mathbf{P}_{D,S}^{\dagger}$ is a function of $e_{D,S}^2$. For a small $e_{D,S}$, the second item is negligible as compared with the first item, and $\Delta\mathbf{P}_{D,S}^{\dagger}$ can be approximated as $\Delta\mathbf{P}_{D,S}^{\dagger} \cong \left(\mathbf{P}_{D,S}^{H}\mathbf{P}_{D,S}\right)^{-1}\Delta\mathbf{P}_{D,S}^{H}$ to simplify the analysis. Similarly, $\left(\hat{\mathbf{P}}_2^{\mathrm{AF}}\right)^{\dagger}$ and $\left(\hat{\mathbf{P}}_2^{\mathrm{DF}}\right)^{\dagger}$ can also be represented as

$$\left(\hat{\mathbf{P}}_2^{\mathrm{AF}}\right)^{\dagger} \cong \left(\mathbf{P}_2^{\mathrm{AF}}\right)^{\dagger} + \underbrace{\left((\mathbf{P}_2^{\mathrm{AF}})^{H}(\mathbf{P}_2^{\mathrm{AF}})\right)^{-1}}_{\Delta(\hat{\mathbf{P}}_2^{\mathrm{AF}})^{\dagger}}$$

and

$$\left(\hat{\mathbf{P}}_2^{\mathrm{DF}}\right)^{\dagger} \cong \left(\mathbf{P}_2^{\mathrm{DF}}\right)^{\dagger} + \Delta\left(\hat{\mathbf{P}}_2^{\mathrm{DF}}\right)^{\dagger}$$

and the LS channel estimation for $\tilde{\mathbf{h}}_{D,S}$, $\tilde{\mathbf{h}}_{R_k,S}$, $\mathbf{h}_{DRS}$ and $\mathbf{h}_{DR}$ are given by $\hat{\tilde{\mathbf{h}}}_{b,S} = \hat{\mathbf{P}}_{b,S}^{\dagger}\mathbf{r}_{b,1}$, $\hat{\mathbf{h}}_{DRS} = \left(\hat{\mathbf{P}}_2^{\mathrm{AF}}\right)^{\dagger}\tilde{\mathbf{r}}_{D,2}^{\mathrm{AF}}$ and $\hat{\mathbf{h}}_{DR} = \left(\hat{\mathbf{P}}_2^{\mathrm{DF}}\right)^{\dagger}\mathbf{r}_{D,2}^{\mathrm{DF}}$, respectively, where $b \in \{D, R_k\}$. The MSE of the channel estimation by considering the frequency offset errors can be derived, respectively, as

$$\begin{aligned}\mathrm{MSE}\left(\hat{\tilde{\mathbf{h}}}_{b,S}\right) &= \frac{1}{L}\mathbb{E}\left\{\left\|\hat{\tilde{\mathbf{h}}}_{b,S} - \tilde{\mathbf{h}}_{b,S}\right\|_2^2\right\} \\ &= \frac{\mathrm{trace}\left\{\left(\mathbf{P}_{b,S}^H\mathbf{P}_{b,S}\right)^{-1}\mathbf{J}_{b,S}\mathbf{\Phi}_{b,S}\right\}}{L}\cdot\sigma_e^2 + \frac{(N-\mathcal{N}_p)\cdot\mathrm{trace}\left\{\mathbf{\Phi}_{b,S}\right\}}{L\mathcal{N}_p} + \frac{\sigma_w^2}{\alpha\mathcal{N}_p\bar{P}},\end{aligned} \tag{2.25}$$

$$\begin{aligned}\mathrm{MSE}\left(\hat{\mathbf{h}}_{DRS}\right) &= \frac{1}{(2L-1)M}\mathbb{E}\left\{\left\|\hat{\tilde{\mathbf{h}}}_{DRS} - \tilde{\mathbf{h}}_{DRS}\right\|_2^2\right\} \\ &= \frac{\mathrm{trace}\left\{\left((\mathbf{P}_2^{\mathrm{AF}})^H\mathbf{P}_2^{\mathrm{AF}}\right)^{-1}\mathbf{J}_{DRS}\mathbf{\Phi}_2^{\mathrm{AF}}\right\}}{(2L-1)M}\cdot\sigma_e^2 + \frac{N-\mathcal{N}_p}{\mathcal{N}_p}\cdot\frac{\mathrm{trace}\left\{\mathbf{\Phi}_2^{\mathrm{AF}}\right\}}{(2L-1)M} \\ &\quad + \frac{\sigma_w^2}{\alpha\mathcal{N}_p\bar{P}}\cdot\frac{\sum_{k=1}^{M}\mathrm{trace}\left\{\mathbf{\Phi}_{D,R_k}^{\mathrm{AF}}\right\}}{(2L-1)M} + \frac{M(\alpha\bar{P}+\sigma_w^2)\sigma_w^2}{\alpha(1-\alpha)\mathcal{N}_p\bar{P}^2},\end{aligned} \tag{2.26}$$

$$\begin{aligned}\mathrm{MSE}\left(\hat{\mathbf{h}}_{DR}\right) &= \frac{1}{Lm}\mathbb{E}\left\{\left\|\hat{\tilde{\mathbf{h}}}_{DR} - \tilde{\mathbf{h}}_{DR}\right\|_2^2\right\} \\ &= \frac{\mathrm{trace}\left\{\left((\mathbf{P}_2^{\mathrm{DF}})^H\mathbf{P}_2^{\mathrm{DF}}\right)^{-1}\mathbf{J}_{DR}\mathbf{\Phi}_2^{\mathrm{DF}}\right\}}{Lm}\cdot\sigma_e^2 + \frac{N-\mathcal{N}_p}{\mathcal{N}_p}\cdot\frac{\mathrm{trace}\left\{\mathbf{\Phi}_2^{\mathrm{DF}}\right\}}{Lm} + \frac{m\sigma_w^2}{(1-\alpha)\mathcal{N}_p\bar{P}},\end{aligned} \tag{2.27}$$

$$\mathbf{\Phi}_{b,S} = \mathbb{E}\left\{\tilde{\mathbf{h}}_{b,S}\tilde{\mathbf{h}}_{b,S}^{H}\right\}, \tag{2.28a}$$

$$\mathbf{J}_{D,S} = \mathbf{J}_{R_k,S} = \alpha N\bar{P}\mathbf{F}_{(L)}\mathbf{X}_{S}^{pH}\mathbf{F}^{H}\mathbf{\Omega}^{2}\mathbf{F}\mathbf{X}_{S}^{p}\mathbf{F}_{(L)}^{H}, \tag{2.28b}$$

$$\mathbf{J}_{DRS} = Q_1^2(\alpha)\cdot\mathrm{diag}\left\{\mathbf{T}_1,\cdots,\mathbf{T}_M\right\}, \tag{2.28c}$$

$$\mathbf{J}_{DR} = \frac{(1-\alpha)N\bar{P}}{m}\cdot\mathrm{diag}\left\{\mathbf{T}_1^{\mathrm{DF}},\cdots,\mathbf{T}_m^{\mathrm{DF}}\right\}, \tag{2.28d}$$

$$\mathbf{T}_i^{\mathrm{AF}} = \mathbf{F}_{(2L-1)}\mathbf{X}_{R_i}^{pH}\mathbf{F}^{H}\mathbf{\Omega}^{2}\mathbf{F}\mathbf{X}_{R_i}^{p}\mathbf{F}_{(2L-1)}^{H}, \tag{2.28e}$$

$$\mathbf{T}_i^{\mathrm{DF}} = \mathbf{F}_{(L)}\mathbf{X}_{R_i}^{pH}\mathbf{F}^{H}\mathbf{\Omega}^{2}\mathbf{F}\mathbf{X}_{R_i}^{p}\mathbf{F}_{(L)}^{H}. \tag{2.28f}$$

2.4 Effect of Frequency Offset and Channel Estimation Errors on PEP

Although the BER of conventional (noncooperative) OFDM with frequency offset has been studied [99, 111], the application of the BER results to a cooperative OFDM uplink is not straightforward. First, the effective $S \to R \to D$ channel in the AF mode is the convolution of $S \to R$ and $R \to D$ channels. It is proven in [91] that the $S \to R \to D$ channel is not Gaussian. Second, in DF mode, the relays retransmit only if there is no decoding error. Since the OFDM channel is usually a frequency-selective fading channel, some subcarriers may suffer deep fading. If the subcarriers are modulated independently, it is very difficult to correctly decode all the subcarriers. In this section, after the analysis of SINR, the PEP of cooperative OFDM by considering both frequency offset and channel estimation errors will be derived.

2.4.1 SINR Analysis

First Time Slot

Without loss of generality, we assume that $\hat{\tilde{\mathbf{h}}}_{D,S} = \tilde{\mathbf{h}}_{D,S} + \Delta\tilde{\mathbf{h}}_{D,S}$, where $\Delta\tilde{\mathbf{h}}_{D,S}$ represents the estimation error of $\tilde{\mathbf{h}}_{D,S}$. The received vector $\mathbf{y}_{D,1}$ can be demodulated as

$$\begin{aligned}\mathbf{r}_{D,1} &= \mathbf{F}^H\mathbf{y}_{D,1} = \sqrt{\alpha N\bar{P}}\mathbf{E}^{\text{cir}}_{D,S}\mathbf{X}_S\mathbf{F}^H_{(L)}\tilde{\mathbf{h}}_{D,S} + \mathbf{F}^H\mathbf{w}_{D,1} \\ &= \underbrace{\sqrt{\alpha N\bar{P}}\mathbf{E}^{\text{diag}}_{D,S}\mathbf{X}_S\mathbf{F}^H_{(L)}\tilde{\mathbf{h}}_{D,S}}_{\boldsymbol{\mu}_{D,1}} + \underbrace{\underbrace{\sqrt{\alpha N\bar{P}}\mathbf{E}^{\text{off}}_{D,S}\mathbf{X}_S\mathbf{F}^H_{(L)}\tilde{\mathbf{h}}_{D,S}}_{\text{interference}} + \mathbf{F}^H\mathbf{w}_{D,1}}_{\boldsymbol{\xi}_{D,1}},\end{aligned} \tag{2.29}$$

where we decompose $\mathbf{E}^{\text{cir}}_{D,S}$ as $\mathbf{E}^{\text{cir}}_{D,S} = \mathbf{E}^{\text{diag}}_{D,S} + \mathbf{E}^{\text{off}}_{D,S}$, with $\mathbf{E}^{\text{diag}}_{D,S}$ being a diagonal matrix that $[\mathbf{E}^{\text{diag}}_{D,S}]_{ii} = [\mathbf{E}^{\text{cir}}_{D,S}]_{ii}$, and $\mathbf{E}^{\text{off}}_{D,S}$ comprising all the off-diagonal elements of $\mathbf{E}^{\text{cir}}_{D,S}$, $\boldsymbol{\mu}_{D,1}$ is the useful signal of $\mathbf{r}_{D,1}$, and $\boldsymbol{\xi}_{D,1}$ represents the interference plus noise of $\mathbf{r}_{D,1}$.

The signal of the n-th tap can be demodulated as

$$\frac{\hat{\tilde{\mathbf{h}}}^*_{D,S}[n]\cdot\mathbf{r}_{D,1}[n]}{\left|\hat{\tilde{\mathbf{h}}}_{D,S}[n]\right|^2} = \frac{\tilde{\mathbf{h}}^*_{D,S}[n]\cdot\boldsymbol{\mu}_{D,1}[n]}{\left|\hat{\tilde{\mathbf{h}}}_{D,S}[n]\right|^2} + \frac{\Delta\tilde{\mathbf{h}}^*_{D,S}[n]\cdot\boldsymbol{\mu}_{D,1}[n]}{\left|\hat{\tilde{\mathbf{h}}}_{D,S}[n]\right|^2} + \frac{\hat{\tilde{\mathbf{h}}}^*_{D,S}[n]\cdot\boldsymbol{\xi}_{D,1}[n]}{\left|\hat{\tilde{\mathbf{h}}}_{D,S}[n]\right|^2}. \tag{2.30}$$

The SINR of (2.30) is given by

$$\bar{\gamma}_{DS,n} = \frac{\mathbb{E}\left\{\left|\tilde{\mathbf{h}}^*_{D,R,S}[n]\cdot\boldsymbol{\mu}_{D,1}[n]\right|^2\right\}}{\mathbb{E}\left\{\left|\Delta\tilde{\mathbf{h}}^*_{D,S}[n]\cdot\boldsymbol{\mu}_{D,1}[n]\right|^2\right\} + \mathbb{E}\left\{\left|\hat{\tilde{\mathbf{h}}}^*_{D,S}[n]\cdot\boldsymbol{\xi}_{D,1}[n]\right|^2\right\}}. \tag{2.31}$$

Equation (2.31) can be simplified as

$$\bar{\gamma}_{DS,n} = \frac{\alpha\bar{P}\cdot\left|\tilde{\mathbf{h}}_{D,S}[n]\right|^2\cdot\beta_e}{\sigma^2_{\text{AF},1} + \left(\alpha\bar{P}\cdot\beta_e + \frac{\sigma^2_{\text{AF},1}}{\left|\tilde{\mathbf{h}}_{D,S}[n]\right|^2}\right)\cdot\text{MSE}\left(\hat{\tilde{\mathbf{h}}}_{D,S}\right)}, \tag{2.32}$$

where $\beta_e = 1 - \frac{\pi^2\sigma_e^2}{3} + \frac{\pi^4\sigma_e^4}{20}$ and $\sigma^2_{\text{AF},1} = \frac{\mathcal{L}_u\alpha\pi^2\sigma_e^2\bar{P}}{3} + \sigma_w^2$.

Second Time Slot of the AF Mode

The received vector $\mathbf{y}_{D,2}^{\mathrm{AF}}$ can be demodulated as

$$\mathbf{r}_{D,2}^{\mathrm{AF}} = \mathbf{F}^H \mathbf{y}_{D,2}^{\mathrm{AF}} = \underbrace{\sum_{k=1}^{M} Q_1(\alpha)\mathbf{E}_{D,R_k,S}^{\mathrm{diag}}\mathbf{X}_S\mathbf{F}_{(2L-1)}^H\tilde{\mathbf{h}}_{D,R_k,S}}_{\boldsymbol{\mu}_{D,2}^{\mathrm{AF}}} + \underbrace{\underbrace{\sum_{k=1}^{M} Q_1(\alpha)\mathbf{E}_{D,R_k,S}^{\mathrm{off}}\mathbf{X}_S\mathbf{F}_{(2L-1)}^H\tilde{\mathbf{h}}_{D,R_k,S}}_{\text{interference}} + \sum_{k=1}^{M} Q_2(\alpha)\mathbf{E}_{D,R_k}^{\mathrm{cir}}\mathbf{W}_\eta\mathbf{F}_{(L)}^H\tilde{\mathbf{h}}_{D,R_k} + \mathbf{F}^H\mathbf{w}_{D,2}}_{\boldsymbol{\xi}_{D,2}^{\mathrm{AF}}}, \tag{2.33}$$

where $\mathbf{E}_{D,R_k,S}^{\mathrm{cir}} = \mathbf{E}_{D,R_k,S}^{\mathrm{diag}} + \mathbf{E}_{D,R_k,S}^{\mathrm{off}}$. The SINR of (2.33) is given by

$$\bar{\gamma}_{DRS,n} = \frac{\mathbb{E}\left\{\left|\left(\sum_{k=1}^{M}\tilde{\mathbf{h}}_{D,R_k,S}[n]\right)^* \cdot \boldsymbol{\mu}_{D,2}^{\mathrm{AF}}[n]\right|^2\right\}}{\mathbb{E}\left\{\left|\left(\sum_{k=1}^{M}\Delta\tilde{\mathbf{h}}_{D,R_k,S}[n]\right)^* \cdot \boldsymbol{\mu}_{D,2}^{\mathrm{AF}}[n]\right|^2\right\} + \mathbb{E}\left\{\left|\left(\sum_{k=1}^{M}\hat{\tilde{\mathbf{h}}}_{D,R_k,S}[n]\right)^* \cdot \boldsymbol{\xi}_{D,2}^{\mathrm{AF}}[n]\right|^2\right\}}. \tag{2.34}$$

and (2.34) can be simplified as

$$\bar{\gamma}_{DRS,n} = \frac{\alpha(1-\alpha)\bar{P}^2\left|\sum_{k=1}^{M}\tilde{\mathbf{h}}_{D,R_k,S}[n]\right|^2 \cdot \beta_e}{M\sigma_{\mathrm{AF},2}^2(\alpha\bar{P}+\sigma_w^2) + M\left(\alpha(1-\alpha)\bar{P}^2\cdot\beta_e + \frac{M\sigma_{\mathrm{AF},2}^2(\alpha\bar{P}+\sigma_w^2)}{\left|\sum_{k=1}^{M}\tilde{\mathbf{h}}_{D,R_k,S}[n]\right|^2}\right)\cdot \mathrm{MSE}\left(\hat{\mathbf{h}}_{DRS}\right)}, \tag{2.35}$$

where $\sigma_{\mathrm{AF},2}^2 = \dfrac{2\mathcal{L}_u(M^2-M+1)\alpha(1-\alpha)\pi^2\sigma_e^2\bar{P}^2}{3M(\alpha\bar{P}+\sigma_w^2)} + \dfrac{\mathcal{L}_u\alpha\pi^2\sigma_e^2\bar{P}}{3} + \dfrac{\mathcal{L}_u(M+1)(1-\alpha)\bar{P}\sigma_w^2}{\alpha\bar{P}+\sigma_w^2} + \sigma_w^2$.

Second Time Slot of the DF Mode

The received vector $\mathbf{y}_{D,2}^{\mathrm{DF}}$ can be demodulated as

$$\mathbf{r}_{D,2}^{\mathrm{DF}} = \underbrace{\sum_{k=1}^{m}\sqrt{\frac{(1-\alpha)N\bar{P}}{m}}\mathbf{E}_{D,R_k}^{\mathrm{diag}}\mathbf{X}_{R_k}\mathbf{F}_{(L)}^{H}\tilde{\mathbf{h}}_{D,R_k}}_{\boldsymbol{\mu}_{D,2}^{\mathrm{DF}}} + \underbrace{\underbrace{\sum_{k=1}^{m}\sqrt{\frac{(1-\alpha)N\bar{P}}{m}}\mathbf{E}_{D,R_k}^{\mathrm{off}}\mathbf{X}_{R_k}\mathbf{F}_{(L)}^{H}\tilde{\mathbf{h}}_{D,R_k}}_{\text{interference}} + \mathbf{F}^{H}\mathbf{w}_{D,2}}_{\boldsymbol{\xi}_{D,2}^{\mathrm{DF}}}. \tag{2.36}$$

Similarly, the SINR of (2.36) in the n-th tap is given by

$$\begin{aligned}\bar{\gamma}_{DR,m,n} &= \frac{\mathbb{E}\left\{\left|\left(\sum_{k=1}^{m}\tilde{\mathbf{h}}_{D,R_k}[n]\right)^{*}\cdot\boldsymbol{\mu}_{D,2}^{\mathrm{DF}}[n]\right|^{2}\right\}}{\mathbb{E}\left\{\left|\left(\sum_{k=1}^{m}\Delta\tilde{\mathbf{h}}_{D,R_k}[n]\right)^{*}\cdot\boldsymbol{\mu}_{D,2}^{\mathrm{DF}}[n]\right|^{2}\right\}+\mathbb{E}\left\{\left|\left(\sum_{k=1}^{m}\hat{\tilde{\mathbf{h}}}_{D,R_k}[n]\right)^{*}\cdot\boldsymbol{\xi}_{D,2}^{\mathrm{DF}}[n]\right|^{2}\right\}} \\ &= \frac{(1-\alpha)\bar{P}\cdot\left|\sum_{k=1}^{m}\tilde{\mathbf{h}}_{D,R_k}[n]\right|^{2}\cdot\beta_e}{m\sigma_{\mathrm{DF},2}^{2}+m\left(\mathcal{L}_u(1-\alpha)\bar{P}\cdot\beta_e+\frac{m\sigma_{\mathrm{DF},2}^{2}}{\left|\sum_{k=1}^{m}\tilde{\mathbf{h}}_{D,R_k}[n]\right|^{2}}\right)\cdot\mathrm{MSE}\left(\hat{\mathbf{h}}_{DR}\right)},\end{aligned} \tag{2.37}$$

where $\sigma_{\mathrm{DF},2}^{2} = \dfrac{\mathcal{L}_u(1-\alpha)\pi^2\sigma_e^2\bar{P}}{3}+\sigma_w^2$.

2.4.2 PEP for the AF Mode

An orthogonal space-time signal matrix $\bar{\mathbf{X}}_S = [\tilde{\mathbf{X}}_S(1), \tilde{\mathbf{X}}_S(2), \cdots, \tilde{\mathbf{X}}_S(T)]$, which is $N\times T$ matrix, is assumed. The probability that $\bar{\mathbf{X}}_S$ will be mistaken for another code $\bar{\mathbf{L}}_S$ is upper bounded by [112]:

$$\mathrm{P}_{\mathrm{r}}^{\mathrm{AF}}\left\{\bar{\mathbf{X}}_S\to\bar{\mathbf{L}}_S\middle|0<\alpha<1\right\}\le\left(\prod_{n=0}^{2L-2}\frac{1}{1+\frac{\bar{\gamma}_{DRS,n}\ell_n}{4}}\right)\left(\prod_{n=0}^{L-1}\frac{1}{1+\frac{\bar{\gamma}_{DS,n}\ell_n}{4}}\right), \tag{2.38}$$

where $\bar{\gamma}_{DS,n}$ and $\bar{\gamma}_{DRS,n}$ represent the SINRs of the $S\to D$ and $S\to R\to D$ channels, respectively, in the n-th multipath tap, and ℓ_n is the n-th eigenvalue of $\left(\bar{\mathbf{X}}_S-\bar{\mathbf{L}}_S\right)\left(\bar{\mathbf{X}}_S-\bar{\mathbf{L}}_S\right)^{H}$. In the high SINR regim with $\sigma_e^2\to 0$, $\bar{\gamma}_{DS,n}$ and $\bar{\gamma}_{DRS,n}$ can be approximated as

$$\lim_{\substack{\sigma_e^2\to 0\\ \mathrm{SNR}\to\infty}}\bar{\gamma}_{DS,n}\to\alpha\mathrm{SNR}\cdot\left|\tilde{\mathbf{h}}_{D,S}[n]\right|^{2}$$

and

$$\lim_{\substack{\sigma_e^2\to 0\\ \mathrm{SNR}\to\infty}} \bar{\gamma}_{DRS,n} \to \frac{\alpha(1-\alpha)\mathrm{SNR}\cdot\left|\sum_{k=1}^{M}\tilde{\mathbf{h}}_{D,R_k,S}[n]\right|^2}{M\left[\frac{\mathcal{L}_u(M+1)(1-\alpha)}{\alpha}+1\right]}$$

where $\mathrm{SNR}=\bar{P}/\sigma_w^2$ denotes the average SNR, and (2.38) can be rewritten as

$$\begin{aligned}&\lim_{\substack{\sigma_e^2\to 0\\ \mathrm{SNR}\to\infty}} \mathrm{P}_{\mathrm{r}}^{\mathrm{AF}}\left\{\bar{\mathbf{X}}_S\to\bar{\mathbf{L}}_S\middle|0<\alpha<1\right\}\\ &\le\underbrace{\left(\frac{4\left[\frac{\mathcal{L}_u(M+1)(1-\alpha)}{\alpha}+1\right]}{\alpha(1-\alpha)\mathrm{SNR}}\right)^{2L-1}\left(\frac{4}{\alpha\mathrm{SNR}}\right)^{L}}_{\text{multipath diversity gain}}\times\underbrace{\left(\prod_{n=0}^{2L-2}\frac{M}{\left|\sum_{k=1}^{M}\tilde{\mathbf{h}}_{D,R_k,S}[n]\right|^2\ell_n}\right)}_{\text{multi-relay diversity gain}}\left(\prod_{n=0}^{L-1}\frac{1}{\left|\tilde{\mathbf{h}}_{D,S}[n]\right|^2\ell_n}\right).\end{aligned}\tag{2.39}$$

When L is small, the M-order multi-relay diversity dominates the diversity gain in a high SINR regime, and a larger M implies a smaller PEP.

2.4.3 PEP for the DF Mode

In DF mode, each relay decodes the received signal from S. The relays with decoding errors will not retransmit. By using P_{relay} to represent the average probability of decoding error at each relay, the probability that m out of M relays successfully decode the received signal is a Binomial distribution, i.e., $P_{\mathrm{relay},m}=\binom{M}{m}(1-P_{\mathrm{relay}})^m P_{\mathrm{relay}}^{M-m}$. We also use $P_{S\to D}$ to represent the probability of the decoding error at D in the first time slot. P_{relay} and $P_{S\to D}$ are given, respectively, by

$$P_{\mathrm{relay}}=\mathrm{P}_{\mathrm{r}}\left\{\bar{\mathbf{X}}_S\to\bar{\mathbf{L}}_S\middle|0<\alpha<1;R_k\right\}\le\prod_{n=0}^{L-1}\frac{1}{1+\frac{\bar{\gamma}_{R_kS,n}\ell_n}{4}},\tag{2.40a}$$

$$P_{S\to D}=\mathrm{P}_{\mathrm{r}}\left\{\bar{\mathbf{X}}_S\to\bar{\mathbf{L}}_S\middle|0<\alpha<1;D\right\}\le\prod_{n=0}^{L-1}\frac{1}{1+\frac{\bar{\gamma}_{DS,n}\ell_n}{4}},\tag{2.40b}$$

where $\bar{\gamma}_{R_kS,n}$ represent the SINR of the $S\to R_k$ channel in the n-th tap. From the SINR analysis of the first time slot, $\bar{\gamma}_{R_kS,n}$ is given by

$$\bar{\gamma}_{R_kS,n}=\frac{\alpha\bar{P}\cdot\left|\tilde{\mathbf{h}}_{R_k,S}[n]\right|^2\cdot\beta_e}{\sigma_{\mathrm{DF},1}^2+\left(\alpha\bar{P}\cdot\beta_e+\frac{\sigma_{\mathrm{DF},1}^2}{\left|\tilde{\mathbf{h}}_{R_k,S}[n]\right|^2}\right)\cdot\mathrm{MSE}\left(\hat{\tilde{\mathbf{h}}}_{R_k,S}\right)}$$

where $\sigma^2_{\mathrm{DF},1} = \dfrac{\alpha\pi^2\sigma_e^2\bar{P}}{3} + \sigma_w^2$.

In the second time slot, the m relays with correct decoding will retransmit. The PEP that $\bar{\mathbf{X}}_S$ will be mistaken for another codeword $\bar{\mathbf{L}}_S$ is upper bounded by

$$\mathrm{P}^{\mathrm{DF}}_{\mathrm{r},m}\left\{\bar{\mathbf{X}}_S \to \bar{\mathbf{L}}_S \middle| 0<\alpha<1\right\} \le \prod_{n=0}^{L-1} \frac{1}{1+\frac{\bar{\gamma}_{DR,m,n}\ell_n}{4}}, \tag{2.41}$$

where $\bar{\gamma}_{DR,m,n}$ represents the SINR of the $R \to D$ channel in the n-th multipath tap. From the derived $\bar{\gamma}_{DR,m,n}$ in (2.36), the averaged PEP of the DF mode is upper bounded by

$$\overline{\mathrm{PEP}^{\mathrm{DF}}} \le P_{S\to D} \cdot \sum_{m=0}^{M} P_{\mathrm{relay},m}\mathrm{P}^{\mathrm{DF}}_{\mathrm{r},m}\left\{\bar{\mathbf{X}}_S \to \bar{\mathbf{L}}_S \middle| 0<\alpha<1\right\}. \tag{2.42}$$

In the high SINR regime with $\sigma_e^2 \to 0$, (2.41) can be approximated as

$$\lim_{\substack{\sigma_e^2\to 0\\ \mathrm{SNR}\to\infty}} \mathrm{P}^{\mathrm{AF}}_{\mathrm{r}}\left\{\bar{\mathbf{X}}_S \to \bar{\mathbf{L}}_S \middle| 0<\alpha<1\right\} \le \underbrace{\left(\frac{4}{(1-\alpha)\mathrm{SNR}}\right)^{L}}_{\text{multipath diversity gain}} \times \underbrace{\left(\prod_{n=0}^{L-1}\frac{m}{\left|\sum_{k=1}^{m}\tilde{\mathbf{h}}_{D,R_k}[n]\right|^2\ell_n}\right)}_{\text{multi-relay diversity gain}}. \tag{2.43}$$

A comparison of (2.39) and (2.43) shows that for a given M, in a high SINR regime with $\sigma_e^2 \to 0$, the AF mode outperforms the DF mode in terms of diversity gain. However, in real systems, the DF mode usually outperforms the AF mode because of the following reasons. First, Lemma 1 and Lemma 2 tell us that for a given L, the maximum number of active relays used in the DF mode is almost twice that of the AF mode, and the achievable cooperative diversity gain in the DF mode is much higher than that obtained in the AF mode. Second, by considering the frequency offset, the OFDM transmission is usually interference limited, and the diversity gain obtained in the AF mode may be deteriorated by the interference and noise that accumulated in the relays. The interference-mitigation capability in DF mode provides a performance advantage over the AF mode in the low SINR regime. A brief performance comparison between the AF and DF modes is shown in Table 2.1.

Table 2.1: Performance Comparison Between AF and DF Modes

Relaying Mode	AF	DF
Complexity	Low	High
Channel Estimation Accuracy	Low	High
Maximum Concatenated Channel Delay	$2L_{max}-1$	L_{max}
Maximum Number of Relays	$\left\lfloor \frac{N}{2L_{max}-1} \right\rfloor$	$\left\lfloor \frac{N}{L_{max}} \right\rfloor$
Capacity to Combat Multipath-fading	Low	High
Achievable Diversity Gain	Low	High
PEP	High	Low

2.5 Numerical Results

The PEP of the proposed channel estimation schemes for systems with frequency offsets is evaluated. The total power consumption is kept constant, and the PEP as a function of power allocation ratio α is first evaluated. The performance comparison between the proposed pilot designs for the AF and DF relaying modes is then performed for different channel lengths L. After that, the PEP performance as a function of frequency offset variance, i.e. σ_ε^2, is evaluated. Finally, for a given σ_ε^2, the PEP performance as the SNR increases is simulated.

Only uniform power-delay profiles are considered for brevity, i.e., $\mathbb{E}\left\{|h_{R_k,S}(l)|^2\right\} = 1/L$ and $\mathbb{E}\left\{|h_{D,R_k}(l)|^2\right\} = \mathbb{E}\left\{|h_{D,S}(l)|^2\right\} = \mathcal{L}_u/L$, where $l = 0, 1, 2, \cdots, L-1$. The number of subcarriers is $N = 128$. The SNR of the pilot subcarriers as SNR $= \bar{P}/\sigma_w^2$. Identical average powers are assigned to both pilot and data subcarriers. Independent and identical distributed (i.i.d.) frequency offset estimation errors are assumed for $S \to R$, $R \to D$ and $S \to R \to D$ channels with a variance σ_e^2.

The normalized MSE for channel estimation is shown as a function of the power allocation ratio (see Figure 2.10). The MSEs of the $S \to R$ and $S \to D$ links are monotonically decreasing functions of α, whereas those for the $S \to R \to D$ (for the AF mode) and $R \to D$ (for the DF mode) links are monotonically increasing functions of α. Although the normalized MSE for the $R \to D$ link in DF mode is always smaller

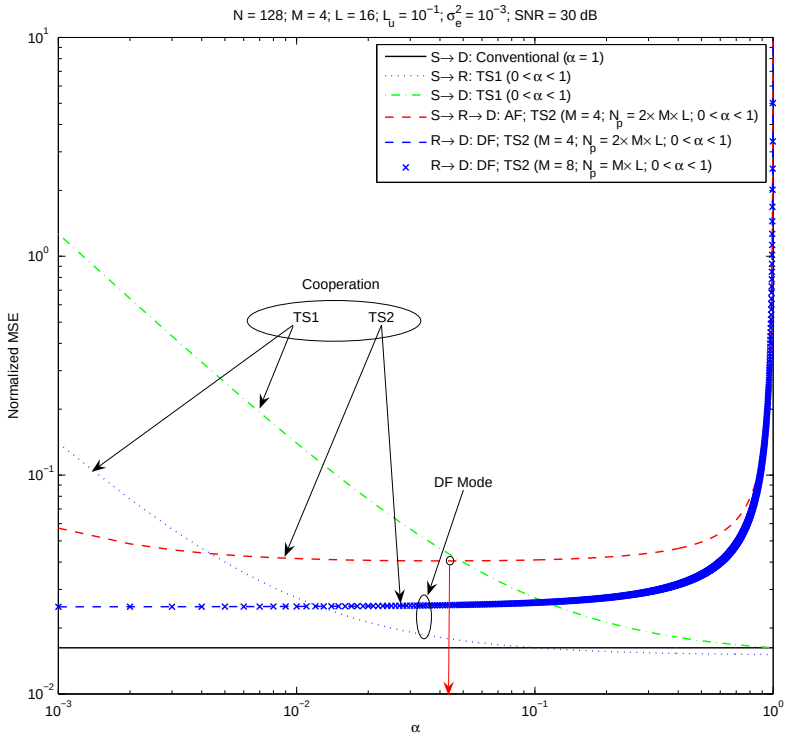

Figure 2.10: Normalized MSE of channel estimation in either conventional transmission ($\alpha = 1$) or the proposed cooperative transmission ($0 < \alpha < 1$).

than that for the $S \to R \to D$ link in AF mode for each α, this result does not mean that the DF mode always outperforms the AF mode in terms of the channel estimation error, because the estimation error in the $S \to R$ link for the DF mode also contributes some impairments to the decoding. However, in each relaying mode, an optimal α can be found to optimize the performance of the relay OFDM system.

The PEP of the proposed cooperative transmission with both frequency offset and channel estimation errors is illustrated in Figures 2.11 - 2.15. From Section 2.3.3, the channel estimation MSE is a function of the variance of the frequency offset estimation error (i.e., σ_e^2), so that σ_e^2 is used as the only parameter of impairment. For Figure 2.11 to Figure 2.13, $\mathcal{L}_u$ is set to 10^{-1}. All the eigenvalues of $\left(\bar{\mathbf{X}}_S - \bar{\mathbf{L}}_S\right)\left(\bar{\mathbf{X}}_S - \bar{\mathbf{L}}_S\right)^H$ are set

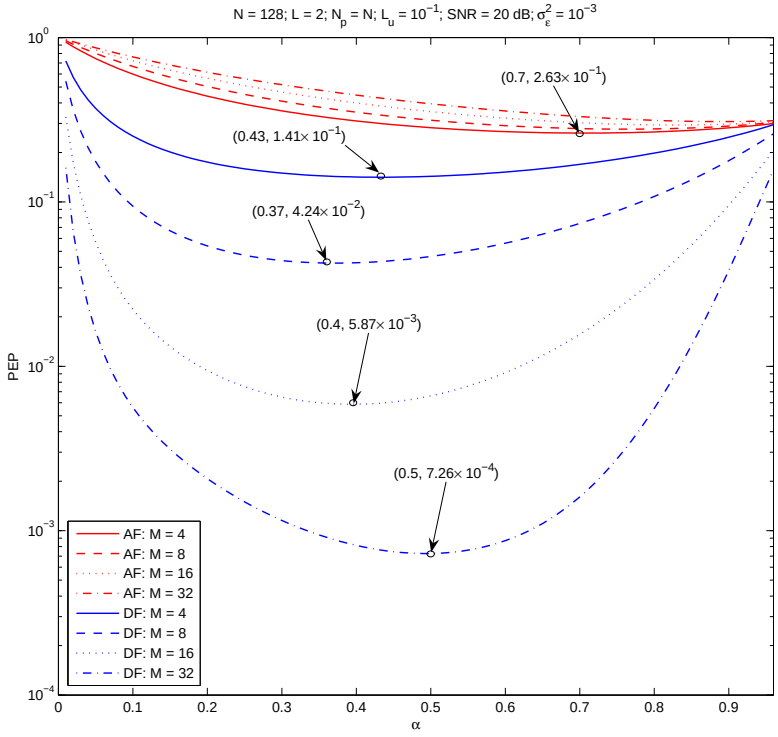

Figure 2.11: PEP of the proposed cooperative transmission with $L = 2$ and $\sigma_e^2 = 10^{-3}$.

to 1.

The performances of the AF and DF modes are compared for $L = 2$ and $\sigma_e^2 = 10^{-3}$ in Figure 2.11. Since the DF spatial diversity gain is proportional to the number of relays M, a larger number of active relays results in a lower PEP. In contrast, a larger number of AF relays results in a worse PEP performance. This difference can be explained as follows. In AF mode, interference and noise accumulate in each relay, and the interference due to frequency offset is not Gaussian when σ_e^2 is large. Since this interference cannot be averaged out by using more relays, the diversity gain will deteriorate by this process of accumulation. However, the DF mode eliminates the interference and noise. It is this interference-mitigation capability that guarantees that the DF mode will achieve a better PEP performance with more relays. When $M = 16$

and 32, the PEP performances of the AF mode are monotonically decreasing functions of the power-allocation ratio. That is, the AF mode cannot improve the diversity gain through cooperative transmission. However, when $M \leq 16$, it achieves a diversity gain. For each M, an optimal α that minimizes the PEP can be found. As compared to the AF mode, the DF mode can always achieve a diversity gain for each M.

Although the optimal PEP performance improves as the number of relays increases, increasing too many results in a degradation. This finding can be explained as follows. For a small number of relays, the performance is noise and/or interference limited, and the effective SINR of the $S \to R \to D$ channels can be improved by increasing the number of relays. As the number of relays increases, the power allocation to each relay decreases, and the cooperation becomes power limited once the number of relays is beyond a threshold. The effective SINR of the $S \to R \to D$ channels becomes lower in a power-limited environment if more relays are used.

For a fixed $\sigma_e^2 = 10^{-3}$, but the channel order is increasing to 4 and 16, the PEP performance is shown in Figures 2.12 and 2.13, respectively. When $L \leq 4$, the optimal (M, α) can always be found to make the DF mode outperform the AF mode in terms of PEP performance. Note that for each relaying mode, a larger channel order results in a higher interference and noise in the $S \to R$, $R \to D$, $S \to D$ and $S \to R \to D$ channels. This higher interference and noise degrade the SINR. However, for a given number of relays, since a $(2L - 1)$-order multipath diversity gain can be obtained in the AF mode [see (2.38)], this gain may compensate for the performance loss due to SINR degradation. When the channel order is not large (e.g., in this simulation, $L \leq 16$ is required), the multipath diversity gain dominates the performance of the AF mode, and the PEP performance may be improved as the channel order increases. If the channel order continuously increases (e.g., to 16), the cooperation channel becomes power-limited, and the SINR degradation in each tap will deteriorate the multipath diversity gain. Increasing the channel order degrades the PEP performance in the DF mode, because this mode can obtain only a L-order multipath diversity gain, as shown

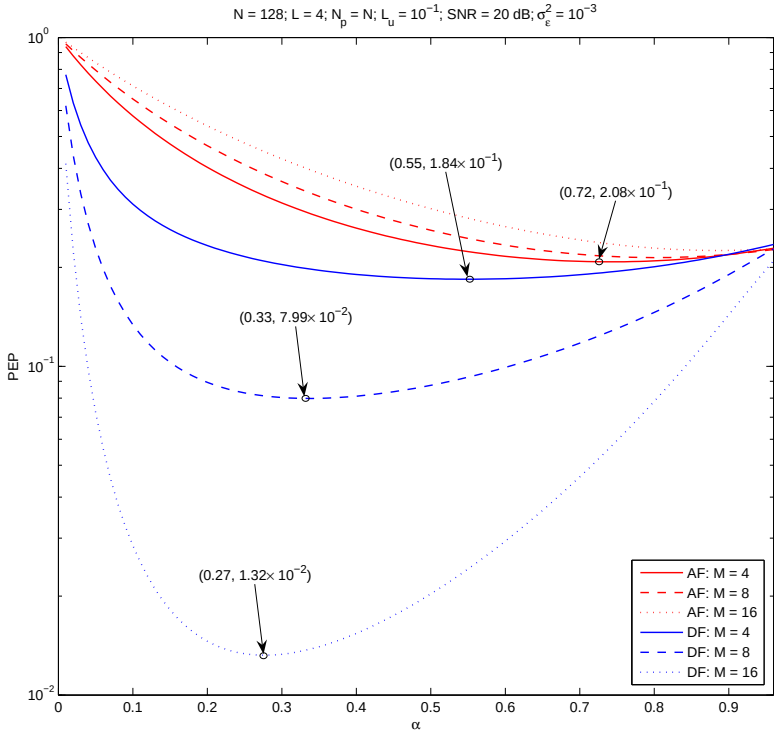

Figure 2.12: PEP of the proposed cooperative transmission with $L = 4$ and $\sigma_e^2 = 10^{-3}$.

by (2.42).

The PEP performance as a function of σ_e^2 is shown in Figure 2.14, which considers ($L = 4$, $M = 16$) and ($L = 8$, $M = 8$). Both AF and DF mode PEPs monotonically increase with σ_e^2. For each number of relays, the DF mode always outperforms the AF mode for a small σ_e^2, although both modes approach the same PEP performance for large σ_e^2 (i.e., the system is interference rather than noise limited, and the diversity gain cannot be improved through cooperation).

The PEP performances as functions of SNR are shown in Figure 2.15 for $L = 4$, $M = 16$, and $\sigma_e^2 = 10^{-2}$ and 10^{-3}. Since the system is noise limited for a small σ_e^2 ($\sigma_e^2 = 10^{-3}$), the relays realize the spatial diversity gain. The PEP performance of the DF mode is about 9 dB better than that of the AF mode at an error rate of 5×10^{-3}.

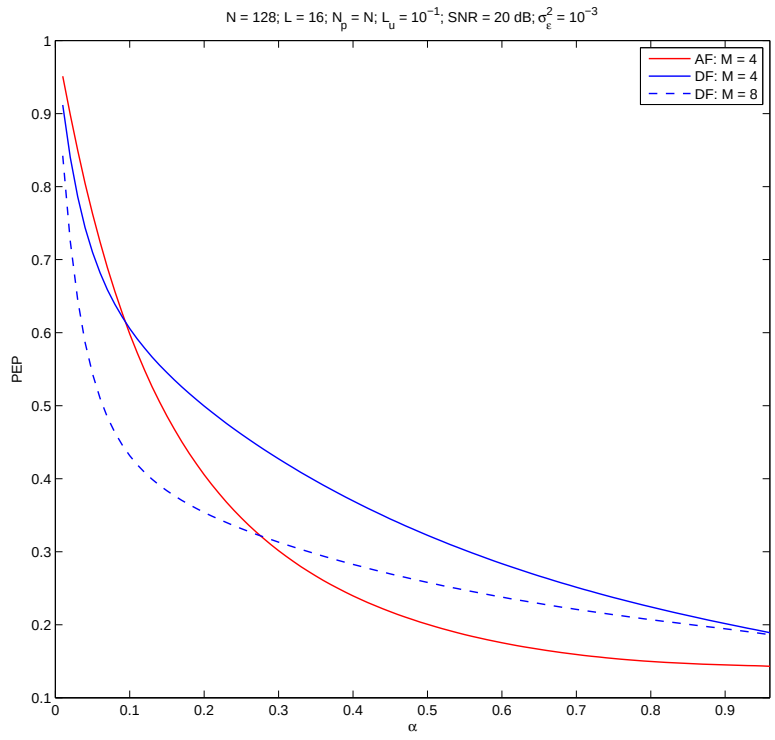

Figure 2.13: PEP of the proposed cooperative transmission with $L = 16$ and $\sigma_e^2 = 10^{-3}$.

As σ_e^2 increases to 10^{-2}, the system becomes interference limited, and an error floor appears in both the AF and the DF modes. In this environment, the performance increases to about 11.3 dB ; i.e., the DF mode has a higher interference-mitigation capability than the AF mode.

2.6 Conclusions

Channel estimation for cooperative AF or DF OFDM systems with frequency offsets has been considered. A two-time-slot cooperative channel-estimation protocol has been proposed. For a given channel order L, the maximum number of relays operating in the AF and the DF modes were shown to be $\lfloor N/(2L-1) \rfloor$ and $\lfloor N/L \rfloor$, respectively.

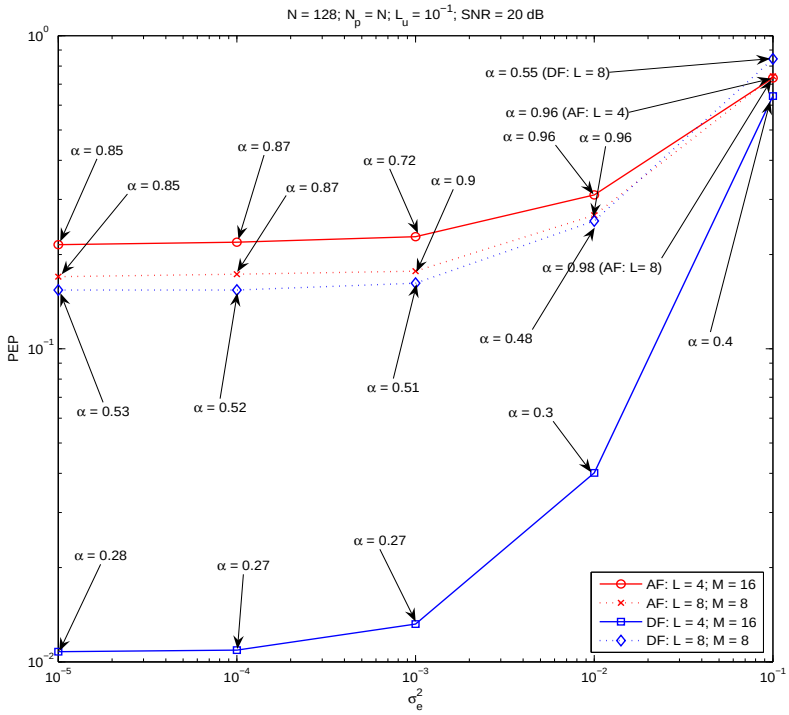

Figure 2.14: PEP of the proposed cooperative transmission as a function of σ_e^2 with $L = 4, 8$.

As a result, the latter achieves more diversity gain than the former. The PEP performance of an orthogonal block code in the proposed cooperative transmission was also evaluated by considering both the frequency offset and channel-estimation errors. The optimal power allocation between the source and a set of relays (AF or DF) was derived to minimize the PEP. For both relaying modes, a larger channel order results in increased interference and noise, which degrades the SINR. Since the AF mode can realize a $(2L - 1)$-order multipath diversity gain, it performs better as the channel order increases provided that the channel order is not too large. Unlike AF relays, DF relays will suffer a PEP performance degradation when the channel order increases, because the L-order multipath diversity gain can not compensate for the SINR loss. Interference will increase if more relays are used in the AF mode, which results in

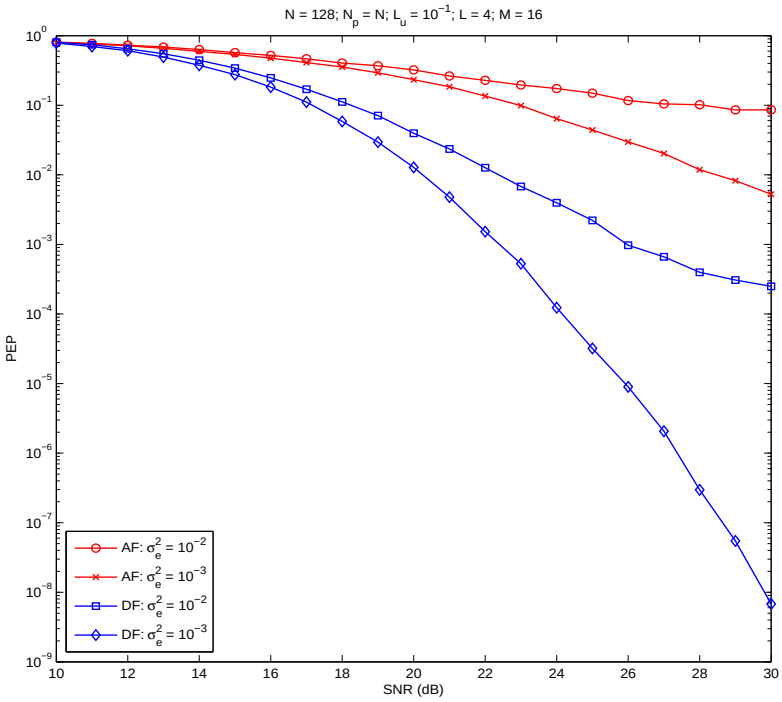

Figure 2.15: PEP of the proposed cooperative transmission as a function of SNR with $L = 4$, $M = 16$ and $\sigma_e^2 = 10^{-2}, 10^{-3}$.

degradation of performance. The interference-mitigation capability of the DF mode improves performance by allowing the use more relays, and when the channel order is smaller than 16, they outperforms the AF mode in terms of PEP.

Chapter 3

BER of MIMO OFDM Systems with Frequency Offset and Channel Estimation Errors

The BER of MIMO OFDM systems with frequency offset and channel estimation errors is analyzed in this chapter [101]. ICI and inter-antenna interference (IAI) due to the residual frequency offsets are analyzed, and the average SINR is derived. The BER of MIMO OFDM is derived as an infinite series. Two receiver combining techniques to improve the BER are MRC and EGC. Their BERs are also derived.

3.1 Introduction

MIMO OFDM faces several technical challenges. First, these systems are highly sensitive to the frequency offset, which introduces ICI and thereby significantly degrades the system performance. Second, channel estimation becomes increasingly difficult when the number of antennas increases. For these reasons, many frequency offset and channel estimators have been proposed for MIMO OFDM systems [113–116]. For SISO OFDM, several estimators of channel, frequency offset or both have already been developed [13,52,117]. The frequency offset estimation schemes for MIMO OFDM proposed in [113,114] use training sequences composed of repeated data. Optimal training signal design for MIMO OFDM channel estimation has been considered in [115]. A recursive channel and frequency offset estimator for MIMO OFDM is discussed in [116].

Previously, the performance degradation due to frequency offset is evaluated in terms of SINR for SISO OFDM systems [13, 16, 118]. Although such an SINR analysis has the merit of being mathematically simple, it is obvious that the BER analysis characterizes the performance degradation more accurately [99, 100, 119, 120]. The ICI is approximated to be a Gaussian RV in [119] to obtain an analytical BER expression for AWGN channels. A more accurate BER expression that exploits the moments of the ICI distribution has been proposed in [120]. The characteristic functions method is used in [100] to derive exact BER of systems with frequency offset and AWGN. For multipath fading channels, the BER is evaluated in [99] also by exploiting the Gaussian approximation of the ICI. However, [99] assumes that the channel is perfectly known at the receiver and that the frequency offset estimation error is negligible. For MIMO OFDM systems, the BER has been analyzed with channel estimation errors in [121].

Although some estimators are highly accurate, their performance ultimately cannot exceed the CRLB [122]. Both the residual frequency offset and channel estimation errors after frequency offset correction and channel equalization degrade the system performance. The BER analysis for MIMO OFDM with both frequency offset and channel estimation errors is thus motivated. This analysis will use the statistics of the residual frequency offset and channel estimation errors.

3.2 MIMO OFDM Signal Model

The structure of a MIMO OFDM link with N_t transmit antennas and N_r receive antennas has been shown in Figure 1.5 in Chapter 1. The transmitter maps the source bit stream to several streams of complex modulation symbols from a complex constellation such as PSK or QAM. A $N \times 1$ vector $\mathbf{x}_i$ is used to represent the frequency-domain symbols sent by the i-th transmit antenna, where $i \in \{1, 2, \cdots, N_t\}$. The time-domain OFDM symbols for the i-th transmit antenna is generated by taking IDFT of $\mathbf{x}_i$, i.e., $\mathbf{m}_i = \sqrt{\frac{E_s}{N_t}}\mathbf{F}\mathbf{x}_i$, where E_s is the total transmit power, and $\mathbf{F}$ is the $N \times N$ IDFT matrix.

Each entry of $\mathbf{x}_i$ is assumed to be i.i.d. RV with mean zero and unit variance; i.e., $\sigma_x^2 = \mathbb{E}\{|\mathbf{x}_i[n]|^2\} = 1$ for $1 \le i \le N_t$ and $0 \le n \le N-1$. Then, a CP is inserted on each $\mathbf{x}_i$ to mitigate ISI. Finally, the data frame is converted to an RF signal for transmission on each transmit antenna.

The discrete channel response between the k-th receive antenna and i-th transmit antenna is $\mathbf{h}_{k,i} = [h_{k,i}(0), h_{k,i}(1), \cdots, h_{k,i}(L_{k,i}-1), \mathbf{0}^T_{L_{max}-L_{k,i}}]^T$, where $L_{k,i}$ is the maximum delay between the i-th transmit and the k-th receive antennas, and $L_{max} = \max\{L_{k,i} : 1 \le i \le N_t, 1 \le k \le N_r\}$. Uncorrelated taps are assumed for each antenna pair (k,i); i.e., $\mathbb{E}\{h^*_{k,i}(m)h_{k,i}(n \ne m)\} = 0$ when $n \ne m$. The corresponding frequency-domain channel attenuation matrix is given by $\mathbf{H}_{k,i} = \text{diag}\left\{H^{(0)}_{k,i}, H^{(1)}_{k,i}, \cdots, H^{(N-1)}_{k,i}\right\}$ with $H^{(n)}_{k,i} = \sum_{d=0}^{L_{k,i}-1} h_{k,i}(d)e^{-\jmath\frac{2\pi nd}{N}}$ representing the channel attenuation at the n-th subcarrier. The channel power profiles are normalized as $\sum_{d=0}^{L_{k,i}-1} |h_{k,i}(d)|^2 = 1$ for all (k,i). The covariance of channel frequency response is given by

$$C_{H^{(n)}_{k,i}H^{(l)}_{p,q}} = \sum_{d=0}^{L_{max}-1} \mathbb{E}\left\{h^*_{k,i}(d)h_{p,q}(d)\right\} e^{-\frac{\jmath 2\pi d(l-n)}{N}} \quad 0 \le d \le L_{max}, 0 \le l, n \le N-1. \tag{3.1}$$

$\varepsilon_{k,i}$ is used to represent the normalized frequency offset between the i-th transmit and k-th receive antenna. The frequency offsets $\varepsilon_{k,i}$ for all (k,i) are modeled as zero-mean i.i.d. RVs. By considering the channel gains and frequency offsets, the received vector can be represented as

$$\mathbf{y} = [\mathbf{y}_1^T, \mathbf{y}_2^T, \cdots, \mathbf{y}_{N_r}^T]^T, \tag{3.2}$$

where

$$\mathbf{y}_k = \sqrt{\frac{E_s}{N_t}} \sum_{i=1}^{N_t} \mathbf{E}_{k,i}\mathbf{F}\mathbf{H}_{k,i}\mathbf{x}_i + \mathbf{w}_k$$

with $\mathbf{E}_{k,i} = \text{diag}\left\{1, e^{\jmath\frac{2\pi\varepsilon_{k,i}}{N}}, \ldots, e^{\jmath\frac{2\pi\varepsilon_{k,i}(N-1)}{N}}\right\}$, and $\mathbf{w}_k$ is a vector of AWGN with $\mathbf{w}_k[n] \sim \mathcal{CN}(0, \sigma_w^2)$. Note that the channel state information is available at the receiver, but not at the transmitter. Consequently, the transmit power is equally allocated among all the transmit antennas.

3.3 SINR Analysis in MIMO OFDM Systems

Spatial-multiplexing MIMO will be treated, where independent data streams are mapped to distinct OFDM symbols and are transmitted simultaneously from transmit antennas. The received vector $\mathbf{y}_k$ at the k-th receive antenna is thus a superposition of the transmit signals from all the N_t transmit antennas. When demodulating $\mathbf{x}_i$, the signals from the transmit antennas other than the i-th transmit antenna constitute IAI.

Assume that $\varepsilon_{k,i}$ and $\mathbf{H}_{k,j}$ for each $(1 \leq j \leq N_t, j \neq i)$ have been estimated imperfectly; i.e., $\hat{\varepsilon}_{k,i} = \varepsilon_{k,i} + \Delta\varepsilon_{k,i}$ and $\hat{\mathbf{H}}_{k,j} = \mathbf{H}_{k,j} + \Delta\mathbf{H}_{k,j}$, where $\Delta\varepsilon_{k,j}$ and $\Delta\mathbf{H}_{k,j} = \text{diag}\left\{\Delta H_{k,j}^{(0)}, \cdots, \Delta H_{k,j}^{(N-1)}\right\}$ are estimation errors of $\varepsilon_{k,j}$ and $\mathbf{H}_{k,j}$ ($\Delta H_{k,j}^{(n)} = \hat{H}_{k,j}^{(n)} - H_{k,j}^{(n)}$ represents the estimation error of $H_{k,j}^{(n)}$). Assume that each $\mathbf{x}_{j\neq i}$ is demodulated with negligible error. After estimating $\varepsilon_{k,i}$, i.e., $\hat{\varepsilon}_{k,i} = \varepsilon_{k,i} + \Delta\varepsilon_{k,i}$, $\varepsilon_{k,i}$ can be compensated for, and $\mathbf{x}_i$ can be demodulated as

$$\begin{aligned}
\mathbf{r}_{k,i} &= \mathbf{F}^H \hat{\mathbf{E}}_{k,i}^H \left(\mathbf{y}_k - \sqrt{\frac{E_s}{N_t}} \sum_{j=1, j\neq i}^{N_t} \hat{\mathbf{E}}_{k,j} \mathbf{F} \hat{\mathbf{H}}_{k,j} \mathbf{x}_j \right) \\
&= \sqrt{\frac{E_s}{N_t}} \underbrace{\mathbf{F}^H \hat{\mathbf{E}}_{k,i}^H \mathbf{E}_{k,i} \mathbf{F} \mathbf{H}_{k,i} \mathbf{x}_i}_{\mathbf{s}_{k,i}} \\
&\quad + \underbrace{\sqrt{\frac{E_s}{N_t}} \sum_{j=1, j\neq i}^{N_t} \mathbf{F}^H \hat{\mathbf{E}}_{k,i}^H \left(\mathbf{E}_{k,j} \mathbf{F} \mathbf{H}_{k,j} - \hat{\mathbf{E}}_{k,j} \mathbf{F} \hat{\mathbf{H}}_{k,j} \right) \mathbf{x}_j}_{\boldsymbol{\Upsilon}_{k,i}} + \underbrace{\mathbf{F}^H \hat{\mathbf{E}}_{k,i}^H \mathbf{w}_k}_{\tilde{\mathbf{w}}_{k,i}},
\end{aligned} \tag{3.3}$$

where $\hat{\mathbf{E}}_{k,j}$ is derived from $\mathbf{E}_{k,j}$ by replacing $\varepsilon_{k,j}$ with $\hat{\varepsilon}_{k,j}$, and $\boldsymbol{\Upsilon}_{k,i}$ and $\tilde{\mathbf{w}}_{k,i}$ are the residual IAI and AWGN components of $\mathbf{r}_{k,i}$.

3.3.1 SINR Analysis without Receiver Combining

The SINR is derived for the i-th transmit antenna signal at the k-th receive antenna. The signals transmitted by antennas other than the i-th antenna are interference, which would be eliminated before demodulating the desired signal of the i-th transmit antenna. Existing interference cancelation algorithms [123–126], can be applied here.

Based on (3.3), the n-th subcarrier $(0 \le n \le N-1)$ of the i-th transmit antenna can be demodulated as

$$\begin{aligned}
\mathbf{r}_{k,i}[n] &= \sqrt{\frac{E_s}{N_t}}\mathbf{s}_{k,i}[n] + \boldsymbol{\Upsilon}_{k,i}[n] + \tilde{\mathbf{w}}_{k,i}[n] \\
&= \sqrt{\frac{E_s}{N_t}} m_{k,i}^{(n)} H_{k,i}^{(n)} \mathbf{x}_i[n] + \underbrace{\sqrt{\frac{E_s}{N_t}} \sum_{l \neq n} m_{k,i}^{(l)} H_{k,i}^{(l)} \mathbf{x}_i[l]}_{\eta_{k,i}^{(n)} = H_{k,i}^{(n)} \alpha_{k,i}^{(n)} + \beta_{k,i}^{(n)}} \\
&\quad + \underbrace{\sqrt{\frac{E_s}{N_t}} \sum_{j=1, j\neq i}^{N_t} m_{k,j}^{(n)} H_{k,j}^{(n)} \mathbf{x}_j[n]}_{\lambda_{k,i}^{(n)}} - \underbrace{\sqrt{\frac{E_s}{N_t}} \sum_{j=1, j\neq i}^{N_t} \hat{m}_{k,j}^{(n)} \hat{H}_{k,j}^{(n)} \mathbf{x}_j[n]}_{\hat{\lambda}_{k,i}^{(n)}} \\
&\quad + \underbrace{\sqrt{\frac{E_s}{N_t}} \sum_{l \neq n} \sum_{j=1, j\neq i}^{N_t} m_{k,j}^{(l)} H_{k,j}^{(l)} \mathbf{x}_j[l]}_{\xi_{k,i}^{(n)}} - \underbrace{\sqrt{\frac{E_s}{N_t}} \sum_{l \neq n} \sum_{j=1, j\neq i}^{N_t} \hat{m}_{k,j}^{(l)} \hat{H}_{k,j}^{(l)} \mathbf{x}_j[l]}_{\hat{\xi}_{k,i}^{(n)}} + \tilde{\mathbf{w}}_{k,i}[n] \\
&= \sqrt{\frac{E_s}{N_t}} m_{k,i}^{(n)} H_{k,i}^{(n)} \mathbf{x}_i[n] + H_{k,i}^{(n)} \alpha_{k,i}^{(n)} + \beta_{k,i}^{(n)} + \Delta\lambda_{k,i}^{(n)} + \Delta\xi_{k,i}^{(n)} + \tilde{\mathbf{w}}_{k,i}[n],
\end{aligned} \tag{3.4}$$

where

$$\begin{aligned}
m_{k,i}^{(l)} &= \frac{\sin\left[\pi\left(l - n - \Delta\varepsilon_{k,i}\right)\right]}{N \sin\left[\frac{\pi(l-n-\Delta\varepsilon_{k,i})}{N}\right]} e^{\frac{\jmath\pi(N-1)(l-n-\Delta\varepsilon_{k,i})}{N}}, \\
m_{k,j\neq i}^{(l)} &= \frac{\sin\left[\pi\left(l - n + \varepsilon_{k,j} - \hat{\varepsilon}_{k,i}\right)\right]}{N \sin\left[\frac{\pi(l-n+\varepsilon_{k,j}-\hat{\varepsilon}_{k,i})}{N}\right]} e^{\frac{\jmath\pi(N-1)(l-n+\varepsilon_{k,j}-\hat{\varepsilon}_{k,i})}{N}}, \\
\hat{m}_{k,j\neq i}^{(l)} &= \frac{\sin\left[\pi\left(l - n + \hat{\varepsilon}_{k,j} - \hat{\varepsilon}_{k,i}\right)\right]}{N \sin\left[\frac{\pi(l-n+\hat{\varepsilon}_{k,j}-\hat{\varepsilon}_{k,i})}{N}\right]} e^{\frac{\jmath\pi(N-1)(l-n+\hat{\varepsilon}_{k,j}-\hat{\varepsilon}_{k,i})}{N}}, \quad 0 \le l \le N-1.
\end{aligned}$$

$\eta_{k,i}^{(n)}$ is decomposed as $\eta_{k,i}^{(n)} = H_{k,i}^{(n)}\alpha_{k,i}^{(n)} + \beta_{k,i}^{(n)}$, which is the ICI contributed by subcarriers other than the n-th subcarrier of transmit antenna i. We can easily prove that $\alpha_{k,i}^{(n)}$ and $\beta_{k,i}^{(n)}$ are zero-mean RVs subject to the following assumptions.

1. $\varepsilon_{k,i}$ is an i.i.d. RV with mean zero and variance σ_ϵ^2 for each (k,i).
2. $\Delta\varepsilon_{k,i}$ is an i.i.d. RV with mean zero and variance σ_{res}^2 for each (k,i).
3. $H_{k,i}^{(n)} \sim \mathcal{CN}(0,1)$ for each (k,i,n).

4. $\Delta H_{k,i}^{(n)}$ is an i.i.d. RV with mean zero and variance $\sigma_{\Delta H}^2$ for each (k,i,n).

5. $\varepsilon_{k,i}$, $\Delta\varepsilon_{k,i}$, $H_{k,i}^{(n)}$ and $\Delta H_{k,i}^{(n)}$ are independent of each other for each (k,i).

Given these assumptions, $\mathrm{Var}\left\{\alpha_{k,i}^{(n)}\right\}$ and $\mathrm{Var}\left\{\beta_{k,i}^{(n)}\right\}$ are derived, respectively, as

$$\begin{aligned}\mathrm{Var}\left\{\alpha_{k,i}^{(n)}\right\} &= \frac{E_s}{N_t}\cdot\mathbb{E}\left\{\left|C^{-1}_{H_{k,i}^{(n)}H_{k,i}^{(n)}}\right|^2\sum_{l\neq n}\left|m_{k,i}^{(l)}C_{H_{k,i}^{(l)}H_{k,i}^{(n)}}\right|^2\right\}\\ &\cong \frac{E_s}{N_t}\cdot\mathbb{E}\left\{\sum_{l\neq n}\left|\frac{\sin(\pi\Delta\varepsilon_{k,i})}{N\sin\left[\frac{\pi(l-n)}{N}\right]}\right|^2\cdot\left|\sum_{d=0}^{L_{max}-1}\mathbb{E}\left\{|h_{k,i}(d)|^2\right\}e^{-\frac{\jmath 2\pi d(l-n)}{N}}\right|^2\right\} \qquad (3.5)\\ &= \frac{\pi^2\sigma_{res}^2E_s}{N_t}\sum_{l\neq n}\frac{\left|C_{H_{k,i}^{(n)}H_{k,i}^{(l)}}\right|^2}{N^2\sin^2\left[\frac{\pi(l-n)}{N}\right]}\end{aligned}$$

and

$$\begin{aligned}\mathrm{Var}\left\{\beta_{k,i}^{(n)}\right\} &= \frac{E_s}{N_t}\cdot\mathbb{E}\left\{\sum_{l\neq n}\left|m_{k,i}^{(l)}\right|^2\left(C_{H_{k,i}^{(l)}H_{k,i}^{(l)}}-C^{-1}_{H_{k,i}^{(n)}H_{k,i}^{(n)}}\left|C_{H_{k,i}^{(l)}H_{k,i}^{(n)}}\right|^2\right)\right\}\\ &\cong \frac{\pi^2\sigma_{res}^2E_s}{3N_t}-\mathrm{Var}\left\{\alpha_{k,i}^{(n)}\right\},\end{aligned} \qquad (3.6)$$

where $C_{H_{k,i}^{(l)}H_{k,i}^{(n)}}$ is given by (3.1). $\Delta\lambda_{k,i}^{(n)}=\lambda_{k,i}^{(n)}-\hat{\lambda}_{k,i}^{(n)}$ is the interference contributed by the n-th subcarrier of the interfering transmit antennas, i.e., the co-subcarrier inter-antenna-interference (CSIAI), and $\Delta\xi_{k,i}^{(n)}=\xi_{k,i}^{(n)}-\hat{\xi}_{k,i}^{(n)}$ is the ICI contributed by the subcarriers other than the n-th subcarrier of the interfering transmit antennas, i.e., the inter-carrier-inter-antenna-interference (ICIAI). The demodulation of $\mathbf{x}_i[n]$ is degraded by either $\eta_{k,i}^{(n)}$ or IAI (CSIAI plus ICIAI). Assume that the integer-part of frequency offset has been estimated and corrected, and only the fractional-part frequency offset offset is considered. Considering small frequency offsets, the following requirements are assumed to be satisfied:

1. $|\varepsilon_{k,j}|\ll 1$ for all (k,j).

2. $|\hat{\varepsilon}_{k,i}|+|\varepsilon_{k,j}|<1$ for all (k,i,j).

3. $|\hat{\varepsilon}_{k,i}|+|\hat{\varepsilon}_{k,j}|<1$ for all (k,i,j).

Condition 1 requires that each frequency offset should be much smaller than 1, and conditions 2 and 3 require that the sum of any two frequency offsets (or the frequency offset estimation results) should not exceed 1. The last two conditions are satisfied only if the estimation error does not exceed 0.5. If all these three conditions are satisfied simultaneously, we can represent $\lambda_{k,i}^{(n)}$, $\hat{\lambda}_{k,i}^{(n)}$, $\xi_{k,i}^{(n)}$ and $\hat{\xi}_{k,i}^{(n)}$ as

$$\lambda_{k,i}^{(n)} = \sqrt{\frac{E_s}{N_t}} \sum_{j=1,j\neq i}^{N_t} m_{k,j}^{(n)} H_{k,j}^{(n)} \mathbf{x}_j[n] = \sqrt{\frac{E_s}{N_t}} \sum_{j=1,j\neq i}^{N_t} \frac{\sin\left[\pi\left(\varepsilon_{k,j}-\hat{\varepsilon}_{k,i}\right)\right]}{N\sin\left[\frac{\pi\left(\varepsilon_{k,j}-\hat{\varepsilon}_{k,i}\right)}{N}\right]} H_{k,j}^{(n)} \mathbf{x}_j[n], \tag{3.7}$$

$$\hat{\lambda}_{k,i}^{(n)} = \sqrt{\frac{E_s}{N_t}} \sum_{j=1,j\neq i}^{N_t} \hat{m}_{k,j}^{(n)} \hat{H}_{k,j}^{(n)} \mathbf{x}_j[n] = \sqrt{\frac{E_s}{N_t}} \sum_{j=1,j\neq i}^{N_t} \frac{\sin\left[\pi\left(\hat{\varepsilon}_{k,j}-\hat{\varepsilon}_{k,i}\right)\right]}{N\sin\left[\frac{\pi\left(\hat{\varepsilon}_{k,j}-\hat{\varepsilon}_{k,i}\right)}{N}\right]} \hat{H}_{k,j}^{(n)} \mathbf{x}_j[n], \tag{3.8}$$

$$\begin{aligned} \xi_{k,i}^{(n)} &= \sqrt{\frac{E_s}{N_t}} \sum_{l\neq n} \sum_{j=1,j\neq i}^{N_t} m_{k,j}^{(l)} H_{k,j}^{(l)} \mathbf{x}_j[l] \\ &\cong \sqrt{\frac{E_s}{N_t}} \sum_{l\neq n} \sum_{j=1,j\neq i}^{N_t} \frac{(-1)^{(l-n)}\sin\left[\pi\left(\varepsilon_{k,j}-\hat{\varepsilon}_{k,i}\right)\right]}{N\sin\left[\frac{\pi(l-n)}{N}\right]} e^{\frac{j\pi(N-1)(l-n)}{N}} H_{k,j}^{(l)} \mathbf{x}_j[l], \end{aligned} \tag{3.9}$$

and

$$\begin{aligned} \hat{\xi}_{k,i}^{(n)} &= \sqrt{\frac{E_s}{N_t}} \sum_{l\neq n} \sum_{j=1,j\neq i}^{N_t} \hat{m}_{k,j}^{(l)} \hat{H}_{k,j}^{(l)} \mathbf{x}_j[l] \\ &= \sqrt{\frac{E_s}{N_t}} \sum_{l\neq n} \sum_{j=1,j\neq i}^{N_t} \frac{\sin\left[\pi\left(l-n+\hat{\varepsilon}_{k,j}-\hat{\varepsilon}_{k,i}\right)\right]}{N\sin\left[\frac{\pi(l-n+\hat{\varepsilon}_{k,j}-\hat{\varepsilon}_{k,i})}{N}\right]} e^{\frac{j\pi(N-1)(l-n)}{N}} \hat{H}_{k,j}^{(l)} \mathbf{x}_j[l] \\ &\cong \sqrt{\frac{E_s}{N_t}} \sum_{l\neq n} \sum_{j=1,j\neq i}^{N_t} \frac{(-1)^{(l-n)}\sin\left[\pi\left(\hat{\varepsilon}_{k,j}-\hat{\varepsilon}_{k,i}\right)\right]}{N\sin\left[\frac{\pi(l-n)}{N}\right]} e^{\frac{j\pi(N-1)(l-n)}{N}} \hat{H}_{k,j}^{(l)} \mathbf{x}_j[l]. \end{aligned} \tag{3.10}$$

Therefore, the interference due to the n-th subcarrier of transmit antenna is

$$\begin{aligned} \Delta\lambda_{k,i}^{(n)} &= \lambda_{k,i}^{(n)} - \hat{\lambda}_{k,i}^{(n)} \\ &= \sqrt{\frac{E_s}{N_t}} \sum_{j=1,j\neq i}^{N_t} \left[\frac{\pi^2\left(\varepsilon_{k,j}-\hat{\varepsilon}_{k,i}+\frac{\Delta\varepsilon_{k,j}}{2}\right) H_{k,j}^{(n)} \Delta\varepsilon_{k,j}}{3} - \left(1-\frac{\pi^2\left(\hat{\varepsilon}_{k,j}-\hat{\varepsilon}_{k,i}\right)^2}{6}\right) \Delta H_{k,j}^{(n)} \right] \mathbf{x}_j[n] \\ &\quad + o(\Delta\varepsilon_{k,j}, \Delta H_{k,j}) \end{aligned} \tag{3.11}$$

and

$$\begin{aligned}\Delta\xi_{k,i}^{(n)} &= \xi_{k,i}^{(n)} - \hat{\xi}_{k,i}^{(n)} \\ &= \sqrt{\frac{E_s}{N_t}} \sum_{l\neq n} \sum_{j=1,j\neq i}^{N_t} \frac{(-1)^{l-n+1} e^{\frac{\jmath\pi(N-1)(l-n)}{N}}}{N \sin\left[\frac{\pi(l-n)}{N}\right]} \\ &\quad \cdot \left[\pi \cos\left(\pi\left(\varepsilon_{k,j} - \hat{\varepsilon}_{k,i} + \frac{\Delta\varepsilon_{k,j}}{2}\right)\right) H_{k,j}^{(l)} \Delta\varepsilon_{k,j} + \sin\left(\pi\left(\hat{\varepsilon}_{k,j} - \hat{\varepsilon}_{k,i}\right)\right) \Delta H_{k,j}^{(l)}\right] \mathbf{x}_j[l] \\ &\quad + o(\Delta\varepsilon_{k,j}, \Delta H_{k,j})\end{aligned} \tag{3.12}$$

with $o(\Delta\varepsilon_{k,j}, \Delta H_{k,j})$ representing the higher order item of $\Delta\varepsilon_{k,j}$ and $\Delta H_{k,j}$. It is easy to show that $\Delta\lambda_{k,i}^{(n)}$ and $\Delta\xi_{k,i}^{(n)}$ are zero-mean RVs, and that their variances are given by

$$\begin{aligned}\mathbb{E}\left\{\left|\Delta\lambda_{k,i}^{(n)}\right|^2\right\} &= \frac{E_s}{N_t} \sum_{j=1,j\neq i}^{N_t} \mathbb{E}\left\{\left[\frac{\pi^2\left(\varepsilon_{k,j} - \hat{\varepsilon}_{k,i} + \frac{\Delta\varepsilon_{k,j}}{2}\right) H_{k,j}^{(n)} \Delta\varepsilon_{k,j}}{3}\right]^2\right\} \\ &\quad + \frac{E_s}{N_t} \sum_{j=1,j\neq i}^{N_t} \mathbb{E}\left\{\left[\left(1 - \frac{\pi^2\left(\hat{\varepsilon}_{k,j} - \hat{\varepsilon}_{k,i}\right)^2}{6}\right) \Delta H_{k,j}^{(n)}\right]^2\right\} \\ &\cong \frac{(N_t-1)\pi^4 E_s}{9N_t}\left(2\sigma_\epsilon^2\sigma_{res}^2 + \sigma_{res}^4 + \frac{\mathbb{E}\left\{\Delta\varepsilon_{k,j}^4\right\}}{4}\right) \\ &\quad + \frac{(N_t-1)E_s}{N_t} \cdot \sigma_{\Delta H}^2 \cdot \left[1 + \frac{\pi^4\left(\mathbb{E}\left\{\varepsilon_{k,j}^4\right\} + 8\sigma_\epsilon^2\sigma_{res}^2 + 2\sigma_\epsilon^4 + 2\sigma_{res}^4\right)}{18} - \frac{2\pi^2\left(\sigma_\epsilon^2 + \sigma_{res}^2\right)}{3}\right]\end{aligned} \tag{3.13}$$

and

$$\begin{aligned}\mathbb{E}\left\{\left|\Delta\xi_{k,i}^{(n)}\right|^2\right\} &= \frac{E_s}{N_t} \sum_{l\neq n} \sum_{j=1,j\neq i}^{N_t} \frac{1}{N^2 \sin^2\left[\frac{\pi(l-n)}{N}\right]} \\ &\quad \cdot \mathbb{E}\left\{\left[\pi \cos\left(\pi\left(\varepsilon_{k,j} - \hat{\varepsilon}_{k,i} + \frac{\Delta\varepsilon_{k,j}}{2}\right)\right) H_{k,j}^{(l)} \Delta\varepsilon_{k,j} + \sin\left(\pi\left(\hat{\varepsilon}_{k,j} - \hat{\varepsilon}_{k,i}\right)\right) \Delta H_{k,j}^{(l)}\right]^2\right\} \\ &\cong \frac{(N_t-1)E_s}{3N_t}\left[\pi^2\sigma_{res}^2 - \pi^4\left(2\sigma_\epsilon^2\sigma_{res}^2 + \sigma_{res}^4 + \frac{\mathbb{E}\left\{\Delta\varepsilon_{k,j}^4\right\}}{4}\right)\right] \\ &\quad + \frac{2(N_t-1)\pi^2 E_s}{3N_t}\left(\sigma_\epsilon^2 + \sigma_{res}^2\right)\sigma_{\Delta H}^2.\end{aligned} \tag{3.14}$$

After averaging out frequency offset $\varepsilon_{k,i}$, frequency offset estimation error $\Delta\varepsilon_{k,i}$ and channel estimation error $\Delta H_{k,i}^{(n)}$ for each (k,i), the average SINR of $\mathbf{r}_{k,i}[n]$ (parameterized by only $H_{k,i}^{(n)}$) is

$$\begin{aligned}
&\bar{\gamma}_{k,i}\left(n\middle|H_{k,i}^{(n)}\right) \\
&\quad\triangleq \frac{\mathbb{E}\left\{\left|\sqrt{\frac{E_s}{N_t}}m_{k,i}^{(n)}H_{k,i}^{(n)}\mathbf{x}_i[n]\right|^2\right\}}{\mathbb{E}\left\{\left|\eta_{k,i}^{(n)}+\Delta\lambda_{k,i}^{(n)}+\Delta\xi_{k,i}^{(n)}+\tilde{\mathbf{w}}_{k,i}[n]\right|^2\right\}} \\
&\quad\cong \frac{\frac{E_s}{N_t}\cdot\sigma_m^2\cdot\left|H_{k,i}^{(n)}\right|^2}{\left|H_{k,i}^{(n)}\right|^2\cdot\mathrm{Var}\left\{\alpha_{k,i}^{(n)}\right\}+\underbrace{\frac{\pi^2\sigma_{res}^2E_s}{3N_t}-\mathrm{Var}\left\{\alpha_{k,i}^{(n)}\right\}+\mathbb{E}\left\{\left|\Delta\lambda_{k,i}^{(n)}\right|^2\right\}+\mathbb{E}\left\{\left|\Delta\xi_{k,i}^{(n)}\right|^2\right\}+\sigma_w^2}_{\nu}},
\end{aligned} \tag{3.15}$$

where $\sigma_m^2=\mathbb{E}\left\{\left|m_{k,i}^{(n)}\right|^2\right\}=1-\frac{\pi^2\sigma_{res}^2}{3}+\frac{\pi^4\mathbb{E}\left\{\Delta\varepsilon_{k,j}^4\right\}}{36}$ and ν is independent of (k,i,n).

For signal demodulation in MIMO OFDM, diversity reception can be exploited to improve the receive SINR. In the following, EGC and MRC are considered.

3.3.2 SINR Analysis with EGC

In order to demodulate the signal transmitted by the i-th transmit antenna, the N_r receive antennas are co-phased and combined to improve the receiving diversity. Therefore, the EGC output is given by

$$\begin{aligned}
\mathbf{r}_i^{\mathrm{EGC}}[n] &= \sum_{k=1}^{N_r}e^{-\jmath\theta_{k,i}^{(n)}}\mathbf{r}_{k,i}[n] \\
&= \sum_{k=1}^{N_r}\sqrt{\frac{E_s}{N_t}}e^{-\jmath\theta_{k,i}^{(n)}}m_{k,i}^{(n)}H_{k,i}^{(n)}\mathbf{x}_i[n]+\sum_{k=1}^{N_r}e^{-\jmath\theta_{k,i}^{(n)}}\left(\eta_{k,i}^{(n)}+\Delta\lambda_{k,i}^{(n)}+\Delta\xi_{k,i}^{(n)}+\tilde{\mathbf{w}}_{k,i}[n]\right),
\end{aligned} \tag{3.16}$$

where $\theta_{k,i}^{(n)} = \arg\left\{m_{k,i}^{(n)} H_{k,i}^{(n)}\right\}$. After averaging out $\varepsilon_{k,i}$, $\Delta\varepsilon_{k,i}$ and $\Delta H_{k,i}^{(n)}$ for each (k,i), the average SINR of $\mathbf{r}_i^{\mathrm{EGC}}[n]$ is given by

$$\begin{aligned}\bar{\gamma}_i^{\mathrm{EGC}}\left(n\middle|H_{1,i}^{(n)},\cdots,H_{N_r,i}^{(n)}\right) &\triangleq \frac{\mathbb{E}\left\{\left|\sum_{k=1}^{N_r}\sqrt{\frac{E_s}{N_t}}e^{-\jmath\theta_{k,i}^{(n)}}m_{k,i}^{(n)}H_{k,i}^{(n)}\mathbf{x}_i[n]\right|^2\right\}}{\mathbb{E}\left\{\left|\sum_{k=1}^{N_r}e^{-\jmath\theta_{k,i}^{(n)}}\left(\eta_{k,i}^{(n)}+\Delta\lambda_{k,i}^{(n)}+\Delta\xi_{k,i}^{(n)}+\tilde{\mathbf{w}}_{k,i}[n]\right)\right|^2\right\}} \\ &\cong \frac{\frac{E_s}{N_t}\cdot\sigma_m^2\cdot\left(\sum_{k=1}^{N_r}\left|H_{k,i}^{(n)}\right|^2+\sum_{k\neq l}\left|H_{k,i}^{(n)}\right|\cdot\left|H_{l,i}^{(n)}\right|\right)}{\sum_{k=1}^{N_r}\left|H_{k,i}^{(n)}\right|^2\cdot\mathrm{Var}\left\{\alpha_{k,i}^{(n)}\right\}+N_r\nu}.\end{aligned} \tag{3.17}$$

When N_r is large enough, (3.17) can be further simplified as

$$\bar{\gamma}_i^{\mathrm{EGC}}\left(n\middle|H_{1,i}^{(n)},\cdots,H_{N_r,i}^{(n)}\right)\cong\frac{\frac{E_s}{N_t}\cdot\sigma_m^2\cdot\left(\sum_{k=1}^{N_r}\left|H_{k,i}^{(n)}\right|^2+\frac{N_r(N_r-1)\pi}{4}\right)}{\sum_{k=1}^{N_r}\left|H_{k,i}^{(n)}\right|^2\cdot\mathrm{Var}\left\{\alpha_{k,i}^{(n)}\right\}+N_r\nu}. \tag{3.18}$$

3.3.3 SINR Analysis with MRC

In a MIMO OFDM system with N_r receive antennas, based on the channel estimation $\hat{H}_{k,i}^{(n)} = H_{k,i}^{(n)} + \Delta H_{k,i}^{(n)}$ for each (k,i,n), the received signal at all the N_r receive antennas can be combined by using MRC, and therefore the combined output is given by

$$\begin{aligned}\mathbf{r}_i^{\mathrm{MRC}}[n] &= \frac{\sum_{k=1}^{N_r}\omega_{k,i}\mathbf{r}_{k,i}[n]}{\sum_{k=1}^{N_r}\left|\omega_{k,i}\right|^2} \\ &= \frac{\sqrt{\frac{E_s}{N_t}}\sum_{k=1}^{N_r}\left|H_{k,i}^{(n)}\right|^2\left|m_{k,i}^{(n)}\right|^2\mathbf{x}_i[n]}{\sum_{k=1}^{N_r}\left|\omega_{k,i}\right|^2}+\frac{\sqrt{\frac{E_s}{N_t}}\sum_{k=1}^{N_r}\Delta H_{k,i}^{(n)H}H_{k,i}^{(n)}\left|m_{k,i}^{(n)}\right|^2\mathbf{x}_i[n]}{\sum_{k=1}^{N_r}\left|\omega_{k,i}\right|^2} \\ &\quad+\frac{\sum_{k=1}^{N_r}\omega_{k,i}\left(\eta_{k,i}^{(n)}+\Delta\lambda_{k,i}^{(n)}+\Delta\xi_{k,i}^{(n)}+\tilde{\mathbf{w}}_{k,i}[n]\right)}{\sum_{k=1}^{N_r}\left|\omega_{k,i}\right|^2},\end{aligned} \tag{3.19}$$

where $\omega_{k,i} = \left(\hat{H}_{k,i}^{(n)} m_{k,i}^{(n)}\right)^*$. After averaging out $\varepsilon_{k,i}$, $\Delta\varepsilon_{k,i}$ and $\Delta H_{k,i}^{(n)}$ for each (k,i), the average SINR of $\mathbf{r}_i^M[n]$ is

$$\begin{aligned}
&\bar{\gamma}_i^{\mathrm{MRC}}\left(n\middle|H_{1,i}^{(n)},\cdots,H_{N_r,i}^{(n)}\right) \\
&\triangleq \frac{\mathbb{E}\left\{\left|\sqrt{\frac{E_s}{N_t}}\sum_{k=1}^{N_r}\left|H_{k,i}^{(n)}\right|^2\left|m_{k,i}^{(n)}\right|^2\mathbf{x}_i[n]\right|^2\right\}}{\mathbb{E}\left\{\left|\sqrt{\frac{E_s}{N_t}}\sum_{k=1}^{N_r}\Delta H_{k,i}^{(n)*}H_{k,i}^{(n)}\left|m_{k,i}^{(n)}\right|^2\mathbf{x}_i[n]\right|^2\right\}+\mathbb{E}\left\{\left|\sum_{k=1}^{N_r}\omega_{k,i}^*\left(\eta_{k,i}^{(n)}+\Delta\lambda_{k,i}^{(n)}+\Delta\xi_{k,i}^{(n)}+\tilde{\mathbf{w}}_{k,i}[n]\right)\right|^2\right\}} \\
&\cong \frac{\frac{E_s}{N_t}\cdot\sigma_m^2\cdot\left(\sum_{k=1}^{N_r}\left|H_{k,i}^{(n)}\right|^2\right)^2}{\sum_{k=1}^{N_r}\left|H_{k,i}^{(n)}\right|^4\cdot\mathrm{Var}\left\{\alpha_{k,i}^{(n)}\right\}+\sum_{k=1}^{N_r}\left|H_{k,i}^{(n)}\right|^2\underbrace{\left[\nu+\left(\frac{E_s}{N_t}+\mathrm{Var}\left\{\alpha_{k,i}^{(n)}\right\}\right)\sigma_{\Delta H}^2\right]}_{\nu'}+N_r\cdot\nu\cdot\sigma_{\Delta H}^2} \\
&= \frac{\frac{E_s}{N_t}\cdot\sigma_m^2\cdot\sum_{k=1}^{N_r}\left|H_{k,i}^{(n)}\right|^2}{\left(\sum_{k=1}^{N_r}\left|H_{k,i}^{(n)}\right|^2-\frac{\sum_{k\neq l}\left|H_{k,i}^{(n)}\right|^2\left|H_{l,i}^{(n)}\right|^2}{\sum_{k=1}^{N_r}\left|H_{k,i}^{(n)}\right|^2}\right)\mathrm{Var}\left\{\alpha_{k,i}^{(n)}\right\}+\nu'+\frac{N_r\cdot\nu\cdot\sigma_{\Delta H}^2}{\sum_{k=1}^{N_r}\left|H_{k,i}^{(n)}\right|^2}},
\end{aligned} \tag{3.20}$$

where $\nu' = \left[\nu+\left(\frac{E_s}{N_t}+\mathrm{Var}\left\{\alpha_{k,i}^{(n)}\right\}\right)\sigma_{\Delta H}^2\right]$. When N_r is large enough, (3.20) can be further simplified as

$$\begin{aligned}
\bar{\gamma}_i^{\mathrm{MRC}}\left(n\middle|H_{1,i}^{(n)},\cdots,H_{N_r,i}^{(n)}\right) &\cong \frac{\frac{E_s}{N_t}\cdot\sigma_m^2\cdot\sum_{k=1}^{N_r}\left|H_{k,i}^{(n)}\right|^2}{\left(\sum_{k=1}^{N_r}\left|H_{k,i}^{(n)}\right|^2-\frac{\sum_{k\neq l}\left|H_{k,i}^{(n)}\right|^2\left|H_{l,i}^{(n)}\right|^2}{\sum_{k=1}^{N_r}\left|H_{k,i}^{(n)}\right|^2}\right)\mathrm{Var}\left\{\alpha_{k,i}^{(n)}\right\}+\nu'+\frac{N_r\cdot\nu\cdot\sigma_{\Delta H}^2}{\sum_{k=1}^{N_r}\left|H_{k,i}^{(n)}\right|^2}} \\
&\cong \frac{\frac{E_s}{N_t}\cdot\sigma_m^2\cdot\sum_{k=1}^{N_r}\left|H_{k,i}^{(n)}\right|^2}{\left(\sum_{k=1}^{N_r}\left|H_{k,i}^{(n)}\right|^2-(N_r-1)\right)\mathrm{Var}\left\{\alpha_{k,i}^{(n)}\right\}+\nu'+\nu\cdot\sigma_{\Delta H}^2}.
\end{aligned} \tag{3.21}$$

3.4 BER Performance

The BER as a function of SINR in MIMO OFDM is derived in this section. We consider M-ary square QAM with Gray bit mapping. Rugini and Banelli developed the BER

of SISO OFDM with frequency offset [99]. The BER analysis in [99] is now extended to MIMO OFDM.

As discussed in [99,127,128], the BER for the i-th transmit antenna with the input constellation being M-ary square QAM (Gray bit mapping) can be represented as

$$P_{BER}(\gamma_i) = \sum_{j=1}^{\sqrt{M}-1} a_j^M \operatorname{erfc}\left(\sqrt{b_j^M \gamma_i}\right), \tag{3.22}$$

where a_j^M and b_j^M are specified by signal constellation, γ_i is the average SINR of the i-th transmit antenna, and $\operatorname{erfc}(x) = \frac{2}{\sqrt{\pi}} \int_x^\infty e^{-u^2} \mathrm{d}u$ is the error function.

Note that in MIMO OFDM systems, the SINR at each subcarrier is a RV parameterized by the frequency offset and channel attenuation. In order to derive the average SINR of MIMO OFDM systems, (3.22) should be averaged over the distribution of γ_i as

$$\begin{aligned}\bar{P}_{BER}(\gamma_i) &= \sum_{j=1}^{\sqrt{M}-1} a_j^M \int_{\gamma_i} \operatorname{erfc}\left(\sqrt{b_j^M \gamma_i}\right) f(\gamma_i)\, \mathrm{d}\gamma_i \\ &= \sum_{j=1}^{\sqrt{M}-1} a_j^M \int_{\mathbf{H}_i} \int_{\mathcal{E}_i} \int_{\mathbf{v}_i} \int_{\mathbf{\Phi}_i} \operatorname{erfc}\left(\sqrt{b_j^M \gamma_i}\right) \cdot f(\mathbf{H}_i) f(\mathcal{E}_i) f(\mathbf{v}_i) f(\mathbf{\Phi}_i)\, \mathrm{d}\mathbf{H}_i \mathrm{d}\mathcal{E}_i \mathrm{d}\mathbf{v}_i \mathrm{d}\mathbf{\Phi}_i,\end{aligned} \tag{3.23}$$

where $\mathbf{H}_i = [\mathbf{H}_{1,i}, \cdots, \mathbf{H}_{N_r,i}]$, $\mathcal{E}_i = [\varepsilon_{1,i}, \cdots, \varepsilon_{N_r,i}]^T$, $\mathbf{v}_i = [\Delta\varepsilon_{1,i}, \cdots, \Delta\varepsilon_{N_r,i}]^T$, and $\mathbf{\Phi}_i = [\Delta\mathbf{H}_{1,i}, \cdots, \Delta\mathbf{H}_{N_r,i}]$. Since obtaining a close-form solution of (3.23) appears to be impossible, an infinite-series approximation of $\bar{P}_{BER}$ is developed. In [99], the average is expressed as an infinite series of generalized hypergeometric functions.

From [129, page 939], $\operatorname{erfc}(x)$ can be represented as an infinite series

$$\operatorname{erfc}(x) = \frac{2}{\sqrt{\pi}} \sum_{m=1}^{\infty} (-1)^{(m+1)} \frac{x^{(2m-1)}}{(2m-1)(m-1)!}. \tag{3.24}$$

Therefore, (3.23) can be rewritten as

$$\begin{aligned}\bar{P}_{BER}(\gamma_i) &= \sum_{j=1}^{\sqrt{M}-1} a_j^M \int_{\gamma_i} \frac{2}{\sqrt{\pi}} \sum_{m=1}^{\infty} (-1)^{(m+1)} \frac{(\sqrt{b_j^M \gamma_i})^{(2m-1)}}{(2m-1)(m-1)!} \mathrm{d}\gamma_i \\ &= \frac{2}{\sqrt{\pi}} \sum_{j=1}^{\sqrt{M}-1} a_j^M \sum_{m=1}^{\infty} \frac{(-1)^{(m+1)} (b_j^M)^{(m-\frac{1}{2})}}{(2m-1)(m-1)!} \\ &\quad \cdot \underbrace{\int_{\mathbf{H}_i} \int_{\mathcal{E}_i} \int_{\mathbf{v}_i} \int_{\mathbf{\Phi}_i} (\gamma_i)^{(m-\frac{1}{2})} f(\mathbf{H}_i) f(\mathcal{E}_i) f(\mathbf{v}_i) f(\mathbf{\Phi}_i) \mathrm{d}\mathbf{H}_i \mathrm{d}\mathcal{E}_i \mathrm{du}\mathbf{v}_i \mathrm{du}\mathbf{\Phi}_i}_{D_{i;m}},\end{aligned} \tag{3.25}$$

where $D_{i;m}$ depends on the type of combining. Note that γ_i has been derived in Section 3.3, and that for the n-th subcarrier ($0 \le n \le N-1$), $\varepsilon_{k,i}$, $\Delta\varepsilon_{k,i}$ and $\Delta H_{k,i}^{(n)}$ for each (k,i) have been averaged out. Therefore, γ_i in (3.25) can be replaced by $\bar{\gamma}_i(n)$; i.e., the average BER can be expected over subcarrier n ($0 \le n \le N-1$), and finally $\bar{P}_{BER}$ can be simplified as

$$\bar{P}_{BER}(\bar{\gamma}_i(n)) = \frac{2}{\sqrt{\pi}} \sum_{j=1}^{\sqrt{M}-1} a_j^M \sum_{m=1}^{\infty} \frac{(-1)^{(m+1)} (b_j^M)^{(m-\frac{1}{2})}}{(2m-1)(m-1)!} \cdot D_{i;m}, \tag{3.26}$$

where $D_{i;m}$ is based on $\bar{\gamma}_i(n)$ instead of γ_i. We first define $\varpi = \frac{E_s}{N_t} \cdot \sigma_m^2$ and $\mu = \mathrm{Var}\left\{\alpha_{k,i}^{(n)}\right\}$, which will be used in the following. The recursive definition for $D_{i;m}$ for the following reception methods: (1) demodulation without combining, (2) EGC, and (3) MRC, will be given.

Note that the SINR for no combining, EGC or MRC is a function of the second-order statistics of the channel and frequency offset estimation errors (although the interference also comprises the fourth-order statistics of the frequency offset estimation errors, it is negligible as compared to the second-order statistics for small estimation errors). Any probability distribution with zero mean and the same variance will result in the same SINR. Therefore, the exact distributions need not be specified. However, when the BER is derived by using an infinite-series approximation, the actual distribution

of the frequency offset estimation errors is required. In the following sections, the frequency offset estimation errors are assumed i.i.d. Gaussian RVs with mean zero and variance σ_ϵ^2.

3.4.1 BER without Receiver Combining

The BER measured at the k-th receive antenna for the i-th transmit antenna can be approximated by (3.26) with $D_{i;m}^k$ instead of $D_{i;m}$ being used here; i.e.,

$$\bar{P}_{BER}^k\left(\bar{\gamma}_{k,i}\left(n\middle|H_{k,i}^{(n)}\right)\right) = \frac{2}{\sqrt{\pi}}\sum_{j=1}^{\sqrt{M}-1} a_j^M \sum_{m=1}^{\infty} \frac{(-1)^{(m+1)}\left(b_j^M\right)^{(m-\frac{1}{2})}}{(2m-1)(m-1)!}\cdot D_{i;m}^k. \tag{3.27}$$

When $m > 2$, we have $D_{i;m}^k = \frac{\varpi\left[(2m-3)\mu+\nu\right]}{\mu^2(m-\frac{3}{2})}\cdot D_{i;m-1}^k - \frac{\varpi^2}{\mu^2}\cdot D_{i;m-2}^k$, as derived in Appendix A. I. The initial condition is given by

$$D_{i;1}^k = \int_0^\infty \frac{\varpi^{\frac{1}{2}}h^{\frac{1}{2}}}{(\mu h+\nu)^{\frac{1}{2}}}e^{-h}\mathrm{d}h. \tag{3.28}$$

3.4.2 BER with EGC

For a MIMO OFDM system with EGC reception, the average BER can be approximated by (3.26) with $D_{i;m}^{\mathrm{EGC}}$ instead of $D_{i;m}$ being used here; i.e.,

$$\bar{P}_{BER}^{\mathrm{EGC}}\left(\gamma_i^{\mathrm{EGC}}\left(n\middle|H_{1,i}^{(n)},\cdots,H_{N_r,i}^{(n)}\right)\right) = \frac{2}{\sqrt{\pi}}\sum_{j=1}^{\sqrt{M}-1} a_j^M \sum_{m=1}^{\infty} \frac{(-1)^{(m+1)}\left(b_j^M\right)^{(m-\frac{1}{2})}}{(2m-1)(m-1)!}\cdot D_{i;m}^{\mathrm{EGC}}. \tag{3.29}$$

Defining $\nu^E = N_r\nu$, $\sigma_{\mathrm{EGC}}^2 = \frac{(N_r!)^2}{8\left[\left(N_r-\frac{1}{2}\right)\cdots\frac{1}{2}\right]^2}$, $\tilde{\nu}^E = \nu^E - \frac{\mu N_r(N_r-1)\pi}{4}$ and $\tilde{\mu} = 2\sigma_{\mathrm{EGC}}^2\cdot\mu$, when $m > 2$, we have

$$D_{i;m}^{\mathrm{EGC}} = \frac{2\sigma_{\mathrm{EGC}}^2\varpi\left[(2m+N_r-4)\tilde{\mu}(N_r-1)!+\tilde{\nu}^E\right]}{\tilde{\mu}^2(m-\frac{3}{2})(N_r-1)!}\cdot D_{i;m-1}^{\mathrm{EGC}} - \frac{(2\sigma_{\mathrm{EGC}}^2\varpi)^2(m+N_r-\frac{5}{2})}{\tilde{\mu}^2(m-\frac{3}{2})}\cdot D_{i;m-2}^{\mathrm{EGC}}, \tag{3.30}$$

as derived in Appendix A.2. The initial condition is given by

$$D_{i;1}^{\mathrm{EGC}} = \frac{(2\sigma_{\mathrm{EGC}}^2\varpi)^{\frac{1}{2}}}{(N_r-1)!}\int_0^\infty \frac{h^{(N_r-\frac{1}{2})}}{(\tilde{\mu}h+\tilde{\nu}^E)^{\frac{1}{2}}}e^{-h}\mathrm{d}u h. \tag{3.31}$$

3.4.3 BER with MRC

For a MIMO OFDM system with channel knowledge at the receiver, the receiving diversity can be optimized by using MRC, and the average BER can be approximated by (3.26) with $D_{i;m}^{\mathrm{MRC}}$ instead of $D_{i;m}$ being used here; i.e.,

$$\bar{P}_{BER}^{\mathrm{MRC}}\left(\gamma_i^{\mathrm{MRC}}\left(n\middle|H_{1,i}^{(n)},\cdots,H_{N_r,i}^{(n)}\right)\right)=\frac{2}{\sqrt{\pi}}\sum_{j=1}^{\sqrt{M}-1}a_j^M\sum_{m=1}^{\infty}\frac{(-1)^{(m+1)}\left(b_j^M\right)^{(m-\frac{1}{2})}}{(2m-1)(m-1)!}\cdot D_{i;m}^{\mathrm{MRC}}. \quad (3.32)$$

By defining $\nu^M=\nu'+\nu\cdot\sigma_{\Delta H}^2$, $D_{i;m}^{\mathrm{MRC}}$ with $m>2$ is given by

$$D_{i;m}^{\mathrm{MRC}}=\frac{\varpi\left[(2m+N_r-4)\mu(N_r-1)!+\tilde{\nu}^M\right]}{\mu^2(m-\frac{3}{2})(N_r-1)!}\cdot D_{i;m-1}^{\mathrm{MRC}}-\frac{\varpi^2(m+N_r-\frac{5}{2})e^{-(N_r-1)}}{\mu^2(m-\frac{3}{2})}\cdot D_{i;m-2}^{\mathrm{MRC}}, \quad (3.33)$$

as derived in Appendix A.3. The initial condition is given by

$$D_{i;1}^{\mathrm{MRC}}=\frac{e^{-(N_r-1)}\varpi^{\frac{1}{2}}}{(N_r-1)!}\int_0^{\infty}\frac{h^{(N_r-\frac{1}{2})}}{(\mu h+\tilde{\nu}^M)^{\frac{1}{2}}}e^{-h}\mathrm{d}u h. \quad (3.34)$$

3.4.4 Complexity of the Infinite-Series Representation of BER

Infinite-series BER expression (3.27), (3.29) or (3.32) must be truncated in practice. The truncation error is negligible if the number of terms is large enough: [130] shows that when the number of terms is as large as 50, the finite-order approximation is good. In this case, a total of $151\sqrt{M}$ multiplication and $101\sqrt{M}$ summation operations are needed to calculate the BER for each combining scheme.

3.5 Numerical Results

Quasi-static MIMO wireless channels are assumed; i.e., the channel impulse response is fixed over one OFDM symbol period but changes across the symbols. The simulation parameters are defined in Table 3.2.

The SINR degradation due to the residual frequency offsets is analyzed in Figure 3.16 for $\sigma_{\Delta H}^2=0.01$ and SNR =10 dB. The SINR degradation increases with σ_{res}^2.

Table 3.2: Parameters for BER Simulation in MIMO OFDM Systems

Subcarrier Modulation	QPSK; 16-QAM
DFT Length	128
σ^2_{res}	10^{-3};10^{-4}
$\sigma^2_{\Delta H}$	10^{-4}
MIMO Parameters	$(N_t = 1, 2;\ N_r = 1, 2, 4)$
Receiving Combining	Without Combining; EGC; MRC

Because of IAI due to the multiple transmit antennas, the SINR performance of MIMO OFDM with $(N_t = 2, N_r = 2)$ is worse than that of SISO OFDM, even though EGC or MRC is applied to exploit the receiving diversity. IAI in MIMO OFDM can be suppressed by increasing the number of receive antennas. In this simulation, when $N_r = 4$, the average SINR with either EGC or MRC will be higher than that of SISO OFDM system. For each MIMO scenario, MRC outperforms EGC.

The BER degradation due to the residual frequency offsets is shown in Figure 3.17 for $\sigma^2_{\Delta H} = 10^{-3}$ and $E_b/N_0 = 10\,\text{dB}$ (E_b/N_0 is the bit energy per noise per Hz). The BER for 4-phase PSK (QPSK) or 16-QAM subcarrier modulation is considered. Just as with the case of SINR, the BER degrades with large σ^2_{res}. For example, when $(N_t = 2, N_r = 2)$ and $\sigma^2_{res} = 10^{-5}$ for QPSK (16-QAM), a BER of 7×10^{-3} (2.5×10^{-2}) or 6×10^{-3} (2×10^{-2}) is achieved with EGC or MRC at the receiver, respectively. When σ^2_{res} is increased to 10^{-2}, a BER of 2×10^{-2} (6×10^{-2}) or 1×10^{-2} (5.5×10^{-2}) can be achieved with EGC or MRC, respectively.

Figures 3.18 - 3.23 compare BERs of QPSK and 16-QAM with different combining methods. Figure 3.18 and Figure 3.19 consider SISO OFDM. The BER is degraded due to the frequency offset and channel estimation errors. For a fixed channel estimation variance error $\sigma^2_{\Delta H}$, a larger variance of frequency offset estimation error, i.e., σ^2_{res}, implies a higher BER. For example, if $\sigma^2_{\Delta H} = 10^{-4}$, $E_b/N_0 = 20$ dB and $\sigma^2_{res} = 10^{-4}$, the BER with QPSK (16-QAM) is about 1.8×10^{-3} (5.5×10^{-3}); when σ^2_{res} is increased to 10^{-3}, the BER with QPSK (16-QAM) increases to 4.3×10^{-3} (1.5×10^{-2}).

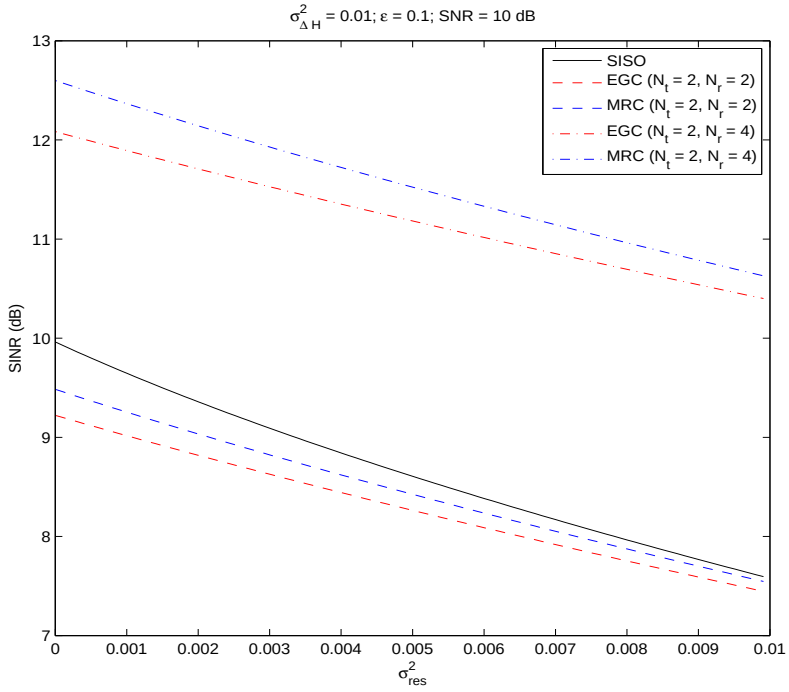

Figure 3.16: SINR reduction due to the residual frequency offset in MIMO OFDM systems.

IAI appears with multiple transmit antennas, and the BER will degrade as IAI increases. Note that since IAI cannot be totally eliminated in the presence of frequency offset and channel estimation errors, a BER floor occurs at the high SNR. IAI can be reduced considerably by exploiting the receiving diversity by using either EGC or MRC, as shown in Figures 3.20 - 3.23. Without receiver combining, the BER is much worse than that in SISO OFDM, simply because of the SINR degradation due to IAI. For example, when $N_t = N_r = 2$ and $\sigma^2_{\Delta H} = 10^{-4}$, the BER with QPSK is about 5.5×10^{-3} when $\sigma^2_{res} = 10^{-4}$, which is much higher than that in SISO OFDM (the BER for SISO OFDM is 1.8×10^{-3}), as shown in Figure 3.20. For a given number of receive antennas, MRC can achieve a lower BER than that with EGC, provided that an accurate channel estimation is assumed at the receiver. For example, when $N_t = N_r = 2$ and $\sigma^2_{\Delta H} = 10^{-4}$, the BER with QPSK is about 5.5×10^{-3} when $\sigma^2_{res} = 10^{-4}$, which is three times of

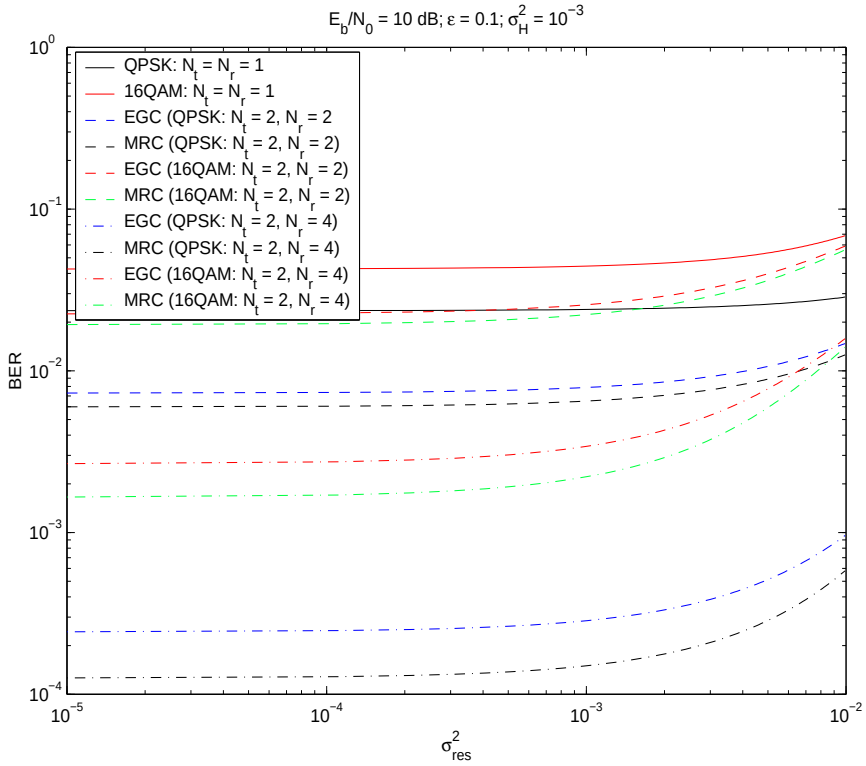

Figure 3.17: BER degradation due to the residual frequency offset in MIMO OFDM systems.

that of SISO OFDM (which is about 1.8×10^{-3}) as shown in Figure 3.21. For a given number of receive antennas, MRC can achieve a lower BER than that achieved with EGC, but the receiver requires accurate channel estimation. For example, in Figure 3.21, when $\sigma^2_{\Delta H} = 10^{-4}$ with $N_t = N_r = 2$ and 16-QAM, the performance improvement of EGC (MRC) over that without combining is about 5.5 dB (6 dB), and that performance improvement increases to 7.5 dB (8.5 dB) if σ^2_{res} is increased to 10^{-3}. By increasing the number of receive antennas to 4, this performance improvement is about 8.2 dB (9 dB) for EGC (MRC) with $\sigma^2_{\Delta H} = 10^{-4}$, or 11 dB (13.9 dB) for EGC (MRC) with $\sigma^2_{\Delta H} = 10^{-3}$, as shown in Figure 3.23.

The theoretical BER approximation are accurate at low SNR with/without diversity combining. However, the simulation and theory results diverge as the SNR increases,

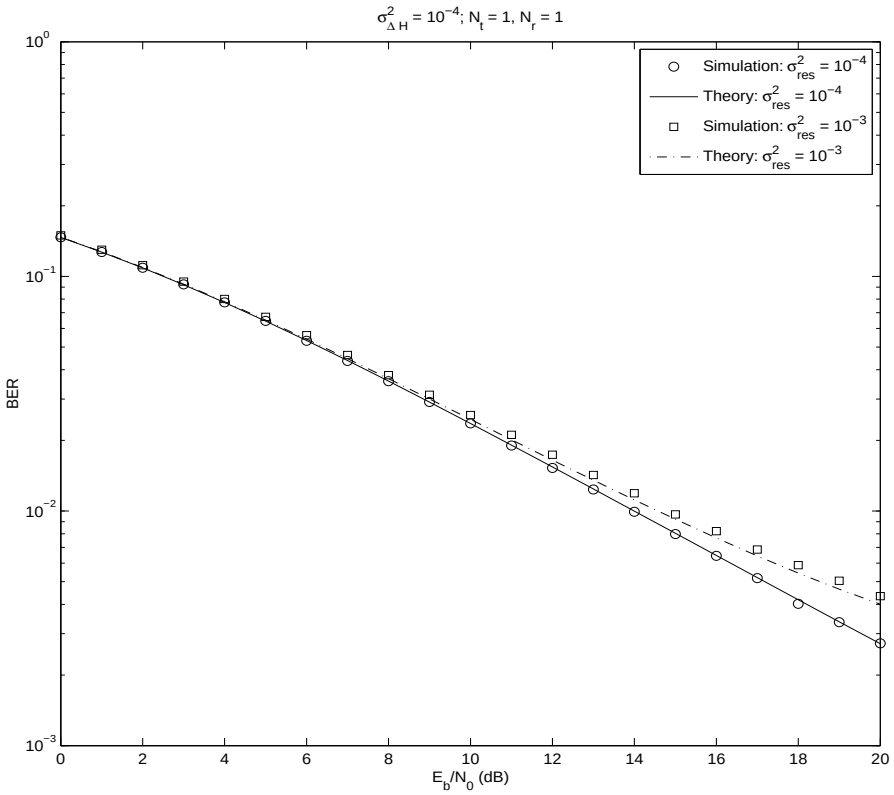

Figure 3.18: BER with QPSK when ($N_t = 1, N_r = 1$).

especially when σ^2_{res} is large. For example, in Figure 3.23, with 16-QAM, when ($N_t = 2$, $N_r = 4$) and $\sigma^2_{res} = 10^{-3}$, about 1 dB difference exists between the simulation and the theoretical result for either EGC or MRC at high SNR. This discrepancy is due to several reasons. As the SNR increases, the systems become interference-limited. When N, N_t and N_r are not large enough, the interferences may not be well approximated as Gaussian RVs with zero mean. In addition, with either EGC or MRC reception, the phase rotation or channel attenuation of the receive sub-streams should be estimated, and their estimation accuracy will also affect the combined SINR. The instant large phase or channel estimation error also contributes a deviation to the BER when using EGC or MRC.

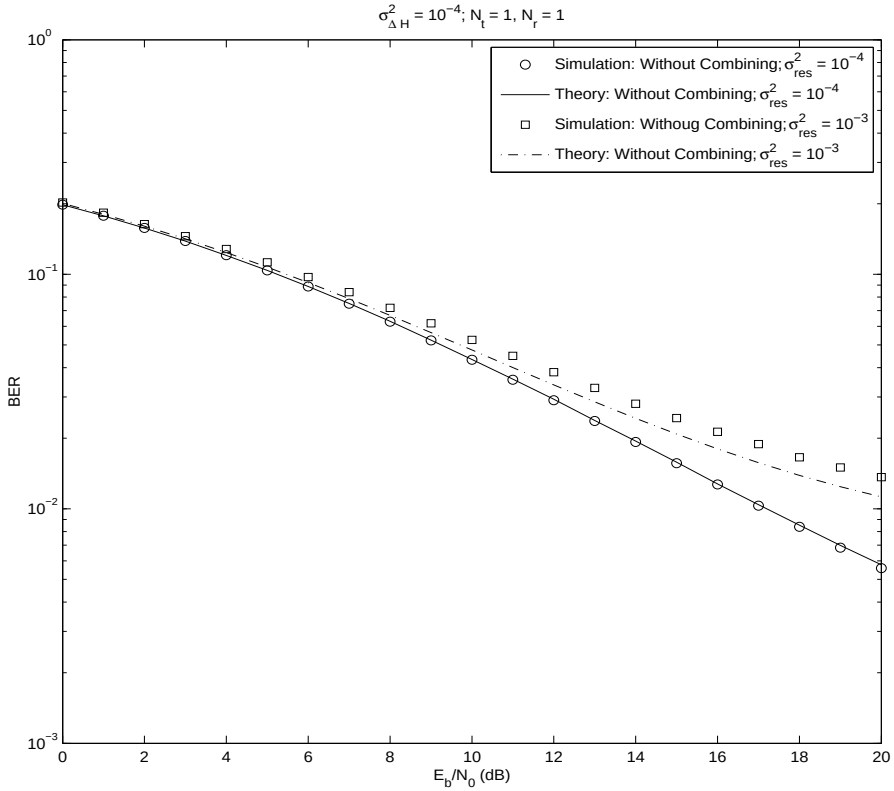

Figure 3.19: BER with 16-QAM when $(N_t = 1, N_r = 1)$.

3.6 Conclusions

In practical systems, neither the frequency offset nor the channel can be perfectly estimated, and the residual frequency offset and channel estimation errors impact the BER performance. The BER is thus needed to be analyzed under imperfect channel and frequency offset estimation condition. Based on our analysis, the acceptable accuracy range of the frequency offset and the channel estimation can be obtained for the desired BER performance.

The BER of MIMO OFDM due to the frequency offset and channel estimation errors has been analyzed in this chapter. The BER expressions for multiple-antenna

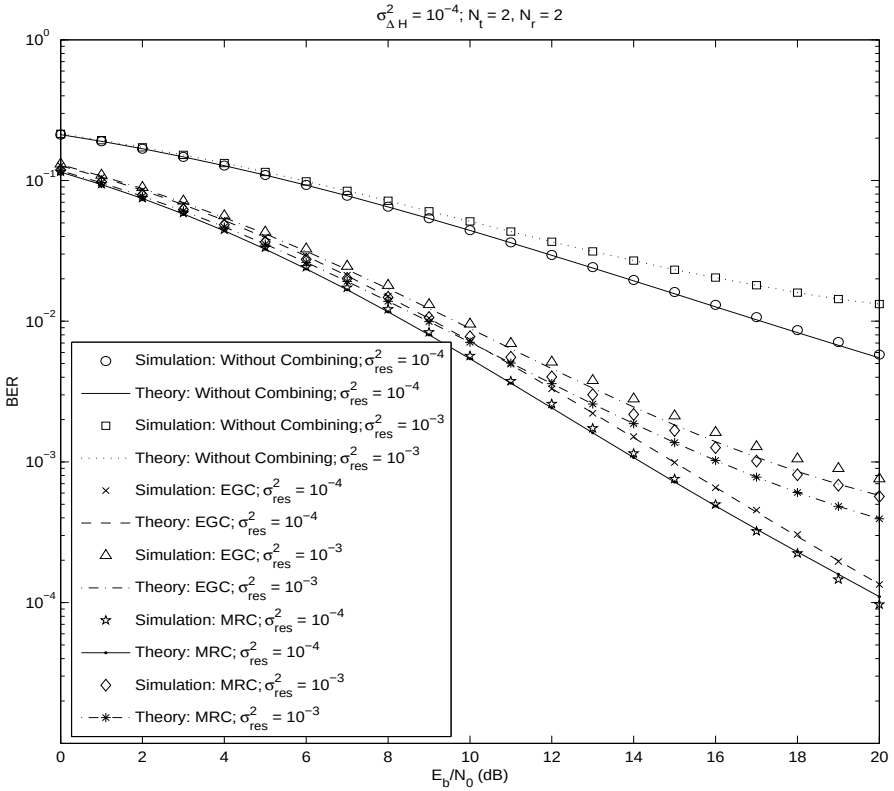

Figure 3.20: BER with QPSK when $(N_t = 2, N_r = 2)$.

reception with EGC and MRC were derived. These expressions are in infinite-series form, and can be truncated in practice. The simulation results show that the truncation error is negligible if the number of terms is larger than 50.

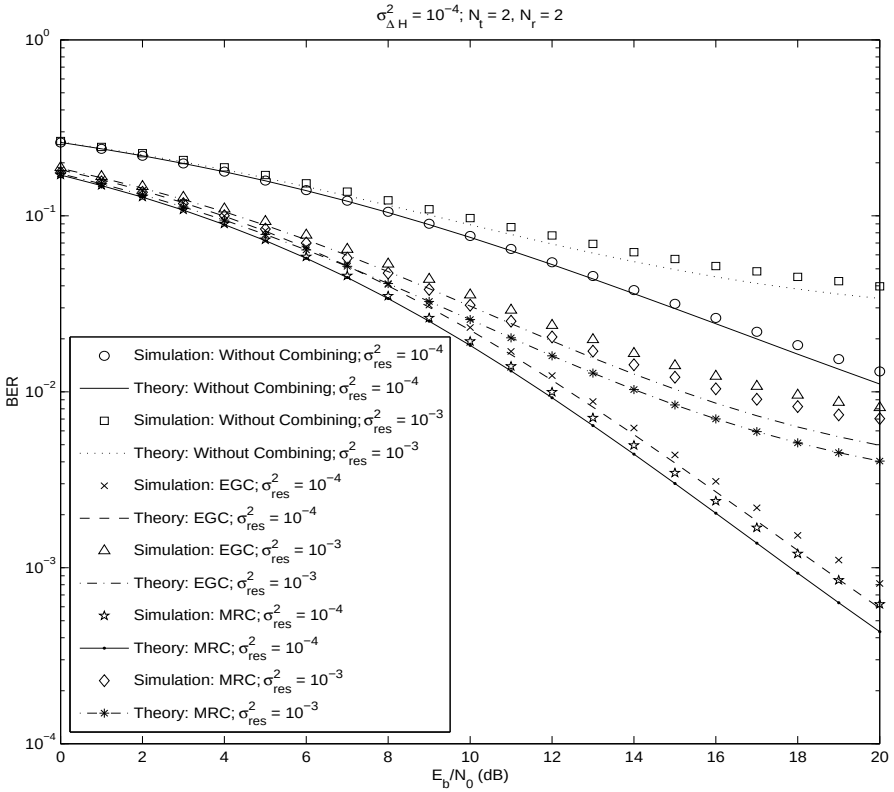

Figure 3.21: BER with 16-QAM when $(N_t = 2, N_r = 2)$.

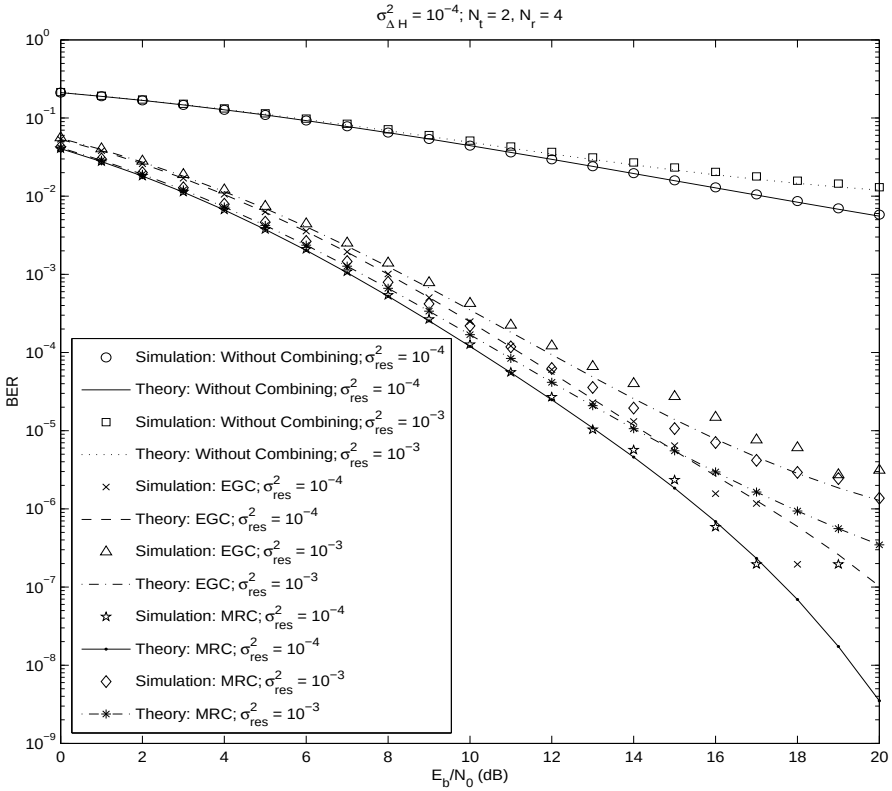

Figure 3.22: BER with QPSK when $(N_t = 2, N_r = 4)$.

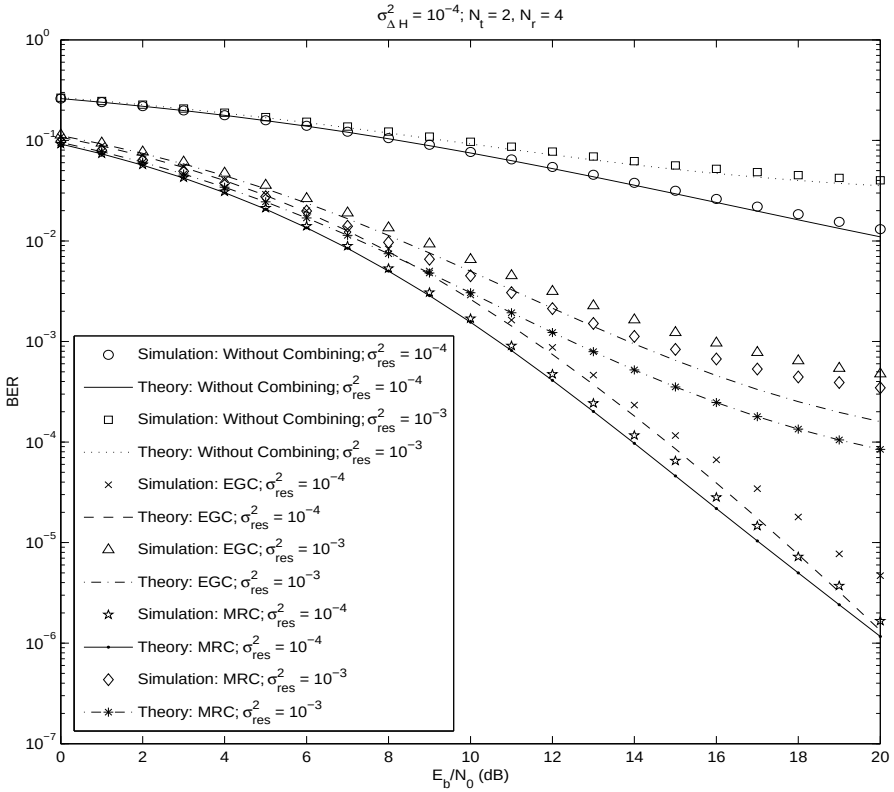

Figure 3.23: BER with 16-QAM when $(N_t = 2, N_r = 4)$.

Chapter 4

Robust OFDMA Uplink Frequency Offset Estimation

In this chapter, the uplink frequency offset estimation of OFDMA systems is investigated [131]. The OFDMA system uses a general subcarrier allocation scheme, where subcarrier group allocated to each user need not be contiguous. By analyzing multiple access interference (MAI), the CRLB for the variance of frequency offset estimation of each user is derived. Successive interference cancelation (SIC)-based frequency offset estimation is considered. An estimate of the variance of frequency offset is derived as a function of SINR and SNR. An estimation of the range of frequency offset is derived for uniformly distributed frequency offsets. Based on this estimate of the range of frequency offsets, the accuracy of existing algorithms can be improved. Thus, new versions of the SIC-based frequency offset estimation and differential estimation algorithms are derived.

4.1 Introduction

As described in Chapter 1, OFDMA systems have the advantages of the high flexibility in resource management due to dynamic subcarrier assignment strategy and the simplified equalization in the frequency domain which is inherited from OFDM. Despite these features, the design of an OFDMA system poses several technical challenges. One basic issue is related to the stringent requirement on frequency synchronization, which is critically important for the OFDMA uplink. Without accurate compensation

of the frequency offset, ICI as well as MAI are generated due the loss of subcarrier orthogonality. Moreover, the uplink frequency offset estimation for such systems is a multiple-parameter estimation problem and, hence, is much more difficult than the downlink case.

The synchronization issues for OFDMA uplink have been widely researched [95–98, 132, 133]. Reference [95] discusses a CP-based timing and frequency offset synchronization. Timing and frequency offset synchronization algorithms for generalized asynchronous and quasi-synchronous OFDMA systems are developed in [96] using null subcarriers and subcarrier hopping. A high-resolution blind frequency offset estimator is proposed in [132] using second-order statistics, however, it requires multiple OFDMA blocks per estimation. A reliable one-block OFDMA uplink synchronization algorithm is proposed in [97]. A high-performance maximum-likelihood (ML) algorithm for both synchronization and channel estimation for an OFDMA uplink transmission is studied in [133], and the complexity is reduced by employing an alternating projection method (this method simplifies the problem of multidimensional optimization into several 1-dimensional optimization problems). An iterative time and frequency synchronization scheme using the space-alternating generalized expectation-maximization algorithm for interleaved OFDMA uplink systems is proposed in [98].

The performance of such algorithms is a function of the received SINR. When the frequency offsets of all the active users are large, each user signal is subject to heavy MAI, and therefore, the frequency offset estimation for each user will be considerably degraded. This degradation can be 10 dB or more for some systems in the high SNR region. This chapter studies the OFDMA uplink frequency offset estimation by utilizing the SNR and SINR parameters.

4.2 OFDMA Uplink Signal Model

The base station first performs uplink time and frequency offset estimation, and then, the estimates are sent through a downlink control channel to the users to help their time and frequency adjustment. Perfect timing synchronization is assumed, so only the uplink frequency offset estimation is discussed. Note that the OFDMA uplink frequency offset estimation can be subdivided into two phases, i.e., acquisition and tracking. When a user starts accessing a base station, its instantaneous frequency offset may be very large, and an acquisition algorithm is needed to estimate and correct this large frequency offset. Channel estimation will also be performed after acquisition. After acquisition, the residual frequency offset of this user will be well within a finite range, e.g., within ±0.5 subcarrier spacing, and this user will run in the tracking phase. At the tracking phase, pilot/training-based algorithms can be performed to estimate the frequency offset with high accuracy. Only the frequency offset tracking phase will be considered, and CSI of each user is assumed to be available at the base station.

An OFDMA uplink transmission with M users is described in Figure 4.24, where Δf represents the subcarrier bandwidth. The total number of the subcarriers is N. An $N \times 1$ vector $\underline{\mathbf{x}}_k$ represents the frequency-domain symbols sent by the k-th user, where $k \in \{1, 2, \cdots, M\}$. The i-th entry of $\underline{\mathbf{x}}_k$ ($\underline{x}_k[i]$) is nonzero if and only if the i-th subcarrier is allocated to the k-th user, where $i \in \{1, 2, \cdots, N\}$. G_k represents the subcarrier group allocated to the k-th user (the elements of G_k are indexes of all the subcarriers), and $\mathcal{N}_k$ represents the cardinality of G_k). Note that $\bigcap_{k \neq l} G_k G_l = \varnothing$ and $\bigcup_{k=1}^{M} G_k \subseteq \{0, 1, \cdots, N-1\}$. $\underline{\mathbf{x}}_k$ can also be simplified into a $\mathcal{N}_k \times 1$ vector $\mathbf{x}_k$ by deleting all the zero entries of $\underline{\mathbf{x}}_k$ and keeping the non-zero entries unchanged.

The time-domain transmit vector for the k-th user is given by

$$\mathbf{s}_k = \mathbf{F}\underline{\mathbf{x}}_k = \mathbf{F}_k \mathbf{x}_k, \tag{4.1}$$

where $\mathbf{F}$ denotes the $N \times N$ IDFT matrix, and $\mathbf{F}_k$ is an $N \times \mathcal{N}_k$ IDFT matrix that is specified by G_k ($\mathbf{F}_k$ can be generated from $\mathbf{F}$ by deleting all the columns with the

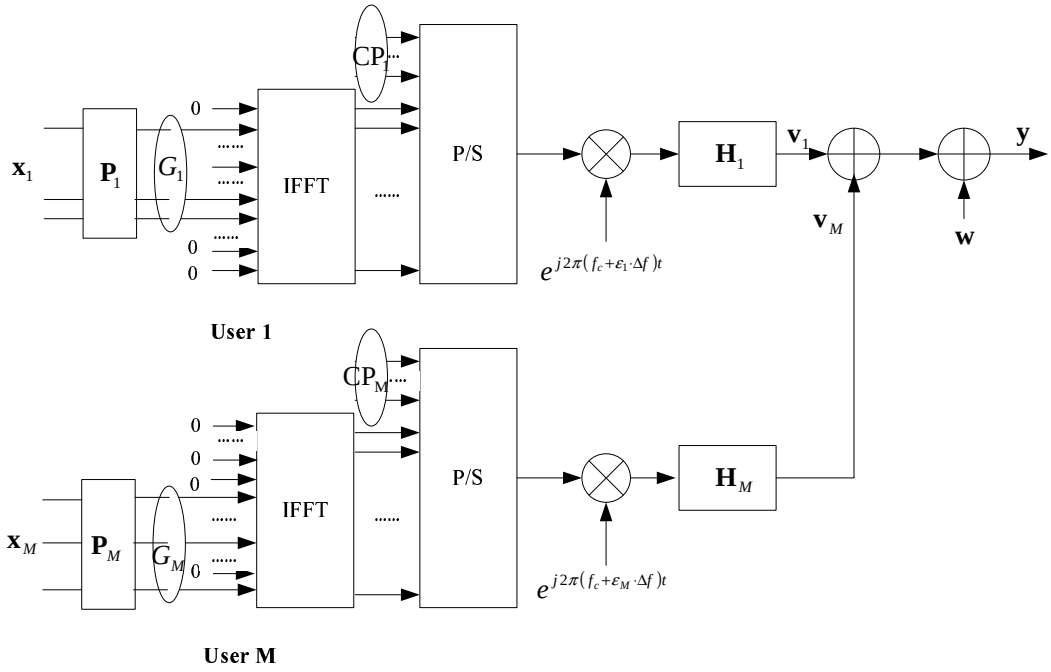

Figure 4.24: Structure of OFDMA uplink transmission.

column indexes not belonging to G_k). A CP of length N_g is appended to each symbol to mitigate the ISI.

The discrete-time channel impulse response associated with the k-th user is $\mathbf{h}_k = [h_k(0), h_k(1), \cdots, h_k(L_k - 1)]^T$, where L_k is the maximum delay of the k-th user. The channel frequency response matrix of the k-th user is given by $\mathbf{H}_k = \text{diag}\left\{H_k^i : i \in G_k\right\}$. The received signal at the base station can be represented as

$$\mathbf{y} = \sum_{k=1}^{M} \mathbf{y}_k = \sum_{k=1}^{M} \left(\mathbf{E}_k \underbrace{\mathbf{F}_k \mathbf{H}_k \mathbf{\Phi}_k \mathbf{x}_k}_{\mathbf{s}_k} + \mathbf{w}_k \right), \tag{4.2}$$

where $\mathbf{\Phi}_k = \text{diag}\left\{\sqrt{P_i} : i \in G_k\right\}$ with P_i representing the power allocation to the i-th subcarrier, and $\mathbf{E}_k$ is given by $\mathbf{E}_k = \text{diag}\left\{1, e^{\frac{j2\pi\varepsilon_k}{N}}, \cdots, e^{\frac{j2\pi\varepsilon_k(N-1)}{N}}\right\}$ with ε_k representing the normalized frequency offset of the k-th user, respectively. $\mathbf{w}_k$ in (4.2) is a AWGN vector added to the signal space of the k-th user with $\mathbf{w}_k[i] \sim \mathcal{CN}(0, \sigma_w^2)$.

Let $\mathbf{s}_k$ be the training sequence transmitted by the k-th user. The received signal $\mathbf{y}$ is a complex Gaussian random vector with the PDF [134]:

$$f(\mathbf{y}) = \frac{1}{(\pi)^N \det[\mathbf{C}]} \exp\left\{-(\mathbf{y}-\mathbf{s})^H \mathbf{C}^{-1}(\mathbf{y}-\mathbf{s})\right\}, \tag{4.3}$$

where $\mathbf{s} = \sum_{k=1}^{M} \mathbf{s}_k$, and $\mathbf{C} = \mathbb{E}\left\{(\mathbf{y}-\mathbf{s})(\mathbf{y}-\mathbf{s})^H\right\}$. The frequency offsets of different users are assumed to be i.i.d RVs with zero mean and variance of σ_ϵ^2 (not necessarily Gaussian). For an unbiased frequency offset estimator $\hat{\varepsilon}_k$, the CRLB is given by $\mathrm{Var}\{\hat{\varepsilon}_k|\mathbf{y}^M\} \geq [\mathbf{\Lambda}_M^{-1}]_{kk}$, where the kl-th element of Fisher information matrix (FIM) $\mathbf{\Lambda}_M$ is

$$[\mathbf{\Lambda}_M]_{kl} = \mathrm{trace}\left(\left(\mathbf{C}^M\right)^{-1} \frac{\partial \mathbf{C}^M}{\partial \varepsilon_k} \left(\mathbf{C}^M\right)^{-1} \frac{\partial \mathbf{C}^M}{\partial \varepsilon_l}\right), \tag{4.4}$$

as given by [135].

In a multiple-access system, the unknown parameters of interfering users can be treated as nuisance parameters, which will degrade the estimation accuracy of the parameters of interest. Regarding OFDMA uplink frequency offset estimation, the following result holds.

Lemma 1—Estimation Error Increases: The OFDMA uplink frequency offset estimation error for each user will not reduce as the number of interfering users increases.

Proof: For an OFDMA uplink transmission with a total of $(M-1)$ users accessing a base station, the received vector is defined as

$$\tilde{\mathbf{y}} = \sum_{k=1}^{M-1} \mathbf{y}_k = \sum_{k=1}^{M-1} \left(\mathbf{E}_k \underbrace{\mathbf{F}_k \mathbf{H}_k \mathbf{\Phi}_k \mathbf{x}_k}_{\mathbf{s}_k} + \mathbf{w}_k\right). \tag{4.5}$$

The covariance matrix of $\tilde{\mathbf{y}}$ is represented as $\tilde{\mathbf{C}}$. Define the current FIM as $\mathbf{\Lambda}_{M-1}$ where $[\mathbf{\Lambda}_{M-1}]_{kl} = \mathrm{trace}\big(\tilde{\mathbf{C}}^{-1}(\partial\tilde{\mathbf{C}}/\partial\varepsilon_k)\tilde{\mathbf{C}}^{-1}(\partial\tilde{\mathbf{C}}/\partial\varepsilon_l)\big)$. If a new user (the M-th user) is accessing the base station, the receive vector and its covariance matrix are $\mathbf{y}$ and $\mathbf{C}$, respectively, and the new FIM is

$$\mathbf{\Lambda}_M = \begin{bmatrix} \mathbf{\Lambda}_{M-1} & \mathbf{b} \\ \mathbf{b}^H & [\mathbf{\Lambda}_M]_{MM} \end{bmatrix}, \tag{4.6}$$

where $\mathbf{b}$ is a $(M-1)\times 1$ vector with $b[k] = \text{trace}\big(\mathbf{C}^{-1}(\partial\mathbf{C}/\partial\varepsilon_k)\mathbf{C}^{-1}(\partial\mathbf{C}/\partial\varepsilon_M)\big)$, $1 \le k \le M-1$, and $[\mathbf{\Lambda}_M]_{MM} = \text{trace}\big(\mathbf{C}^{-1}(\partial\mathbf{C}/\partial\varepsilon_M)\mathbf{C}^{-1}(\partial\mathbf{C}/\partial\varepsilon_M)\big)$. The inverse of $\mathbf{\Lambda}_M$ can be represented as

$$\mathbf{\Lambda}_M^{-1} = \begin{bmatrix} \mathbf{\Lambda}_{M-1}^{-1} & \mathbf{0} \\ \mathbf{0}^H & 0 \end{bmatrix} + \begin{bmatrix} -\mathbf{\Lambda}_{M-1}^{-1}\mathbf{b} \\ 1 \end{bmatrix} \left([\mathbf{\Lambda}_M]_{MM} - \mathbf{b}^H\mathbf{\Lambda}_{M-1}^{-1}\mathbf{b}\right)^{-1} \begin{bmatrix} -\mathbf{b}^H\mathbf{\Lambda}_{M-1}^{-1} & 1 \end{bmatrix}. \tag{4.7}$$

By using $\mathbf{\Lambda}_{M|M-1}^{-1}$ to represent the northwestern $(M-1)\times(M-1)$ sub-matrix of $\mathbf{\Lambda}_M^{-1}$, we have

$$\mathbf{\Lambda}_{M|M-1}^{-1} = \mathbf{\Lambda}_{M-1}^{-1} + \left([\mathbf{\Lambda}_M]_{MM} - \mathbf{b}^H\mathbf{\Lambda}_{M-1}^{-1}\mathbf{b}\right)^{-1}\mathbf{\Lambda}_{M-1}^{-1}\mathbf{b}\mathbf{b}^H\mathbf{\Lambda}_{M-1}^{-1}, \tag{4.8}$$

where $[\mathbf{\Lambda}_M^{-1}]_{MM} = \left([\mathbf{\Lambda}_M]_{MM} - \mathbf{b}^H\mathbf{\Lambda}_{M-1}^{-1}\mathbf{b}\right)^{-1} > 0$. Since $\mathbf{\Lambda}_{M-1}^{-1}\mathbf{b}\mathbf{b}^H\mathbf{\Lambda}_{M-1}^{-1}$ is a nonnegative definite matrix, we have

$$\begin{aligned} [\mathbf{\Lambda}_{M|M-1}^{-1}]_{ii} &= [\mathbf{\Lambda}_{M-1}^{-1}]_{ii} + \left([\mathbf{\Lambda}_M]_{MM} - \mathbf{b}^H\mathbf{\Lambda}_{M-1}^{-1}\mathbf{b}\right)^{-1}[\mathbf{\Lambda}_{M-1}^{-1}\mathbf{b}\mathbf{b}^H\mathbf{\Lambda}_{M-1}^{-1}]_{ii} \\ &\ge [\mathbf{\Lambda}_{M-1}^{-1}]_{ii}, \quad 1 \le i \le M-1. \end{aligned} \tag{4.9}$$

□

Lemma 1 indicates that the MAI increases if the number of users accessing a base station increases. For an unbiased estimator for the k-th user, the CRLB is related to $[\mathbf{\Lambda}_{M-1}^{-1}]_{kk}$, and the following result holds.

Lemma 2—Inequality of FIM: In the OFDMA uplink frequency offset estimation, $[\mathbf{\Lambda}_M^{-1}]_{kk} \ge [\mathbf{\Lambda}_M]_{kk}^{-1}$ for each k.

Proof: Without loss of generality, suppose that the number of users is M, and that the frequency offsets of the different users are i.i.d RVs. From [135, page 1352], for a Hermitian positive define matrix $\mathbf{\Lambda}_M$, the following inequality

$$[\mathbf{\Lambda}_M^{-1}]_{kk} = \left[\mathbf{I}_M \odot \mathbf{\Lambda}_M^{-1}\right]_{kk} \ge [\mathbf{I}_M \odot \mathbf{\Lambda}_M]_{kk}^{-1} = [\mathbf{\Lambda}_M]_{kk}^{-1} \tag{4.10}$$

is always satisfied for each $1 \le k \le M$.

□

In the following, $\mathbf{\Lambda}$ is used to denote the FIM when the number of user of users accessing a base station is not specified. By using Lemma 2, the CRLB for the k-th user is derived as

$$\begin{aligned}\mathrm{Var}\left\{\hat{\varepsilon_k}|\mathbf{y}\right\} &\geq \left[\mathbf{\Lambda}^{-1}\right]_{kk} \geq \left[\mathbf{\Lambda}\right]_{kk}^{-1} \\ &= \frac{1}{\sum\limits_{i=1}^{\mathcal{N}_k}\frac{\left(\frac{\partial\lambda_{k,i}}{\partial\varepsilon_k}\right)^2}{(\lambda_{k,i}+z_{k,i})^2}+\sum\limits_{l\neq k}\sum\limits_{j=1}^{\mathcal{N}_l}\frac{\left(\frac{\partial z_{l,j}}{\partial\varepsilon_k}\right)^2}{(\lambda_{l,j}+z_{l,j})^2}} \\ &= \frac{1}{\alpha_k\cdot\mathrm{SNR}_k^2}+\frac{1}{\beta_k\cdot\mathrm{SNR}_k}+\frac{1}{\varpi_k\cdot\mathrm{SIR}_k},\end{aligned} \tag{4.11}$$

where $\lambda_{k,i}$, and $z_{k,i}$ are defined in Appendix B. 1, α_k, β_k, and ϖ_k are training-sequence-specified coefficients for the k-th user. For a length N training sequence with $N \gg 1$, we always have $1 \ll \alpha_k$, $1 \ll \beta_k$ and $1 \ll \varpi_k$. The first two items in (4.11) are related to the SNR of the k-th user, and the third item to the signal-to-interference ratio (SIR) of the k-th user.

4.3 Interference Analysis in OFDMA Systems

Consider a system with a total of M users accessing a base station. The analysis of the MAI due to the frequency offsets is based on the following assumptions.

1. $\bigcap\limits_{m\neq n} G_m G_n = \varnothing$ and $\bigcup\limits_{m} G_m \subseteq \{0,1,\cdots,N-1\}$, where $m,n \in \{1,2,\cdots,M\}$.
2. $\mathcal{N}_m \ll N$, $1 \leq m \leq M$.
3. ε_m for each m is an i.i.d. RV with zero mean and variance σ_ϵ^2.

4.3.1 Interference Reduction by Using Pre-Projector Method

The CRLB for an OFDMA uplink synchronization is derived in (4.11) and is related to multiple variables. To analyze the received SINR of the k-th user, define a projection matrix $\mathbf{P}_k = \mathbf{F}_k(\mathbf{F}_k^H\mathbf{F}_k)^{-1}\mathbf{F}_k^H = \mathbf{F}_k\mathbf{F}_k^H$, and the signal transmitted by user k is

demodulated as

$$\begin{aligned}\mathbf{r}_k = \mathbf{P}_k\mathbf{y} &= \mathbf{P}_k \sum_l \underbrace{\mathbf{E}_l \underbrace{\mathbf{F}_l\mathbf{H}_l\mathbf{\Phi}_l\mathbf{x}_l}_{\mathbf{s}_l}}_{\mathbf{v}_l} + \mathbf{P}_k\mathbf{w} \\ &= \mathbf{P}_k\mathbf{v}_k + \mathbf{P}_k\sum_{l\neq k}\mathbf{v}_l + \mathbf{P}_k\mathbf{w} = \tilde{\mathbf{s}}_k + \underbrace{\mathbf{\Upsilon}_{k;k} + \mathbf{\Upsilon}_{l\neq k;k}}_{\mathbf{\Upsilon}_k} + \tilde{\mathbf{w}}_k,\end{aligned} \tag{4.12}$$

where $\mathbf{P}_k\mathbf{v}_k = \tilde{\mathbf{s}}_k + \mathbf{\Upsilon}_{k;k}$, with $\tilde{\mathbf{s}}_k$ representing the useful part of the k-th user signal, and $\mathbf{\Upsilon}_{k;k}$ representing the ICI due to ε_k; $\mathbf{\Upsilon}_{l\neq k;k} = \mathbf{P}_k \sum\limits_{l\neq k}\mathbf{v}_l$ represents the interference from interfering users (i.e., MAI); and $\tilde{\mathbf{w}}_k$ is the AWGN added to the signal space of the k-th user. In the following analysis, $\mathbf{\Upsilon}_k = \mathbf{\Upsilon}_{k;k} + \mathbf{\Upsilon}_{l\neq k;k}$ is used to represent the interference on the k-th user (ICI+MAI). By using $\mathbf{P}_k$, the multidimensional estimation problem is reduced to several single-parameter-estimation problems.

From (4.11) and (4.12), the CRLB of the k-th user is

$$\mathrm{Var}\left\{\hat{\varepsilon_k}|\mathbf{r}_k\right\} \geq \frac{1}{\mathrm{trace}\left(\tilde{\mathbf{C}}_k^{-1}\frac{\partial\tilde{\mathbf{C}}_k}{\partial\varepsilon_k}\tilde{\mathbf{C}}_k^{-1}\frac{\partial\tilde{\mathbf{C}}_k}{\partial\varepsilon_k}\right)}, \tag{4.13}$$

where

$$\tilde{\mathbf{C}}_k = \mathbb{E}\left\{\left(\mathbf{r}_k - \mathbf{s}_k\right)\left(\mathbf{r}_k - \mathbf{s}_k\right)^H\right\} \cong \left(\mathbf{I}_N - \Sigma_k^2\right)\mathbf{C}_k \tag{4.14}$$

with $\Sigma_k = \mathrm{diag}\left\{0, -\jmath 2\pi\varepsilon_k/N, \cdots, -\jmath 2\pi\varepsilon_k \times (N-1)/N\right\}$.

Note that

$$\mathrm{trace}\left(\tilde{\mathbf{C}}_k^{-1}\frac{\partial\tilde{\mathbf{C}}_k}{\partial\varepsilon_k}\tilde{\mathbf{C}}_k^{-1}\frac{\partial\tilde{\mathbf{C}}_k}{\partial\varepsilon_k}\right) \leq \mathrm{trace}\left(\mathbf{C}_k^{-1}\frac{\partial\mathbf{C}_k}{\partial\varepsilon_k}\mathbf{C}_k^{-1}\frac{\partial\mathbf{C}_k}{\partial\varepsilon_k}\right) - \frac{8\pi^2(N-1)(2N-1)\varepsilon_k^2}{3N^3}, \tag{4.15}$$

(4.13) can be approximated as

$$\begin{aligned}\mathrm{Var}\left\{\hat{\varepsilon_k}|\mathbf{r}_k\right\} &\geq \frac{1}{\mathrm{trace}\left(\mathbf{C}_k^{-1}\frac{\partial\mathbf{C}_k}{\partial\varepsilon_k}\mathbf{C}_k^{-1}\frac{\partial\mathbf{C}_k}{\partial\varepsilon_k}\right) - \frac{8\pi^2(N-1)(2N-1)\varepsilon_k^2}{3N^3}} \\ &= \frac{1}{\sum\limits_{i=1}^{\mathcal{N}_k}\frac{\left(\frac{\partial\lambda_{k,i}}{\partial\varepsilon_k}\right)^2}{(\lambda_{k,i}+z_{k,i})^2} - \frac{8\pi^2(N-1)(2N-1)\varepsilon_k^2}{3N^3}} > \frac{1}{\sum\limits_{i=1}^{\mathcal{N}_k}\frac{\left(\frac{\partial\lambda_{k,i}}{\partial\varepsilon_k}\right)^2}{(\lambda_{k,i}+z_{k,i})^2}}.\end{aligned} \tag{4.16}$$

4.3.2 SINR Analysis

From (4.12), the receive SINR of user k can be represented as

$$\mathrm{SINR}_k \triangleq \frac{\mathbb{E}\left\{\|\tilde{\mathbf{s}}_k\|_2^2\right\}}{\mathbb{E}\left\{\|\boldsymbol{\Upsilon}_k\|_2^2\right\} + \mathbb{E}\left\{\|\tilde{\mathbf{w}}_k\|_2^2\right\}} = \frac{\mathrm{SNR}_k}{\frac{\pi^2\sigma_\epsilon^2\mathrm{SNR}_k}{3} + 1} \cdot \left(1 - \frac{\pi^2\sigma_\epsilon^2}{3} + \frac{\pi^4\sigma_\epsilon^4}{20}\right), \tag{4.17}$$

as derived in Appendix B. 1. Since $\frac{1}{\mathrm{SINR}_k} = \frac{1}{\mathrm{SNR}_k} + \frac{1}{\mathrm{SIR}_k}$ always holds, SIR_k can be represented as $\mathrm{SIR}_k = \frac{3}{\pi^2\sigma_\epsilon^2}\left(1 - \frac{\pi^2\sigma_\epsilon^2}{3} + \frac{\pi^4\sigma_\epsilon^4}{20}\right)$, and the conditional variance derived in (4.16) is lower bounded as,

$$\mathrm{Var}\left\{\hat{\varepsilon_k}|\mathbf{r}_k\right\} \geq \frac{1}{\alpha_k \cdot \mathrm{SNR}_k^2} + \frac{1}{\beta_k \cdot \mathrm{SNR}_k} + \frac{\pi^2\sigma_\epsilon^2}{3\varpi_k\left(1 - \frac{\pi^2\sigma_\epsilon^2}{3} + \frac{\pi^4\sigma_\epsilon^4}{20}\right)}, \tag{4.18}$$

At a high SNR, the conditional variance becomes $\lim_{\mathrm{SNR}_k \to \infty} \mathrm{Var}\left\{\hat{\varepsilon_k}|\mathbf{r}_k\right\} \geq \frac{\pi^2\sigma_\epsilon^2}{3\varpi_k\left(1 - \frac{\pi^2\sigma_\epsilon^2}{3} + \frac{\pi^4\sigma_\epsilon^4}{20}\right)}$.

The SINR reduction due to the MAI is shown in Figure 4.25. A considerable MAI is added to the user of interest due to the frequency offsets of the interfering users, and a larger σ_ϵ^2 implies a higher MAI. For example, for an SNR of 30 dB, when $\sigma_\epsilon^2 = 10^{-3}$, the received SINR is about 13.6 dB. If σ_ϵ^2 is increased to 10^{-2}, the received SINR is reduced to only about 4.55 dB.

4.3.3 Frequency Offset Analysis

By using a SIC method, e.g., that proposed in [136], the MAI can be iteratively reduced, and at the $(n+1)$-th iteration $(n \geq 1)$, $\mathbf{r}_k$ can be represented as

$$\mathbf{r}_k^{(n+1)} = \tilde{\mathbf{s}}_k^{(n+1)} + \boldsymbol{\Upsilon}_{k;k}^{(n+1)} + \boldsymbol{\Upsilon}_{l<k}^{(n+1)} + \boldsymbol{\Upsilon}_{l>k}^{(n)} + \tilde{\mathbf{w}}_k^{(n+1)}, \tag{4.19}$$

where the superscript $^{(n)}$ denotes the vector value at the n-th iteration, and

$$\tilde{\mathbf{s}}_k^{(n+1)} = \mathbf{P}_k \boldsymbol{\Delta}_k^{(n+1)} \mathbf{s}_k, \tag{4.20a}$$

$$\boldsymbol{\Upsilon}_{k;k}^{(n+1)} = \mathbf{P}_k \left(\mathbf{I}_N - \boldsymbol{\Delta}_k^{(n+1)}\right) \mathbf{s}_k, \tag{4.20b}$$

$$\boldsymbol{\Delta}_k^{(n+1)} = \mathrm{diag}\left\{1, e^{\frac{\jmath 2\pi e_k^{(n+1)}}{N}}, \cdots, e^{\frac{\jmath 2\pi e_k^{(n+1)} \times (N-1)}{N}}\right\}, \tag{4.20c}$$

$$e_k^{(n+1)} = \varepsilon_k - \hat{\varepsilon}_k^{(n+1)}. \tag{4.20d}$$

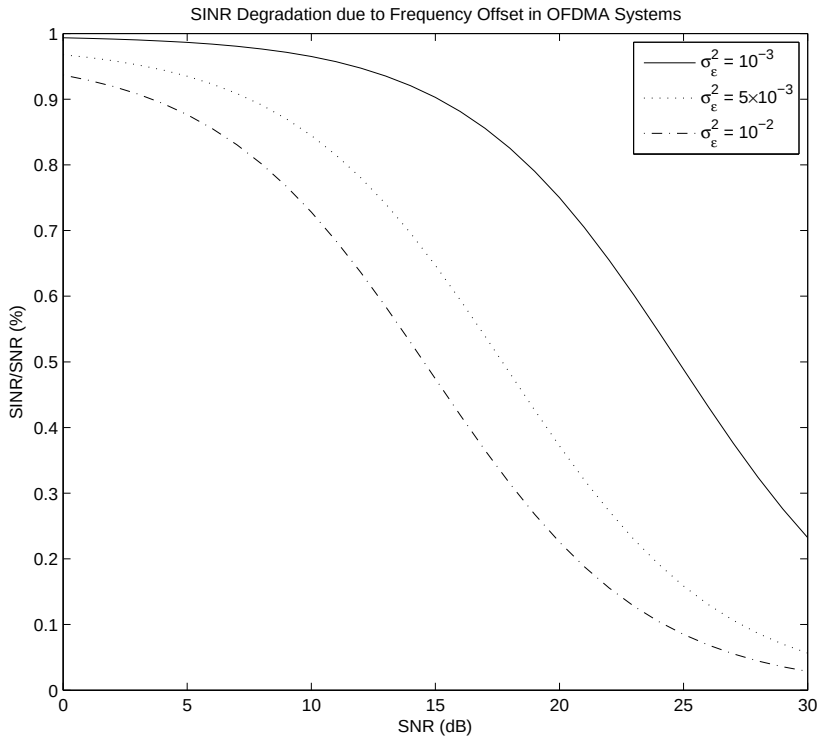

Figure 4.25: SINR reduction introduced by non-zero frequency offset in OFDMA systems.

As n increases, (4.19) converges to its steady state as $\mathbf{r}_k = \tilde{\mathbf{s}}_k + \boldsymbol{\Upsilon}_{k;k} + \boldsymbol{\Upsilon}_{l\neq k} + \tilde{\mathbf{w}}_k$.

Although the MAI can be reduced by using the SIC-based method, it can never be totally eliminated in a noisy environment. In a synchronized OFDMA system (frequency offset acquisition has been performed and most of the frequency offset has been compensated for), the frequency offset of each user is limited with a finite range so that

$$\mathrm{Var}\left\{\hat{\varepsilon_k}|\mathbf{r}_k\right\} = \sigma_\epsilon^2 > \frac{1}{\alpha_k \cdot \mathrm{SNR}_k^2} + \frac{1}{\beta_k \cdot \mathrm{SNR}_k} + \frac{\pi^2\sigma_\epsilon^2}{3\varpi_k}. \tag{4.21}$$

By resolving (4.21), σ_ϵ^2 can be lower bounded as

$$\sigma_\epsilon^2 > \frac{3\varpi_k}{3\varpi_k - \pi^2} \cdot \left(\frac{1}{\alpha_k \cdot \mathrm{SNR}_k^2} + \frac{1}{\beta_k \cdot \mathrm{SNR}_k}\right), \tag{4.22}$$

and as SNR_k increases, $\lim_{\mathrm{SNR}_k \to \infty} \sigma_\epsilon^2 = 0$. Note that the distribution of frequency offsets is not specified here because any distribution with zero mean and variance σ_ϵ^2 satisfies (4.21) and(4.22). For example, without loss of generality, we can assume that $\varepsilon_k \sim \mathcal{N}(0, \sigma_\epsilon^2)$. However, if we assume that ε_k is a uniformly distributed RV with the distribution range $(-\epsilon, \epsilon)$ where $\epsilon > 0$, we have $\epsilon = \sqrt{3}\sigma_\epsilon$, and (4.22) can be rewritten as

$$\epsilon = \sqrt{3}\sigma_\epsilon > \sqrt{\frac{9\varpi_k}{3\varpi_k - \pi^2} \cdot \left(\frac{1}{\alpha_k \cdot \mathrm{SNR}_k^2} + \frac{1}{\beta_k \cdot \mathrm{SNR}_k} \right)}. \tag{4.23}$$

Now σ_ϵ^2 will be analyzed in real systems with a finite SNR. If the training sequence proposed in [13] is used by each user, we have $\alpha_k = \varpi_k = 4\pi^2 N$ and $\beta_k = 2\pi^2 N$ for each k. Figure 4.26 shows σ_ϵ^2 as a function of the SNR and N. When the SNR and N are large enough, σ_ϵ^2 is negligible. For example, when SNR_k=10 dB, σ_ϵ^2 is only about 4×10^{-5} with $N = 128$, and it will reduce to 5×10^{-6} when $N = 1024$.

4.4 Iterative Frequency Offset Estimation

In the OFDMA uplink, frequency offset estimation is a multidimensional-estimation problem. The frequency offset vector $\mathcal{E} = [\varepsilon_1, \varepsilon_2, \cdots, \varepsilon_M]^T$ is estimated based on $\mathbf{y}$. Two iterative algorithms for the frequency offset estimation will be introduced.

4.4.1 ML Estimation

Based on the received training sequence $\mathbf{y}$, an ML estimator of $\mathcal{E}$ is given by

$$\hat{\mathcal{E}}_{ML} = \arg\min_{\hat{\mathcal{E}}} \left\| \mathbf{y} - \sum_l \underbrace{\hat{\mathbf{E}}_l \mathbf{F}_l \mathbf{H}_l \mathbf{\Phi}_l}_{\mathbf{A}_l} \mathbf{x}_l \right\|_2^2 = \arg\min_{\hat{\mathcal{E}}} \left(\mathbf{y} - \sum_l \mathbf{A}_l \mathbf{x}_l \right)^H \left(\mathbf{y} - \sum_l \mathbf{A}_l \mathbf{x}_l \right), \tag{4.24}$$

where

$$\hat{\mathbf{E}}_k = \mathrm{diag}\left\{ e^{\jmath\psi_k}, e^{\jmath\left(\frac{2\pi\hat{\varepsilon}_k}{N} + \psi_k\right)}, \cdots, e^{\jmath\left(\frac{2\pi\hat{\varepsilon}_k \times (N-1)}{N} + \psi_k\right)} \right\}$$

and

$$\hat{\mathcal{E}} = [\hat{\varepsilon}_1, \hat{\varepsilon}_2, \cdots, \hat{\varepsilon}_M]^T.$$

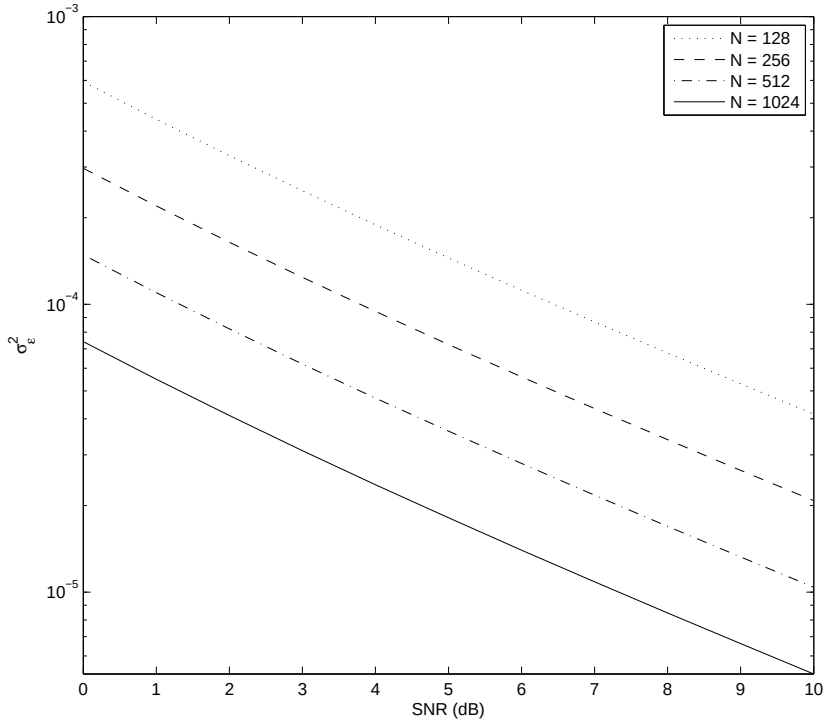

Figure 4.26: Minimum variance of the frequency offset in a noisy OFDMA system.

By taking the partial derivative of $\left(\mathbf{y} - \sum_l \mathbf{A}_l\mathbf{x}_l\right)^H \left(\mathbf{y} - \sum_l \mathbf{A}_l\mathbf{x}_l\right)$ with respect to each l and setting each equation to zero, $\mathbf{x}_l$ can be estimated as

$$\hat{\mathbf{x}}_l = (\mathbf{A}_l^H\mathbf{A}_l)^{-1}\mathbf{A}_l^H\mathbf{y} - \sum_{k\neq l}(\mathbf{A}_l^H\mathbf{A}_l)^{-1}\mathbf{A}_l^H\tilde{\mathbf{P}}_k\mathbf{y}, \quad 1 \leq k, l \leq M, \tag{4.25}$$

where $\tilde{\mathbf{P}}_k = \mathbf{A}_k(\mathbf{A}_k^H\mathbf{A}_k)^{-1}\mathbf{A}_k^H$. By replacing $\mathbf{x}_l$ in (4.24) by using (4.25), (4.24) can be simplified as

$$\hat{\mathcal{E}}_{ML} = \arg\min_{\hat{\varepsilon}} \left\| \mathbf{y} - \sum_l \left(\tilde{\mathbf{P}}_l\mathbf{y} - \sum_{k\neq l} \tilde{\mathbf{P}}_l\tilde{\mathbf{P}}_k\mathbf{y} \right) \right\|_2^2 = \arg\min_{\hat{\varepsilon}} \left\| \mathbf{y} - \sum_l \tilde{\mathbf{P}}_l\mathbf{y} + \sum_{k\neq l} \tilde{\mathbf{P}}_l\tilde{\mathbf{P}}_k\mathbf{y} \right\|_2^2. \tag{4.26}$$

Since a multidimensional parameter estimator is inefficient, a multidimensional estimation is usually decomposed into multiple 1-dimensional estimators to reduce the

complexity [133, 137]. The frequency offset of each user can be iteratively estimated by using (4.26), and this algorithm will converge to its steady state after several iterations. However, $\tilde{\mathbf{P}}_l$ for each l should be calculated at each iteration, and the matrix inverse operation in $\tilde{\mathbf{P}}_l$ complicates $\hat{\mathcal{E}}_{ML}$. In real systems, pilots/training sequences are usually used to estimate the frequency offsets. The MAI can be eliminated by using a SIC-based algorithm, and the estimation performance of the SIC-based algorithm is as good as that of (4.26).

4.4.2 SIC-based Algorithm by Using Known Pilots/Training Sequences

Suppose the number of users that access a base station is M, and the perfect CSI between each user and base station is assumed to be perfectly known at the base station. Note that because the channel estimates will degrade in the presence of the frequency offset, perfect CSI knowledge is not available. However, CSI can be estimated in the presence of the frequency offset by exploiting the received $\{\mathbf{v}_1, \mathbf{v}_2, \cdots, \mathbf{v}_M\}$. For example, some joint channel and frequency offset estimation algorithms are proposed in [138], which can achieve the CSI with a high accuracy.

Based on the joint PDF of $\{\mathbf{v}_1, \mathbf{v}_2, \cdots, \mathbf{v}_M\}$ and $\mathbf{y}$, $\{\mathbf{v}_1, \mathbf{v}_2, \cdots, \mathbf{v}_M\}$ can be estimated as

$$\begin{aligned}
&\{\hat{\mathbf{v}}_1, \hat{\mathbf{v}}_2, \cdots, \hat{\mathbf{v}}_M\} \\
&= \arg\max_{\hat{\mathbf{v}}_M} \{\ln f(\hat{\mathbf{v}}_M | \hat{\mathbf{v}}_{M-1}, \cdots, \hat{\mathbf{v}}_1; \mathbf{y})\} + \arg \max_{\{\hat{\mathbf{v}}_1, \cdots, \hat{\mathbf{v}}_{M-1}\}} \{\ln f(\hat{\mathbf{v}}_{M-1}, \cdots, \hat{\mathbf{v}}_1; \mathbf{y})\} \\
&= \sum_{m=1}^{M} \arg\max_{\hat{\mathbf{v}}_m} \left\{ \ln f\left(\hat{\mathbf{v}}_m | \mathbf{y} - \sum_{l=1}^{m-1} \hat{\mathbf{v}}_l \right) \right\} + \ln f(\mathbf{y}) \\
&= \sum_{m=1}^{M} \arg\max_{\hat{\mathbf{v}}_m} \left\| \hat{\mathbf{v}}_m^H \left(\mathbf{y} - \sum_{l=1}^{m-1} \hat{\mathbf{v}}_l \right) \right\|_2^2 .
\end{aligned} \tag{4.27}$$

User $(l+1)$ estimates $\mathbf{v}_{l+1}$ based on $\left(\mathbf{y} - \sum_{m=1}^{l} \hat{\mathbf{v}}_m\right)$, which can be performed after the synchronization of the previous l users, where $l \leq M-1$. There is a substantial tradeoff

between the estimation accuracy and the number of iterations in (4.27), and, in each iteration, the estimation accuracy of $\hat{\mathbf{v}}_m$ depends on that of $\hat{\mathbf{v}}_{l\neq m}$. Note that, usually, there is no closed-form solution for (4.27), and the frequency offsets that maximize (4.27) should be searched in a given range to optimize the cost function. This search range must be sufficiently large to reduce the probability that the actual offset is outside it.

4.5 Improving Estimators by Exploiting the Frequency Offset Variance in OFDMA Uplink

In an OFDMA uplink transmission, the performances of the conventional estimators are sensitive to SINR [13, 76]. The frequency offset of the m-th user ε_m is assumed to be an i.i.d. RV with zero mean and variance σ_ϵ^2. If σ_ϵ^2 is known as a *priori*, it can be used to improve the estimation accuracy.

Note that CSI is critical in some pilot-based frequency offset algorithms, and the variance of the frequency offsets cannot be correctly estimated without CSI. The enhanced frequency offset estimation in the single-user scenario with CSI is discussed in [139], where the frequency offset estimation by using pilot/training symbols, null subcarriers, or their combination is analyzed.

The OFDMA receiver structure for an uplink frequency offset estimation is shown in Figure 4.27. The SNR/SINR estimates for each user are used to estimate σ_ϵ^2, and the estimate is used to improve the frequency offset estimation. In (4.17), SINR is derived as a function of σ_ϵ^2, and this function is invertible. Therefore, using SNR_k and SINR_k, an estimate of σ_ϵ^2 is given by

$$\hat{\sigma}_\epsilon^2 = \frac{10\mathrm{SNR}_k(\mathrm{SINR}_k+1) - 10\sqrt{\mathrm{SNR}_k^2(\mathrm{SINR}_k+1)^2 - \frac{9}{5}\mathrm{SNR}_k(\mathrm{SNR}_k-\mathrm{SINR}_k)}}{3\pi^2\mathrm{SNR}_k}. \quad (4.28)$$

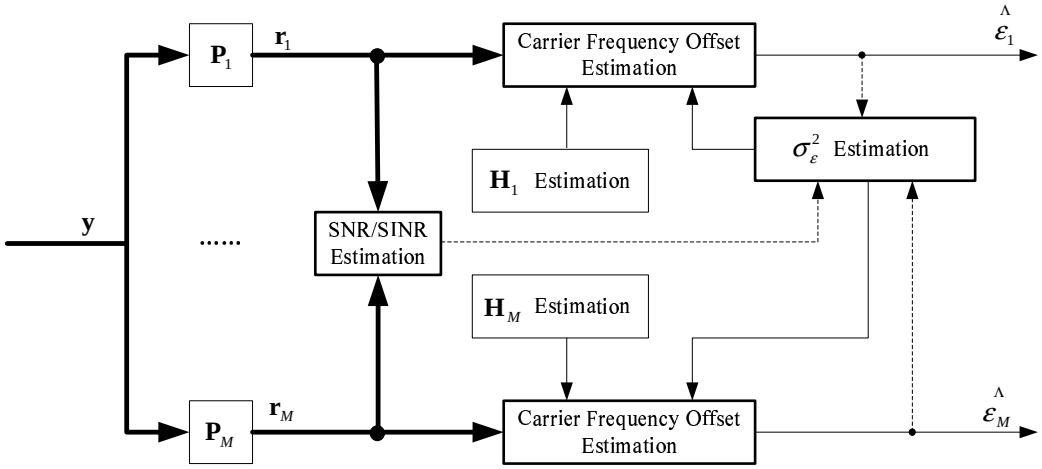

Figure 4.27: Receiver structure for OFDMA uplink frequency offset estimation.

Note that an estimate of σ_ϵ^2 is not sufficient to specify the actual distribution of frequency offsets. However, if σ_ϵ^2 is available, some reasonable distributions can be assumed to improve the frequency offset estimation. For example, if ε_k is a uniformly distributed RV with the distribution range $(-\epsilon_k, \epsilon_k)$, the maximum deviationis given by

$$\hat{\epsilon}_k = \sqrt{3}\hat{\sigma}_\epsilon = \frac{\sqrt{10\mathrm{SNR}_k(\mathrm{SINR}_k+1) - 10\sqrt{\mathrm{SNR}_k^2(\mathrm{SINR}_k+1)^2 - \frac{9}{5}\mathrm{SNR}_k(\mathrm{SNR}_k - \mathrm{SINR}_k)}}}{\pi\sqrt{\mathrm{SNR}_k}}. \tag{4.29}$$

Several high-quality SNR estimators have been proposed in [140–142]. For example, by modulating each subcarrier of each user with a PSK signal, a well-known non-data-aided estimator proposed in [140] can be used to estimate SNR_k as

$$\hat{\mathrm{SNR}}_k = \frac{\sqrt{2m_2^2 - m_4}}{m_2 - \sqrt{2m_2^2 - m_4}}, \tag{4.30}$$

where $m_2 = \frac{1}{\mathcal{N}_k}\left(\mathbf{F}_k^H\mathbf{y}\right)^H\left(\mathbf{F}_k^H\mathbf{y}\right)$ and $m_4 = \frac{1}{\mathcal{N}_k}\sum_{i=0}^{\mathcal{N}_k-1}\left\{\left(\mathbf{F}_k^H\mathbf{y}\right)[i]\right\}^4$. When $\mathcal{N}_k$ is large enough, the performance of (4.30) is independent of the frequency offset.

The SINR of user k, i.e., SINR_k, can be estimated as

$$\text{SINR}_k \cong \frac{\left|\left(\mathbf{F}_k^H \mathbf{y}\right)^H \mathbf{x}_k\right|^2}{\left\|\mathbf{F}_k^H \mathbf{y}\right\|_2^2 - \left|\left(\mathbf{F}_k^H \mathbf{y}\right)^H \mathbf{x}_k\right|^2}, \tag{4.31}$$

where $\mathbf{x}_k$ represents the training sequence transmitted by the k-th user. Figure 4.28 illustrates the SINR estimation accuracy with $N = 256$ and $\sigma_\epsilon^2 = 3.3 \times 10^{-3}$. The simulation results show that the SINR for each user can be accurately estimated based on (4.31). For an OFDMA uplink transmission with M users accessing a base station, σ_ϵ^2 can be represented as

$$\sigma_\epsilon^2 = \max\left\{\hat{\sigma}_{\epsilon_1}^2, \hat{\sigma}_{\epsilon_2}^2, \cdots, \hat{\sigma}_{\epsilon_M}^2, \frac{1}{M}\sum_{i=1}^{M} \hat{\varepsilon}_i^2\right\}, \tag{4.32}$$

where $\hat{\varepsilon}_k$ represents the currently estimated ε_k, and $\hat{\sigma}_{\epsilon_i}^2$ represents the estimated σ_ϵ^2 for the i-th user. If uniformly distributed RVs with the distribution range $(-\epsilon, \epsilon)$ are used to approximate the actual distribution of the frequency offsets, ϵ can be represented as

$$\epsilon = \max\{\sqrt{3}\hat{\sigma}_{\epsilon_1}, \sqrt{3}\hat{\sigma}_{\epsilon_2}, \cdots, \sqrt{3}\hat{\sigma}_{\epsilon_M}, |\hat{\varepsilon}_1|, |\hat{\varepsilon}_2|, \cdots, |\hat{\varepsilon}_M|\}. \tag{4.33}$$

4.5.1 The SIC-based Algorithm with the Variance of the Frequency Offsets

Using the training sequences, an OFDMA uplink Frequency offset estimation can be performed via the SIC-based method, as given in (4.27). The performance of (4.27) can be improved by exploiting the variance of the frequency offset of each user [the same goes for (4.26)]. The idea is to search ε_k for each k subject to $\text{Var}\{\varepsilon_k\} = \sigma_\epsilon^2$ to optimize the cost function, as given by Algorithm 1, which is an improved version of (4.27). The search complexity can be minimized by using a probability distribution with the smaller range given the variance. For example, if ε_k is assumed uniformly distributed with variance σ_ϵ^2, then the search interval is $(-\sqrt{3}\sigma_\epsilon, \sqrt{3}\sigma_\epsilon)$. However, if a Gaussian

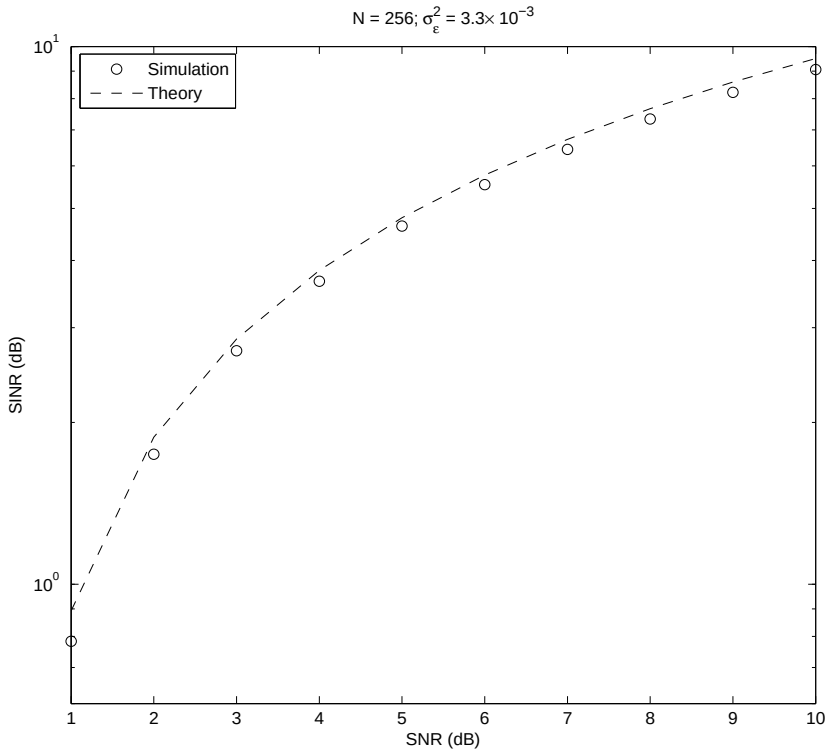

Figure 4.28: SINR estimation in OFDMA uplink.

$\varepsilon_k \sim \mathcal{N}(0, \sigma_\epsilon^2)$ is assumed, the search range increases to an infinite area. Because of this fact, the use of the uniform distribution to model the frequency offset is preferable. In the following, the uniform distribution is shown to be a good approximation to the actual distribution. The performance degradation due to the mismatch between the uniform distribution and the actual distribution will also be analyzed.

Algorithm 1: SIC-based Estimator with ϵ Knowledge

Iteration 0:

for $m = 1$ to M

$\hat{\mathbf{v}}_m^{(0)} = \mathbf{0}_N$; $\mathbf{y}_m^{(0)} = \mathbf{0}_N$; $\mathbf{k}_m^{(0)} = \mathbf{0}_N$;

end

end ***Iteration*** 0 ;

$\vdots$

Iteration $(i+1)$:

for $m = 1$ to M

$\mathbf{k}_m^{(i+1)} = \mathbf{y} - \sum_{l=1}^{m-1} \mathbf{y}_l^{(i+1)} - \sum_{l=m+1}^{k} \mathbf{y}_l^{(i)}$;

$\hat{\mathbf{v}}_m^{(i+1)} = \arg\max_{-\epsilon<\hat{\varepsilon}_m<\epsilon} \left\| \hat{\mathbf{v}}_m^H \mathbf{k}_m^{(i+1)} \right\|_2^2$;

$\mathbf{y}_m^{(i+1)} = \hat{\mathbf{v}}_m^{(i+1)}$;

end

end ***Iteration*** $(i+1)$;

$\vdots$

end Algorithm 1.

Figure 4.29 compares the performance of the SIC-based estimators with and without the variance estimation. The total number of subcarriers is 256, and the number of users is 16. Perfect channel and initial phase estimation is assumed. The estimators with/without the variance estimate reach the same accuracy, albeit at the different converging speeds. Equation (4.27) without the variance estimation converges to its steady state in five iterations, but Algorithm 1 converges in two iterations.

4.5.2 Conventional Differential Algorithms with the Variance Knowledge

The SIC-based algorithms can perform the OFDMA uplink frequency offset estimation with high accuracy. However, channel and initial phase estimation is required, which complicates the use of the algorithm in a high-mobility environment. Differential algorithms are proposed in many classical frequency offset estimators, where a training sequence comprising two or more identical replicas is usually used [13, 76, 143]. Their performance is independent of the initial phases, and if the channel does not change during the training sequence period, the frequency offsets can be estimated without

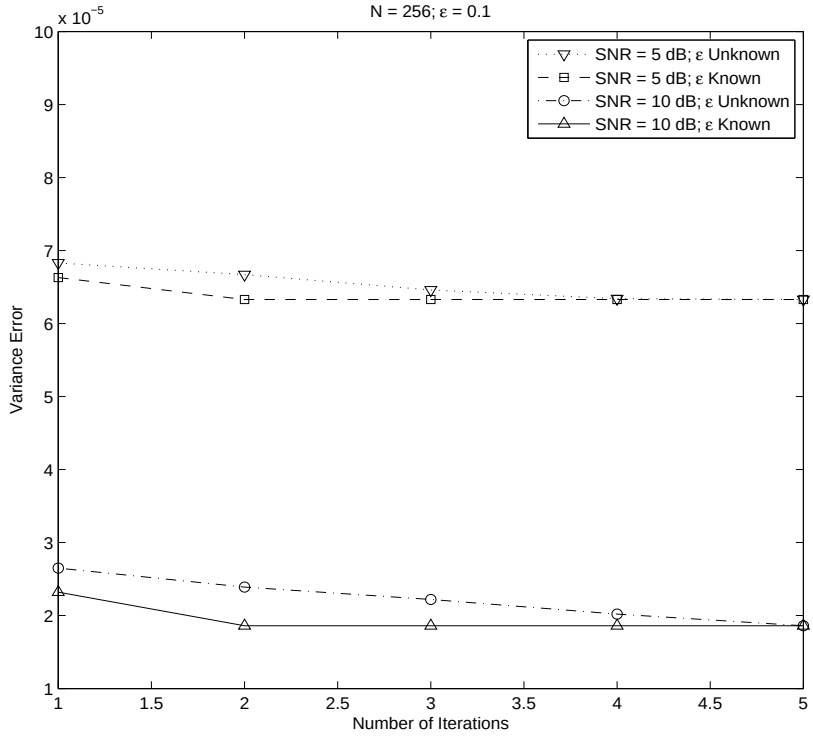

Figure 4.29: SIC-based frequency offset estimation.

the CSI knowledge.

Some original differential algorithms for OFDM systems, e.g., [13, 76], can also be used for an OFDMA uplink transmission, and the LS or ML principle can be applied for each user to perform the frequency offset estimation. Assuming that M users access a base station, with e_k representing the frequency offset estimation error of the k-th user ($1 \le k \le M$), the frequency offset estimation vector can be represented as

$$\tilde{\mathcal{E}}_{\mathrm{LS}} = \left[\hat{\varepsilon}_1, \cdots, \hat{\varepsilon}_M\right]^T = \underbrace{\left[\varepsilon_1, \cdots, \varepsilon_M\right]^T}_{\mathcal{E}} + \underbrace{\left[e_1, \cdots, e_M\right]^T}_{\mathbf{e}}, \tag{4.34}$$

where $\hat{\varepsilon}_k = \arg\min_{\hat{\varepsilon}_k} \left\| \mathbf{P}_k \mathbf{y} - \hat{\mathbf{E}}_k \mathbf{s}_k \right\|_2^2$. For the conditionally unbiased estimations, $\mathbb{E}\{\mathbf{e}\} = \mathbf{0}_M$, and the variance matrix of $\mathbf{e}$ is given by $\mathrm{Var}\{\tilde{\mathcal{E}}_{\mathrm{LS}}\} = \mathbb{E}\{\mathbf{e}\mathbf{e}^H\} = \mathbf{C}_e$.

The MAI due to the frequency offsets will degrade the estimation accuracy of (4.34),

Table 4.3: Subcarrier Allocation in OFDMA Uplink Transmission (Bandwidth = 10 MHz, DFT Length = 256, CP = 16)

Number of Users	16
Number of Subcarriers Allocated	224
Number of Guard Band Subcarriers	32
Subcarrier Allocation	Interleaved
Normalized Frequency Offset	Uniformly distributed in $(-\epsilon, \epsilon)$
Training Sequence Used	Like in [13]
Maximum Multipath Delays (μs)	0.8
Initial Phase	Uniformly distributed in (0,2π)

and this performance loss partially comes from our lack of knowledge of the frequency offset variance. Under the assumption of uniform distribution for the frequency offsets, (4.34) can be improved as $\tilde{\mathcal{E}}_\epsilon = [\hat{\varepsilon}_{\epsilon,1}, \cdots, \hat{\varepsilon}_{\epsilon,M}]^T$, where $\hat{\varepsilon}_{\epsilon,k} = \arg\min_{-\epsilon<\hat{\varepsilon}_k<\epsilon} \left\| \mathbf{P}_k \mathbf{y} - \hat{\mathbf{E}}_k \mathbf{s}_k \right\|_2^2$ for each k. From [122], the covariance matrix of the estimation error of $\tilde{\mathcal{E}}_\epsilon$ is lower bounded by $\widetilde{\mathbf{M}} = \left(\mathbf{C}_{\mathcal{E}\mathcal{E}}^{-1} + \mathbf{C}_e^{-1}\right)^{-1}$, where $\mathbf{C}_{\mathcal{E}\mathcal{E}} = \sigma_\epsilon^2 \mathbf{I}_M$. If $\mathbb{E}\{e_k e_{l\neq k}\} = 0$ is satisfied for each k, $\widetilde{\mathbf{M}}$ is reduced to

$$\widetilde{\mathbf{M}} = \text{diag}\left\{ \frac{1}{\tilde{\sigma}_1^2}, \frac{1}{\tilde{\sigma}_2^2}, \cdots, \frac{1}{\tilde{\sigma}_M^2} \right\}. \tag{4.35}$$

where $\tilde{\sigma}_i^2 = (1/\sigma_\epsilon^2) + (1/\text{Var}\{e_i\})$

4.6 Numerical Results

A wireless OFDMA system with a bandwidth of 10 MHz and 256 subcarriers is considered, and a length-16 CP is used. QPSK modulation is used in all subcarriers, and the interleaved subcarriers allocation is performed among different users to exploit the frequency diversity. A Rayleigh fading channel is considered for each uses, as shown in Table 4.3.

The estimator proposed in [13] (a differential frequency offset estimator based on a training sequence comprising two identical replicas) is used as an example to illustrate the performance improvement with knowledge of the frequency offsets. Note that

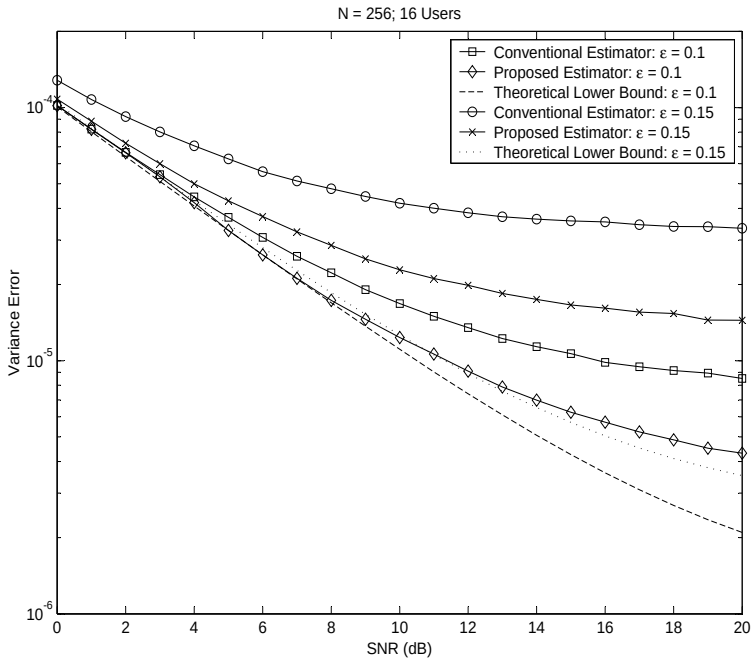

Figure 4.30: Performance comparison between conventional estimator and the proposed estimator.

the performance of any conventional algorithm can be improved by exploiting this knowledge.

Figure 4.30 shows the performance improvement in the conventional estimators with (4.33) or without (4.33). In this simulation, all the users are assumed to run at the frequency offset tracking phase, and a larger ϵ implies a higher estimation error in either the conventional estimator (that without using the frequency offset variance) or the proposed one (that with the frequency offset variance). A performance floor always appears at a high SNR in either the conventional estimator or the proposed one

Table 4.4: Subcarrier Allocation in OFDMA Uplink Transmission with New Accessed Users (Bandwidth = 10 MHz, DFT Length = 256, CP = 16)

Number of Users in Tracking Phase	16
Number of Subcarriers Allocated	224
Number of Guard Band Subcarriers	32
Subcarrier Allocation	Interleaved
Normalized Frequency Offset in Tracking Phase	Uniformly distributed in $(-\epsilon, \epsilon)$
Number of New Accessed Users	1; 2; 3; 4
Normalized Frequency Offset of New User	Uniformly distributed in $(-1.6, 1.6)$
Training Sequence Used	Like in [13]
Maximum Multipath Delays (μs)	0.8
Initial Phase	Uniformly distributed in (0,2π)

due to the unreducible MAI. The estimation accuracy in the conventional estimator can be improved by exploiting the knowledge of the variance, and this performance improvement becomes larger as the SNR increases. For example, when ϵ = 0.1, the performance improvement of an algorithm with variance knowledge over one without can be up to 3 dB at a high SNR.

In an OFDMA uplink, the users may dynamically access or depart from a base station. A new accessing user may have an instantaneously large frequency offset, causing a heavy MAI to its frequency-domain neighbors. Table 4.4 shows a scenario of the base station, where 16 current users are running at the tracking phase, and this simulation considers the case that only one new user is starting to access the base station. The new user has an initial frequency offset of 1.6 times the subcarrier spacing. Note that the integer frequency offset in the new user should be estimated and corrected by using an acquisition algorithm, e.g., as in [13, 144].

The performance degradation of the frequency offset estimation in tracking users, due to the large frequency offset of the new accessing user, is shown in Figure 4.31. A considerable performance degradation appears in the conventional estimator (without variance knowledge); the proposed estimator with variance knowledge is more robust

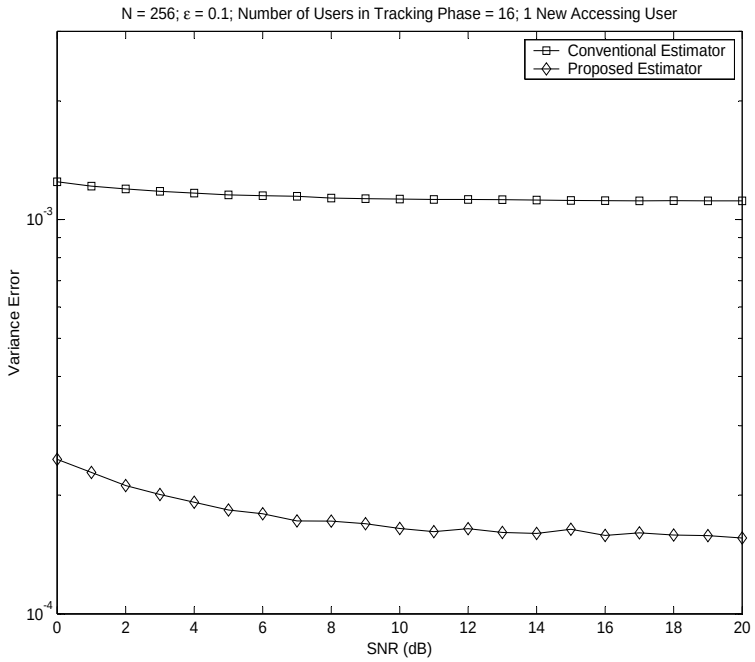

Figure 4.31: Performance comparison between conventional estimator and the proposed estimator when there is one new user accessing the base station.

for combating the instantaneously large MAI. For example, at a SNR of 10 dB, the variance error in the conventional estimator is about 1.13×10^{-3}, and this error can be reduced to about 1.65×10^{-4} in the proposed estimator.

A much heavier MAI is generated if there are multiple new users simultaneously accessing the base station, as shown in Figure 4.32, where the simulation parameters are also defined in Table 4.4. This simulation keeps SNR = 10 dB unchanged, and one to four new users access the base station. In this case, the instant interference on the existing users is mainly contributed by these new users. The proposed estimator

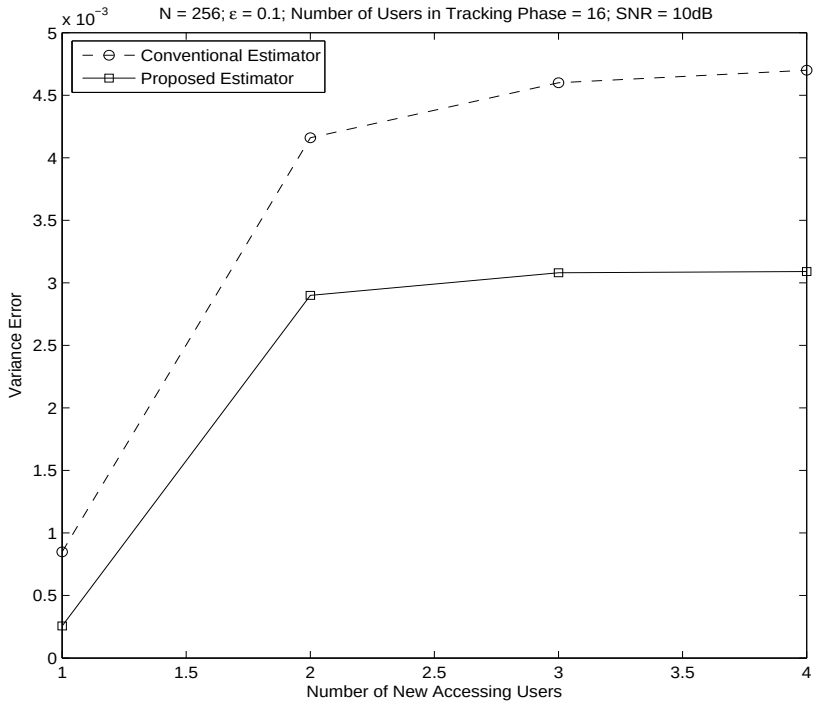

Figure 4.32: Performance comparison between conventional estimator and the proposed estimator when there are multiple new users simultaneously accessing the base station.

considerably outperforms the conventional estimator. For example, with two new users accessing the base station, the variance error for the conventional estimator is about 4.16×10^{-3}, and that for the proposed estimator is about 2.9×10^{-3}. For the case of four new users, the variance error for the conventional estimator increases to about 4.7×10^{-3}, and that for the proposed estimator is 3.08×10^{-3}.

Thus far, the frequency offsets for different users were assumed to be uniformly distributed RVs. In real systems, the actual distribution may be not uniform, and, hence, a uniformly distributed RV mismatches the distribution of ε_k. However, the exact distribution may be well approximated by a uniform distribution. For example, assuming that the actual distribution is Gaussian with $\varepsilon_k \sim \mathcal{N}(0, \sigma_\epsilon^2)$, the probability of ε_k being outside of the range $(-\sqrt{3}\sigma_\epsilon, \sqrt{3}\sigma_\epsilon)$ is $P\left\{|\varepsilon_k| > \sqrt{3}\sigma_\epsilon\right\} \cong 0.0833$; i.e., most

of the realization of ε_k falls into the range $(-\sqrt{3}\sigma_\epsilon, \sqrt{3}\sigma_\epsilon)$. Since a uniform distributed RV with a range $(-\sqrt{3}\sigma_\epsilon, \sqrt{3}\sigma_\epsilon)$ can also result in a variance of σ_ϵ^2, we can set $\epsilon = \sqrt{3}\sigma_\epsilon$ and use this uniform distribution to approximate the actual distribution. For OFDMA uplink frequency offset estimation with the proposed estimator, σ_ϵ is first estimated by using (4.32), and then set $\hat{\epsilon} = \sqrt{3}\hat{\sigma}_\epsilon$ [or directly use (4.33)] to approximate ε_k as an uniformly distributed RV in $(-\hat{\epsilon}, \hat{\epsilon})$. Figure 4.33 compares the performance of the conventional estimator with or without variance knowledge when all the user frequency offsets are i.i.d. Gaussian RVs. The simulation results show that $\varepsilon_k \sim \mathcal{N}(0, \sigma_\epsilon^2)$ can be well approximated as a uniformly distributed RV with $\epsilon = \sqrt{3}\sigma_\epsilon$, and that at a high SNR, the prior variance knowledge can provide a performance improvement of about 3 dB.

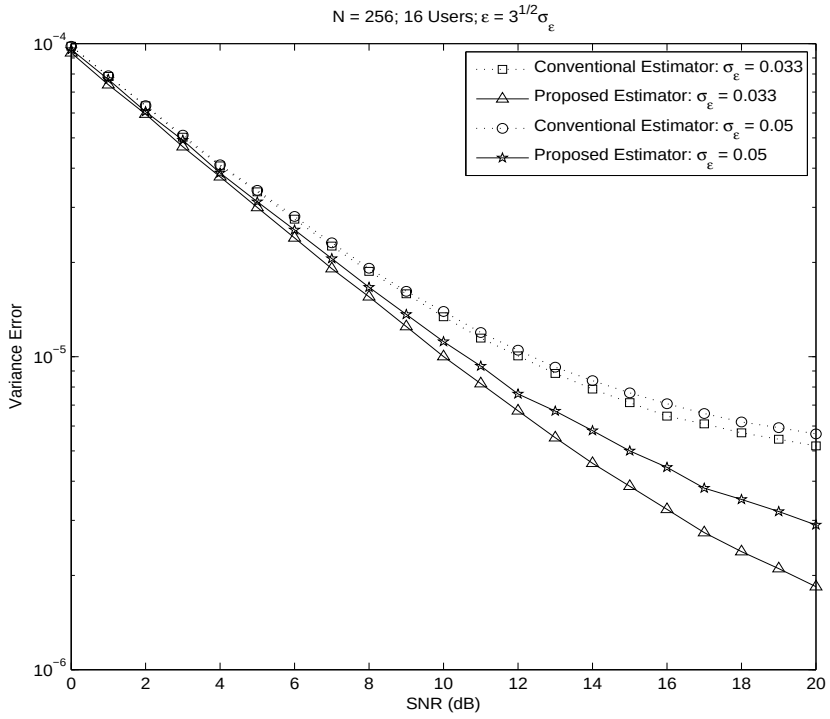

Figure 4.33: Performance comparison between conventional estimator and the proposed estimator by using a uniform RV to approximate the Gaussian distributed frequency offsets.

4.7 Conclusions

This chapter has discussed the OFDMA uplink frequency offset estimation, and the performance degradation in the estimation due to MAI has been analyzed. The variance of the frequency offset of each user may be estimated through MAI analysis. This estimate of the variance of frequency offsets helps to improve the robustness and accuracy of the frequency offset estimation. For an OFDMA uplink with all the accessed users running at the tracking phase, the frequency offset of each user can be assumed to be an i.i.d. RV with zero mean and a variance of σ_ϵ^2, and a uniformly distributed RV can be used to approximate the actual distribution of the frequency offset. The simulation results prove the validity of this uniform approximation.

Chapter 5

OFDMA Uplink Frequency Offset Estimation via Cooperative Relaying

Frequency offset estimation for an OFDMA uplink for AF relays and a new type of relay called decode-and-compensate-and-forward (DcF) relays are studied in this chapter [145]. Multiple relays are considered, and the relay with the best $S \rightarrow R$ channel is chosen to perform re-transmission, where S and R represent the source and the relay nodes. Power allocation between S and R can be adaptively adjusted to optimize the cooperative scheme in terms of frequency offset error variance. When CSI is available at each mobile node, a scheme where the relays adaptively switch between the cooperative and conventional (no relaying) transmissions is proposed to optimize the frequency offset estimation.

5.1 Introduction

In the literature, many relay studies focused on flat-fading channels, where single-carrier systems are of interest [39, 146, 147]. However, the use of relays in frequency-selective broadband channels is important as well. A popular solution against frequency-selective fading is OFDM. Cooperative OFDM relay networks and cooperative OFDMA are, thus, increasingly important.

As is common to all OFDM-based systems, cooperative OFDMA systems are also

sensitive to frequency offsets, which generate ICI and MAI. Although the frequency offset estimation in OFDMA has been widely investigated [97, 98, 133, 148], these conventional algorithms may perform poorly in fading, especially when the subcarriers allocated to one user are too few, and all these subcarriers are in a deep fading simultaneously. The impact of fading can be alleviated by using cooperative relaying [36,147,149,150]. The frequency offset estimation for cooperative OFDMA systems is thus motivated.

When the frequency offset is only induced by the mismatch between the transmitter and receiver oscillators, both the $S \to R \to D$ and $S \to D$ links have the same frequency offset. The relays can operate in either the conventional AF or the new DcF mode. A DcF relay estimates the frequency offset between the source and itself, and modifies the training sequence retransmitted to D. In this way, both training sequences transmitted over $S \to D$ and $S \to R \to D$ links have the same frequency offset. Thus, using these two transmissions, D can generate two frequency offset estimates, which can be linearly combined to minimize the MSE. The training-sequence and/or pilot-aided frequency offset estimation is considered. The proposed scheme can improve the performance of conventional training/pilot-based frequency offset estimation algorithm.

5.2 Cooperative OFDMA Uplink Signal Model

The total number of subcarriers is assumed to be N, and each node is allocated N_u unique subcarriers. The subcarriers allocated to node a is denoted by the set G_a. $\mathbf{F}_a$ is an $N \times N_u$ submatrix of IDFT matrix $\mathbf{F}$ for node a.

In the following, S represents the source node and R_k, $k \in \{1, \ldots, M\}$, represent the kth relay, where $M \geq 1$ is the total number of relays. For each (S, D), $\varepsilon_{SD} = \varepsilon_{SR} + \varepsilon_{RD}$ is satisfied, where ε_{ab} represents the frequency offset between nodes a and b. The proposed DcF mode works as follows. If R can estimate ε_{SR} with a high accuracy based on a received training sequence, it can re-generate the training sequence by

multiplying the kth sample of the training sequence with $e^{\frac{\jmath 2\pi k\hat{\varepsilon}_{SR}}{N}}$ ($\hat{\varepsilon}_{SR}$ is an estimate of $\hat{\varepsilon}_{SR}$), and then forwards the resulting training sequence to D. Since the frequency offsets observed through $S \rightarrow D$ and $S \rightarrow R \rightarrow D$ are identical (i.e., equal to ε_{SD}), node D has two copies of the same training sequence with the same frequency offset. In this way, the relay transmission helps the frequency offset estimation process at D. Since a two-time-slot period is required in the proposed scheme, it doubles the overhead requirement as compared to the conventional scheme. However, the power consumption in the proposed scheme is the same as the conventional one.

5.2.1 Channel Model

For a pair of nodes $a, b \in \{S, R_1, \ldots, R_M\}$, a frequency selective quasi-static fading channel with channel response $\tilde{\mathbf{h}}_{\mathbf{ab}} = \left[h_{ab}(0), h_{ab}(1), \ldots, h_{ab}(L_m - 1)\right]^T$ is assumed. The maximum channel length for any (a, b) is L_m. G_b represents the subcarrier group allocated to the bth node. The $N_u \times N_u$ frequency channel response matrix is given by $\mathbf{H}_{ab} = \text{diag}\{H_{ab}(g_1), H_{ab}(g_2), \ldots, H_{ab}(g_{N_u})\}$, where $g_i \in G_b, 1 \in i \in N_u$, and $H_{a,b}(n) = \sum_{d=0}^{L_m-1} h_{a,b}(d) e^{-\frac{\jmath 2\pi nd}{N}}$ is the channel frequency response at the nth subcarrier. For each $1 \leq k \leq M$, the following assumptions are made for the channel coefficients:

1. $h_{R_kS}(i) \sim \mathcal{CN}(0, \sigma^2_{S_sca}(i))$, where $\sum_{i=0}^{L_m-1} \sigma^2_{S_sca}(i) = 1$; $H_{R_kS}(n) \sim \mathcal{CN}(0, 1)$, where $n \in G_s$.

2. $h_{DR_k}(i), h_{DS}(i) \sim \mathcal{CN}(0, \sigma^2_{L_sca}(i))$, where $\sum_{i=0}^{L_m-1} \sigma^2_{L_sca}(i) = \mathcal{L}_u < 1$; $H_{DR_k}(n), H_{DS}(n) \sim \mathcal{CN}(0, \mathcal{L}_u)$.

5.2.2 The First Time Slot

In the first time slot, the received signal at node D and the relay R_k can be represented as

$$\mathbf{Y}_{D,1} = \underbrace{\mathbf{E}_{SD}\mathbf{F}_S\mathbf{H}_{SD}\mathbf{\Phi}_{S,1}}_{\mathbf{V}_{SD,1}}\mathbf{X}_{S,1} + \underbrace{\overbrace{\sum_{R_k\neq S}\underbrace{\mathbf{E}_{R_kD}\mathbf{F}_{R_k}\mathbf{H}_{R_kD}\mathbf{\Phi}_{R_k,1}}_{\mathbf{V}_{R_kD,1}}\mathbf{X}_{R_k,1}}^{\text{interference}} + \mathbf{W}_{D,1}}_{\mathbf{\Xi}_{D,1}}, \tag{5.1a}$$

$$\mathbf{Y}_{R_k,1} = \underbrace{\mathbf{E}_{SR_k}\mathbf{F}_S\mathbf{H}_{SR_k}\mathbf{\Phi}_{S,1}}_{\mathbf{V}_{SR_k,1}}\mathbf{X}_{S,1} + \underbrace{\overbrace{\sum_{R_l\neq S,R_k}\underbrace{\mathbf{E}_{R_lR_k}\mathbf{F}_{R_l}\mathbf{H}_{R_lR_k}\mathbf{\Phi}_{R_l,1}}_{\mathbf{V}_{R_l,R_k}}\mathbf{X}_{R_l,1}}^{\text{interference}} + \mathbf{W}_{R_k}}_{\mathbf{\Xi}_{R_k,1}}, \tag{5.1b}$$

where $\mathbf{Y}_{D,1}$ and $\mathbf{Y}_{R_k,1}$ are $N\times T$ matrices, and $\mathbf{E}_{ab} = \text{diag}\left\{1, e^{\frac{\jmath 2\pi\varepsilon_{ab}}{N}}, \ldots, e^{\frac{\jmath 2\pi\varepsilon ab(N-1)}{N}}\right\}$. We assume that the oscillators of the mobile nodes should be calibrated with the oscillator of the base station and, therefore, that each $\varepsilon_{zD}, z \in \{S, R_1, \ldots, R_M\}$, can be approximated as an i.i.d. RV with mean zero and variance σ_ε^2 (but not necessarily Gaussian). Since $\varepsilon_{SD} = \varepsilon_{SR_k} + \varepsilon_{R_kD}$ holds, we have Var $\{\varepsilon_{zD}\} = \sigma_\epsilon^2$ and Var $\{\varepsilon_{SR_k}\} =$ Var$\{\varepsilon_{SD} - \varepsilon_{R_kD}\} = 2\sigma_\epsilon^2$, $z \in \{S, R_1, \ldots, R_M\}$. Identical power is allocated to each pilot subcarrier. We also assume that $\alpha N_u\bar{P}$ is allocated to node S in the first time slot, and that in the second time slot, the relay uses the remaining power, i.e., $(1-\alpha)N_u\bar{P}$, where $\bar{P}$ represents the average power of each subcarrier, and $0 < \alpha < 1$. Therefore, $\mathbf{\Phi}_{S,1} = \mathbf{\Phi}_{R_l,1} = \sqrt{\alpha\bar{P}}\mathbf{I}_{N_u}$ are $N_u \times N_u$ diagonal matrices with each diagonal entry representing the transmit power of one subcarrier of nodes S and R_l, respectively, in the first time slot. $\mathbf{X}_{a,1} = [\mathbf{x}_{a,1}(0), \ldots, \mathbf{x}_{a,1}(T-1)]$, which is an $N_u\times T$ matrix ($T = 1, 2, \ldots$), represents the transmit matrix of node a, and we assume that $[\mathbf{X}_{a,1}]_{mn} \sim \mathcal{CN}(0,1)$. $\mathbf{W}_a$ and $\mathbf{W}_{D,1}$ are $N_u \times T$ matrices of AWGN with $\{\mathbf{W}_a[m], \mathbf{W}_{D,1}[m]\} \sim \mathcal{CN}(0, \sigma_w^2)$.

Using the similar process of the SINR analysis in Chapter 4, the effective SINR at

nodes D and R_k is given by

$$\gamma_{SD,1} = \frac{\mathbb{E}\left\{\text{trace}\left\{\mathbf{F}_s^H \mathbf{V}_{SD,1} \mathbf{X}_{S,1} \mathbf{X}_{S,1}^H \mathbf{V}_{SD,1}^H \mathbf{F}_s\right\}\right\}}{\mathbb{E}\left\{\text{trace}\left\{\mathbf{F}_s^H \mathbf{\Xi}_{D,1} \mathbf{\Xi}_{D,1}^H \mathbf{F}_s\right\}\right\}} = \frac{\alpha\bar{P}\beta_1 \cdot \mathbb{E}\{\nu_{SD}\}}{\frac{\mathcal{L}_u \pi^2 N_u \sigma_\epsilon^2 \alpha\bar{P}}{3} + N_u\sigma_w^2} = \frac{\mathcal{L}_u \alpha\bar{P}\beta_1}{\frac{\mathcal{L}_u \pi^2 \sigma_\epsilon^2 \alpha\bar{P}}{3} + \sigma_w^2}, \tag{5.2a}$$

$$\gamma_{SR_k,1} = \frac{\mathbb{E}\left\{\text{trace}\left\{\mathbf{F}_s^H \mathbf{V}_{SR_k,1} \mathbf{X}_{S,1} \mathbf{X}_{S,1}^H \mathbf{V}_{SR_k,1}^H \mathbf{F}_s\right\}\right\}}{\mathbb{E}\left\{\text{trace}\left\{\mathbf{F}_s^H \mathbf{\Xi}_{R_k,1} \mathbf{\Xi}_{R_k,1}^H \mathbf{F}_s\right\}\right\}} = \frac{\alpha\bar{P}\beta_2 \cdot \mathbb{E}\{\nu_{SR_k}\}}{\frac{2\pi^2 N_u \sigma_\epsilon^2 \alpha\bar{P}}{3} + N_u\sigma_w^2} = \frac{\alpha\bar{P}\beta_2}{\frac{2\pi^2 \sigma_\epsilon^2 \alpha\bar{P}}{3} + \sigma_w^2}, \tag{5.2b}$$

where $\nu_{Sb} = \text{trace}\{\mathbf{H}_{Sb}\mathbf{H}_{Sb}^H\}$, $\beta_1 = \left(1 - \frac{\pi^2\sigma_\epsilon^2}{3} + \frac{\pi^4\sigma_\epsilon^4}{20}\right)$ and $\beta_2 = \left(1 - \frac{2\pi^2\sigma_\epsilon^2}{3} + \frac{\pi^4\sigma_\epsilon^4}{5}\right)$.

Assume that the subcarriers allocated to each node are not contiguous, and the distance between any two neighboring subcarriers is assumed to be large enough to make the correlation between them be negligible. Therefore, each ν_{Sb} is a central *chi-square* RV with $2N_u$ degrees of freedom [2, page 41]. From [2, page 42], for a threshold $T_h > 0$, the probability that $\nu_{Sb} < N_u \cdot T_h$ is given by

$$P_r\{\nu_{Sb} < N_u \cdot T_h\} = 1 - e^{-N_u \cdot T_h} \sum_{k=0}^{N_u - 1} \frac{(N_u \cdot T_h)^k}{k!}. \tag{5.3}$$

For a larger N_u, a smaller outage probability $P_r\{\nu_{Sb} < N_u \cdot T_h\}$ is obtained, i.e., a more robust wireless channel is obtained, as shown in Figure 5.34.

5.2.3 The Second Time Slot

In the second time slot, suppose that all nodes have CSI. Only one relay is chosen for re-transmission. The active relay R_s may be chosen by maximizing the composite channel gains:

$$R_s = \arg \max_{R_1,\ldots,R_M} \{\nu_{SR_1}, \ldots, \nu_{SR_M}\}. \tag{5.4}$$

It was proven by [151] that the opportunistic relaying strategy by using the "best" relay to perform re-transmission is optimal in terms of outage probability. The PDF of ν_{SRk} is given by $f(\nu) = \frac{1}{(N_u - 1)!}\nu^{N_u - 1}e^{-\nu}$. The PDF of $\nu_{\max} = \max\{\nu_{SR_1}, \ldots, \nu_{SR_M}\}$

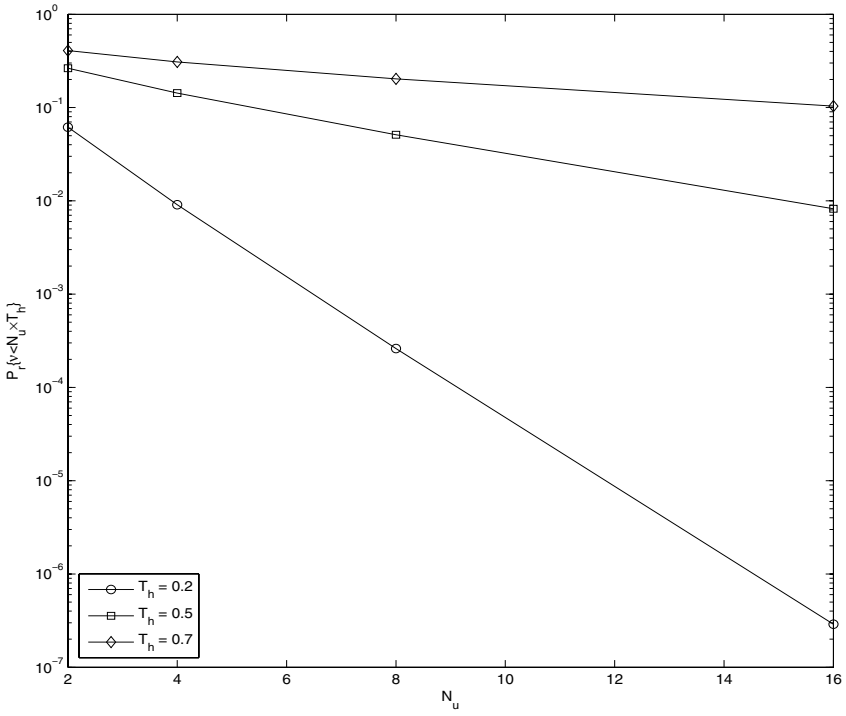

Figure 5.34: Channel outage probability as a function of N_u in OFDMA.

is therefore $f(\nu_{\max}) = M\left(1 - e^{-\nu_{\max}\sum_{m=0}^{N_u-1}\frac{\nu_{\max}^m}{m!}}\right)\frac{\nu_{\max}^{N_u-1}e^{-\nu_{\max}}}{(N_u-1)!}$, and the expectation of $\nu_{\max}$ is derived as

$$\bar{\nu}_{\max} = \int_0^\infty \nu_{\max} f(\nu_{\max})\mathrm{d}\nu_{\max} = M\sum_{k=0}^{M-1}\binom{M-k}{k}\sum_{n=0}^{(N_u-1)(M-k)}\frac{g_k^{(n)}(0)}{(M-k)^2(M-k-1)!}, \tag{5.5}$$

where $g_k(x) = \left(\sum_{m=0}^{N_u-1}\frac{x^m}{m!}\right)^{M-k}$, and $g_k^{(n)}(0) = \frac{d^{(n)}g_k(x)}{dx^n}|_{x=0}$ represents the n-order derivative of $g_k(x)$ with $x = 0$.

The PDF of $\nu_{\max}$ as a function of M is shown in Figure 5.35 with $N = 1024$ and $N_u = 16$. Figure 5.35 shows that the peak of $f(\nu_{\max})$ shifts to the right as M increases, and that, accordingly, $\bar{\nu}_{\max}$ increases as M increases. For example, when $M = 2$, $\bar{\nu}_{\max} = 18.2$; if we increase M to 8, we have $\bar{\nu}_{\max} = 22.1$, and $\bar{\nu}_{\max}= 23.8$ if we further increase

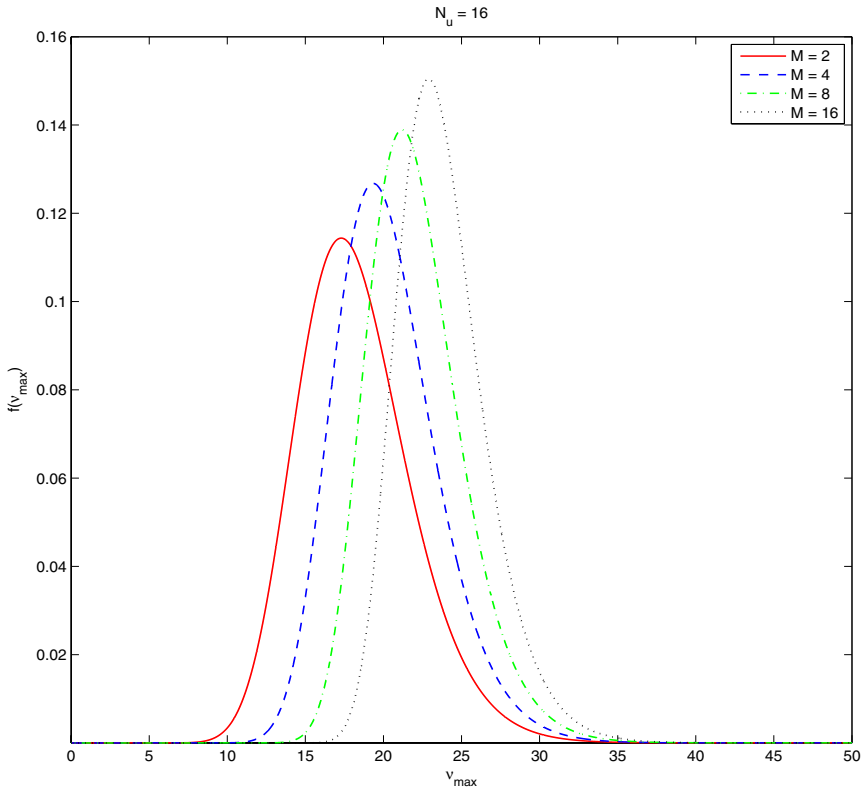

Figure 5.35: PDF of $\nu_{\max}$ in cooperation OFDMA uplink transmission.

M to 16. For a constant N_u, since a larger M implies a higher spatial diversity gain, we can finally improve the robustness of the training sequence transmission and, as a result, reduce the frequency offset estimation error.

AF Mode

In the AF mode, R_s simply re-transmits the received training sequence to D. The received training sequence at node D in the second time slot is

$$\begin{aligned}\mathbf{Y}_{D,2}^{\mathrm{AF}} &= \rho_{SR_s}\mathbf{E}_{R_sD}\mathbf{F}_S\mathbf{H}_{R_sD}\mathbf{\Phi}_{R_s,2}\mathbf{F}_S^H\mathbf{Y}_{R_s,1} + \sum_{R_k\neq S,R_s}\mathbf{E}_{R_kD}\mathbf{F}_{R_k}\mathbf{H}_{R_kD}\mathbf{\Phi}_{R_k,2}\mathbf{X}_{R_k,2} + \mathbf{W}_{D,2} \\ &= \underbrace{\rho_{SR_s}\mathbf{E}_{R_sD}\mathbf{F}_S\mathbf{H}_{R_s,D}\mathbf{F}_S^H\mathbf{V}_{SR_s}}_{\mathbf{V}_{SRD,2}^{\mathrm{AF}}}\mathbf{X}_{S,1} + \tilde{\mathbf{W}}_{D,2}^{\mathrm{AF}},\end{aligned} \tag{5.6}$$

where

$$\begin{aligned}\tilde{\mathbf{W}}_{D,2}^{\mathrm{AF}} &= \rho_{SR_s}\mathbf{E}_{R_sD}\mathbf{F}_S\mathbf{H}_{R_sD}\mathbf{\Phi}_{R_s,2}\mathbf{F}_S^H\sum_{R_l\neq S,R_s}\mathbf{V}_{R_lR_s}\mathbf{X}_{R_l,1} + \rho_{SR_s}\mathbf{E}_{R_sD}\mathbf{F}_S\mathbf{H}_{R_sD}\mathbf{\Phi}_{R_s,2}\mathbf{F}_S^H\mathbf{W}_{R_s} \\ &\quad + \sum_{R_k\neq S,R_s}\mathbf{E}_{R_kD}\mathbf{F}_{R_k}\mathbf{H}_{R_kD}\mathbf{\Phi}_{R_k,2}\mathbf{X}_{R_k,2} + \mathbf{W}_{D,2},\end{aligned}$$

$\mathbf{\Phi}_{R_s,2} = \sqrt{\dfrac{(1-\alpha)\bar{P}}{M}}\mathbf{I}_{N_u}$ represents the power consumed in R_s for re-transmission in the second time slot, and $\rho_{SR_s} = \sqrt{\dfrac{N_u}{\alpha\bar{\nu}_{\max}\bar{P}} + N_u\sigma_w^2}$ represents the amplifying coefficients of R_s.

The received SINR is given by

$$\begin{aligned}\gamma_2^{\mathrm{AF}} &= \frac{\mathbb{E}\left\{\mathrm{trace}\left\{\mathbf{F}_S^H\mathbf{V}_{SRD,2}^{\mathrm{AF}}\mathbf{X}_{S,1}\mathbf{X}_{S,1}^H(\mathbf{V}_{SRD,2}^{\mathrm{AF}})^H\mathbf{F}_S\right\}\right\}}{\mathbb{E}\left\{\mathrm{trace}\left\{\mathbf{F}_S^H\tilde{\mathbf{W}}_{D,2}^{\mathrm{AF}}(\tilde{\mathbf{W}}_{D,2}^{\mathrm{AF}})^H\mathbf{F}_S\right\}\right\}} \\ &= \frac{\mathcal{L}_u\alpha(1-\alpha)\bar{P}^2\beta_1\beta_2\mathbb{E}\left\{\bar{\nu}_{\max}\nu_{R_sD}\right\}}{\frac{2\mathcal{L}_u\alpha\bar{P}\pi^2N_u\sigma_\epsilon^2}{3} + N_u\sigma_w^2 + \left(\frac{\mathcal{L}_u(1-\alpha)\bar{P}\pi^2N_u\sigma_\epsilon^2)}{3} + N_u\sigma_w^2\right)\xi_{SR_s}},\end{aligned} \tag{5.7}$$

where $\xi_{SR_s} = \mathcal{L}_u\alpha\bar{P}\beta_2\bar{\nu}_{\max} + \dfrac{2\mathcal{L}_u\alpha\bar{P}\pi^2N_u\sigma_\epsilon^2}{3} + N_u\sigma_w^2$.

DcF Mode

In this mode, the relay first identifies the received training sequence, and then re-generates this training sequence and re-transmits it. After performing the demodulating and decoding, the node R_s should estimate ε_{SR_s}; i.e., $\hat{\varepsilon}_{SR_s,1} = \varepsilon_{SR_s} + e_{SR_s,1}$, ($e_{SR_s,1}$

represents the estimation error of $\hat{\varepsilon}_{SR_s,1}$), and then uses $\hat{\varepsilon}_{SR_s,1}$ to pre-compensate for the frequency offset between S and R_s to re-generate the training sequence. The received training sequence at D is

$$\mathbf{Y}_{D,2}^{\mathrm{DcF}} = \underbrace{\mathbf{E}_{R_sD}\mathbf{F}_S\mathbf{H}_{RsD}\mathbf{\Phi}_{R_s,2}\mathbf{F}_S^H\hat{\mathbf{E}}_{SR_s}\mathbf{F}_S}_{\mathbf{V}_{SRD,2}^{\mathrm{DcF}}}\mathbf{X}_s + \underbrace{\sum_{R_k\neq S,R_s}\mathbf{E}_{R_kD}\mathbf{F}_{R_k}\mathbf{H}_{R_kD}\mathbf{\Phi}_{R_k,2}\mathbf{X}_{R_k,2} + \mathbf{W}_{D,2}}_{\tilde{\mathbf{W}}_{D,2}^{\mathrm{DcF}}}, \tag{5.8}$$

where $\hat{\mathbf{E}}_{SR_s} = \mathrm{diag}\left\{1, e^{\frac{\jmath 2\pi\hat{\varepsilon}_{SR_s,1}}{N}}, \ldots, e^{\frac{\jmath 2\pi\hat{\varepsilon}_{SR_s,1}(N-1)}{N}}\right\}$.

The average SINR in the node D is

$$\gamma_2^{\mathrm{DcF}} = \frac{\mathbb{E}\left\{\mathrm{trace}\left\{\mathbf{K}^{\mathrm{DcF}}\right\}\right\}}{\mathbb{E}\left\{\mathrm{trace}\left\{\mathbf{F}_S^H\tilde{\mathbf{W}}_{D,2}^{\mathrm{DcF}}\left(\tilde{\mathbf{W}}_{D,2}^{\mathrm{DcF}}\right)^H\mathbf{F}_S\right\}\right\}} = \frac{(1-\alpha)\bar{P}\beta_1\cdot\mathbb{E}\left\{\nu_{R_sD}\right\}}{\frac{\mathcal{L}_u\pi^2N_u\sigma_\epsilon^2(1-\alpha)\bar{P}}{3}+N_u\sigma_w^2}, \tag{5.9}$$

where $\mathbf{K}^{\mathrm{DcF}} = \mathbf{F}_S^H\mathbf{V}_{SRD,2}^{\mathrm{DcF}}\hat{\mathbf{E}}_{SR_s}\mathbf{X}_S\mathbf{X}_S^H\hat{\mathbf{E}}_{SR_s}^H\left(\mathbf{V}_{SRD,2}^{\mathrm{DcF}}\right)^H\mathbf{F}_S$.

5.3 Frequency Offset Estimation in the Cooperative Scheme

The training sequences received in the first and the second time slots can be used by D to estimate frequency offset. The first time slot frequency offset ε_{SD} can be estimated as $\hat{\varepsilon}_{SD,1} = \varepsilon_{SD} + e_{SD,1}$, where $e_{SD,1}$ is an estimation error. From [13,148], for an unbiased estimator $\hat{\varepsilon}_{SD,1}$, the CRLB can be represented as

$$\mathrm{Var}\left\{e_{SD,1}|\nu_{SD}\right\} \geq \frac{1}{\mathcal{A}_T\cdot\gamma_{SD,1}}, \tag{5.10}$$

where $\mathcal{A}_T$ is a positive coefficient specified by the structure of the training sequence $\mathbf{X}_S$. For example, if the training sequence proposed in [13] is used, it can be shown that $\mathcal{A}_T = 4\pi^2N_u$. Similarly, the frequency offset estimation at node R_s can be represented as $\hat{\varepsilon}_{SR_s,1} = \varepsilon_{SR_s} + e_{SR_s,1}$. For an unbiased estimator, the CRLB is

$$\mathrm{Var}\left\{e_{SR_s,1}|\nu_{SR_s}\right\} \geq \frac{1}{\mathcal{A}_T\cdot\gamma_{SR_s,1}}. \tag{5.11}$$

The frequency offset estimation in the second time slot depends on the relaying mode. Denote $\hat{\varepsilon}_{SR_sD,2} = \varepsilon_{SD} + e_{SR_sD,2}$ as the estimate of ε_{SD} in the second time slot. The CRLB for the AF mode is given by

$$\mathrm{Var}\left\{e_{SR_sD,2}|\nu_{SR_s},\nu_{R_sD};\mathrm{AF}\right\} \geq \frac{1}{\mathcal{A}_T \cdot \gamma_2^{\mathrm{AF}}}. \tag{5.12}$$

In the DcF mode, the estimation error $\varepsilon_{SR_s,1}$ will be accumulated and propagated to the final result, and the CRLB is given by

$$\begin{aligned}\mathrm{Var}\left\{e_{SR_sD,2}|\nu_{SR_s},\nu_{R_sD};\mathrm{DcF}\right\} &= \mathrm{Var}\left\{e_{SR_S,1}|\nu_{SR_S}\right\} + \mathrm{Var}\left\{e_{R_sD,2}|\nu_{R_sD}\right\} \\ &\geq \frac{1}{\mathcal{A}_T}\left(\frac{1}{\gamma_{SR_s,1}} + \frac{1}{\gamma_2^{DcF}}\right)\end{aligned} \tag{5.13}$$

Since the frequency offset estimates in both the first and second time slots are conditionally unbiased with mean ε_{SD}, these two estimates can be combined to improve the estimation accuracy. From [122, chapter 6], the estimation results in a two-time-slot period can be combined to be

$$\hat{\varepsilon}_{SD} = \lambda_1\hat{\varepsilon}_{SD,1} + \lambda_2\hat{\varepsilon}_{SR_sD,2} = \varepsilon_{SD} + \underbrace{\lambda_1 e_{SD,1} + \lambda_2 e_{SR_sD,2}}_{e_{SD}}, \tag{5.14}$$

where λ_1 and λ_2 are two non-negative coefficients, and $\lambda_1 + \lambda_2 = 1$. $e_{SD,1}$ and $e_{SR_sD,2}$ are uncorrelated. The variance error of $\hat{\varepsilon}_{SD}$ is given by

$$\mathrm{Var}\left\{e_{SD}|\nu_{SD},\nu_{DR_s},\nu_{R_sD}\right\} = \lambda_1^2\mathrm{Var}\left\{e_{SD,1}|\nu_{SD}\right\} + \lambda_2^2\mathrm{Var}\left\{e_{SR_sD,2}|\nu_{SR_s},\nu_{R_sD}\right\}. \tag{5.15}$$

In the AF mode, for a given α and $(\nu_{SD},\nu_{SR_s},\nu_{RsD})$, the optimal λ_1 and λ_2, i.e., $\lambda_{1,\mathrm{opt}}^{\mathrm{AF}} = \dfrac{\gamma_{SD,1}}{\gamma_{SD,1}+\gamma_2^{\mathrm{AF}}}$ and $\lambda_{2,\mathrm{opt}}^{\mathrm{AF}} = \dfrac{\gamma_2^{\mathrm{AF}}}{\gamma_{SD,1}+\gamma_2^{\mathrm{AF}}}$, are used to minimize the variance of e_{SD} as

$$\mathrm{Var}\left\{e_{SD}|0<\alpha<1;\nu_{SD},\nu_{SR_s},\nu_{R_sD};\lambda_{1,\mathrm{opt}}^{\mathrm{AF}},\lambda_{2,\mathrm{opt}}^{\mathrm{AF}}\right\} \geq \frac{1}{\mathcal{A}_T\left(\gamma_{SD,1}+\gamma_2^{\mathrm{AF}}\right)}. \tag{5.16}$$

In the DcF mode, when $\lambda_{1,\mathrm{opt}}^{\mathrm{DcF}} = \dfrac{1}{1+\frac{\gamma_{SD,1}\left(\gamma_{SR_s,1}+\gamma_2^{\mathrm{DcF}}\right)}{\gamma_{SR_s,1}\gamma_2^{\mathrm{DcF}}}}$ and $\lambda_{2,\mathrm{opt}}^{\mathrm{DcF}} = \dfrac{\gamma_{SD,1}\left(\gamma_{SR_s,1}+\gamma_2^{\mathrm{DcF}}\right)}{\gamma_{SR_s,1}\gamma_2^{\mathrm{DcF}}+\gamma_{SD,1}\left(\gamma_{SR_s,1}+\gamma_2^{\mathrm{DcF}}\right)}$, the minimum variance of e_{SD} can be obtained

as

$$\mathrm{Var}\left\{e_{SD}|0\le\alpha\le 1;\nu_{SD},\nu_{SR_s},\nu_{R_sD};\lambda_{1,\mathrm{opt}}^{\mathrm{DcF}},\lambda_{2,\mathrm{opt}}^{\mathrm{DcF}}\right\}\ge\frac{1}{\mathcal{A}_T(\gamma_{SD,1}+\frac{\gamma_{SR_s,1}\gamma_2^{\mathrm{DcF}}}{\gamma_{SR_s,1}+\gamma_2^{DcF}})}. \tag{5.17}$$

Both (5.16) and (5.17) are functions of α and can be minimized by using the optimal α. However, the optimal α depends on whether or not the base station sends CSI to the mobile nodes. With feedback, the mobile nodes can adaptively optimize α based on the current $(\nu_{SD},\nu_{SR_s},\nu_{R_sD})$ values. If the base station does not feedback CSI, α can be optimized based on only the statistical information of $(\nu_{SD},\nu_{SR_s},\nu_{R_sD})$.

5.3.1 Without CSI Feedback from the Base Station

In this case, the optimal α should minimize the expected variance error as

$$\alpha_{\mathrm{WF}}^{\mathrm{AF}}=\arg\min_{0\le\alpha\le 1}\mathbb{E}_\nu\left\{\frac{1}{\mathcal{A}_T(\gamma_{SD,1}+\gamma_2^{\mathrm{AF}})}\right\},\quad(\mathrm{AF}) \tag{5.18a}$$

$$\alpha_{\mathrm{WF}}^{\mathrm{DcF}}=\arg\min_{0\le\alpha\le 1}\mathbb{E}_\nu\left\{\frac{1}{\mathcal{A}_T(\gamma_{SD,1}+\frac{\gamma_{SR_s,1}\gamma_2^{DcF}}{\gamma_{SR_s,1}+\gamma_2^{\mathrm{DcF}}})}\right\},\quad(\mathrm{DcF}) \tag{5.18b}$$

for the AF and DcF modes, respectively, where the expectation is performed with respect to $(\nu_{SD},\nu_{SR_s},\nu_{R_sD})$. By taking the partial derivative of (5.18) with respect to α and setting the result to zero, the optimal α for either the AF or DcF mode can be achieved by resolving the function, if the closed-form solution is available. Actually, we can also find the optimal α that maximizes (5.18) numerically. The numerical method is used in the later simulation.

5.3.2 With CSI Feedback from the Base Station

The optimal α derived in Section 5.3.1 does not change as the current channel changes, so that neither $\alpha_{\mathrm{WF}}^{\mathrm{AF}}$ nor $\alpha_{\mathrm{WF}}^{\mathrm{DcF}}$ is always optimal in each channel realization. If the base station sends the current CSI to the mobile nodes, a lower variance error can be achieved by adaptively optimizing α based on the current CSI. For a given $(\nu_{SD},\nu_{SR_s},\nu_{R_sD})$, the

adaptively optimized α is given by

$$\alpha_{\mathrm{FB}}^{\mathrm{AF}} = \arg\min_{0\le\alpha\le1}\left\{\frac{1}{\mathcal{A}_T\left(\gamma_{SD,1}+\gamma_2^{\mathrm{AF}}\right)}\right\}, \quad \text{(AF)} \tag{5.19a}$$

$$\alpha_{\mathrm{FB}}^{\mathrm{DcF}} = \arg\min_{0\le\alpha\le1}\left\{\frac{1}{\mathcal{A}_T\left(\gamma_{SD,1}+\frac{\gamma_{SR_s,1}\gamma_2^{DcF}}{\gamma_{SR_s,1}+\gamma_2^{\mathrm{DcF}}}\right)}\right\}, \quad \text{(DcF)} \tag{5.19b}$$

for the AF and DcF modes, respectively.

5.3.3 Adaptive Switching Between Cooperative and Conventional Non-Cooperative Transmissions

A hybrid cooperative scheme is proposed to adaptively optimize the transmission, as shown in Figure 5.36. The basic idea is: for a given (M, σ_ϵ^2, SNR), if there is an α ($0 < \alpha < 1$) to make the cooperative transmission outperform the conventional transmission or vice versa, the transmitter switches accordingly. Since the base station may either send CSI to the mobile nodes or not, the cooperative transmission may be performed in two cases: (1) if the base station does not feedback CSI, the second switch should be switched to "21" to perform "Without Feedback" cooperation. $\alpha_{\mathrm{WF}}^{\mathrm{AF}}$ (or $\alpha_{\mathrm{WF}}^{\mathrm{DcF}}$) will be used for the AF (or DcF) mode; and (2) if the base station sends the CSI to the mobile nodes, the second switch should be switched to "22" to perform "With Feedback" cooperation, and $\alpha_{\mathrm{FB}}^{\mathrm{AF}}$ (or $\alpha_{\mathrm{FB}}^{\mathrm{DcF}}$) should be used for the AF (or DcF) mode in this case. An information-sharing scheme should be performed between S and R_s to guarantee that an identical α will be used by them in the same transmission.

5.4 Numerical Results

An OFDMA uplink system with IDFT length of 1024 is simulated. A CP of length 64 is used. An equal allocation of subcarriers per node is made. The number of relays is M. Frequency offsets are assumed to be i.i.d. RVs with mean zero and variance σ_ϵ^2. The algorithm proposed in [13] is used to verify the performance improvement

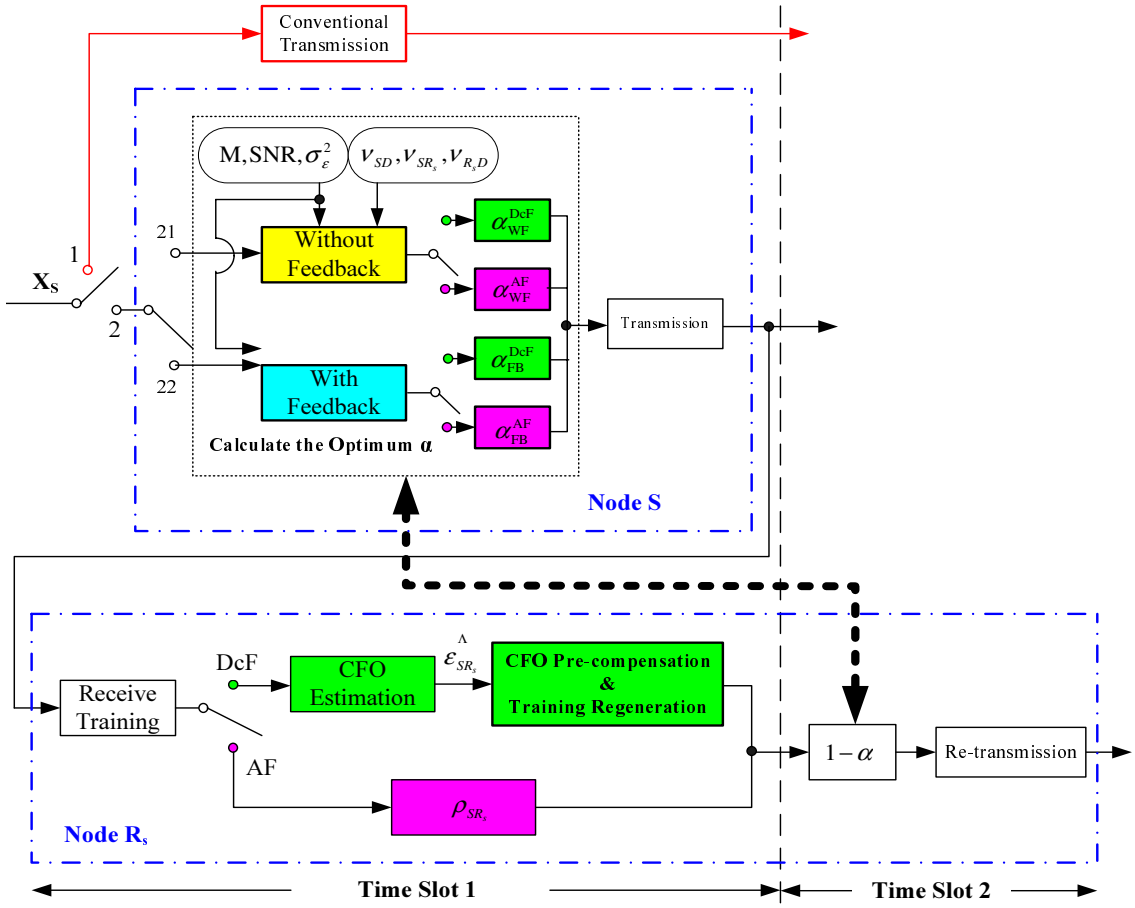

Figure 5.36: Adaptive cooperation in OFDMA uplink frequency offset estimation.

obtained by using cooperative relays, i.e., $T = 2$. The training sequence is known to all the nodes.

Figure 5.37 compares the variance of errors of the proposed cooperative scheme as a function of α and that of the conventional estimation ($\alpha = 1$), where SNR = 20 dB and $M = 16$. When $\sigma_\epsilon^2 = 10^{-2}$, the AF and DcF cooperative schemes outperforms conventional estimation when $0.11 < \alpha < 1$ and $0.65 < \alpha < 1$, respectively. When $\sigma_\epsilon^2 = 10^{-3}$, the corresponding ranges of α are $0.13 < \alpha < 1$ and $0.56 < \alpha < 1$, respectively. For each α, the AF mode always outperforms the DcF mode. From Figure 5.37, the

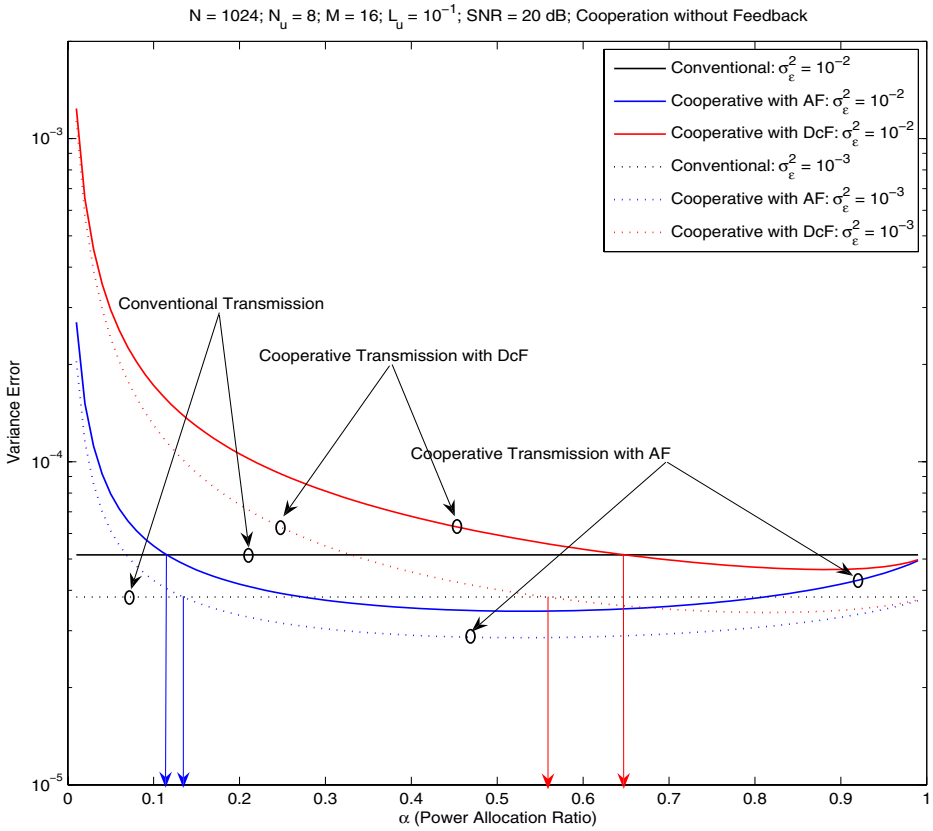

Figure 5.37: Cooperative frequency offset estimation as a function of α without feedback from the base station.

optimal α, i.e., $\alpha_{\mathrm{WF}}^{\mathrm{AF}}$ and $\alpha_{\mathrm{WF}}^{\mathrm{DcF}}$, can easily be found. For example, $\sigma_\epsilon^2 = 10^{-2}$, we have $\alpha_{\mathrm{WF}}^{\mathrm{AF}} = 0.53$ (with a variance error 2.85×10^{-5}) and $\alpha_{\mathrm{WF}}^{\mathrm{DcF}} = 0.81$ (with a variance error 3.42×10^{-5}).

Since the power allocation between S and R_s can be adaptively optimized in each transmission if the CSI is available to the nodes, the performance gains can then be further improved. For example, in Table 5.5, with SNR = 20 dB and $\sigma_\epsilon^2 = 10^{-1}$, the performance improvement of AF (or DcF) mode over the conventional scheme is 2.2 dB (or 0.4 dB) if the base station does not send CSI. If it does, the performance advantage increases to 4.9 dB and 1.7 dB for the AF and DcF modes, respectively.

Table 5.5: Performance Improvement in the Proposed Cooperative Scheme With and Without Feedback from the Base Station over the Conventional Non-cooperative Algorithm

Without Feedback; M=16								
SNR	20dB				30dB			
σ_ϵ^2	10^{-4}	10^{-3}	10^{-2}	10^{-1}	10^{-4}	10^{-3}	10^{-2}	10^{-1}
AF	1.19	1.21	1.669	2.217	1.533	2.072	3.473	3.236
DcF	0.492	0.438	0.401	0.412	0.454	0.529	0.427	0.471
With Feedback; M=16								
SNR	20dB				30dB			
σ_ϵ^2	10^{-4}	10^{-3}	10^{-2}	10^{-1}	10^{-4}	10^{-3}	10^{-2}	10^{-1}
AF	25.35	20.17	10.48	4.95	19.97	10.58	5.56	3.48
DcF	15.86	15.55	6.66	1.75	15.56	6.65	1.73	0.6

Table 5.6 evaluates the performance of the proposed scheme as a function of M when the base station sends CSI to the mobile nodes. In this simulation, for each M, the variances of estimation error for $\alpha_{\text{FB}}^{\text{AF}}$ (for the AF mode) and $\alpha_{\text{FB}}^{\text{DcF}}$ (for the DcF mode) are evaluated. In either the AF or DcF mode, the variance decreases monotonically with M. As mentioned above for Table 5.5, a performance advantage over the conventional scheme can also be achieved in the cooperative scheme with feedback. The AF mode still outperforms the DcF mode. For example, when $\sigma_\epsilon^2 = 10^{-2}$ and $M = 16$, the variance error achieved in the DcF mode is 1.098×10^{-5}, but that achieved in the AF mode is 4.56×10^{-6}. We can explain this finding as follows: in the interference-limited cooperative transmission, the interference due to the frequency offset in $S \to R_s$ link is twice that of either the $S \to D$ or $R_s \to D$ link. In the DcF relaying mode, R_s should estimate ε_{SR_s}, and the estimation error will be accumulated and propagated to the final result. When the frequency offset is large, the error in R_s will dominate the overall variance error, as given by (5.17). However, this error propagation from R_s to D can be mitigated in the AF mode.

The BER performance of the proposed cooperative scheme with CSI feedback from the base station is evaluated in Figure 5.38. The subcarrier modulation is either QPSK

Table 5.6: Performance Improvement in the Proposed Cooperative Scheme with Feedback as a Function of M

Transmission Mode		Variance Errors: N=1024, N_u=8, $\mathcal{L}_u$ = 10^{-1}, SNR=20dB, σ_ϵ^2 = 10^{-2}				
Conventional Transmission	M	2	4	8	16	32
	Error	5.15×10^{-5}	5.15×10^{-5}	5.15×10^{-5}	5.15×10^{-5}	5.15×10^{-5}
AF Relaying	M	2	4	8	16	32
	Error	4.603×10^{-6}	4.585×10^{-6}	4.572×10^{-6}	4.562×10^{-6}	4.554×10^{-6}
DcF Relaying	M	2	4	8	16	32
	Error	1.134×10^{-5}	1.121×10^{-5}	1.109×10^{-5}	1.1089×10^{-5}	1.1087×10^{-5}

or 16-QAM. The AF mode always outperforms the DcF mode in terms of BER if there are frequency offset errors, and this gap increases as the SNR increases. In both relaying modes, the BER performance improves with M. However, the performance improvement in the AF mode is more than that in the DcF mode. We can explain this finding as follows: in the AF mode, frequency offset estimation error is dominated by the effective SINR of both the $S \rightarrow D$ and $S \rightarrow Rs \rightarrow D$ links, and more relays reduce the SINR degradation due to the frequency offset error. Whereas the frequency offset estimation error in the DcF mode is dominated by the estimation error accumulated in the relay, and hence more relays yield diminishing returns on the amount of SINR improvement.

5.5 Conclusions

This chapter discussed the improved OFDMA uplink frequency offset estimation by using cooperative relaying. A new DcF relaying mode was developed. The idea is to adjust for the frequency offset in the $S \rightarrow R$ so that both $S \rightarrow R \rightarrow D$ link and $S \rightarrow D$ link have the same frequency offset. The training sequence received in both $S \rightarrow D$ and $S \rightarrow R \rightarrow D$ links can then be used to estimate the frequency offset, and the two estimates can be linearly combined to minimize the variance error. Further

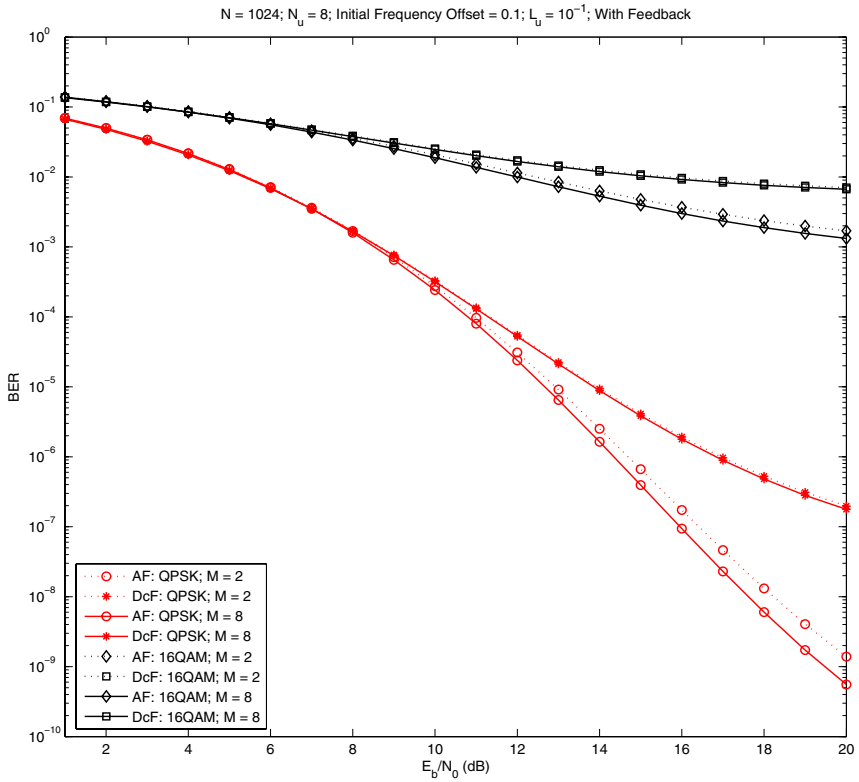

Figure 5.38: BER by using the proposed cooperative frequency offset estimation with feedback from the base station.

improvement is possible by adjusting the power allocation ratio between the source and the relay. When CSI is available, the relays can adaptively switch between the cooperative and conventional modes, and this proposed adaptation yields gains 4.95 dB and 1.75 dB over the conventional non-cooperative scheme for the AF and DcF modes, respectively, in low SINR. Although the DcF mode outperforms the AF mode in terms of channel capacity and BER with the same frequency offset, the AF mode obtains the performance advantage over the DcF mode by considering the frequency offset estimation, because the frequency offset error in the DcF mode is higher than that in the AF mode. At high SNR, the AF mode outperforms the DcF mode by about

4.1 dB for QPSK, and this gap is 7 dB for 16-QAM.

Chapter 6

Conclusions and Future Work

6.1 Conclusions

In this thesis, new channel and frequency offset estimation algorithms and their performance for several OFDM systems have been investigated. These were proposed in Chapters 2 to 5.

Chapter 2 discussed channel estimation for AF and DF relaying cooperative OFDM systems with frequency offsets. A two-time-slot cooperative channel-estimation protocol was proposed. Pilot designs for AF and DF relays were derived with the goal to eliminate IRI. For a given channel order L, the maximum number of AF and DF relays was constrained to be $\lfloor N/(2L-1) \rfloor$ and $\lfloor N/L \rfloor$, respectively. In the presence of both frequency offset and channel estimation errors, the PEP of an orthogonal block code in the proposed cooperative transmission was derived. The optimal power allocation between the source and relays was also derived to minimize the PEP. The PEP performance comparison of AF and DF relays was made with the different number of relays and channel orders.

Chapter 3 focused on the BER evaluation of MIMO OFDM systems. The frequency offset and channel estimation errors, which are unavoidable in practical systems, were considered. By analyzing the interference between subcarriers and antennas, the SINR was derived. The approximate BER was derived for multiple-antenna reception with EGC and MRC. Simulations demonstrated the accuracy of the theoretical analysis. The results give insight of the impact of the frequency offset and channel estimation errors on the system BER performance.

Chapter 4 discussed the frequency offset estimation in the uplink OFDMA. A general subcarrier allocation scheme was considered. In this scheme, each user subcarrier group need not to be contiguous. The key idea is to improve the accuracy of frequency offset estimation by exploiting the estimated value of the variance of frequency offset.

By analyzing ICI and MAI, which occur in multi-user accessing the OFDMA systems, the CRLB for the variance of frequency offset estimation of each user was first derived and further expressed as the function of the SNR. An estimation of the variance of the frequency offset was derived as a function of SINR and SNR. For uniformly distributed frequency offsets, an estimation of the range of frequency offsets was derived. Based on this estimate of the range of frequency offsets, the accuracy of existing algorithms can be improved. Successive interference cancelation (SIC) frequency offset estimator was considered. With the knowledge of the range of frequency offsets, new versions of the SIC-based frequency offset estimation algorithm, as well as differential estimation algorithms, were derived. The improvement of the frequency offset estimation was confirmed with simulation results.

Chapter 5 also considered the frequency offset estimation for an OFDMA uplink, but with cooperative relays. The accuracy of frequency offsets was improved by using the cooperation of the system. Two types of relays were studied, AF relays and DcF relays. The destination first generates the frequency offset estimation of the transmission from the source in the first time slot, and then the transmission from the selected relay in the second time slot. The two frequency offset estimations were combined to minimize the frequency offset estimation MSE. When CSI is available at each mobile node, power allocation between the source and the relay can be adaptively adjusted to optimize the cooperative scheme in terms of the variance of frequency offset estimation error. A scheme, where with the CSI knowledge, the relays adaptively switch between the cooperative and conventional transmissions, was proposed to optimize the frequency offset estimation. Although the frequency offset estimation accuracy in the

DcF mode is somewhat worse than the AF mode, both modes outperform the conventional transmission. However, DcF relays outperform AF relays in terms of channel capacity and BER.

6.2 Future Work

Frequency offset and/or channel estimation for OFDM systems has attracted great interest in the wireless communication community. The trend of combing OFDM with other advanced techniques brings forth many challenges. The following are several possible research topics.

The thesis has investigated channel estimation for cooperative OFDM. The number of pilots needed for channel estimation was found to increase with the number of relays. Thus, when the number of relays is large, more pilots are required, resulting in a reduced data throughput. Channel estimation techniques should be developed to reduce the number of needed pilots, and some signal processing knowledge maybe used to short the channel, while keep or even improve estimation accuracy.

Blind or semi-blind channel estimation methods can increase the system throughput because pilots are not used. These techniques have been intensively studied for conventional (i.e. non-relaying) systems. They may be extended to cooperative OFDM/OFDMA systems. Frequency offset estimation by using such techniques is also worth studying.

The cooperative systems that have been considered in Chapter 3 and Chapter 6 can be categorized as one hop relay networks. Other cooperative networks include two-way relay networks and multiple hop networks. Frequency offset and/or channel estimation for these networks, especially when combined with OFDM, is challenging and can be investigated.

This thesis only discussed channel estimation for slow-fading channels. However,

along with the popularity of the wireless systems, higher velocity of mobiles are expected, which results in time-varying or doubly-selective channels. Channel estimation techniques for OFDM systems operating in time-varying channels can be developed.

In cooperative systems, due to each node has its own oscillator, the frequency difference between each node exists, i.e., multiple frequency offsets are generated. These multiple frequency offsets indeed make the system complex and the estimation of frequency offsets hard. The system model in the presence of frequency offsets is expected to be built based on cooperative protocols. The impact of frequency offsets thus can be analyzed later. The frequency offset estimation is expected to explore the inner structure of the cooperation protocols. Other methods to mitigate the frequency offsets for cooperative OFDM systems, such as frequency offset mitigating codes and designing data detection algorithms with frequency offset estimation errors are also of interest.

In Chapter 3, the transmission power on each relay is assumed to be same. However, each relay might have its own power limitation. The channel estimation with the power limitation of each relay meets the practical scenarios.

Time synchronization is required to identify when individual OFDM symbols start and end. The symbol-level time synchronization defines the DFT window; i.e., the set of samples used to calculate DFT of each received OFDM symbol. Although, time synchronization has been intensively investigated in non-relay OFDM systems, in cooperative systems, due to the physically distributed relays, the time offset might be quite large. Time offset estimation and mitigation can be investigated for cooperative systems.

Appendix A

$D_{i;m}^{k}$ in Chapter 3

A.1 $D_{i;m}^{k}$ for Without Combining

Without loss of generality, the signal transmitted by the i-th transmit antenna is assumed to be demodulated at the k-th receive antenna. For each (k,i,n), $H = \left|H_{k,i}^{(n)}\right|$ has a probability density function (PDF) $f(H) = 2H \cdot e^{-H^2}$. When $m > 2$, $D_{i;m}^{k}$ can be represented as

$$\begin{aligned} D_{i;m}^{k} &= \int_0^\infty \left(\sqrt{\bar{\gamma}_{k,i}\left(n\middle|H_{k,i}^{(n)}\right)}\right)^{2m-1} f(H)\,\mathrm{d}H \\ &= \int_0^\infty \frac{\varpi^{(m-\frac{1}{2})} H^{(2m-1)}}{(\mu H^2+\nu)^{(m-\frac{1}{2})}} e^{-H^2}\mathrm{d}H^2 \\ &= \frac{(m-\frac{1}{2})\varpi^{(m-\frac{1}{2})}}{\mu(m-\frac{3}{2})} \int_0^\infty \frac{h^{(m-\frac{3}{2})}e^{-h}}{(\mu h+\nu)^{(m-\frac{3}{2})}}\mathrm{d}h - \frac{\varpi^{(m-\frac{1}{2})}}{\mu(m-\frac{3}{2})} \int_0^\infty \frac{h^{(m-\frac{1}{2})}e^{-h}}{(\mu h+\nu)^{(m-\frac{3}{2})}}\mathrm{d}h \\ &= \frac{\varpi(m-\frac{1}{2})}{\mu(m-\frac{3}{2})} \cdot D_{i;m-1}^{k} - \frac{\varpi^{(m-\frac{1}{2})}}{\mu(m-\frac{3}{2})} \int_0^\infty \frac{h^{(m-\frac{1}{2})}e^{-h}}{(\mu h+\nu)^{(m-\frac{3}{2})}}\mathrm{d}h, \end{aligned} \tag{A.1}$$

where $h = H^2$. (A.1) can be further derived as

$$\begin{aligned} D_{i;m}^{k} &= \frac{\varpi(m-\frac{1}{2})}{\mu(m-\frac{3}{2})} \cdot D_{i;m-1}^{k} - \frac{\varpi^{(m-\frac{1}{2})}}{\mu(m-\frac{3}{2})} \int_0^\infty \frac{h^{(m-\frac{1}{2})}e^{-h}}{(\mu h+\nu)^{(m-\frac{3}{2})}}\mathrm{d}h \\ &= \frac{\varpi(m-\frac{1}{2})}{\mu(m-\frac{3}{2})} \cdot D_{i;m-1}^{k} + \frac{\varpi^{(m-\frac{1}{2})}\nu}{\mu^2(m-\frac{3}{2})} \int_0^\infty \frac{h^{(m-\frac{3}{2})}e^{-h}}{(\mu h+\nu)^{(m-\frac{3}{2})}}\mathrm{d}h \\ &\quad - \frac{\varpi^{(m-\frac{1}{2})}}{\mu^2(m-\frac{3}{2})} \underbrace{\int_0^\infty \frac{h^{(m-\frac{3}{2})}e^{-h}}{(\mu h+\nu)^{(m-\frac{5}{2})}}\mathrm{d}h}_{Z_i^k} \\ &= \frac{\varpi(m-\frac{1}{2})}{\mu(m-\frac{3}{2})} \cdot D_{i;m-1}^{k} + \frac{\varpi\nu}{\mu^2(m-\frac{3}{2})} \cdot D_{i;m-1}^{k} - \frac{\varpi^{(m-\frac{1}{2})}}{\mu^2(m-\frac{3}{2})} \cdot Z_i^k. \end{aligned} \tag{A.2}$$

From the last step of (A.1), $D_{i;m-1}^k$ can be represented as a function of $D_{i;m-2}^k$ and Z_i^k:

$$\begin{aligned} D_{i;m-1}^k &= \frac{\varpi(m-\frac{3}{2})}{\mu(m-\frac{5}{2})} \cdot D_{i;m-2}^k - \frac{\varpi^{(m-\frac{3}{2})}}{\mu(m-\frac{5}{2})} \int_0^\infty \frac{h^{(m-\frac{3}{2})} e^{-h}}{(\mu h+\nu)^{(m-\frac{5}{2})}} \mathrm{d}h \\ &= \frac{\varpi(m-\frac{3}{2})}{\mu(m-\frac{5}{2})} \cdot D_{i;m-2}^k - \frac{\varpi^{(m-\frac{3}{2})}}{\mu(m-\frac{5}{2})} \cdot Z_i^k. \end{aligned} \tag{A.3}$$

By resolving (A.3), Z_i^k can be represented as

$$Z_i^k = \frac{\varpi(m-\frac{3}{2}) \cdot D_{i;m-2}^k - \mu(m-\frac{5}{2}) \cdot D_{i;m-1}^k}{\varpi^{(m-\frac{3}{2})}}. \tag{A.4}$$

By replacing Z_i^k in (A.2) with (A.4), $D_{i;m}^k$ can be finally simplified as

$$\begin{aligned} D_{i;m}^k &= \frac{\varpi(m-\frac{1}{2})}{\mu(m-\frac{3}{2})} \cdot D_{i;m-1}^k + \frac{\varpi\nu}{\mu^2(m-\frac{3}{2})} \cdot D_{i;m-1}^k - \frac{\varpi^{(m-\frac{1}{2})}}{\mu^2(m-\frac{3}{2})} \cdot Z \\ &= \frac{\varpi(m-\frac{1}{2})}{\mu(m-\frac{3}{2})} \cdot D_{i;m-1}^k + \frac{\varpi\nu}{\mu^2(m-\frac{3}{2})} \cdot D_{i;m-1}^k + \frac{\varpi(m-\frac{5}{2})}{\mu(m-\frac{3}{2})} \cdot D_{i;m-1}^k - \frac{\varpi^2}{\mu^2} \cdot D_{i;m-2}^k \\ &= \frac{\varpi\left[(2m-3)\mu+\nu\right]}{\mu^2(m-\frac{3}{2})} \cdot D_{i;m-1}^k - \frac{\varpi^2}{\mu^2} \cdot D_{i;m-2}^k. \end{aligned} \tag{A.5}$$

A.2 $D_{i;m}^{\mathbf{EGC}}$ for EGC

Without loss of generality, consider the demodulation of the signal transmitted by the i-th transmit antenna. Define

$$\nu^E = \sum_{k=1}^{N_r} \left(\frac{\pi^2 \sigma_{res}^2 E_s}{3N_t} - \mathrm{Var}\left\{\alpha_{k,i}^{(n)}\right\} + \mathbb{E}\left\{\left|\Delta\lambda_{k,i}^{(n)}\right|^2\right\} + \mathbb{E}\left\{\left|\Delta\xi_{k,i}^{(n)}\right|^2\right\} + \sigma_w^2 \right) = N_r\nu \tag{A.6}$$

and $H_{\mathrm{EGC}} = \sum_{k=1}^{N_r} \left| H_{k,i}^{(n)} \right|$. Like in Appendix I, when $m > 2$, $D_{i;m}^{\mathrm{EGC}}$ can be represented as

$$\begin{aligned}
D_{i;m}^{\mathrm{EGC}} &= \int_0^{\infty} \left(\sqrt{\bar{\gamma}_i^E \left(n \middle| H_{1,i}^{(n)}, \cdots, H_{N_r,i}^{(n)} \right)} \right)^{2m-1} f\left(H_{\mathrm{EGC}}\right) \mathrm{d}H_{\mathrm{EGC}} \\
&= \int_0^{\infty} \frac{\varpi^{(m-\frac{1}{2})} H_{\mathrm{EGC}}^{(2m-1)}}{\left(\mu \left(H_{\mathrm{EGC}}^2 - \frac{N_r(N_r-1)\pi}{4} \right) + \nu^E \right)^{(m-\frac{1}{2})}} \cdot \frac{H_{\mathrm{EGC}}^{(2N_r-2)}}{2^{N_r} \sigma_{\mathrm{EGC}}^{2N_r} (N_r-1)!} \cdot e^{-\frac{H_{\mathrm{EGC}}^2}{2\sigma_{\mathrm{EGC}}^2}} \mathrm{d}H_{\mathrm{EGC}}^2 \\
&= \frac{(m+N_r-\frac{3}{2})(2\sigma_{\mathrm{EGC}}^2 \varpi)^{(m-\frac{1}{2})}}{\tilde{\mu}(m-\frac{3}{2})(N_r-1)!} \int_0^{\infty} \frac{h^{(m+N_r-\frac{5}{2})} e^{-h}}{\left(\tilde{\mu}h + \tilde{\nu}^E\right)^{(m-\frac{3}{2})}} \mathrm{d}h \\
&\quad - \frac{(2\sigma_{\mathrm{EGC}}^2 \varpi)^{(m-\frac{1}{2})}}{\tilde{\mu}(m-\frac{3}{2})(N_r-1)!} \int_0^{\infty} \frac{h^{(m+N_r-\frac{3}{2})} e^{-h}}{\left(\tilde{\mu}h + \tilde{\nu}^E\right)^{(m-\frac{3}{2})}} \mathrm{d}h \\
&= \frac{2\sigma_{\mathrm{EGC}}^2 \varpi (m+N_r-\frac{3}{2})}{\tilde{\mu}(m-\frac{3}{2})} \cdot D_{i;m-1}^{\mathrm{EGC}} - \frac{(2\sigma_{\mathrm{EGC}}^2 \varpi)^{(m-\frac{1}{2})}}{\tilde{\mu}(m-\frac{3}{2})(N_r-1)!} \int_0^{\infty} \frac{h^{(m+N_r-\frac{3}{2})} e^{-h}}{\left(\tilde{\mu}h + \tilde{\nu}^E\right)^{(m-\frac{3}{2})}} \mathrm{d}h,
\end{aligned} \tag{A.7}$$

where $\tilde{\nu}^E = \nu^E - \dfrac{\mu N_r(N_r-1)\pi}{4}$, $h = \dfrac{H_{\mathrm{EGC}}^2}{2\sigma_{\mathrm{EGC}}^2}$, $\sigma_{\mathrm{EGC}}^2 = \dfrac{(N_r!)^2}{8\left[\left(N_r-\frac{1}{2}\right)\cdots\frac{1}{2}\right]^2}$ and $\tilde{\mu} = 2\sigma_{\mathrm{EGC}}^2 \cdot \mu$. (A.7) can be further simplified as

$$\begin{aligned}
D_{i;m}^{\mathrm{EGC}} &= \frac{2\sigma_{\mathrm{EGC}}^2 \varpi (m+N_r-\frac{3}{2})}{\tilde{\mu}(m-\frac{3}{2})} \cdot D_{i;m-1}^{\mathrm{EGC}} - \frac{(2\sigma_{\mathrm{EGC}}^2 \varpi)^{(m-\frac{1}{2})}}{\tilde{\mu}(m-\frac{3}{2})(N_r-1)!} \int_0^{\infty} \frac{h^{(m+N_r-\frac{3}{2})} e^{-h}}{\left(\tilde{\mu}h + \tilde{\nu}^E\right)^{(m-\frac{3}{2})}} \mathrm{d}h \\
&= \frac{2\sigma_{\mathrm{EGC}}^2 \varpi (m+N_r-\frac{3}{2})}{\tilde{\mu}(m-\frac{3}{2})} \cdot D_{i;m-1}^{\mathrm{EGC}} - \frac{(2\sigma_{\mathrm{EGC}}^2 \varpi)^{(m-\frac{1}{2})} \tilde{\nu}^E}{\tilde{\mu}^2(m-\frac{3}{2})(N_r-1)!} \int_0^{\infty} \frac{h^{(m+N_r-\frac{5}{2})} e^{-h}}{\left(\tilde{\mu}h + \tilde{\nu}^E\right)^{(m-\frac{3}{2})}} \mathrm{d}h \\
&\quad - \frac{\varpi^{(m-\frac{1}{2})}}{\mu^2(m-\frac{3}{2})(N_r-1)!} \underbrace{\int_0^{\infty} \frac{h^{(m+N_r-\frac{5}{2})} e^{-h}}{\left(\mu h + \nu^E\right)^{(m-\frac{5}{2})}} \mathrm{d}h}_{Z_i^{\mathrm{EGC}}} \\
&= \frac{2\sigma_{\mathrm{EGC}}^2 \varpi (m+N_r-\frac{3}{2})}{\tilde{\mu}(m-\frac{3}{2})} \cdot D_{i;m-1}^{\mathrm{EGC}} + \frac{2\sigma_{\mathrm{EGC}}^2 \varpi \tilde{\nu}^E}{\tilde{\mu}^2(m-\frac{3}{2})(N_r-1)!} \cdot D_{i;m-1}^{\mathrm{EGC}} \\
&\quad - \frac{(2\sigma_{\mathrm{EGC}}^2 \varpi)^{(m-\frac{1}{2})}}{\tilde{\mu}^2(m-\frac{3}{2})(N_r-1)!} \cdot Z_i^{\mathrm{EGC}}.
\end{aligned} \tag{A.8}$$

From the last step of (A.7), $D_{i;m-1}^{\mathrm{EGC}}$ can be represented as a function of $D_{i;m-2}^{\mathrm{EGC}}$ and Z_i^{EGC};

$$\begin{aligned} D_{i;m-1}^{\mathrm{EGC}} &= \frac{2\sigma_{\mathrm{EGC}}^2\varpi(m+N_r-\frac{5}{2})}{\tilde{\mu}(m-\frac{5}{2})}\cdot D_{i;m-2}^{\mathrm{EGC}} - \frac{(2\sigma_{\mathrm{EGC}}^2\varpi)^{(m-\frac{3}{2})}}{\tilde{\mu}(m-\frac{5}{2})(N_r-1)!}\int_0^{\infty}\frac{h^{(m+N_r-\frac{5}{2})}e^{-h}}{(\tilde{\mu}h+\tilde{\nu}^E)^{(m-\frac{5}{2})}}\mathrm{d}h \\ &= \frac{2\sigma_{\mathrm{EGC}}^2\varpi(m+N_r-\frac{5}{2})}{\tilde{\mu}(m-\frac{5}{2})}\cdot D_{i;m-2}^{\mathrm{EGC}} - \frac{(2\sigma_{\mathrm{EGC}}^2\varpi)^{(m-\frac{3}{2})}}{\tilde{\mu}(m-\frac{5}{2})(N_r-1)!}\cdot Z_i^{\mathrm{EGC}}. \end{aligned} \tag{A.9}$$

By resolving (A.9), Z_i^{EGC} can be represented as

$$Z_i^{\mathrm{EGC}} = \frac{2\sigma_{\mathrm{EGC}}^2\varpi(m+N_r-\frac{5}{2})(N_r-1)!\cdot D_{i;m-2}^{\mathrm{EGC}} - \tilde{\mu}(m-\frac{5}{2})(N_r-1)!\cdot D_{i;m-1}^{\mathrm{EGC}}}{(2\sigma_{\mathrm{EGC}}^2\varpi)^{(m-\frac{3}{2})}}. \tag{A.10}$$

By replacing Z_i^{EGC} in (A.8) with (A.10), $D_{i;m}^{\mathrm{EGC}}$ can be finally simplified as

$$\begin{aligned} D_{i;m}^{\mathrm{EGC}} &= \frac{2\sigma_{\mathrm{EGC}}^2\varpi(m+N_r-\frac{3}{2})}{\tilde{\mu}(m-\frac{3}{2})}\cdot D_{i;m-1}^{\mathrm{EGC}} + \frac{2\sigma_{\mathrm{EGC}}^2\varpi\tilde{\nu}^E}{\tilde{\mu}^2(m-\frac{3}{2})(N_r-1)!}\cdot D_{i;m-1}^{\mathrm{EGC}} \\ &\quad - \frac{(2\sigma_{\mathrm{EGC}}^2\varpi)^{(m-\frac{1}{2})}}{\tilde{\mu}^2(m-\frac{3}{2})(N_r-1)!}\cdot Z^{\mathrm{EGC}} \\ &= \frac{2\sigma_{\mathrm{EGC}}^2\varpi\left[(2m+N_r-4)\tilde{\mu}(N_r-1)!+\tilde{\nu}^E\right]}{\tilde{\mu}^2(m-\frac{3}{2})(N_r-1)!}\cdot D_{i;m-1}^{\mathrm{EGC}} - \frac{(2\sigma_{\mathrm{EGC}}^2\varpi)^2(m+N_r-\frac{5}{2})}{\tilde{\mu}^2(m-\frac{3}{2})}\cdot D_{i;m-2}^{\mathrm{EGC}}. \end{aligned} \tag{A.11}$$

A.3 $D_{i;m}^{\mathrm{MRC}}$ for MRC

Without loss of generality, consider the demodulation of the signal transmitted by the i-th transmit antenna. Define $H_{\mathrm{MRC}} = \sqrt{\sum_{k=1}^{N_r}\left|H_{k,i}^{(n)}\right|^2}$. When $m > 2$, $D_{i;m}^{\mathrm{MRC}}$ can be

represented as

$$
\begin{aligned}
D_{i;m}^{\mathrm{MRC}} &= \int_0^{\infty} \left(\sqrt{\bar{\gamma}_i^M \left(n \middle| H_{1,i}^{(n)}, \cdots, H_{N_r,i}^{(n)} \right)} \right)^{2m-1} f\left(H_{\mathrm{MRC}}\right) \mathrm{d}H_{\mathrm{MRC}} \\
&= 2^{N_r} \int_0^{\infty} \frac{\varpi^{(m-\frac{1}{2})} H_{\mathrm{MRC}}^{(2m-1)}}{\left(\mu\left[H_{\mathrm{MRC}}^2 - (N_r-1)\right] + \nu^M\right)^{(m-\frac{1}{2})}} \cdot \frac{H_{\mathrm{MRC}}^{(2N_r-2)}}{(N_r-1)!} \cdot e^{-H_{\mathrm{MRC}}^2} \mathrm{d}H_{\mathrm{MRC}}^2 \\
&= \frac{2^{N_r}(m+N_r-\frac{3}{2}) e^{-(N_r-1)} \varpi^{(m-\frac{1}{2})}}{\mu(m-\frac{3}{2})(N_r-1)!} \int_0^{\infty} \frac{h^{(m+N_r-\frac{5}{2})} e^{-h}}{\left(\mu h + \tilde{\nu}^M\right)^{(m-\frac{3}{2})}} \mathrm{d}h \\
&\quad - \frac{2^{N_r} e^{-(N_r-1)} \varpi^{(m-\frac{1}{2})}}{\mu(m-\frac{3}{2})(N_r-1)!} \int_0^{\infty} \frac{h^{(m+N_r-\frac{3}{2})} e^{-h}}{\left(\mu h + \tilde{\nu}^M\right)^{(m-\frac{3}{2})}} \mathrm{d}h \\
&= \frac{\varpi(m+N_r-\frac{3}{2}) e^{-(N_r-1)}}{\mu(m-\frac{3}{2})} \cdot D_{i;m-1}^{\mathrm{MRC}} - \frac{2^{N_r} e^{-(N_r-1)} \varpi^{(m-\frac{1}{2})}}{\mu(m-\frac{3}{2})(N_r-1)!} \int_0^{\infty} \frac{h^{(m+N_r-\frac{3}{2})} e^{-h}}{\left(\mu h + \tilde{\nu}^M\right)^{(m-\frac{3}{2})}} \mathrm{d}h,
\end{aligned}
\tag{A.12}
$$

where $h = H_{\mathrm{MRC}}^2$ and $\tilde{\nu}^M = \nu^M - \mu(N_r - 1)$. (A.12) can be further simplified as

$$
\begin{aligned}
D_{i;m}^{\mathrm{MRC}} &= \frac{\varpi(m+N_r-\frac{3}{2}) e^{-(N_r-1)}}{\mu(m-\frac{3}{2})} \cdot D_{i;m-1}^{\mathrm{MRC}} - \frac{2^{N_r} e^{-(N_r-1)} \varpi^{(m-\frac{1}{2})}}{\mu(m-\frac{3}{2})(N_r-1)!} \int_0^{\infty} \frac{h^{(m+N_r-\frac{3}{2})} e^{-h}}{\left(\mu h + \tilde{\nu}^M\right)^{(m-\frac{3}{2})}} \mathrm{d}h \\
&= \frac{\varpi(m+N_r-\frac{3}{2}) e^{-(N_r-1)}}{\mu(m-\frac{3}{2})} \cdot D_{i;m-1}^{\mathrm{MRC}} \\
&\quad - \frac{2^{N_r} e^{-(N_r-1)} \varpi^{(m-\frac{1}{2})}}{\mu^2(m-\frac{3}{2})(N_r-1)!} \int_0^{\infty} \frac{\left(\mu h - \tilde{\nu}^M + \tilde{\nu}^M\right) \cdot h^{(m+N_r-\frac{5}{2})} e^{-h}}{\left(\mu h + \tilde{\nu}^M\right)^{(m-\frac{3}{2})}} \mathrm{d}h \\
&= \frac{\varpi(m+N_r-\frac{3}{2}) e^{-(N_r-1)}}{\mu(m-\frac{3}{2})} \cdot D_{i;m-1}^{\mathrm{MRC}} - \frac{2^{N_r} e^{-(N_r-1)} \varpi^{(m-\frac{1}{2})} \tilde{\nu}^M}{\mu^2(m-\frac{3}{2})(N_r-1)!} \int_0^{\infty} \frac{h^{(m+N_r-\frac{5}{2})} e^{-h}}{\left(\mu h + \tilde{\nu}^M\right)^{(m-\frac{3}{2})}} \mathrm{d}h \\
&\quad - \frac{2^{N_r} e^{-(N_r-1)} \varpi^{(m-\frac{1}{2})}}{\mu^2(m-\frac{3}{2})(N_r-1)!} \underbrace{\int_0^{\infty} \frac{h^{(m+N_r-\frac{5}{2})} e^{-h}}{\left(\mu h + \tilde{\nu}^M\right)^{(m-\frac{5}{2})}} \mathrm{d}h}_{Z_i^{\mathrm{MRC}}} \\
&= \frac{\varpi(m+N_r-\frac{3}{2}) e^{-(N_r-1)}}{\mu(m-\frac{3}{2})} \cdot D_{i;m-1}^{\mathrm{MRC}} + \frac{\varpi \tilde{\nu}^M e^{-(N_r-1)}}{\mu^2(m-\frac{3}{2})(N_r-1)!} \cdot D_{i;m-1}^{\mathrm{MRC}} \\
&\quad - \frac{2^{N_r} e^{-(N_r-1)} \varpi^{(m-\frac{1}{2})}}{\mu^2(m-\frac{3}{2})(N_r-1)!} \cdot Z_i^{\mathrm{MRC}}.
\end{aligned}
\tag{A.13}
$$

From the last step of (A.12), $D_{i;m-1}^{\mathrm{MRC}}$ can be represented as a function of $D_{i;m-2}^{\mathrm{MRC}}$ and Z_i^{MRC};

$$\begin{aligned} D_{i;m-1}^{\mathrm{MRC}} &= \frac{e^{-(N_r-1)}\varpi(m+N_r-\frac{5}{2})}{\mu(m-\frac{5}{2})}\cdot D_{i;m-2}^{\mathrm{MRC}} - \frac{2^{N_r}e^{-(N_r-1)}\varpi^{(m-\frac{3}{2})}}{\mu(m-\frac{5}{2})(N_r-1)!}\int_0^{\infty}\frac{h^{(m+N_r-\frac{5}{2})}e^{-h}}{(\mu h+\tilde{\nu}^M)^{(m-\frac{5}{2})}}\mathrm{d}h \\ &= \frac{\varpi(m+N_r-\frac{5}{2})e^{-(N_r-1)}}{\mu(m-\frac{5}{2})}\cdot D_{i;m-2}^{\mathrm{MRC}} - \frac{2^{N_r}e^{-(N_r-1)}\varpi^{(m-\frac{3}{2})}}{\mu(m-\frac{5}{2})(N_r-1)!}\cdot Z_i^{\mathrm{MRC}}. \end{aligned} \tag{A.14}$$

By resolving (A.14), Z_i^{MRC} can be represented as

$$Z_i^{\mathrm{MRC}} = \frac{\varpi(m+N_r-\frac{5}{2})(N_r-1)!\cdot D_{i;m-2}^{\mathrm{MRC}} - \mu(m-\frac{5}{2})(N_r-1)!e^{(N_r-1)}\cdot D_{i;m-1}^{\mathrm{MRC}}}{2^{N_r}\varpi^{(m-\frac{3}{2})}}. \tag{A.15}$$

By replacing Z_i^{MRC} in (A.13) with (A.15), $D_{i;m}^{\mathrm{MRC}}$ can be finally simplified as

$$\begin{aligned} D_{i;m}^{\mathrm{MRC}} &= \frac{\varpi(m+N_r-\frac{3}{2})e^{-(N_r-1)}}{\mu(m-\frac{3}{2})}\cdot D_{i;m-1}^{\mathrm{MRC}} + \frac{\varpi\tilde{\nu}^M e^{-(N_r-1)}}{\mu^2(m-\frac{3}{2})(N_r-1)!}\cdot D_{i;m-1}^{\mathrm{MRC}} \\ &\quad - \frac{2^{N_r}e^{-(N_r-1)}\varpi^{(m-\frac{1}{2})}}{\mu^2(m-\frac{3}{2})(N_r-1)!}\cdot Z^{\mathrm{MRC}} \\ &\quad - \frac{\varpi^2(m+N_r-\frac{5}{2})e^{-(N_r-1)}}{\mu^2(m-\frac{3}{2})}\cdot D_{i;m-2}^{\mathrm{MRC}} \\ &= \frac{\varpi\left[(2m+N_r-4)\mu(N_r-1)!+\tilde{\nu}^M\right]}{\mu^2(m-\frac{3}{2})(N_r-1)!}\cdot D_{i;m-1}^{\mathrm{MRC}} - \frac{\varpi^2(m+N_r-\frac{5}{2})e^{-(N_r-1)}}{\mu^2(m-\frac{3}{2})}\cdot D_{i;m-2}^{\mathrm{MRC}}. \end{aligned} \tag{A.16}$$

Appendix B

Appendix for Chapter 5

B.1 Analysis of FIM

The covariance matrix $\mathbf{C}$ can be rewritten as

$$\begin{aligned}\mathbf{C} &= \sum_k \mathbb{E}\left\{(\mathbf{y}_k - \mathbf{s}_k)(\mathbf{y}_k - \mathbf{s}_k)^H\right\} + \sum_k \underbrace{\sum_{k\neq l} \underbrace{\mathbb{E}\left\{(\mathbf{y}_k - \mathbf{s}_k)(\mathbf{y}_l - \mathbf{s}_l)^H\right\}}_{\mathbf{Z}_{kl}}}_{\mathbf{Z}_k} \\ &= \sum_k (\mathbf{C}_k + \mathbf{Z}_k),\end{aligned} \tag{B.1}$$

where $\mathbf{C}_k = \mathbb{E}\left\{(\mathbf{y}_k - \mathbf{s}_k)(\mathbf{y}_k - \mathbf{s}_k)^H\right\}$, and $\mathbf{Z}_{kl} = \mathbb{E}\left\{(\mathbf{y}_k - \mathbf{s}_k)(\mathbf{y}_l - \mathbf{s}_l)^H\right\}$ is the MAI matrix of the k-th user, which is contributed by the l-th user. For the nonzero frequency offsets, $\sum_{k\neq l} \mathbf{Z}_{kl} \neq \mathbf{O}_N$. We can decompose $\mathbf{C}$ as

$$\mathbf{C} = \sum_k (\mathbf{C}_k + \mathbf{Z}_k) = \sum_k \mathbf{U}\left(\mathbf{D}_k + \tilde{\mathbf{D}}_k\right)\mathbf{U}^H, \tag{B.2}$$

where $\mathbf{U}$ is a $N \times N$ Unitary matrix, $\mathbf{D}_k = \mathrm{diag}\{0, \cdots, \lambda_{k,1}, \cdots, \lambda_{k,\mathcal{N}_k}, \cdots, 0\}$ with $\lambda_{k,i}$ representing the i-th eigenvalue of $\mathbf{C}_k$, and $\tilde{\mathbf{D}}_k = \mathrm{diag}\{0, \cdots, z_{k,1}, \cdots, z_{k,\mathcal{N}_k}, \cdots, 0\}$ with $z_{k,i}$ representing the i-th eigenvalue of $\mathbf{Z}_k$. The index of $z_{k,i}$ is identical to that of $\lambda_{k,i}$ for each i. Therefore, $\mathbf{C}^{-1}$ can be represented as $\mathbf{C}^{-1} = \sum_k \mathbf{U}\left(\mathbf{D}_k + \tilde{\mathbf{D}}_k\right)^{-1}\mathbf{U}^H$, where $\left(\mathbf{D}_k + \tilde{\mathbf{D}}_k\right)^{-1} = \mathrm{diag}\{0, \cdots, (\lambda_{k,1} + z_{k,1})^{-1}, \cdots, (\lambda_{k,\mathcal{N}_k} + z_{k,\mathcal{N}_k})^{-1}, \cdots, 0\}$.

We also have

$$\begin{aligned}\frac{\partial \mathbf{C}}{\partial \varepsilon_k} &= \frac{\partial (\mathbf{C}_k + \mathbf{Z}_k)}{\partial \varepsilon_k} + \sum_{l\neq k} \frac{\partial (\mathbf{C}_l + \mathbf{Z}_l)}{\partial \varepsilon_k} \\ &= \mathbf{U} \cdot \mathrm{diag}\left\{0, \cdots, \frac{\partial(\lambda_{k,1} + z_{k,1})}{\partial \varepsilon_k}, \cdots, \frac{\partial(\lambda_{k,\mathcal{N}_k} + z_{k,\mathcal{N}_k})}{\partial \varepsilon_k}, \cdots, 0\right\} \cdot \mathbf{U}^H \\ &\quad + \sum_{l\neq k} \mathbf{U} \cdot \mathrm{diag}\left\{0, \cdots, \frac{\partial(\lambda_{l,1} + z_{l,1})}{\partial \varepsilon_k}, \cdots, \frac{\partial(\lambda_{l,\mathcal{N}_l} + z_{l,\mathcal{N}_l})}{\partial \varepsilon_k}, \cdots, 0\right\} \cdot \mathbf{U}^H.\end{aligned} \tag{B.3}$$

Note that $\mathbf{Z}_k$ is the MAI contributed by users other than k and is not a function of ε_k; therefore, $\partial\mathbf{Z}_k/\partial\varepsilon_k = \mathbf{O}_N$. $\mathbf{C}_l$ is also not a function of ε_k, so $\partial\mathbf{C}_l/\partial\varepsilon_k = \mathbf{O}_N$. From the above discussion, we have

$$\begin{aligned}\frac{\partial\mathbf{C}}{\partial\varepsilon_k} &= \frac{\partial\mathbf{C}_k}{\partial\varepsilon_k} + \sum_{l\neq k}\frac{\partial\mathbf{Z}_l}{\partial\varepsilon_k} \\ &= \mathbf{U}\cdot\operatorname{diag}\left\{0,\cdots,\frac{\partial\lambda_{k,1}}{\partial\varepsilon_k},\cdots,\frac{\partial\lambda_{k,\mathcal{N}_k}}{\partial\varepsilon_k},\cdots,0\right\}\cdot\mathbf{U}^H \\ &\quad + \sum_{l\neq k}\mathbf{U}\cdot\operatorname{diag}\left\{0,\cdots,\frac{\partial z_{l,1}}{\partial\varepsilon_k},\cdots,\frac{\partial z_{l,\mathcal{N}_l}}{\partial\varepsilon_k},\cdots,0\right\}\cdot\mathbf{U}^H.\end{aligned} \tag{B.4}$$

When $l \neq k$, the kl-th element of FIM can be represented as

$$[\mathbf{\Lambda}]_{kl} = \sum_{i=1}^{\mathcal{N}_k}\frac{\frac{\partial\lambda_{k,i}}{\partial\varepsilon_k}\frac{\partial z_{k,i}}{\partial\varepsilon_l}}{(\lambda_{k,i}+z_{k,i})^2} + \sum_{j=1}^{\mathcal{N}_l}\frac{\frac{\partial\lambda_{l,j}}{\partial\varepsilon_l}\frac{\partial z_{l,j}}{\partial\varepsilon_k}}{(\lambda_{l,j}+z_{l,j})^2} + \sum_{n\neq k,l}\sum_{p=1}^{\mathcal{N}_n}\frac{\frac{\partial^2 z_{n,p}}{\partial\varepsilon_k\partial\varepsilon_l}}{(\lambda_{n,p}+z_{n,p})^2}, \tag{B.5}$$

and the kk-th element of FIM is given by

$$[\mathbf{\Lambda}]_{kk} = \sum_{i=1}^{\mathcal{N}_k}\frac{\left(\frac{\partial\lambda_{k,i}}{\partial\varepsilon_k}\right)^2}{(\lambda_{k,i}+z_{k,i})^2} + \sum_{l\neq k}\sum_{j=1}^{\mathcal{N}_l}\frac{\left(\frac{\partial z_{l,j}}{\partial\varepsilon_k}\right)^2}{(\lambda_{l,j}+z_{l,j})^2}. \tag{B.6}$$

B.2 SINR Analysis

Without loss of generality, suppose that M users accessed a base station, and the k-th user is selected as the user of interest. The average SINR of user k is

$$\mathrm{SINR}_k = \frac{\mathbb{E}\left\{\|\tilde{\mathbf{s}}_k\|_2^2\right\}}{\mathbb{E}\left\{\|\mathbf{\Upsilon}_k\|_2^2\right\}+\mathbb{E}\left\{\|\tilde{\mathbf{w}}_k\|_2^2\right\}} = \frac{\mathbb{E}\left\{\sum_{n\in G_k}\left|\sqrt{P_n}\mathbf{x}_k[n]H_k^n\cdot\frac{\sin(\pi\varepsilon_k)}{N\sin(\frac{\pi\varepsilon_k}{N})}\right|^2\right\}}{\mathbb{E}\left\{\sum_{n\in G_k}\left|\mathcal{I}_k(n)+\mathcal{I}_{l\neq k}(n)\right|^2\right\}+\mathbb{E}\left\{\left\|\mathbf{F}_k^H\mathbf{w}\right\|_2^2\right\}}, \tag{B.7}$$

where

$$\mathcal{I}_k(n) = \sum_{i\in G_k, i\neq n}\sqrt{P_i}\mathbf{x}_k[i]H_k^i\frac{\sin[\pi(i-n+\varepsilon_k)]}{N\sin\left[\frac{\pi(i-n+\varepsilon_k)}{N}\right]}, \tag{B.8}$$

and

$$\mathcal{I}_{l\neq k}(n) = \sum_{l=1,l\neq k}^{M}\sum_{i\in G_l}\sqrt{P_i}\mathbf{x}_l[i]H_l^i\frac{\sin[\pi(i-n+\varepsilon_l)]}{N\sin\left[\frac{\pi(i-n+\varepsilon_l)}{N}\right]}. \tag{B.9}$$

We also assume that $\mathbb{E}\{|\mathbf{x}_i[m]|^2\} = \sigma_x^2 = 1$, and $\sigma_w^2 = \dfrac{\mathbb{E}\left\|\mathbf{F}_k^H \mathbf{w}[n]\right\|_2^2}{\mathcal{N}_k} = \dfrac{\mathbb{E}\left\|\mathbf{w}\right\|_2^2}{N}$.

Note that $\sin[\pi(i-n+\varepsilon_l)] = (-1)^{i-n}\sin(\pi\varepsilon_l) \cong (-1)^{i-n}\pi\varepsilon_l$, and $\sin\left[\dfrac{\pi(i-n+\varepsilon_l)}{N}\right] \cong \sin\left[\dfrac{\pi(i-n)}{N}\right]$, when $\varepsilon_l \ll 1$. Therefore, we have

$$\mathcal{I}_k(n) = \sum_{i\in G_k, i\neq n} \sqrt{P_i}\mathbf{x}_k[i]H_k^i \frac{\sin[\pi(i-n+\varepsilon_k)]}{N\sin\left[\frac{\pi(i-n+\varepsilon_k)}{N}\right]} \cong \underbrace{\sum_{i\in G_k, i\neq n} \frac{(-1)^{i-n}\sqrt{P_i}\mathbf{x}_k[i]H_k^i\pi}{N\sin\left[\frac{\pi(i-n)}{N}\right]}}_{\eta_k(n)} \cdot\varepsilon_k, \tag{B.10}$$

and

$$\mathcal{I}_{l\neq k}(n) = \sum_{l=1,l\neq k}^{M}\sum_{i\in G_l} \sqrt{P_i}\mathbf{x}_l[i]H_l^i \frac{\sin[\pi(i-n+\varepsilon_l)]}{N\sin\left[\frac{\pi(i-n+\varepsilon_l)}{N}\right]} \cong \underbrace{\sum_{l=1,l\neq k}^{M}\sum_{i\in G_l} \frac{(-1)^{i-n}\sqrt{P_i}\mathbf{x}_l[i]H_l^i\pi}{N\sin\left[\frac{\pi(i-n)}{N}\right]}}_{\eta_l(n)} \cdot\varepsilon_l. \tag{B.11}$$

Then,

$$\mathrm{SINR}_k = \frac{\mathbb{E}\left\{\sum\limits_{n\in G_k}\left|\sqrt{P_n}\mathbf{x}_k[n]H_k^n\right|^2\right\}\cdot\mathbb{E}\left\{\left|\frac{\sin(\pi\varepsilon_k)}{N\sin\left(\frac{\pi\varepsilon_k}{N}\right)}\right|^2\right\}}{\sum\limits_{n\in G_k}\mathbb{E}\left\{\left|\eta_k(n)\cdot\varepsilon_k + \sum\limits_{l=1,l\neq k}^{M}\eta_l(n)\cdot\varepsilon_l\right|^2\right\} + \mathbb{E}\left\{\left\|\mathbf{F}_k^H\mathbf{w}\right\|_2^2\right\}}. \tag{B.12}$$

Note that $\eta_k(n)$, as well as each $\eta_{l\neq k}(n)$, is a RV with mean zero. If we assume that $\mathbb{E}\{\mathbf{x}_k[n]\mathbf{x}_l^*[m]\} = 0$ for $k \neq l$ or $n \neq m$, the average interference of the subcarrier n is

$$\mathbb{E}\left\{\left|\eta_k(n)\cdot\varepsilon_k + \sum_{l=1,l\neq k}^{M}\eta_l(n)\cdot\varepsilon_l\right|^2\right\} = \sum_{i\neq n}\frac{\pi^2\sigma_\epsilon^2\kappa_n}{N^2\sin^2\left[\frac{\pi(i-n)}{N}\right]}, \tag{B.13}$$

where $\kappa_n = \mathbb{E}\left\{\left|\sqrt{P_i}H_m^i\right|^2\right\}$. When N is large enough, and almost all the subcarriers are allocated, we have $\sum_{i\neq n}\left(1/N^2\sin^2\left[\pi(i-n)/N\right]\right) \cong \sum_{i\neq n}\left(1/\pi^2(i-n)^2\right) \cong 1/3$, and

$$\mathrm{SINR}_k \cong \frac{\mathrm{SNR}_k}{\frac{\pi^2\sigma_\epsilon^2\mathrm{SNR}_k}{3}+1}\cdot\left(1-\frac{\pi^2\sigma_\epsilon^2}{3}+\frac{\pi^4\sigma_\epsilon^4}{20}\right), \tag{B.14}$$

where $\mathrm{SNR}_k = \dfrac{\mathbb{E}\{\kappa_n\}}{\sigma_w^2}$ represents the average received SNR of the k-th user and σ_ϵ^2 is the variance of the frequency offsets.

Bibliography

[1] S. Sesia, I. Toufik, and M. Baker, *LTE The UMTS Long Term Evolution From Theory To Practice*. John Wiley & Sons Ltd., 2009.

[2] J. G. Proakis, *Digital Communications*, 4th ed. McGraw-Hill, 2000.

[3] G. L. Stüber, J. R. Barry, S. W. McLaughlin, Y. Li, M. A. Ingram, and T. G. Pratt, "Broadband MIMO-OFDM wireless communications," *Proc. IEEE*, vol. 92, no. 2, pp. 271–294, Feb. 2004.

[4] A. J. Paulraj, D. A. Gore, and R. U. Nabar, *Introduction to space-time wireless communications*. Cambridge University Press, 2003.

[5] Y. Li and G. L. Stüber, *Orthogonal Frequency Division Multiplexing for Wireless Communications*. Springer Science+Business Media, Inc., 2006.

[6] A. Greenspan, M. Klerer, J. Tomcik, R. Canchi, and J. Wilson, "IEEE 802.20: Mobile broadband wireless access for the twenty-first century," *IEEE Commun. Mag.*, vol. 46, no. 7, pp. 56–63, Jul. 2008.

[7] ETSI, "Digital video bradcasting (DVB): framing structure, channel coding and modulation for digital terrestrial television," ETSI EN 300 744 v1.5.1, April 2004. [Online]. Available: http://www.etsi.org.

[8] ——, "Digital audio bradcasting (DAB) to mobile, portable and fixed receivers," ETSI EN 300 401 v1.4.1, Jan. 2006. [Online]. Available: http://www.etsi.org.

[9] T. de Couasnon, R. Monnier, and J. B. Rault, "OFDM for digital TV broadcasting," *Signal Processing*, vol. 39, no. 1-2, pp. 1–31, Sep. 1994.

[10] R. V. Nee and R. Prasad, *OFDM for Wireless Multimedia Communications*. Boston: Artech House Publishers, 2000.

[11] D. Tse and P. Viswanath, *Fundamentals of Wireless Communication.* Cambridge University Press, 2005.

[12] T. S. Rappaport, *Wireless Communications Principles and Practice*, 2nd ed. Prentice Hall, 2002.

[13] P. H. Moose, "A technique for orthogonal frequency division multiplexing frequency offset correction," *IEEE Trans. Commun.*, vol. 42, no. 10, pp. 2908–2914, Oct. 1994.

[14] N. Watanabe, K. Takazawa, and J. Kusano, "Doubly rotated quartz crystal resonator for miniaturized VC-TCXO in mobile phone," in *IEEE International Frequency Control Symposium and PDA Exhibition*, New Orleans, LA, May 2002, pp. 119–127.

[15] C. F. Li, Y. S. Chu, J. S. Ho, and W. H. Sheen, "Cell search in WCDMA under large-frequency and clock errors: Algorithms to hardware implementation," *IEEE Trans. Circuits Syst.*, vol. 55, no. 2, pp. 659–671, Mar. 2008.

[16] T. Pollet, M. Blade, and M. Moeneclaey, "BER sensitivity of OFDM systems to carrier frequency offset and Weiner phase noise," *IEEE Trans. Commun.*, vol. 43, no. 234, pp. 191–193, Feb. 1995.

[17] G. Tsoulos, *MIMO Sytems Technology For Wireless Communications.* CRC Press, 2006.

[18] G. Foschini and M. J. Gans, "On limits of wireless communications in a fading environment when using multiple antennas," *Wirel. Pers. Commun. (Netherlands)*, vol. 6, no. 3, pp. 311–335, Jan. 1998.

[19] A. J. Paulraj, D. A. Gore, R. U. Nabar, and H. Bölcskei, "An overview of MIMO communications - a key to gigabit wireless," *Proc. IEEE*, no. 2, pp. 198–218, Feb. 2004.

[20] A. van Zelst and T. C. W. Schenk, "Implementation of a MIMO OFDM-based wireless LAN system," *IEEE Trans. Signal Processing*, vol. 52, no. 2, pp. 483–494, Feb. 2004.

[21] V. Tarokh, N. Seshadri, and A. R. Calderbank, "Space-time codes for high data rate wireless communication: Performance criterion and code construction," *IEEE Trans. Inform. Theory*, vol. 44, no. 2, pp. 744–765, Mar. 1998.

[22] S. M. Alamouti, "A simple transmit diversity technique for wireless communications," *IEEE J. Select. Areas Commun.*, vol. 16, no. 8, pp. 1451–1458, Oct. 1998.

[23] E. Telatar, "Capacity of multi-antenna Gaussian channels," *Euro. Trans. Telecommun.*, vol. 10, no. 6, pp. 585–595, Nov. 1999.

[24] G. J. Foschini, "Layered space-time architecture for wireless communication in a fading environment when using multi-element antennas," *Bell Labs. Tech. J.*, vol. 1, pp. 41–59, Autumn 1996.

[25] L. Zheng and D. Tse, "Diversity and multiplexing: A fundamental tradeoff in multiple-antenna channels," *IEEE Trans. Inform. Theory*, vol. 49, no. 5, pp. 1073–1096, May 2003.

[26] S. Alamouti, "A simple transmit diversity technique for wireless communications," *IEEE J. Select. Areas Commun.*, vol. 16, no. 8, pp. 1451–1458, Oct. 1998.

[27] V. Tarokh, N. Seshadri, and A. R. Calderbank, "Space-time block codes from orthogonal designs," *IEEE Trans. Inform. Theory*, vol. 45, no. 5, pp. 1456–1467, Jul. 1999.

[28] W. Zhang and C. Tellambura, "Performance of joint transmit and receive antenna selection with orthogonal space-time coding," *IEEE Trans. Veh. Technol.*, vol. 5, no. 5, pp. 2631–2635, 2010.

[29] Telecommunications Industry Association, "TIA/EIA physical layer standard for CDMA2000 spread spectrum systems, revision C," TIA/EIA/IS-2002-2.

[30] 3rd Generation partnership Project, "Technical specification group radio access network: Physical channels and mapping of transport channels onto physical channels (FDD) (release 1999)," v.3.2.0, 2000-2003.

[31] P. W. Wolniansky, G. J. Foschini, G. D. Golden, and R. A. Valenzuela, "V-BLAST: an architecture for realizing very high data rates over the rich scattering wireless channels," in *ISSSE, invited paper*, Pisa, Italy, 1998, pp. 198–218.

[32] T. Roman, M. Enescu, and V. Koivunen, "Joint time-Domain trackink of channel and frequency offsets for MIMO OFDM systems," *Wirel. Pers. Commun. (Netherlands)*, vol. 31, no. 1-2, pp. 181–200, 2004.

[33] Z.-F. Tan and G.-P. Lei, "Robust uplink carrier frequency offset estimation in MIMO-OFDM systems," in *Proc. Int. Conf. on Wireless Communications, Networking and Mobile Computing (WiCOM)*, Beijing, Sep. 2009, pp. 1–6.

[34] K. J. R. Liu, A. K. Sadek, W. Su, and A. Kwasinski, *Cooperative communications and networking*. Cambridge University Press, 2009.

[35] J. N. Laneman and G. W. Wornell, "Distributed space-time-block-coded protocols for exploiting cooperative diversity in wireless networks," *IEEE Trans. Inform. Theory*, vol. 49, pp. 2415–2425, Oct. 2003.

[36] J. N. Laneman, D. N. C. Tse, and G. W. Wornell, "Cooperative diversity in wireless networks: Efficient protocols and outage behavior," *IEEE Trans. Inform. Theory*, vol. 50, no. 12, pp. 3062–3080, Dec. 2004.

[37] A. Sendonaris, E. Erkip, and B. Aazhang, "User cooperation diversity Part I: System description," *IEEE Trans. Commun.*, vol. 51, no. 11, pp. 1927–1938, Nov. 2003.

[38] X. Guo, W. Ma, Z. Guo, X. Shen, and Z. Hou, "Adaptive resource reuse scheduling for multihop relay wireless network based on multicoloring," *IEEE Commun. Lett.*, vol. 12, no. 3, pp. 176–178, Mar. 2008.

[39] R. U. Nabar, H. Boelcskei, and F. W. Kneubheuler, "Fading relay channel: performance limits and space-time signal design," *IEEE J. Select. Areas Commun.*, vol. 22, no. 6, pp. 1099–1109, Aug. 2004.

[40] R. U. Nabar and H. Boelcskei, "Space-time signal design fro fading relay channels," in *Proc. IEEE Global Telecommn. Conf. (GLOBECOM)*, San Francisco, CA, Dec. 2003.

[41] K. J. R. Liu, A. K. Sadek, W. Su, and A. Kwasinski, *Cooperative Communications and Networking*. Cambridge University Press, 2009.

[42] M. Morelli, C. C. J. Kuo, and M. O. Pun, "Synchronization techniques for orthogonal frequency division multiple access (OFDMA): A tutorial review," *Proc. IEEE*, vol. 95, no. 7, pp. 1394–1427, Jul. 2007.

[43] P. Xia, S. Zhou, and G. B. Giannakis, "Adaptive MIMO-OFDM based on partial channel state information," *IEEE Trans. Signal Processing*, vol. 52, no. 1, pp. 202–213, Jan. 2004.

[44] H. Bölcskei and E. ZURICH, "MIMO-OFDM wireless systems: basics, perspectives, and challenges," *IEEE Trans. Wireless Commun.*, vol. 13, no. 4, pp. 31–37, Aug. 2006.

[45] R. W. Heath., Jr., and G. B. Giannakis, "Exploiting input cyclostationary for blind channel identification in OFDM syslems," *IEEE Trans. Signal Processing*, vol. 47, no. 3, pp. 848–856, Mar. 1999.

[46] B. Muquet, M. de Courville, and P. Duhamel, "Subspace-based blind and semi-blind channel estimation for OFDM systems," *IEEE Trans. Signal Processing*, vol. 50, no. 7, pp. 1699–1712, Jul. 2002.

[47] X. Cai and A. N. Akansu, "A subspace method for blind channel identification in OFDM systems," in *Proc. IEEE Int. Conf. Communications (ICC)*, vol. 2, New Orleans, LA, Jun. 2000, pp. 929–933.

[48] C. Li and S. Roy, "Subspace-based blind channel estimation for OFDM by exploiting virtual carriers," *IEEE Trans. Wireless Commun.*, vol. 2, no. 1, pp. 141–150, Jan. 2003.

[49] Y. Song, S. Roy, and L. A. Akers, "Joint blind estimation of channel and data symbols in OFDM," in *Proc. IEEE Vehicular Technology Conf. (VTC)*, vol. 1, May 2000, pp. 46–50.

[50] S. Zhou and G. B. Giannakis, "Finite-alphabet based channel estimation for OFDM and related multilcarrier systems," *IEEE Trans. Commun.*, vol. 49, no. 8, pp. 1402–1414, Aug. 2001.

[51] J. J. van de Beek, O. Edfors, M. Sandell, S. K. Wilson, and P. O. Borjesson, "On channel estimation in OFDM systems," in *Proc. IEEE Vehicular Technology Conf. (VTC)*, vol. 2, 1995, pp. 815–819.

[52] O. Edfors, M. Sandell, J.-J. van de Beek, S. K. Wilson, and P. O. Borjesson, "OFDM channel estimation by singular value decomposition," *IEEE Trans. Commun.*, vol. 46, no. 7, pp. 931–939, Jul. 1998.

[53] Y. Li, L. J. Cimini, Jr., and N. R. Sollenberger, "Robust channel estimation for OFDM systems with rapid dispersive fading channels," *IEEE Trans. Commun.*, vol. 46, no. 7, pp. 902–915, Jul. 1998.

[54] C. Oberli and B. Daneshrad, "Channel estimation for MIMO-OFDM with training overhead trade-off," in *Proc. IEEE Int. Symposium on Personal, Indoor and Mobile Radio Commun. (PIMRC)*, Sep. 2004, pp. 1787–1791.

[55] P. Marques, A. Pereira, and A. Gameiro, "Pilot and data aided channel estimation for uplink MC-CDMA mobile systems," in *EUSIPCO*, Antalya, Turkey, Sep. 2005, pp. 891–895.

[56] M. Morelli and U. Mengali, "A comparison of pilot-aided channel estimation methods for OFDM systems," *IEEE Trans. Signal Processing*, vol. 49, pp. 3065–3073, Dec. 2001.

[57] D. Shen, Z. Diao, K.-K. Wong, and V. O. K. Li, "Analysis of pilot assisted channel estimators for OFDM systems with transmit diversity," *IEEE Trans. Broadcast*, vol. 52, no. 2, pp. 193–202, Jun. 2006.

[58] M. Hsieh and C.Wei, "Channel estimation for OFDM systems based on comb-type pilot arrangement in frequency-selective fading channels," *IEEE Trans. Consumer Electron.*, vol. 44, no. 1, pp. 217–225, Feb. 1998.

[59] Y. Li, "Pilot-symbol-aided channel estimation for OFDM in wireless systems," *IEEE Trans. Veh. Technol.*, vol. 49, no. 4, pp. 1207–1215, Jul. 2000.

[60] X. Hou, S. Li, D. Liu, C. Yin, and G. Yue, "On two-dimensional adaptive channel estimation in OFDM systems," in *Proc. IEEE Vehicular Technology Conf. (VTC)*, vol. 1, 2004, pp. 498–502.

[61] R. Negi and J. Cioffi, "Pilot tone selection for channel estimation in a mobile OFDM system," *IEEE Trans. Consumer Electron.*, vol. 44, no. 3, pp. 1122–1128, Aug. 1998.

[62] S. Adireddy, L. Long, and H. Viswanathan, "Optimal placement of training

for frequencey-selective block-fading channels," *IEEE Trans. Inform. Theory*, vol. 48, no. 8, pp. 2338–2353, Aug. 2002.

[63] S. Ohno and G. B. Giannakis, "Capacity maximizing MMSE-optimal pilots for wireless OFDM over frequency-selective block Rayleigh-fading channels," *IEEE Trans. Inform. Theory*, vol. 50, no. 9, pp. 2138–2145, Sep. 2002.

[64] M. Dong and L. Tong, "Optimal design and placement of pilot symbols for channel estimation," *IEEE Trans. Signal Processing*, vol. 50, no. 12, pp. 3055–3069, Dec. 2002.

[65] X. Ma, L. Yang, and G. B. Giannakis, "Optimal training for MIMO frequency-selective fading channels," in *Asilomar Conf. on Signals, Systems and computers*, vol. 2, Nov. 2002, pp. 1107–1111.

[66] W. Zhang, X.-G. Xia, and P. C. Ching, "Optimal training and pilot pattern design for OFDM systems in rayleigh fading," *IEEE Trans. Broadcast*, vol. 52, no. 4, pp. 505–514, Dec. 2006.

[67] W. Zhou and W.-H. Lam, "Channel estimation and data detection for OFDM systems over fast-fading and dispersive channels," *IEEE Trans. Veh. Technol.*, vol. 59, no. 3, pp. 1381–1393, Mar. 2010.

[68] N. Lashkarian and S. Kiaei, "Class of cyclic-based estimators for frequency-offset estimation of OFDM systems," *IEEE Trans. Commun.*, vol. 48, no. 12, pp. 2139–2149, Dec. 2000.

[69] J. J. van de Beek, M. Sandell, and P. O. Borjesson, "ML estimation of timing and frequency offset in multicarrier systems," *IEEE Trans. Signal Processing*, vol. 45, no. 7, pp. 1800–1805, Jul. 1997.

[70] H. Liu and U. Tureli, "A high-efficiency carrier estimator for OFDM communications," *IEEE Commun. Lett.*, vol. 2, no. 4, pp. 104–106, Apr. 1998.

[71] U. Tureli, H. Liu, and M. D. Zoltowski, "OFDM blind carriar offset estimation: ESPRIT," *IEEE Trans. Commun.*, vol. 48, no. 9, pp. 1459–1461, Sep. 2000.

[72] U. Tureli, D. Kivanc, and H. Liu, "Experimental and analytical studies on a high-resolution OFDM carrier frequency offset estimator," *IEEE Trans. Veh. Technol.*, vol. 50, no. 2, pp. 629–643, Mar. 2001.

[73] D. Huang and K. B. Letaief, "Carrier frequency offset estimation for OFDM systems using null subcarriers," *IEEE Trans. Commun.*, vol. 54, no. 5, pp. 813–823, May 2006.

[74] M. Ghogho, A. Swami, and G. B. Giannakis, "Optimized null-subcarrier selection for CFO estimation in OFDM over frequency-selective fading channels," in *Proc. IEEE Global Telecommn. Conf. (GLOBECOM)*, vol. 1, San Antonio, TX, Nov. 2001, pp. 202–206.

[75] T. M. Schmidl and D. C. Cox, "Robust frequency and timing synchronization for OFDM," *IEEE Trans. Commun.*, vol. 45, no. 12, pp. 1613–1621, Dec. 1997.

[76] M. Morelli and U. Mengali, "An improved frequency offset estimator for OFDM applications," *IEEE Commun. Lett.*, vol. 3, no. 3, pp. 75–77, Mar. 1999.

[77] Z. Zhang, K. Long, and Y. N. Liu, "Complex efficient carrier frequency offset estimation algorithm in OFDM systems," *IEEE Trans. Broadcast*, vol. 50, no. 2, pp. 159–164, Jun. 2004.

[78] H. Minn, X. Fu, and V. K. Bhargava, "Optimal periodic training design for frequency offset estimation in frequency-offsetive fading channels," *IEEE Trans. Commun.*, vol. 54, no. 6, pp. 1081–1096, Jun. 2006.

[79] F. Classen and H. Meyr, "Frequency synchronization algorithms for OFDM systems suitable for communication over frquency selective fading channels," in

Proc. IEEE Vehicular Technology Conf. (VTC), vol. 3, Stockholm, Sweden, Jun. 1994, pp. 1655–1659.

[80] M. Li and W. Zhang, "A novel method of carrier frequency offset clustered pilot tones for carrier frequency offset estimation in OFDM systems," *IEEE Trans. Consumer Electron.*, vol. 49, no. 4, pp. 965–972, Nov. 2003.

[81] W. Zhang and X.-G. Xia, "Clustered pilot tones for carrier frequency offset estimation in OFDM systems," *IEEE Trans. Wireless Commun.*, vol. 6, no. 1, pp. 101–109, Jan. 2007.

[82] X. Fu and H. Minn, "Modified data-pilot multiplexed scheme for OFDM systems," in *Proc. IEEE Vehicular Technology Conf. (VTC)*, vol. 2, Sep. 2005, pp. 1011–1015.

[83] F. F. Gao, T. Cui, and A. Nallanathan, "Scattered pilots and virtual carrier based frequency offset tracking for OFDM systems: Algorithms, identifiablity, and performance analysis," *IEEE Trans. Commun.*, vol. 54, no. 4, pp. 619–629, Apr. 2008.

[84] J. Lei and T.-S. Ng, "A consistent OFDM carrier frequency offset estimator based on distinctively spaced pilot tones," *IEEE Trans. Wireless Commun.*, vol. 3, no. 2, pp. 588–599, Mar. 2004.

[85] Y. Li, H. Minn, N. Al-Dhahir, and A. R. Calderbank, "Pilot designs for consistent frequency-offset estimation in OFDM systems," *IEEE Trans. Commun.*, vol. 55, no. 5, pp. 864–877, May 2007.

[86] H. K. Song, Y. H. You, J. H. Paik, and Y. S. Cho, "Frequency-offset synchronization and channel estimation for OFDM-based transmission," *IEEE Commun. Lett.*, vol. 4, no. 3, pp. 95–97, Mar. 2000.

[87] X. Ma, H. Kobayash, and S. C. Schwartz, "Joint frequency offset and channel estimation for OFDM," in *Proc. IEEE Global Telecommn. Conf. (GLOBECOM)*, vol. 1, Dec. 2003, pp. 15–19.

[88] N.-L. Hung, L.-N. Tho, and C. K. Chi, "RLS-based joint estimation and tracking of channel response, sampling, and carrier frequency offsets for OFDM," *IEEE Trans. Broadcast*, vol. 55, no. 1, pp. 84–94, Mar. 2009.

[89] T. Cui and C. Tellambura, "Robust joint frequency offset and channel estimation for OFDM systems," in *Proc. IEEE Vehicular Technology Conf. (VTC)*, May 2004, pp. 603–607.

[90] ——, "Joint frequency offset and channel estimation for OFDM systems using pilot symbols and virtual carriers," *IEEE Trans. Wireless Commun.*, vol. 6, no. 4, pp. 1193–1202, Apr. 2007.

[91] C. Patel and G. St*ü*ber, "Channel estimation for amplify and forward relay based cooperation diversity systems," *IEEE Trans. Wireless Commun.*, vol. 6, no. 6, pp. 2348–2356, Jun. 2007.

[92] B. Gedik and M. Uysal, "Two channel estimation methods for amplify-and-forward relay networks," in *Proc. Canadian Conf. on Electrical and Comput. Eng.*, Niagara Falls, ON, May 2008, pp. 616–618.

[93] F. Gao, T. Cui, and A. Nallanathan, "On channel estimation and optimal training design for amplify and forward relay networks," *IEEE Trans. Wireless Commun.*, vol. 7, no. 5, pp. 1907–1916, May 2008.

[94] K. Kim, H. Kim, and H. Park, "OFDM channel estimation for the amply-and-forward cooperative channel," in *Proc. IEEE Vehicular Technology Conf. (VTC)*, Dublin, Apr. 2007, pp. 1642–1646.

[95] J.-J. van de Beek, P. O. Borjesson, M.-L. Boucheret, J. M. D. Landstrom, P. Odling, C. Ostberg, M. Wahlqvist, and S. K. Wilson, "A time and frequency synchronization scheme for multiuser OFDM," *IEEE J. Select. Areas Commun.*, vol. 17, no. 11, pp. 1900–1914, Nov. 1999.

[96] S. Barbarossa, M. Pompili, and G. B. Giannakis, "Channel-independent synchronization of orthogonal frequency division multiple access systems," *IEEE J. Select. Areas Commun.*, vol. 20, no. 2, pp. 474–486, Feb. 2002.

[97] Z. Cao, U. Tureli, and Y.-D. Yao, "Deterministic multiuser carrier frequency offset estimation for interleaved OFDMA uplink," *IEEE J. Select. Areas Commun.*, vol. 52, no. 9, pp. 1585–1594, Sep. 2004.

[98] J.-H. Lee and S.-C. Kim, "Time and frequency synchronization for OFDMA uplink system using the SAGE algorithm," *IEEE Trans. Wireless Commun.*, vol. 6, no. 4, pp. 1176–1181, Apr. 2007.

[99] L. Rugini and P. Banelli, "BER of OFDM systems impaired by carrier frequency offset in multipath fading channels," *IEEE Trans. Wireless Commun.*, vol. 4, no. 5, pp. 2279–2288, Sep. 2005.

[100] K. Sathananthan and C. Tellambura, "Probability of error calculation of OFDM systems with frequency offset," *IEEE Trans. Commun.*, vol. 49, no. 11, pp. 1884–1888, Nov. 2001.

[101] Z. Zhang, W. Zhang, and C. Tellambura, "BER of MIMO-OFDM systems with carrier frequency offset and channel estimation errors," in *Proc. IEEE Int. Conf. Communications (ICC)*, Glasgow, Scotland, Jun. 2007, pp. 5473–5477.

[102] ——, "Cooperative OFDM channel estimation in the presence of frequency offsets," *IEEE Trans. Veh. Technol.*, vol. 58, no. 7, pp. 3447–3459, Sep. 2008.

[103] C. Patel, G. Stüber, and T. Pratt, "Statistical properties of amplify and forward relay fading channels," *IEEE Trans. Veh. Technol.*, vol. 55, no. 1, pp. 1–9, Jan. 2006.

[104] B. Gedik and M. Uysal, "Impact of imperfect channel estimation on the performance of amplify-and-forward relaying," *IEEE Trans. Wireless Commun.*, vol. 8, no. 3, pp. 1468–1479, Mar. 2009.

[105] F. Liu, Z. Chen, X. Zhang, and D. Yang, "Channel estimation for amplify and forward relay in OFDM system," in *Proc. Int. Conf. on Wireless Communications, Networking and Mobile Computing (WiCOM)*, Dalian, Oct. 2008, pp. 1–4.

[106] O.-S. Shin, A. M. Chan, H. T. Kung, and V. Tarokh, "Design of an OFDM cooperative space-time diversity system," *IEEE Trans. Veh. Technol.*, vol. 56, pp. 2203–2215, Jul. 2007.

[107] I. Barhumi, G. Leus, and M. Moonen, "Optimal training design for MIMO OFDM systems in mobile wireless channels," *IEEE Trans. Signal Processing*, vol. 51, no. 6, pp. 1615–1624, Jun. 2003.

[108] H. Minn, X. Fu, and V. K. Bhargava, "Optimal training design for MIMO OFDM channel estimation in the presence of frequency offset and phase noise," *IEEE Trans. Commun.*, vol. 54, no. 10, pp. 1081–1096, Jun. 2006.

[109] M. Ghogho and A. Swami, "Training design for multipath channel and frequency-offset estimation in MIMO systems," *IEEE Trans. Signal Processing*, vol. 54, no. 10, pp. 3957–2339, Oct. 2006.

[110] N. Benvenuto, S. Tomasin, and D. Veronesi, "Multiple frequency offsets estimation and compensation for cooperative networks," in *Proc. IEEE Wireless Commun. and Networking Conf. (WCNC)*, Kowloon, Hong Kong, Mar. 2007, pp. 891–895.

[111] M. Krondorf, T. J. Liang, and G. Fettweis, "Symbol error rate of OFDM systems with carrier frequency offset and channel estimation error in frequency selective fading channels," in *Proc. IEEE Int. Conf. Communications (ICC)*, Glasgow, U. K., Jun. 2007, pp. 5132–5136.

[112] H. Mheidat, M. Uysal, and N. Al-Dhahir, "Equalization techniques for distributed space-time block codes with amplify-and-forward relaying," *IEEE Trans. Signal Processing*, vol. 55, no. 5, pp. 1839–1852, May 2007.

[113] A. N. Mody and G. L. Stüber, "Synchronization for MIMO OFDM systems," in *Proc. IEEE Global Telecommn. Conf. (GLOBECOM)*, San Antonio, TX, Nov. 2001, pp. 509–513.

[114] L.-M. He, "Carrier frequency offset estimation in MIMO OFDM systems," in *Proc. Int. Conf. on Wireless Communications, Networking and Mobile Computing (WiCOM)*, Dalian, Oct. 2008, pp. 1–4.

[115] H. Minn and N. Al-Dhahir, "Optimal training signals for MIMO OFDM channel estimation," *IEEE Trans. Commun.*, vol. 5, no. 5, pp. 1158–1168, May 2006.

[116] T. Roman, M. Enescu, and V. Koivunen, "Recursive estimation of time-varying channel and frequency offset in MIMO OFDM systems," in *Proc. IEEE Int. Symposium on Personal, Indoor and Mobile Radio Commun. (PIMRC)*, vol. 2, Sep. 2003, pp. 1934–1938.

[117] X. Ma, G. B. Giannakis, and S. Barbarossa, "Non-data-aided frequency offset and channel estimation in OFDM and related block transmissions," in *Proc. IEEE Int. Conf. Communications (ICC)*, vol. 6, Helsinki, Finland, Jun. 2001, pp. 1866–1870.

[118] B. Stantchev and G. Fettweis, "Time-variant distortions in OFDM," *IEEE Commun. Lett.*, vol. 4, no. 10, pp. 312–314, Sep. 2000.

[119] T. Keller and L. Hanzo, "Adaptive multicarrier modulation: A convenient framework for time-frequency processing in wireless communications," *Proc. IEEE*, vol. 88, no. 5, pp. 611–640, May 2000.

[120] Y. Zhao and S. G. Häggman, "BER analysis of OFDM communication systems with intercarrier interference," in *Int. Conf. on Commun. Technology*, vol. 2, Beijing, China, Oct. 1998, pp. 1–5.

[121] M. Torabi, S. Aissa, and M. Soleymani, "MIMO-OFDM systems with imperfect channel information: Capacity, outage and BER performance," in *Proc. IEEE Int. Conf. Communications (ICC)*, vol. 12, Istanbul, Jun. 2006, pp. 5342–5347.

[122] S. M. Kay, *Fundamentals of Statistical Signal Processing: Estimation Theory*. Englewood Cliffs, NJ: Prentice-Hall, 1993.

[123] D. N. Dao and C. Tellambura, "Intercarrier interference self-cancellation space-frequency codes for MIMO-OFDM," *IEEE Trans. Veh. Technol.*, vol. 54, no. 5, pp. 1729–1738, Sep. 2005.

[124] T. Tang, R. W. J. Heath, and Jr., "Space-time interference cancellation in MIMO-OFDM systems," *IEEE Trans. Veh. Technol.*, vol. 54, no. 5, pp. 1802–1816, Sep. 2005.

[125] L. Giangaspero, L. Agarossi, G. Paltenghi, S. Okamura, M. Okada, and S. Komaki, "Co-channel interference cancellation based on MIMO OFDM systems," *IEEE Trans. Wireless Commun.*, vol. 9, no. 6, pp. 8–17, Dec. 2002.

[126] A. Stamoulis, S. N. Diggavi, and N. Al-Dhahir, "Intercarrier interference in MIMO OFDM," *IEEE Trans. Signal Processing*, vol. 50, no. 10, pp. 2451–2464, Oct. 2002.

[127] K. Cho and D. Yoon, "On the general BER expression of one- and two-dimensional amplitude modulations," *IEEE Trans. Commun.*, vol. 50, no. 7, pp. 1074–1080, Jul. 2002.

[128] L.-L. Yang and L. Hanzo, "A recursive algorithm for the error probability evaluation of M-QAM," *IEEE Commun. Lett.*, vol. 4, no. 10, pp. 304–306, Oct. 2000.

[129] I. S. Gradshteyn and I. M. Ryzhik, *Table of Integrals, Series, and Products.* Academic Press Inc., 1994.

[130] Z. Zhang and C. Tellambura, "The effect of imperfect carrier frequency offset estimation on OFDMA uplink transmission," *IEEE Trans. Commun.*, vol. 57, no. 4, pp. 1025–1030, Apr. 2009.

[131] Z. Zhang, W. Zhang, and C. Tellambura, "Robust OFDMA uplink synchronization by exploiting the variance of carrier frequency offsets," *IEEE Trans. Veh. Technol.*, vol. 57, no. 5, pp. 3028–3039, 2008.

[132] H. Bolcskei, "Blind high-resolution uplink synchronization of OFDM-based multiple access schemes," in *IEEE Workshop on Signal Processing advances in Wireless Commun.*, May 1999, pp. 166–169.

[133] M.-O. Pun, M. Morelli, and C.-C. Kuo, "Maximum-likelihood synchronization and channel estimation for OFDMA uplink transmissions," *IEEE Trans. Commun.*, vol. 54, no. 4, pp. 726–736, Apr. 2006.

[134] S. Haykin, *Adaptive Filter Theory.* New Jersey: Prentice-Hall, 1996.

[135] H. L. V. Trees, *Detection, Estimation, and Modulation Theory, Part IV, Optimum Array Processing.* New York: Wiley, 2002.

[136] D. Huang and K. Letaief, "An interference-cancellation scheme for carrier frequency offsets correction in OFDMA systems," *IEEE Trans. Commun.*, vol. 53, no. 7, pp. 1155–1165, Jul. 2005.

[137] I. Ziskind and M. Wax, "Maximum likelihood localization of multiple sources by alternating projection," *IEEE Trans. Signal Processing*, vol. 36, no. 10, pp. 1553–1560, Oct. 1988.

[138] T. Cui and C. Tellambura, "Joint channel and frequency offset estimation and training sequence design for MIMO systems over frequency selective channels," in *Proc. IEEE Global Telecommn. Conf. (GLOBECOM)*, vol. 4, Nov./Dec. 2004, pp. 2344–2348.

[139] D. Huang and K. Letaief, "Enhanced carrier frequency offset estimation for OFDM using channel side information," *IEEE Trans. Wireless Commun.*, vol. 5, no. 10, pp. 2784–2793, Oct. 2006.

[140] D. Pauluzzi and N. Beaulieu, "A comparison of SNR estimation techniques for the AWGN channel," *IEEE Trans. Commun.*, vol. 48, no. 10, pp. 1681–1691, Oct. 2000.

[141] A. Wiesel, J. Goldberg, and H. Messer-Yaron, "SNR estimation in time varying fading channels," *IEEE Trans. Commun.*, vol. 54, no. 5, pp. 841–848, May 2006.

[142] P. Gao and C. Tepedelenlioglu, "SNR estimation for nonconstant modulus constellations," *IEEE Trans. Signal Processing*, vol. 53, no. 3, pp. 865–870, Mar. 2005.

[143] H. Minn, X. Fu, and V. K. Bhargava, "Optimal periodic training signal for frequency offset estimation in frequency-selective fading channels," *IEEE Trans. Commun.*, vol. 54, no. 6, pp. 1081–1096, Jun. 2006.

[144] Z. Zhang, M. Zhao, H. Zhou, Y. Liu, and J. Gao, "Frequency offset estimation with fast acquisition in OFDM system," *IEEE Commun. Lett.*, vol. 8, no. 3, pp. 171–173, Mar. 2004.

[145] Z. Z. Zhang, W. Zhang, and C. Tellambura, "Cooperative OFDM channel estimation in presence of frequency offsets," *IEEE Trans. Veh. Technol.*, vol. 58, no. 7, pp. 3347–3459, 2009.

[146] A. Sendonaris, E. Erkip, and B. Aazhang, "User cooperation diversity. Part I. system description," *IEEE Trans. Commun.*, vol. 51, no. 11, pp. 1927 – 1938, Nov. 2003.

[147] M. Yu and J. Li, "Is amplify-and-forward practically better than decode-and-forward or vice versa," in *Proc. IEEE Int. Conf. Acoustics, Speech, and Signal Processing (ICASSP)*, vol. 3, 2005.

[148] M. Morelli, "Timing and frequency synchronization for the uplink of an OFDMA system," *IEEE Trans. Commun.*, vol. 52, no. 2, pp. 296–306, Jan. 2004.

[149] T. C.-Y. Ng and W. Yu, "Joint optimization of relay strategies and resource allocations in cooperative cellular networks," *IEEE J. Select. Areas Commun.*, vol. 25, no. 2, pp. 328–339, Feb. 2007.

[150] Z. Yi and I.-M. Kim, "Joint optimization of relay-precoders and decoders with partial channel side information in cooperative networks," *IEEE J. Select. Areas Commun.*, vol. 25, no. 2, pp. 447–458, Feb. 2007.

[151] A. Bletsas, H. Shin, and M. Z. Win, "Cooperative communications with outage-optimal opportunistic relaying," *IEEE Trans. Wireless Commun.*, vol. 6, no. 9, pp. 3450–3460, Sep. 2007.